Clustering-Induced, Clathrin-Mediated Endocytosis (CIC-ME) for Cancer Therapy

Raimond Heukers

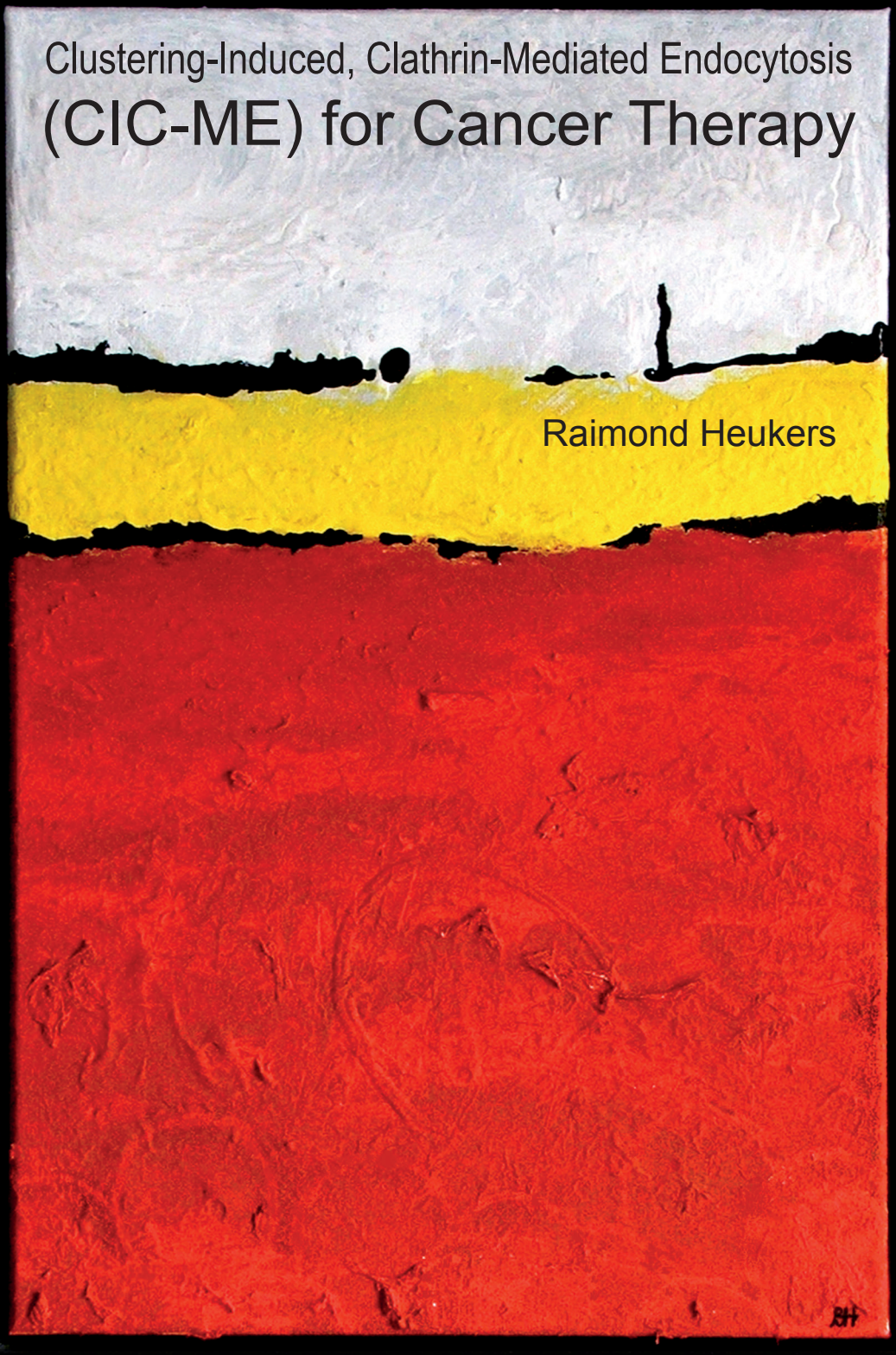

ISBN: 978-90-393-6065-1

Het onderzoek in dit proefschrift werd uitgevoerd in de groep Moleculaire Oncologie, welke onderdeel is van de Cel Biologie groep in het departement Biologie van de faculteit Bètawetenschappen van de Universiteit Utrecht. Het onderzoek werd gefinancieerd door het Focus & Massa project van de Universiteit Utrecht.

Cover: Acryl on canvas by Raimond Heukers

Printed by: Proefschriftmaken.nl || Uitgeverij BOXPress

Clustering-Induced, Clathrin-Mediated Endocytosis (CIC-ME) for Cancer Therapy

Clustering-geïnduceerde, clathrine-gemedieerde endocytosis (CIC-ME) voor kanker therapie

(met een samenvatting in het Nederlands)

Proefschrift

ter verkrijging van de graad van doctor aan de Universiteit Utrecht op gezag van de rector magnificus, prof.dr. G.J. van der Zwaan, ingevolge het besluit van het college voor promoties in het openbaar te verdedigen op maandag 20 januari 2014 des middags te 4.15 uur

door

Raimond Heukers

geboren op 11 juli 1983 te Emmen

Promotor: Prof. dr. C.C. Hoogenraad

Co-promotor: Dr. P. M.P. van Bergen en Henegouwen

“En dan zo op ’n maol: Raoms! Daor giet ‘t hen”

Geertje Heukers-Boxum (2012)

Table of contents

Chapter 1

General introduction

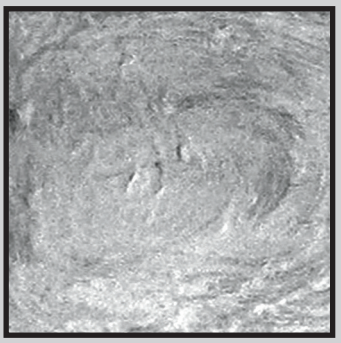

1.1. Cancer and cancer therapy

Despite the many efforts to discover novel ways of treating cancer, it is still a major health problem [1]. Cancer is characterized by the uncontrolled cell growth of cells that have acquired self-sufficiency in growth signalling and/or unlimited replication [2]. Such cells are often insensitive to anti-proliferating signals and are able to evade apoptosis. For therapy, solid tumors are generally removed by surgery. In case of small tumors, metastasis or remainders of tumors after resection, removal is obviously more tedious or simply impossible. In those cases, other approaches like chemo- or radiation therapy are applied. Unfortunately, many systemic therapies like chemotherapy are associated with unwanted side effects, caused by off-target cytotoxicity [3]. Collateral damage is often observed in mucosal cell layers like those found in the intestine. Improvements can be made by enhancing the tumor specificity of such compounds.

1.2. Immunotherapy

Examples of therapies that are directed against specific cancer-related molecules include chemical small molecule inhibitors, siRNAs that interfere with protein synthesis and immunotherapy [4-7]. The latter involves the use of the immune system for the treatment of cancer. Many different monoclonal antibodies (mAbs) have been developed for the treatment of many diseases, including cancer [8]. A few of these have already been tested clinically, such as trastuzumab (anti-HER2), bevacizumab (anti-VEGF), cetuximab, panitumumab, and matuzumab (all directed against EGFR) [9, 10]. Such antibodies act via three mechanisms: activating the antibody-dependent cellular cytotoxicity system, activating the complement-dependent cytotoxicity and blocking tumor-related signalling cascades by either blocking ligand-binding via binding to the ligand-binding spot on the receptor or to the ligands itself. Conventional antibodies like the monoclonal antibodies mentioned above have a molecular weight of ~150 kDa and a size of 14.2 nm × 8.5 nm × 3.8 nm [11]. These antibodies consist of two heavy chains and two light chains (Figure 1A). The heavy chains possess an Fc (fragment crystallisable) domain, which can interact with the human complement system or with effector cells of the immune system [12].

The large size of monoclonal antibodies enables a long circulation time in the body but also suffer from several side effects for their use in cancer therapy. Their size and the so-called ‘binding site barrier’ limit the distribution of antibodies through tissues and their penetration into the tumor [13]. Therefore, many types of smaller antibody formats have been developed, such as antigen-binding fragment (Fab; ~50 kDa), variable fragment (Fv; ~15 kDa), single-chain variable fragment (scFv; ~30 kDa) and so-called minibodies [14-18]. Nevertheless, these formats also have their shortcommings like stability issues and lower binding affinities, compared to intact antibodies [17]. Besides variations of naturally occurring antibodies, synthetic molecules or scaffold proteins, like affibodies, DARPins (designed ankyrin repeat proteins) and fibronectin subunits

have been developed against multiple targets [19-21]. It should be noted that these fragments lack an Fc region and thereby primarily act via binding and competition of disease-related molecules.

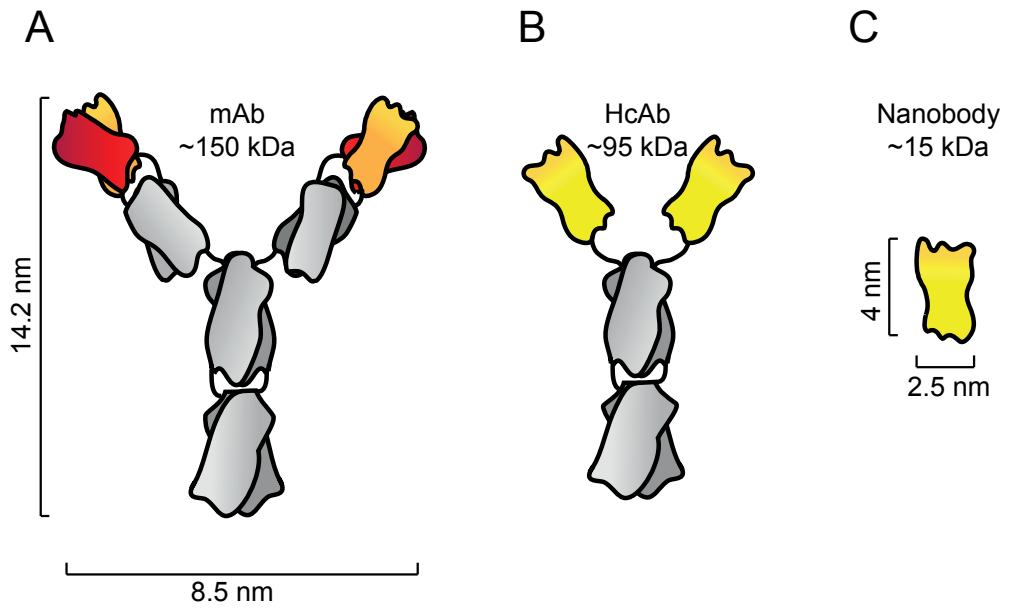

Figure 1. *Schematic overview of different antibody-formats. Conventional antibody (mAb, A), heavy chain only antibody (HcAb, B) and its derivative derived nanobody or VHH (C) and their molecular weight and size are shown [11, 22, 23].*

1.3. Nanobodies

Another example of such small antibody fragments are the so-called nanobodies [23, 24]. These consist of the variable domain of heavy chain only antibodies (HcAbs) and are therefore also known as VHH (Variable domain of the Heavy chain of Heavy chain only antibodies) (Figure 1B and C). HcAbs are ~ 95 kDa antibodies that are typically found in members of the Camelidae family or some primitive fish species like nurse sharks, and are fully functional despite the absence of the light chain and the first constant domain (CH1) [22]. Even though antigen binding occurs only via single epitope-binding domains, HcAbs are able to bind antigens with high binding affinities. Even upon isolation of these epitope binding domains (the actual VHHs or nanobodies), similar antigen binding properties are achieved. Because of their small size (15 kDa), VHHs are considered to be the smallest naturally derived antigen-binding fragments. Since their discovery, many VHHs or nanobodies have been developed to block binding of different types of ligands to treat various types of diseases [11, 15, 24, 25].

1.4. Nanobullets, the intracellular delivery of therapeutic agents

Many in vivo studies show inhibition of tumor growth upon administration of ligand blocking antibodies or nanobodies [26-28, 28]. Unfortunately, ligand blocking and activation of the immune system is often not sufficient to remove a tumor completely and improvements should be made to enhance their antitumor activity [29]. On the other hand, cell killing agents are often not specific, resulting in off-target cytotoxicity. Advantages can be made by the specific delivery of toxic agents to and more importantly into tumor cells. Such so-called 'Nanobullets' combine the specificity of antibodies with the toxicity of a chemotherapeutic agent. Furthermore, the intracellular delivery of therapeutic compounds allows the use of prodrugs that become cytotoxic only upon uptake in tumor cells. This would reduce off-target toxicity and enhance the specific activity of such agents. Examples of such carriers include liposomes, micelles or other nanoparticles, in which the toxic payload is shielded from its environment by encapsulation in a (ideally tumor-targeted) lipid- or protein- based particle. Such encapsulation enhances the circulation time of the therapeutic agent and protects surrounding tissues. However, in order for this intracellular delivery of therapeutic agents via Nanobullets to be successful, a basic understanding on how cells take up material from its surrounding is essential.

1.5. ErbB/HER receptor kinases

Receptor tyrosine kinases maintain cell viability by regulating a balance between surviving signals and apoptosis. Deregulation of such kinases is responsible for many diseases, such as cancer and diabetes and these are therefore important targets for therapy. The ErbB (Erythroblastosis oncogene B) family of receptor kinases consist of four members: ErbB1 or epidermal growth factor receptor (EGFR), ErbB2 (neu, HER2), ErbB3 and ErbB4, and each of these members have different affinities for several growth factors [30]. Two members (EGFR and ErbB4) are completely functional, while ErbB2 has no known ligand and ErbB3 lacks an active kinase domain. Tyrosine phosphorylation of these receptors occurs via direct interaction with the other members of the ErbB receptor family [31]. EGFR often serves as a model tyrosine kinase receptor and its ligand-induced activation and internalization is considered to be well studied [32, 33]. The extracellular part of this 170 kDa transmembrane protein consists of 4 domains of which two are responsible for ligand binding [34]. Ligand binding results in a conformational change of the extracellular, transmembrane and intracellular domains, which enables the formation of an asymmetrical EGFR dimer [34-37]. This interaction is stabilized via both interactions between the extracellular domains and the transmembrane helix [38, 39]. The transmembrane domains of EGFR are homo-dimerized via interaction of two GxxxG-like, so-called GG4- or Sternberg-Gullick- or TMD dimerization motifs [40, 41]. More specifically, a disulfide crosslinking screen revealed that this interaction is most likely mediated by the first, N-terminal, transmembrane dimerization motif [42]. The EGF-induced

conformation change also releases a conformational auto-inhibition, which results in kinase activation and trans-autophosphorylation of its C-terminal tyrosine residues [43]. These phosphotyrosines serve as docking sites for various adaptor proteins involved in signal transduction in proliferative and anti-apoptotic pathways, such as the classical Ras-ERK1/2 (extracellular signal-regulated kinase 1/2) signaling pathway and phospholipase C (PLCγ)/phosphoinositide 3 kinase (PI3K) signaling towards Akt/protein kinase B (PKB) and NFκB (nuclear factor kappa-light-chain-enhancer of activated B cells) [44]. Currently, several antibodies, antibody-conjugates or kinase inhibitors targeting EGFR and/or HER2 are being developed or have already found their way into the clinic [27, 28].

1.6. The hepatocyte growth factor receptor (HGFR or Met)

The hepatocyte growth factor (HGF) receptor (Met) is another type of receptor tyrosine kinase (RTK) that is primarily expressed on epithelial cells and is the only known high affinity receptor for HGF [45]. Binding of HGF to Met activates the receptor, resulting in the phosphorylation of tyrosines in the cytoplasmic tail. Subsequently, the recruitment of a large signaling complex to the intracellular segment of the receptor results in downstream signaling towards the MAPK, STAT and PI3kinase/Akt pathways [45-48]. Met/HGF signaling is crucial during embryogenesis, tissue regeneration and wound healing in the adult life [49-51]. Deregulated signaling is implicated in the development, progression and metastasis of a wide variety of human cancers [51, 52]. Uncontrolled Met/HGF signaling can occur due to: mutational activation, receptor/ligand overexpression, autocrine activation and ligand-independent activation [53, 54]. Due to its specific expression in many human cancers, Met has become an attractive target for cancer therapy, resulting in the development of a variety of Met/HGF signaling inhibitors. These include small Met TK inhibitors, HGF or Met antagonistic antibodies and decoy receptors [52, 55, 56].

1.7. Cellular uptake and ligand-induced negative feedback mechanism

Cells constantly are taking up molecules from their environment. Small molecules like chemicals, amino acids and ions can pass the plasma membrane via diffusion, dedicated channels or ion-pumps. Larger molecules like proteins require the assistance of the plasma membrane. In this case, the plasma membrane forms vesicles, containing these proteins, which eventually pinch-off into the cytosplasm. This process is called endocytosis [57]. Very large materials are taken up via phagocytosis, while smaller molecules can enter just via pinocytosis. The process of pinocytosis can be roughly divided into four different pathways: macropinocytosis, clathrin-mediated endocytosis (CME), caveolin-mediated endocytosis and clathrin-independent endocytosis (CIE) [57, 58].

As many biological systems are in equilibrium, a positive stimulus is often counteracted

by a negative reaction. In case of receptor activation, ligand-induced signalling is neutralised via several negative feedback mechanisms (Figure 2). Both EGFR and Met signalling is attenuated by rapid internalization and subsequent degradation of the receptor-ligand complex [59]. The many processes that occur at the intracellular tail of EGFR, such as post-translational modifications like phosphorylation, ubiquitination and acetylation have all proven to play a role in the rapid ligand-induced endocytosis [60-62]. These mechanisms are thought to act simultaneously as redundant regulators of endocytosis.

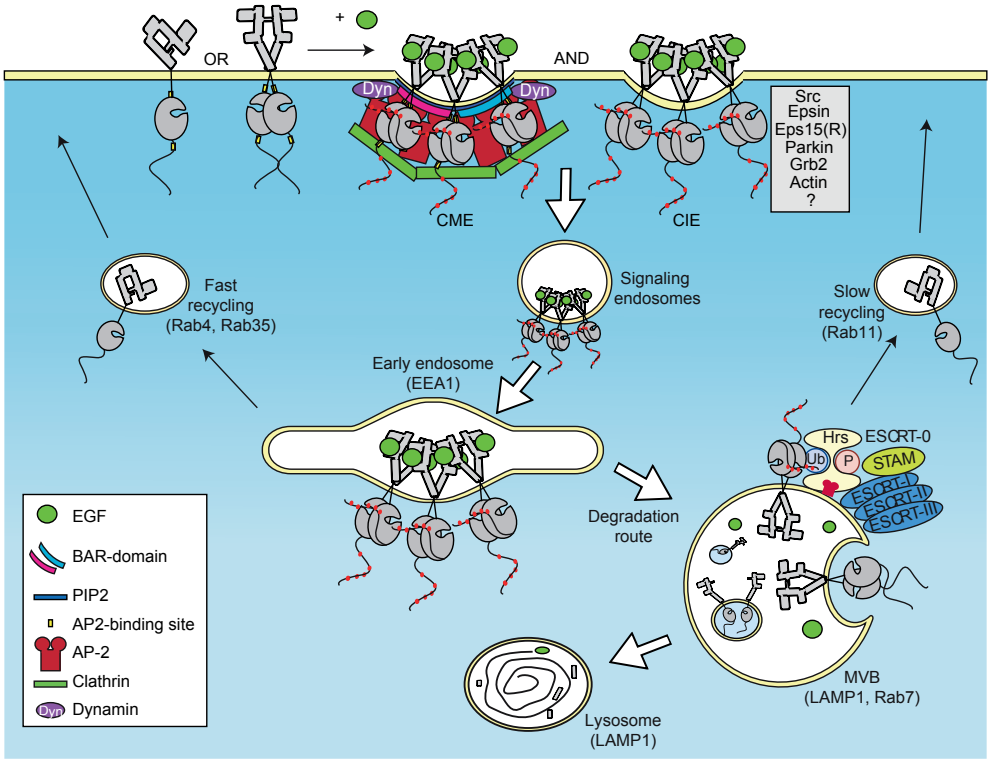

***Figure 2**. Schematic overview of the negative feedback mechanism of EGFR. EGFR can exist on the plasma membrane as monomers or pre-dimers. Upon binding of EGF, the receptors forms higher order clusters and becomes activated due to a conformational change. This activated cluster is then internalized via clathrin-dependent and independent pathways. This process also depends on dynamin, epsin, Eps15(R), BAR-domain-containing proteins and PIP2. Endocytosis results in the formation of signalling endosomes that subsequently fuse into larger early endosomes and the sorting compartments. Receptors are recycled back to the plasma membrane from the early endosomes (fast) or upon sorting to more perinuclear sorting endosomes. Activated and ubiquitinated receptors are sorted to the degradation route towards late endosomes. Ubiquitinated EGFR is recognized by adaptor proteins and subsequently invaginated into interluminal vesicles of the multiple vesicle bodies (MVB) via the ESCRT-complex. Finally MVBs fuse with lysosomal compartments, resulting in degradation of its content.*

On top of the ligand-induced posttranslational modifications of EGFR, activation of the receptor is also accompanied by higher order oligomerization of EGFR [63-66]. Ligand-induced clustering is kinase-dependent and does not seem to be involved in receptor activation [67]. So far, the role for this clustering in the functioning of EGFR is still unclear. Previously, intracellular dimerization of EGFR has been shown to induce or enhance internalization of EGFR independently of its kinase activity [67, 68]. Moreover, clustering via combinations of anti-EGFR antibodies cause the receptors to be internalized [69, 70]. Upon binding of EGF, EGFR is internalized via both CME and CIE. At low, more physiological concentrations of EGF, CME is considered to be the main internalization route [71, 72]. This process also includes a role for the adaptor protein complex 2 (AP2), dynamin, phosphatidylinositol 4,5-bisphosphate (PIP_2) and BAR-domain containing proteins (reviewed by [71]). From the plasma membrane, these internalized signaling endosomes traffic to early endosomes. Subsequently, receptors can either recycle back to the plasma membrane via fast recycling or via slow recycling. Fast recycling already takes place directly from the early endosomes via Rab4 and Rab35 positive vesicles [73], while the slow recycling involves the perinuclear sorting into Rab11 positive recycling endosomes. Active receptors become ubiquitinated via a Cbl-mediated mechanism and these receptors are transported from early endosomes into multiple vesicle bodies (MVBs) via invagination mediated by the ESCRT complexes. Upon fusion of these MVBs with lysosomes, these receptors are eventually degraded [62, 71].

1.8. Scope of this thesis

This thesis focuses on clustering-induced internalization and employs this phenomenon for the intracellular delivery of Nanobullets. For the targeting to tumor cells and the induction of endocytosis, nanobodies directed against EGFR or Met are used. First, a general overview of studies reporting the use of VHHs/nanobodies for cancer therapy is given in **Chapter 2** of this thesis. In **Chapter 3** of this thesis, we have aimed to study the mechanism of clustering-induced endocytosis by using non-agonistic biparatopic VHH-constructs directed against EGFR. This chapter also illustrates that VHHs are a valuable tool to study cell biological mechanisms like endocytosis. In ligand-induced endocytosis, the next step in the negative feedback mechanism of EGFR involves the lysosomal degradation of the receptors (indicated in Figure 2). In **Chapter 4** of this thesis, we have further evaluated the fate of EGFR upon clustering-induced internalization. For this, we have used four previously published tri-epitopic anti-EGFR antibody-fibronectin fusion constructs that are very efficient in inducing clustering-induced endocytosis of EGFR in several cell lines [74]. **Chapter 5** of this thesis describes an example of a 'Nanobullet' targeted to EGFR. Here, nanoparticles consisting of crosslinked albumin were PEGylated and rendered specific against EGFR expressing cells via conjugation to multiple anti-EGFR nanobodies. These

targeted nanoparticles, called nanobody-albumin nanoparticles (NANAPs) serve as vehicles for the intracellular delivery of therapeutic agents, like in this case, the kinase inhibitor 1740864. This inhibitor was reversibly conjugated to the NANAPs via a platinum-based linker that releases upon intracellular endosomal sorting toward the lysosomes. In **Chapter 6** a similar approach was used to develop a biomaterial that facilitates intracellular drug delivery in Met-expressing cells. For that, novel anti-Met nanobodies were selected and coupled to albumin nanoparticles. Subsequently, specific binding, internalization en subcellular routing was assessed. **Chapter 7** describes the development and *in vitro* testing of a novel nanobody-photosensitizer conjugate (NB-PS) for photodynamic therapy (PDT). Also, an internalizing nanobullet was used to further improve the efficacy of PDT. For this, the biparatopic VHH used in Chapter 3 was used for clustering-induced internalization and intracellular delivery and accumulation of the PS IRDye700DX. The research in this thesis is summarized and discussed further in **Chapter 8**.

1.9. References

1. Ferlay, J. *et al*. Estimates of worldwide burden of cancer in 2008: GLOBOCAN 2008. *Int. J. Cancer* **127**, 2893-2917 (2010).
2. Hanahan, D. & Weinberg, R. A. The hallmarks of cancer. *Cell* **100**, 57-70 (2000).
3. Guillot, B., Bessis, D. & Dereure, O. Mucocutaneous side effects of antineoplastic chemotherapy. *Expert Opin. Drug Saf.* **3**, 579-587 (2004).
4. Zhang, J., Yang, P. L. & Gray, N. S. Targeting cancer with small molecule kinase inhibitors. *Nat. Rev. Cancer.* **9**, 28-39 (2009).
5. Meister, G. & Tuschl, T. Mechanisms of gene silencing by double-stranded RNA. *Nature* **431**, 343-349 (2004).
6. Pecot, C. V., Calin, G. A., Coleman, R. L., Lopez-Berestein, G. & Sood, A. K. RNA interference in the clinic: challenges and future directions. *Nat. Rev. Cancer.* **11**, 59-67 (2011).
7. Heemskerk, B., Kvistborg, P. & Schumacher, T. N. The cancer antigenome. *EMBO J.* **32**, 194-203 (2013).
8. Scott, A. M., Wolchok, J. D. & Old, L. J. Antibody therapy of cancer. *Nat. Rev. Cancer.* **12**, 278-287 (2012).
9. Elbakri, A., Nelson, P. N. & Abu Odeh, R. O. The state of antibody therapy. *Hum. Immunol.* **71**, 1243-1250 (2010).
10. Oldham, R. K. & Dillman, R. O. Monoclonal antibodies in cancer therapy: 25 years of progress. *J. Clin. Oncol.* **26**, 1774-1777 (2008).
11. Cortez-Retamozo, V. *et al*. Efficient cancer therapy with a nanobody-based conjugate. *Cancer Res.* **64**, 2853-2857 (2004).
12. Sarma, V. R., Silverton, E. W., Davies, D. R. & Terry, W. D. The three-dimensional structure at 6 A resolution of a human gamma Gl immunoglobulin molecule. *J. Biol. Chem.* **246**, 3753-3759 (1971).
13. Fujimori, K., Covell, D. G., Fletcher, J. E. & Weinstein, J. N. A modeling analysis of monoclonal antibody percolation through tumors: a binding-site barrier. *J. Nucl. Med.* **31**, 1191-1198 (1990).
14. Gong, R., Chen, W. & Dimitrov, D. S. Expression, purification, and characterization of engineered antibody CH2 and VH domains. *Methods Mol. Biol.* **899**, 85-102 (2012).
15. Altintas, I., Kok, R. J. & Schiffelers, R. M. Targeting epidermal growth factor receptor in tumors: from conventional monoclonal antibodies via heavy chain-only antibodies to nanobodies *Eur. J. Pharm. Sci.* **45**, 399-407 (2012).
16. Miller, K. R. *et al*. T cell receptor-like recognition of tumor in vivo by synthetic antibody fragment. *PLoS One* **7**, e43746 (2012).
17. Bell, A. *et al*. Differential tumor-targeting abilities of three single-domain antibody

formats *Cancer Lett.* **289**, 81-90 (2010).
18. Hu, S. *et al*. Minibody: A novel engineered anti-carcinoembryonic antigen antibody fragment (single-chain Fv-CH3) which exhibits rapid, high-level targeting of xenografts. *Cancer Res.* **56**, 3055-3061 (1996).
19. Orlova, A. *et al*. Synthetic affibody molecules: a novel class of affinity ligands for molecular imaging of HER2-expressing malignant tumors. *Cancer Res.* **67**, 2178-2186 (2007).
20. Stumpp, M. T., Binz, H. K. & Amstutz, P. DARPins: a new generation of protein therapeutics. *Drug Discov. Today* **13**, 695-701 (2008).
21. Boersma, Y. L. & Pluckthun, A. DARPins and other repeat protein scaffolds: advances in engineering and applications. *Curr. Opin. Biotechnol.* **22**, 849-857 (2011).
22. Hamers-Casterman, C. *et al*. Naturally occurring antibodies devoid of light chains. *Nature* **363**, 446-448 (1993).
23. Revets, H., De Baetselier, P. & Muyldermans, S. Nanobodies as novel agents for cancer therapy. *Expert Opin. Biol. Ther.* **5**, 111-124 (2005).
24. Roovers, R. C., van Dongen, G. A. & van Bergen en Henegouwen, P. M. Nanobodies in therapeutic applications. *Curr. Opin. Mol. Ther.* **9**, 327-335 (2007).
25. Van Bockstaele, F., Holz, J. B. & Revets, H. The development of nanobodies for therapeutic applications. *Curr. Opin. Investig Drugs* **10**, 1212-1224 (2009).
26. Roovers, R. C. *et al*. A bi-paratopic anti-EGFR nanobody efficiently inhibits solid tumour growth. *Int. J. Cancer* (2011).
27. Friedlander, E., Barok, M., Szollosi, J. & Vereb, G. ErbB-directed immunotherapy: antibodies in current practice and promising new agents. *Immunol. Lett.* **116**, 126-140 (2008).
28. Yarden, Y. & Pines, G. The ERBB network: at last, cancer therapy meets systems biology. *Nat. Rev. Cancer.* **12**, 553-563 (2012).
29. Martinelli, E., De Palma, R., Orditura, M., De Vita, F. & Ciardiello, F. Anti-epidermal growth factor receptor monoclonal antibodies in cancer therapy. *Clin. Exp. Immunol.* **158**, 1-9 (2009).
30. Yarden, Y. The EGFR family and its ligands in human cancer. signalling mechanisms and therapeutic opportunities. *Eur. J. Cancer* **37 Suppl 4**, S3-8 (2001).
31. Graus-Porta, D., Beerli, R. R., Daly, J. M. & Hynes, N. E. ErbB-2, the preferred heterodimerization partner of all ErbB receptors, is a mediator of lateral signaling. *EMBO J.* **16**, 1647-1655 (1997).
32. Citri, A. & Yarden, Y. EGF-ERBB signalling: towards the systems level. *Nat. Rev. Mol. Cell Biol.* **7**, 505-516 (2006).
33. Yarden, Y. & Shilo, B. Z. SnapShot: EGFR signaling pathway. *Cell* **131**, 1018 (2007).
34. Ferguson, K. M. Active and inactive conformations of the epidermal growth factor receptor. *Biochem. Soc. Trans.* **32**, 742-745 (2004).
35. Burgess, A. W. *et al*. An open-and-shut case? Recent insights into the activation of EGF/ErbB receptors. *Mol. Cell* **12**, 541-552 (2003).
36. Jura, N. *et al*. Mechanism for activation of the EGF receptor catalytic domain by the juxtamembrane segment. *Cell* **137**, 1293-1307 (2009).
37. Thiel, K. W. & Carpenter, G. Epidermal growth factor receptor juxtamembrane region regulates allosteric tyrosine kinase activation. *Proc. Natl. Acad. Sci. U. S. A.* **104**, 19238-19243 (2007).
38. Tanner, K. G. & Kyte, J. Dimerization of the extracellular domain of the receptor for epidermal growth factor containing the membrane-spanning segment in response to treatment with epidermal growth factor. *J. Biol. Chem.* **274**, 35985-35990 (1999).
39. Ogiso, H. *et al*. Crystal structure of the complex of human epidermal growth factor and receptor extracellular domains. *Cell* **110**, 775-787 (2002).
40. Mendrola, J. M., Berger, M. B., King, M. C. & Lemmon, M. A. The single transmembrane domains of ErbB receptors self-associate in cell membranes. *J. Biol. Chem.* **277**, 4704-4712 (2002).
41. Sternberg, M. J. & Gullick, W. J. A sequence motif in the transmembrane region of growth factor receptors with tyrosine kinase activity mediates dimerization. *Protein Eng.* **3**, 245-248 (1990).
42. Lu, C. *et al*. Structural evidence for loose linkage between ligand binding and kinase activation in the epidermal growth factor receptor. *Mol. Cell. Biol.* **30**, 5432-5443 (2010).
43. Zhang, X., Gureasko, J., Shen, K., Cole, P. A. & Kuriyan, J. An allosteric mechanism for activation of the kinase domain of epidermal

growth factor receptor. *Cell* **125**, 1137-1149 (2006).
44. Jorissen, R. N. *et al*. Epidermal growth factor receptor: mechanisms of activation and signalling. *Exp. Cell Res.* **284**, 31-53 (2003).
45. Naldini, L. *et al*. Hepatocyte growth factor (HGF) stimulates the tyrosine kinase activity of the receptor encoded by the proto-oncogene c-MET. *Oncogene* **6**, 501-504 (1991).
46. Ferracini, R., Longati, P., Naldini, L., Vigna, E. & Comoglio, P. M. Identification of the major autophosphorylation site of the Met/hepatocyte growth factor receptor tyrosine kinase. *J. Biol. Chem.* **266**, 19558-19564 (1991).
47. Bussolino, F. *et al*. Hepatocyte growth factor is a potent angiogenic factor which stimulates endothelial cell motility and growth. *J. Cell Biol.* **119**, 629-641 (1992).
48. Xiao, G. H. *et al*. Anti-apoptotic signaling by hepatocyte growth factor/Met via the phosphatidylinositol 3-kinase/Akt and mitogen-activated protein kinase pathways. *Proc. Natl. Acad. Sci. U. S. A.* **98**, 247-252 (2001).
49. Birchmeier, C. & Gherardi, E. Developmental roles of HGF/SF and its receptor, the c-Met tyrosine kinase. *Trends Cell Biol.* **8**, 404-410 (1998).
50. Chmielowiec, J. *et al*. c-Met is essential for wound healing in the skin. *J. Cell Biol.* **177**, 151-162 (2007).
51. Birchmeier, C., Birchmeier, W., Gherardi, E. & Vande Woude, G. F. Met, metastasis, motility and more. *Nat. Rev. Mol. Cell Biol.* **4**, 915-925 (2003).
52. Corso, S., Comoglio, P. M. & Giordano, S. Cancer therapy: can the challenge be MET? *Trends Mol. Med.* **11**, 284-292 (2005).
53. Mitra, A. K. *et al*. Ligand-independent activation of c-Met by fibronectin and alpha(5) beta(1)-integrin regulates ovarian cancer invasion and metastasis. *Oncogene* **30**, 1566-1576 (2011).
54. Nakamura, Y. *et al*. Constitutive activation of c-Met is correlated with c-Met overexpression and dependent on cell-matrix adhesion in lung adenocarcinoma cell lines. *Cancer. Sci.* **99**, 14-22 (2008).
55. Liu, X., Newton, R. C. & Scherle, P. A. Developing c-MET pathway inhibitors for cancer therapy: progress and challenges. *Trends Mol. Med.* (2009).
56. Knudsen, B. S. & Vande Woude, G. Showering c-MET-dependent cancers with drugs. *Curr. Opin. Genet. Dev.* **18**, 87-96 (2008).
57. Conner, S. D. & Schmid, S. L. Regulated portals of entry into the cell. *Nature* **422**, 37-44 (2003).
58. Doherty, G. J. & McMahon, H. T. Mechanisms of endocytosis. *Annu. Rev. Biochem.* **78**, 857-902 (2009).
59. Sorkin, A. & Goh, L. K. Endocytosis and intracellular trafficking of ErbBs. *Exp. Cell Res.* **314**, 3093-3106 (2008).
60. Wang, Q., Zhu, F. & Wang, Z. Identification of EGF receptor C-terminal sequences 1005-1017 and di-leucine motif 1010LL1011 as essential in EGF receptor endocytosis. *Exp. Cell Res.* **313**, 3349-3363 (2007).
61. Huang, F., Goh, L. K. & Sorkin, A. EGF receptor ubiquitination is not necessary for its internalization. *Proc. Natl. Acad. Sci. U. S. A.* **104**, 16904-16909 (2007).
62. Goh, L. K., Huang, F., Kim, W., Gygi, S. & Sorkin, A. Multiple mechanisms collectively regulate clathrin-mediated endocytosis of the epidermal growth factor receptor. *J. Cell Biol.* **189**, 871-883 (2010).
63. Clayton, A. H. *et al*. Ligand-induced dimer-tetramer transition during the activation of the cell surface epidermal growth factor receptor-A multidimensional microscopy analysis. *J. Biol. Chem.* **280**, 30392-30399 (2005).
64. Clayton, A. H., Tavarnesi, M. L. & Johns, T. G. Unligated epidermal growth factor receptor forms higher order oligomers within microclusters on A431 cells that are sensitive to tyrosine kinase inhibitor binding. *Biochemistry* **46**, 4589-4597 (2007).
65. Clayton, A. H., Orchard, S. G., Nice, E. C., Posner, R. G. & Burgess, A. W. Predominance of activated EGFR higher-order oligomers on the cell surface. *Growth Factors* **26**, 316-324 (2008).
66. Saffarian, S., Li, Y., Elson, E. L. & Pike, L. J. Oligomerization of the EGF receptor investigated by live cell fluorescence intensity distribution analysis. *Biophys. J.* **93**, 1021-1031 (2007).
67. Hofman, E. G. *et al*. Ligand-induced EGF receptor oligomerization is kinase-dependent and enhances internalization. *J. Biol. Chem.* **285**, 39481-39489 (2010).
68. Wang, Q., Villeneuve, G. & Wang, Z. Control of epidermal growth factor receptor endocytosis by receptor dimerization, rather

than receptor kinase activation. *EMBO Rep.* **6**, 942-948 (2005).
69. Friedman, L. M. *et al*. Synergistic down-regulation of receptor tyrosine kinases by combinations of mAbs: implications for cancer immunotherapy. *Proc. Natl. Acad. Sci. U. S. A.* **102**, 1915-1920 (2005).
70. Spangler, J. B. *et al*. Combination antibody treatment down-regulates epidermal growth factor receptor by inhibiting endosomal recycling. *Proc. Natl. Acad. Sci. U. S. A.* **107**, 13252-13257 (2010).
71. Sorkin, A. & Goh, L. K. Endocytosis and intracellular trafficking of ErbBs. *Exp. Cell Res.* **315**, 683-696 (2009).
72. Wiley, H. S. Anomalous binding of epidermal growth factor to A431 cells is due to the effect of high receptor densities and a saturable endocytic system. *J. Cell Biol.* **107**, 801-810 (1988).
73. Grant, B. D. & Donaldson, J. G. Pathways and mechanisms of endocytic recycling. *Nat. Rev. Mol. Cell Biol.* **10**, 597-608 (2009).
74. Spangler, J. B., Manzari, M. T., Rosalia, E. K., Chen, T. F. & Wittrup, K. D. Triepitopic antibody fusions inhibit cetuximab-resistant BRAF and KRAS mutant tumors via EGFR signal repression. *J. Mol. Biol.* **422**, 532-544 (2012).

Chapter 2

Targeting tumors with nanobodies for cancer therapy

Sabrina Oliveira[1,2], Raimond Heukers[1], Jirawas Sornkom[1], Robbert J. Kok[3], and Paul M. P. van Bergen en Henegouwen[1]

[1] Cell Biology, Department of Biology, Utrecht University, Utrecht, The Netherlands
[2] Department of Pathology, University Medical Center Utrecht, Utrecht, The Netherlands
[3] Department of Pharmaceutics, Utrecht Institute for Pharmaceutical Sciences, Faculty of Science, Utrecht University, Utrecht, The Netherlands

Based on J Control Release. 2013 Sep 11;172(3):607-617.

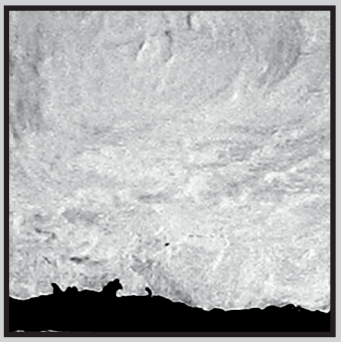

Abstract

The use of monoclonal antibodies has revolutionized both cancer therapy and cancer imaging. Antibodies have been used to directly inhibit tumor cell proliferation and to kill tumor cells via Fc-domain-mediated effector funtions or to target drugs to tumors. Also in molecular imaging, monoclonal antibodies have found their way to the clinic. Nevertheless, distribution within tumors is hampered by their size, leading to insufficient efficacy of cancer treatment and irregular imaging. An attractive alternative for monoclonal antibodies are nanobodies or VHHs. These are the variable domain of heavy-chain antibodies from animals from the *camelidae* family that were first discovered in 1993. Stimulated by the ease of nanobody selection, production, and low immunogenicity potential, a number of nanobodies specific to different disease-related targets have been developed. For cancer therapy, nanobodies have been employed as antagonistic drugs, and more recently, as targeting moieties of effector-domains and of drug delivery systems. In parallel, nanobodies have also been employed for molecular imaging with modalities such as nuclear and optical imaging. In this review, we discuss recent developments in the application of nanobodies as targeting moieties in cancer therapy and cancer imaging. With such a wide range of successful applications, nanobodies have become much more than simple antagonists.

2.1. Introduction

The use of monoclonal antibodies (mAbs) for cancer therapy has been established extensively for over 15 years, with a number of impressive successes both for haematological malignancies and solid tumors treatments [1]. So far, there are 23 mAbs approved by the US Food and Drug Administration (FDA) on the market. Among these include some cancer specific ones like rituximab (anti-CD20), trastuzumab (directed to HER2), bevacizumab (anti-VEGF), alemtuzumab (anti-CD52), cetuximab, panitumumab, and matuzumab (all targeted to EGFR) [2, 3]. These mAbs interfere with the functioning of their target proteins in cancer, either by binding to transmembrane receptors or – in the case of bevacizumab – to the soluble ligand, thereby inhibiting tumor cell proliferation or tumor angiogenesis. As they all possess an intact fragment crystallizable domain, i.e. Fc domain, they can interact with human complement or effector cells of the immune system, which also contributes to their therapeutic efficacy. mAbs have also found their way to the clinic for molecular imaging. In this case, mAbs are used to target radioactive or fluorescent tracers to the tumor, for either PET/SPECT or optical imaging, respectively [4-6]. Lastly, mAbs are used in a variety of targeted nanomedicines, aiming at tumor cell directed delivery of a cytotoxic payload [7]. It is however fair to state that the application of mAbs in both cancer therapy and imaging needs further improvements. mAbs have a molecular weight of ~150 kDa and dimensions of 14.2 nm × 8.5 nm × 3.8 nm [8], which together with the 'binding site barrier' [9] limit the distribution and penetration of the antibodies into the tumor. mAbs typically have several days-weeks of half-life in the bloodstream, which for molecular imaging results in high background levels. Moreover, an important concern of the application of mAbs is their potential to induce immunogenic responses. To avoid unwanted immune responses in patients, mAbs are either completely humanized or produced as a chimeric protein. Altogether, these aspects have urged pharmaceutical companies and scientists to find new antibody formats that provide the same binding specificity of mAbs, but with some of the desired improvements.

As many of the mentioned drawbacks of mAbs are related to their size, large efforts have been made towards the development of smaller antibody formats [10, 11]. Naturally derived or synthetic antigen-binding fragment (Fab; ~50 kDa), variable fragment (Fv; ~15 kDa) and single-chain variable fragment (scFv; ~30 kDa) were vastly tested and engineered to overcome the restrictions of the full-length mAbs (Fig. 1) [10, 12]. Nevertheless, their average activities are still suboptimal due to lower affinities and limited stability, which is especially the case of scFv [13]. Apart from those mentioned above, the minibody - an engineered antibody fragment made by genetically fusing scFv binding domain to human CH3 - was introduced as another candidate for cancer immunotherapy [14]. Furthermore, synthetic molecules or scaffold proteins, such as affibodies and DARPins (designed ankyrin repeat proteins) have been developed, with important successes [15-17]. However, no report has addressed their potential to induce immunological

responses and their added value, compared to the other platforms, still needs to be determined.

By serendipity, a special type of antibody was discovered in animals from the *Camelidae* family by Hamers-Casterman and co-workers in 1993 [18]. These so-called heavy-chain antibodies (HcAbs, ~95 kDa) are fully functional and, despite the absence of light chain and of the first constant domain (CH1), they bind their antigens with similar affinities to those of conventional antibodies [19]. Apart from *Camelidae*, some primitive fish species were also found to produce different types of HcAbs, such as nurse shark and ratfish [20, 21]. Interestingly, the variable domain alone of HcAbs (i.e. VHH) was proven to have sufficient antigen binding properties and, as such, can be considered as the smallest naturally derived antigen-binding fragment with the approximate molecular weight of 15 kDa [22, 23]. The term 'nanobodies' was employed with respect to their size in nanometer range by the Belgian company Ablynx®, and particularly refers to the VHH from camelid species [23-25]. Another term used for nanobodies is single domain antibody (sdAb) [26].

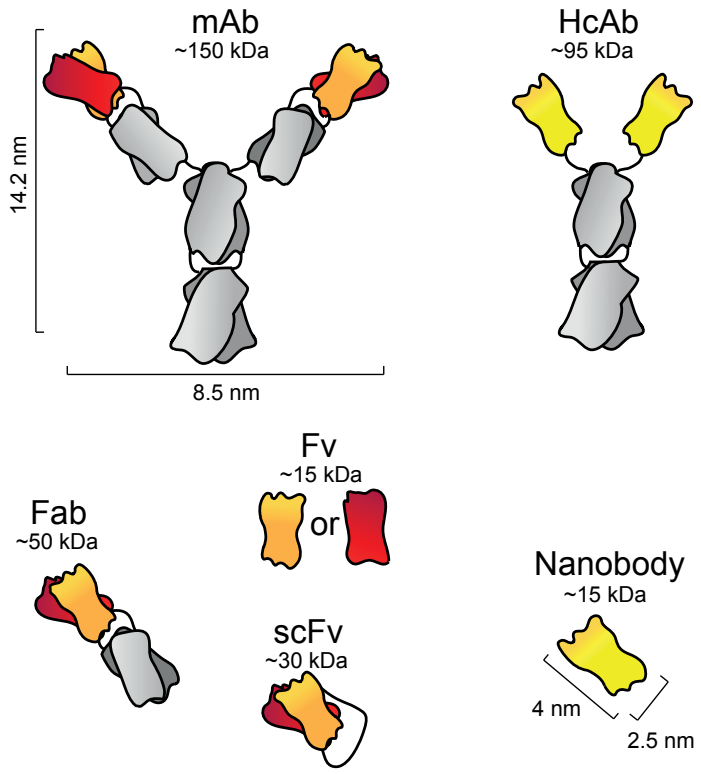

Figure 1. *Antibodies and their fragments. Schematic representation and corresponding molecular weight of (left) a monoclonal antibody, mAb, and its fragments, i.e., Fab', Fv, scFv; and of (right) a heavy chain only antibody, HcAb, together with its antigen-binding fragment, i.e. nanobody or VHH.*

2.2. Nanobodies: structure and characteristics

In 1994, the first detailed sequence of nanobody encoding genes was published by Muyldermans and co-workers, providing more molecular insights regarding their interaction and binding interface [22][1]. The nanobody sequences were shown to have a high degree of identity with the human type 3 VH domain (VH3), which most likely accounts for the low immunogenic potential of nanobodies, as demonstrated in mice [27]. In addition, humanization of nanobodies has been performed before these were transferred into the clinic (Ablynx) [25, 28, 29], further minimizing their immunological potential. In this line, Vincke and colleagues have presented the humanization of dromedary-derived nanobodies resulting in an universal humanized nanobody scaffold [30]. A number of distinctive amino acid substitutions are specifically found in framework 2. In conventional antibodies, this region serves as a part of the hydrophobic VL interface and, consequently, substitutions that have occurred in HcAbs are thought to be the main reason for the high hydrophilicity, stability and higher solubility of VHHs as compared to conventional VH domains, including scFvs. Another interesting difference between VHH and human VH domain is the length of CDRs, which contributes to an increase of the antigen-interacting surface [25, 31]. A longer CDR3 in nanobodies allows it to form a fingerlike structure able to extend into cavities on target proteins, which causes nanobodies to bind to unique epitopes [32, 33]. In contrast, the binding interfaces of Fabs' and other mAbs' derived fragments are more flat and less flexible, limiting the interactions of mAbs and antibody fragments solely to the surface of antigens [34]. Recently, we have determined the crystal structure of an anti-EGFR nanobody (7D12) in complex with the EGFR ectodomain [33]. This nanobody binds directly to domain III thereby sterically blocking EGF-binding. Interestingly, the 7D12 paratope that is binding to EGFR consists of CDR1 and 3, and the CDR2 makes no contact with EGFR (Fig. 2). Moreover, nanobodies have a high refolding capacity even after being exposed to extreme conditions, such as very low/high pH and temperature [35, 36]. It was reported that nanobodies could refold and bind to their targets even after a long incubation period at 80-92^{o}C [37]. This is mainly due to the fact that nanobodies do not aggregate during denaturation and they usually possess only one disulfide bridge. Therefore, nanobodies can easily refold back to their native conformation when the temperature is lowered. Furthermore, because of the modular and single domain characteristic of nanobodies, molecular manipulations for generating multivalent or multispecific single-chain antibodies are relatively easy (Fig. 3). Last, but certainly not less important, while the production of recombinant conventional mAbs is often hampered by aggregation and reduced affinity from mispairing of the VH and VL domains, production of multivalent nanobodies is straightforward and the little post-translational modifications allows the production in bacteria or yeast. With all the characteristics mentioned, nanobodies are very promising building blocks to function as novel antibody molecules for a wide variety of applications [24, 26, 38, 39].

While providing many advantages as mentioned above, the small size of nanobodies could also be a disadvantage. For instance, for conjugation to other molecules (e.g. fluorophores), random chemistry could affect their binding properties more than observed with conventional antibodies. Direct conjugation to a C-terminal cysteine has for instance been used to circumvent this problem [40, 41]. Also, as a result of their preference for conformational epitopes, nanobodies do not always recognize denatured proteins and their application in Western blotting is not always successful. Their small size is also a disadvantage in cancer therapy, as they are rapidly cleared from the bloodstream through kidney glomerular filtration. It was reported by both Huang et al and Gainkam et al that the half-life of a radiolabelled nanobody targeting the epidermal growth factor receptor (EGFR) (^{99m}Tc-8B6) was less than 1.5 hours in the bloodstream of mice [42, 43]. Thus, in terms of therapy, only a small fraction of the total nanobody injected accumulates at the target site, which should be compensated by frequent and high doses regimens. Importantly, a strategy has been employed to prolong nanobodies' half-lives, described by Coppieters et al. [44a] and Tijink et al [44b], who fused a bivalent anti-EGFR nanobody to a nanobody binding to human and mouse serum albumin (α-EGFR-αEGFR-αAlb, Fig. 3) [44a-46]. The half-life of this α-EGFR-αEGFR-αAlb nanobody was prolonged to approximately 2-3 days in mice, which is similar to the half-life of cetuximab, a mAb specific for EGFR [44]. As human serum albumin was shown to have a blood half-life of ~19 days [44, 47, 48], prolongation of half-life of α-EGFR-αEGFR-αAlb can be expected in humans, but remains to be shown. Finally, a disadvantage is nevertheless the absence of an effector domain in nanobodies, which reduces the efficacy of nanobodies in cancer therapy. In conventional antibodies, the Fc domain can trigger

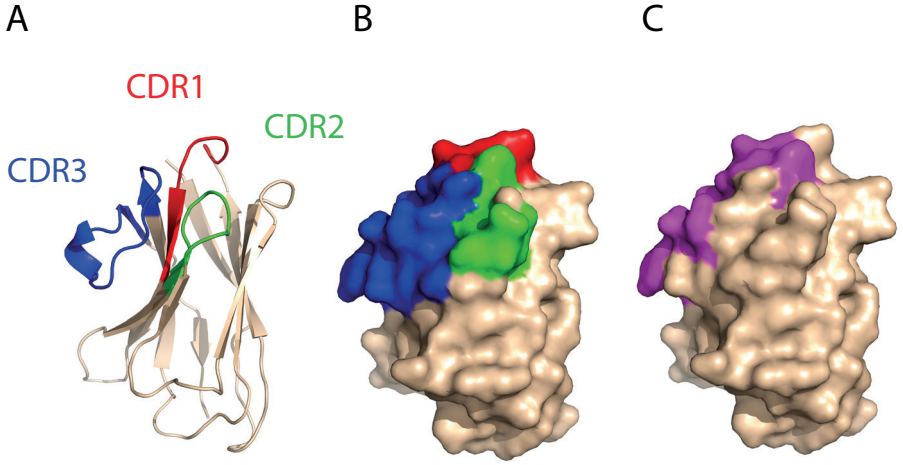

Figure 2. *Crystal structure of anti-EGFR nanobody. A. Cartoon of 7D12 with CDR1, 2 and 3 highlighted in red, green and blue respectively. B. Molecular surface of 7D12 with CDR1,2 and 3 highlighted in red, green and blue respectively. C. View of the paratope of 7D12 binding to EGFR; note that CDR2 (green) does not contribute to the binding to EGFR.*

antibody-dependent cellular cytotoxicity (ADCC) an, antibody-dependent cellular phagocytosis (ADCP) and complement-dependent cytotoxicity (CDC) upon antigen binding [13, 46]. These three mechanisms are known to be important in the process of tumor eradication, as they both contribute to cell lysis activation, and hence apoptosis cascades [49]. For this reason, nanobodies have been fused to a Fc domain, but in this way, the advantage of their small size will be lost [50, 51]. In the next sections of this review, innovative applications for nanobodies will be described, demonstrating the potential and versatility of the nanobodies to be used in different strategies, seeking for the most effective cancer treatment.

2.3. Nanobody applications in cancer immunotherapy

The molecular biology of nanobodies has recently been described in an excellent review by Muyldermans [25]. In the following sections we will describe the use of nanobodies in different platforms for cancer therapy: 1. as antagonistic drugs, 2. as targeting agents of effector domains, and 3. as targeting moieties on the surface of drug delivery systems (Table 1). Each section will refer to the state of the art and possible new developments.

2.3.1. Nanobody antagonists as cancer therapeutic agents

An important strength of the nanobody technology is the versatility of the system that enables the production of a wide variety of nanobodies that bind specifically to the different targets. The most common approach is to first immunize animals from the *Camelidae* family with the protein of interest or cells expressing this protein, resulting in the generation of a large variety of HcAbs. Subsequently, from the collected peripheral blood lymphocytes, a library is constructed enabling the selection of nanobodies through phage display technology [45]. By rationally designed selection approaches, this technology enables the selection of nanobodies with specific characteristics that, for instance, antagonistically block growth factor receptor signaling and, as a result, can inhibit tumor growth. There are two possible strategies: selecting for nanobodies that block the ligand or selecting antagonists of the receptor. It is important to bear in mind that the anti-ligand nanobodies can only be efficiently used when a single ligand is involved in the signaling of the corresponding receptor. For instance, while EGFR can be activated by different ligands, the hepatocyte growth factor (HGF) is the only known ligand for the HGF receptor, i.e. c-Met [52]. Therefore, it is for EGFR inhibition more logical and effective to use an anti-EGFR strategy, rather than the anti-EGF strategy. On the other hand, anti-HGF nanobodies which neutralize the soluble ligand can be successful in case of c-Met inhibition. In the following sections, a number of successful examples of tumor ligand and receptors will be described, together with their corresponding nanobodies.

2.3.1.1. Hepatocyte growth factor (HGF, hepapoietin A; scatter factor)

HGF is a plasminogen-like protein that is secreted by mesenchymal cells as a single inactive peptide and then cleaved by a serine protease into a 69-kDa alpha-chain and 34-kDa beta-chain [53]. HGF has a function in the regulation of cell proliferation, motility and morphogenesis through its interaction with the c-Met receptor. Binding of HGF to c-Met results in the activation of its tyrosine kinase and subsequent signaling cascade [53]. In tumor cells where HGF and c-Met are overexpressed, the enhanced signaling can trigger tumorogenesis and angiogenesis, and prevent apoptosis, which all contribute to the outgrowth of tumors [54]. Several anti-HGF mAbs have been developed, e.g., rilotumumab (AMG102; Amgen) [55] and TAK-701 (Millennium) [56]. Moreover, in 2012, two anti-HGF nanobodies, i.e., 1E2-Alb8 and 6E10-Alb8 were described by Vosjan and co-workers [57]. These nanobodies, which contained the anti-albumin nanobody subunit for prolonged half-life, also presenting a half-life of approximately 2 days, were administered to nude mice with glioblastoma xenografts. The nanobodies specifically accumulated at the tumors, leading to a remarkable inhibition of tumor outgrowth. In fact, after treatment and withdrawal periods, tumors were fully eradicated in four out of six mice by 1E2-Alb8 and in three out of six mice by 6E10-Alb8 [57].

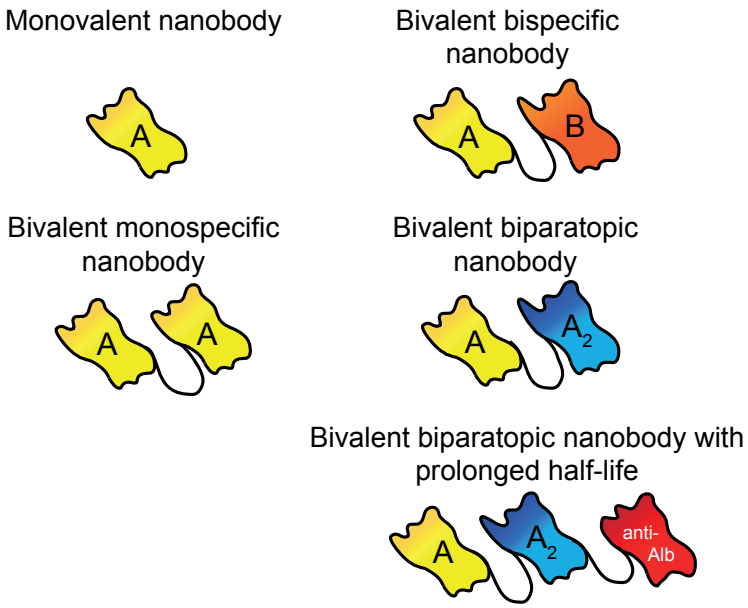

Figure 3. *Schematic illustrations of multivalent nanobodies. Besides the monovalent format (A), nanobodies can be produced in a bivalent format, either monospecific (A-A), bispecific (A-B) when binding to two different targets, or biparatopic (A-A2) when binding to two different epitopes of the same target protein. The bivalency creates avidity which can result in higher affinity towards the antigen. Furthermore, the addition of a third nanobody that binds to serum albumin (anti-Alb) has been employed as a strategy to prolong half-life in the bloodstream.*

2.3.1.2. Vascular endothelial growth factor receptor-2 (VEGFR2)

VEGFR2 is a well studied receptor from the family of human VEGF-receptors 1-3 [58]. During embryogenesis and angiogenesis, VEGFR2 is highly expressed, contributing to the development of new blood-vessels. These receptors have strong tyrosine kinase activity that in turn regulates proliferation and apoptosis via the binding of vascular endothelial growth factor (VEGF) [59]. In tumors, VEGFR2 plays an essential role in inducing tumor angiogenesis and outgrowth. In fact, VEGFR2 and its family members are often found to be overexpressed and dysregulated in many types of cancers, e.g., lung, colon and breast cancers [60]. An anti-VEGFR2 mAb, ramucirumab (IMC-1121B; ImClone Systems) [61], is currently being evaluated in phase III clinical trials, for treatment of breast and gastric cancers. Recently, the first report on VEGFR2-specific nanobodies was published by Behdani et al [62]. The authors raised HcAbs against VEGFR2 in *Camelus dromedaries* and performed several screening assays to select specific nanobodies against VEGFR2. The selected nanobody 3VGR19 binds the receptor with high affinity (Kd = 5.4 nM) and it efficiently inhibited capillary tube formation *in vitro*. Further characterization and *in vivo* assays are eagerly awaited to provide more insights on their potential in cancer therapy, and their efficacy in relation to clinically available anti-angiogenic antibodies.

2.3.1.3. Epidermal growth factor receptor (EGFR or ErbB1)

EGFR belongs to a family of receptor tyrosine kinases (RTKs). EGFR activation can be triggered by a number of extracellular ligands, resulting in diverse intracellular signaling cascades. Besides a moderate expression in many human tissues, such as skin and liver, this receptor is typically overexpressed and dysregulated in a number of epithelial tumors, namely, brain, head and neck, breast and colon tumors [63, 64]. Several EGFR-specific mAbs have been developed with great success, for example, cetuximab (Erbitux) and panitumumab (Vectibix) [65-67]. Anti-EGFR mAbs have shown very impressive results at the preclinical level. However, in the clinic, results have not always corresponded to the expectations [68, 69], which is only partly due to difficulties in assessing EGFR expressions status in patients [70, 71]. This has stimulated further research, seeking for more potent anti-EGFR therapies and also combined therapies. In 2007, Roovers et al have reported, for the first time, the use of functional phage display antibodies selection, together with competitive elution, to develop antagonistic anti-EGFR nanobodies [45]. Importantly, these mono- and bivalent nanobodies were clearly competing with EGF, being the bivalent nanobodies more effective due to the created avidity. *In vitro*, these nanobodies efficiently inhibited EGF-induced signaling and cell proliferation. Furthermore, the albumin-binding subunit allowing longer circulation in the bloodstream was employed for *in vivo* studies, which clearly showed inhibition of outgrowth of A431 subcutaneous human tumor xenografts [45]. In 2011, we introduced a novel format of anti-EGFR nanobodies, i.e. biparatopic nanobodies consisting of

two different nanobodies binding to EGFR, on different epitopes. For *in vivo* studies, the third nanobody unit binding to albumin for prolonged half-life was also included and these were indicated as CONAN-1, from cooperating nanobodies [46]. The anti-EGFR sub-units specifically bound to the domain III of EGFR, blocking the interaction of anti-EGFR mAbs matuzumab or cetuximab to the receptor. CONAN-1 was able to efficiently inhibit EGF-dependent cell proliferation *in vitro,* as well as tumor outgrowth in mice bearing A431 tumor xenografts, with a half-life of approximately 2 days [46]. Although the potency of CONAN-1 in tumor inhibition is beyond the bivalent monospecific nanobodies, it could not outperform the clinically approved mAb cetuximab. One explanation for this is the lack of Fc domain that can trigger ADCC and CDC upon antigen binding [13, 46]. A possibility to overcome the limitation mentioned above is to introduce an artificial conjugation of Fc-tail to nanobodies [50, 51], like other researchers have done to different molecules [72, 73]. In principle, Fc-linked nanbodies could trigger ADCC, ADCP and CDC, resulting in a stronger activity of the nanobody construct. Nevertheless, the Fc-tail conjugation may be a mixed blessing, as it would increase the size of the nanobody and could also lead to non-targeted interaction of the conjugate, for example, to the macrophages, resulting in the accumulation of the construct in liver and spleen [74]. Therefore, a tradeoff between the activity and adverse effects needs to be carefully determined, before one can generalize on the improvements achieved through this modification.

2.3.2. Nanobodies as targeting moieties of effector domains

Another possibility to further increase the therapeutic efficacy of nanobodies would be to use nanobodies as a mean to specifically deliver a certain effector domain (e.g. enzyme or toxin) to or into the target cell. This could be achieved by chemical conjugation of the two units, i.e., nanobody and effector domain or, at an earlier stage, through cloning in order to make a construct that will be produced as a single protein. When produced as a single protein, chances exist that the protein will not be correctly folded, while when chemical conjugation is performed at random, the binding properties of the nanobody could be affected when the conjugation involves amino acids that are for instance present in the CDRs of the nanobody. The already mentioned site-directed conjugation to a C-terminal cysteine would control where the effector domain binds to the nanobody, minimizing the chances of interfering with nanobody's binding properties [40, 41]. In either case, the binding properties of the nanobody conjugated to an effector domain have to be confirmed and the conjugate can only be used when these have not been compromised. Furthermore, in this strategy, the nanobody should assure specific targeting, accumulation, and retention of the conjugate at the tumor (possibly through internalization of the conjugates). Ideally, the effector domain would be very potent, leading to cell death and complete tumor regression, rather than only inhibiting tumor cell proliferation. Also, at the same time, the conjugates would

be safe to normal tissues and only be toxic at the targeted regions (i.e. cancer cells).

The activity of anti-carcinoembrogenic antigen (CEA) nanobodies conjugated with *Enterobacter cloacae* β-lactamase that can efficiently convert non-toxic pro-drugs into cytotoxic compounds was demonstrated by Cortez-Retamozoet al. in 2004 [75]. *In vitro* experiments showed specific distribution of the conjugates at the surface of LS174T cancer cells expressing CEA and *in vivo* studies demonstrated tumor regressions, which led to complete cure of mice bearing xenografts. Although β-lactamase is not a direct effector domain in these studies, the results suggested that *in situ* activation of cytotoxic compounds is indeed possible and highly effective.

Table 1. *Nanobodies in cancer therapy*

Function and target	Combined with	Refs.
1. Antagonistic drugs		
Hepatocyte growth factor (HGF)	-	[57]
Vascular endothelial growth factor receptor-2 (VEGFR2)	-	[62]
Epidermal growth factor receptor (EGFR)	-	[45, 46]
2. Targeting of effector domains		
Carcinoembrogenic antigen (CEA)	*Enterobacter cloacae* β-lactamase	[75]
Vascular endothelial growth factor receptor-2 (VEGFR2)	Pseudomonas exotoxin A	[76]
DNMT1/SHH	Vinorelbine	[77]
Epidermal growth factor receptor (EGFR)	TRAIL	[78]
3. Targeting moiety on drug delivery systems		
Epidermal growth factor receptor (EGFR)	Liposome + AG538	[87, 88, 90]
Epidermal growth factor receptor (EGFR)	Micelles + Doxorubicin	[92-94]
Epidermal growth factor receptor (EGFR)	Albumin nanoparticles + 17864	[97]

Recently, a new conjugate was described consisting of the anti-VEGFR2 nanobody linked to the Pseudomonas exotoxin A (PE38) [76]. The anti-VEGFR2-PE38 conjugate could efficiently bind to the VEGFR2 expressed on the surface of 293KDR cells, resulting in growth inhibition *in vitro*. Although evaluation of this conjugate *in vivo* has not been published yet, especially regarding the toxicity of such conjugate towards the host, the anti-VEGFR2-PE38 conjugate has shown to be a good example of using nanobodies as targeting moieties for cytotoxic effectors.

Nanobodies linked to antineoplastic drugs are an alternative type of conjugates which could be very important in targeted cancer therapy. A bispecific nanobody, targeting DNMT1/SHH, conjugated to the anti-mitotic drug, vinorelbine, has been described as a new therapy for resistant hormone refractory prostate cancer (HRPC) [77]. The results described so far are very promising, though the detailed publication of these data and of further studies regarding the use (and safety) of this anti-DNMT1/SHH-vinorelbine conjugate will further determine the value of this approach.

Recently, we have developed a novel application of anti-EGFR nanobodies for glioblastoma multiform (GBM) therapy [78]. In these experiments, bivalent anti-EGFR nanobodies and their conjugates with tumor necrosis factor-related apoptosis-inducing ligand (nanobody-TRAIL) were produced and secreted by neural stem cells (NSCs). The secreted constructs were shown to have high specificity and sufficient tumor uptake level in GBM both *in vitro* and in *in vivo* experiments. With the advantage of the NSCs that could provide on-site and sustained release of the effective nanobodies, profound effects on the GBM were observed. In these experiments, direct comparison between the activity of the bivalent anti-EGFR nanobody and the activity of the nanobody-TRAIL conjugate have demonstrated that the combination of different therapeutic approaches can lead to novel and more potent cancer therapy.

Altogether, these conjugates would combine the advantages of high specificity of the nanobodies, their intrinsic therapeutic effect as antagonists, and high level of tissue penetration, while providing sufficient tumor destruction properties by the effector domain. Based on the promising results described above, it is tempting to think of many other types of conjugates. Likely, a number of new nanobody-conjugates will be developed in the coming years. In due time, one will know the real feasibility for translation into the clinic and the real potency of the nanobody-conjugates for cancer therapy.

2.3.3. Nanobodies as targeting moieties on drug delivery systems

Instead of linking the targeting molecule (i.e. nanobodies) directly to the effector domain, as discussed above, the therapeutic molecules can also be incorporated in a drug delivery system and be used as a targeting moiety chemically attached to their surface. Drug delivery systems, i.e.

nano-sized drug carriers or nanoparticles with diameter <200 nm, have been widely employed in pharmaceutical sciences in an attempt to: a) protect normal tissues from systemically administered toxic compounds, b) solubilize hydrophobic drugs in lipidic bilayers (e.g. liposomes) or hydrophobic cores (micelles), and/or c) administer large amounts of drugs in one dose, resulting in less administration frequency and reduced chance of immunogenicity [79].

The conjugation of targeting moieties to the surface of drug delivery systems or nanoparticles has gained remarkable attention, as means to improve the specificity of nanoparticles towards tumor cells, in particular via receptor-mediated internalization [7, 80-82]. The majority of drug delivery systems described in literature consists of pegylated (PEG) or surface-charge-shielded nanoparticles (employed to extended blood half-life [83, 84]) that accumulate at the tumor site through the enhanced permeability and retention effect (EPR) [85]. The abnormal structure of rapidly growing tumor vasculature, combined with the lack of proper lymphatic drainage, lead to the accumulation of nanoparticles, provided that they circulate long enough in the bloodstream [86]. Therefore, after extravasation of nanoparticles from the bloodstream into the tumor micro-environment, targeting moieties mediate cell-specific interactions. Nanobodies have also been used for that purpose and the following sections will describe these developments.

2.3.3.1. Nanobody-liposomes

In 2010, we introduced a novel multivalent nanobody-liposome platform to target liposomes specifically to tumor cells overexpressing EGFR [87]. Nanobodies recognizing the ectodomain of EGFR (EGa1) were conjugated to the surface of liposomes via maleimide-PEG-DSPE, which was incorporated during liposome formation. As expected, the EGa1-liposomes associated in a greater extent with A431 human tumor cells overexpressing EGFR, compared to liposomes devoid of nanobody. After binding of EGa1-liposomes to tumor cells via EGFR, receptor-mediated internalization led to a pronounced reduction of EGFR at the cell membrane. This was then followed by degradation of the receptor, i.e. receptor downregulation, and this could significantly inhibit the proliferation of tumor cells *in vitro*. *In vivo*, however, the observed downregulation of EGFR was not sufficient to induce tumor regression. Nevertheless, this study was performed with empty liposomes, i.e. without a drug, thus improvements were still possible. Interestingly, the ability of nanobody-liposomes to induce EGFR downregulation was exclusive to this multivalent format, as other systems, such as, scFv-liposomes or the monovalent nanobody EGa1 could not lead to similar effects [87]. The reason behind this finding still needs to be clarified, but at this point in time we speculate that the decrease of pH upon internalization and consequent acidification of endosomes and lysosomes, does not affect the binding of nanobodies. Nanobodies remain attached to the receptor and, subsequently, not allowing EGFR to be recycled to the cell membrane, but rather directing the multivalent complex to lysosomes for degradation.

In 2012, an improvement to this EGa-1-liposome was introduced by loading the inner compartment of the liposomes with an anti-IGF-1R kinase inhibitor (AG538) [88]. Previous studies have shown close relationship and crosstalk between EGFR and IGF-1R, where these receptors interact with each other on multiple levels, for example, by direct interaction between two receptors, controlling the availability of each others' ligands and through indirect interaction partners, e.g., G protein coupled receptors (GPCR) or other downstream molecules [89]. For these reasons, the new EGa1-AG538-liposome were developed and these had three modes of actions, i.e., inhibition of EGFR and of IGF-1R signaling, and the downregulation of EGFR, as previously described for the EGa1-liposomes [87]. Compared to the empty EGa1-liposomes, the EGa1-AG538-liposome showed stronger inhibition of growth of 14C human head and neck cancer cell line *in vitro* [88]. The report on the *in vivo* evaluation of this combined therapy became available very recently, suggesting that the degree of inhibition induced by EGa1-AG538-liposome on the molecular and cellular level is predictive of the response of tumor xenograft to this combined therapy [90].

Overall, these results encourage new studies with different combinations of tumor-targeting nanobody and liposomes. For instance, it would be of great value to compare nanobody-targeted liposomes containing doxorubicin to the Fab-targeted liposomes loaded with doxorubicin that are currently in clinical trials [91]. Because the concept of nanobody-targeted liposomes is still in its infancy, further studies will give more insights on the efficacy and safety of this nanomedicine format.

2.3.3.2. Nanobody-micelles

The hydrophobic core of polymeric micelles originating from amphiphilic co-polymers is suitable for a variety of hydrophobic drugs, which are otherwise difficult to be delivered through the bloodstream [80].

In 2011, a new nanobody-micelle platform for drug delivery in cancer therapy was introduced. Micelles were made from poly(ethylene glycol)-*b*-poly[N-(2-hydroxypropyl) methacrylamidelactate] (mPEG-*b*-p(HPMAm-Lac_n) block polymers and the EGFR targeting nanobody EGa1 was conjugated to a fraction of the polymer chains at the end of the hydrophilic PEG block. The results were very promising as the EGa1-decorated polymeric micelles could effectively bind to EGFR expressing cells, better than the micelles alone. Furthermore, no binding of the EGa1-polymeric micelles to EGFR negative cells was observed, nor binding to EGFR positive cells in the presence of an excess of EGa1 nanobody, emphasizing the high specificity of the nanobody-micelles [92, 93]. *In vivo*, the EGa1-micelles alone had intrinsic inhibitory properties, due to the presence of the antagonistic nanobody. Inhibition of tumor growth was significantly improved by the encapsulation of doxorubicin in these nanobody-polymeric

micelles, which were more toxic than the untargeted polymeric micelles containing doxorubicin [94]. These results highlight the potential of tumor targeted polymeric micelles and, similarly to the nanobody-liposomes, this opens a new avenue in the field of targeted drug delivery.

2.3.3.3. Nanobody-albumin nanoparticles

The idea of albumin nanoparticles as a drug delivery system was postulated in 1996 by Muller et al. [95]. Being the most abundant protein in the bloodstream, human serum albumin is highly biocompatible and therefore an appealing and safe drug carrier [96]. In 2012, we have published the successful development of novel targeted albumin nanoparticles, i.e. the nanobody-albumin nanoparticles (NANAPS) [97]. These nanoparticles were loaded with a multikinase inhibitor, i.e. 17864, coupled via a platinum based linker to ensure the stable incorporation of the drug in the albumin nanoparticle. The surface of these nanoparticles was coated with maleimidyl functionalized PEG that was linked to the anti-EGFR nanobody EGa1, to provide specificity for binding to EGFR-expressing tumor cells. These NANAPs were efficiently internalized into the 14C cancer cells via the interaction of the nanobody with EGFR. Once inside cells, the compartmentalization in the lysosomes allowed the release of the multikinase inhibitor 17864 from its linker, thereby allowing it to reach its intracellular target site for activity. Inhibition of 14C cells by the NANAPS was observed, while the non-targeted formulations did not induce any inhibition of tumor cell proliferation [97]. These results encourage further studies on the NANAPS platform as a new potent drug carrier system in EGFR-overexpressed cancer therapy.

The examples given on nanobodies conjugated to the surface of drug delivery systems were all employing random conjugation chemistry, nevertheless other conjugation strategies have been proposed. In this context, Reulen and co-workers have produced nanobodies as fusion proteins carrying an intein domain at their C-terminal end, to allow the formation of a reactive thioester for conjugation to nanoparticles via native chemical ligation [98]. Furthermore, these examples all refer to nanoparticles targeting the EGFR, but bearing in mind the possibility to develop nanobodies to any relevant tumor marker, new studies will certainly become available in which nanoparticles target other receptors, namely c-MET and IGF-1R.

2.4. Nanobody for molecular imaging of cancer

Besides therapy, nanobodies have also been developed for molecular imaging of cancer. In this area, nanobodies are particularly interesting, because: a) they are stable and very specific; b) they are able to rapidly distribute through the bloodstream, reaching tissues homogenously; c) they bind tightly to the targets on the surface of cancer cells (and to some extent they are being internalized); d) they are known to have a low immunogenic potential; and e) they are cleared rather quickly when unbound, allowing for the acquisition of images with high tumor-

to-background (T/B) contrast at early time points after their administration [39, 99]. Altogether, nanobodies fulfill the requisites of an ideal probe for successful molecular imaging. Several molecular imaging modalities have been established in the clinic, namely single-photon emission computed tomography (SPECT), positron emission tomography (PET), and, more recently, optical imaging [100, 101]. This section will describe probes based on nanobodies for molecular imaging using different modalities (Table 2).

Table 2. *Nanobodies for cancer molecular imaging*

Modality and target	Tracer	Refs.
1. Nuclear imaging		
Epidermal growth factor receptor (EGFR)	^{99m}Tecnicium	[42, 43, 102]
Epidermal growth factor receptor (EGFR)	^{68}Galium	[104, 105]
Epidermal growth factor receptor – 2 (HER2)	^{177}Lutetium	[103]
Epidermal growth factor receptor – 2 (HER2)	^{99m}Tecnicium	[106]
Epidermal growth factor receptor – 2 (HER2)	^{68}Galium	[107]
2. Ultrasound imaging		
Vascular cell adhesion protein 1 (VCAM1)	-	[108]
3. Optical imaging		
Epidermal growth factor receptor (EGFR)	IRDye800CW	[99]
Epidermal growth factor receptor – 2 (HER2)	IRDye800CW	[40]

2.5. Perspectives on the applications of nanobodies

It has been almost 20 years since the HcAbs were discovered and the nanobodies described, with over 340 published articles (April 2013, web of science). Nanobodies have been vastly selected, tested, engineered and used for various applications. From the antagonistic nanobodies and the nanobodies for targeting of effector domains or of drug delivery systems, to the use of nanobodies for molecular imaging, we have reviewed the most relevant literature in these two areas, i.e. cancer therapy and molecular imaging (Fig. 4). We believe that nanobody development

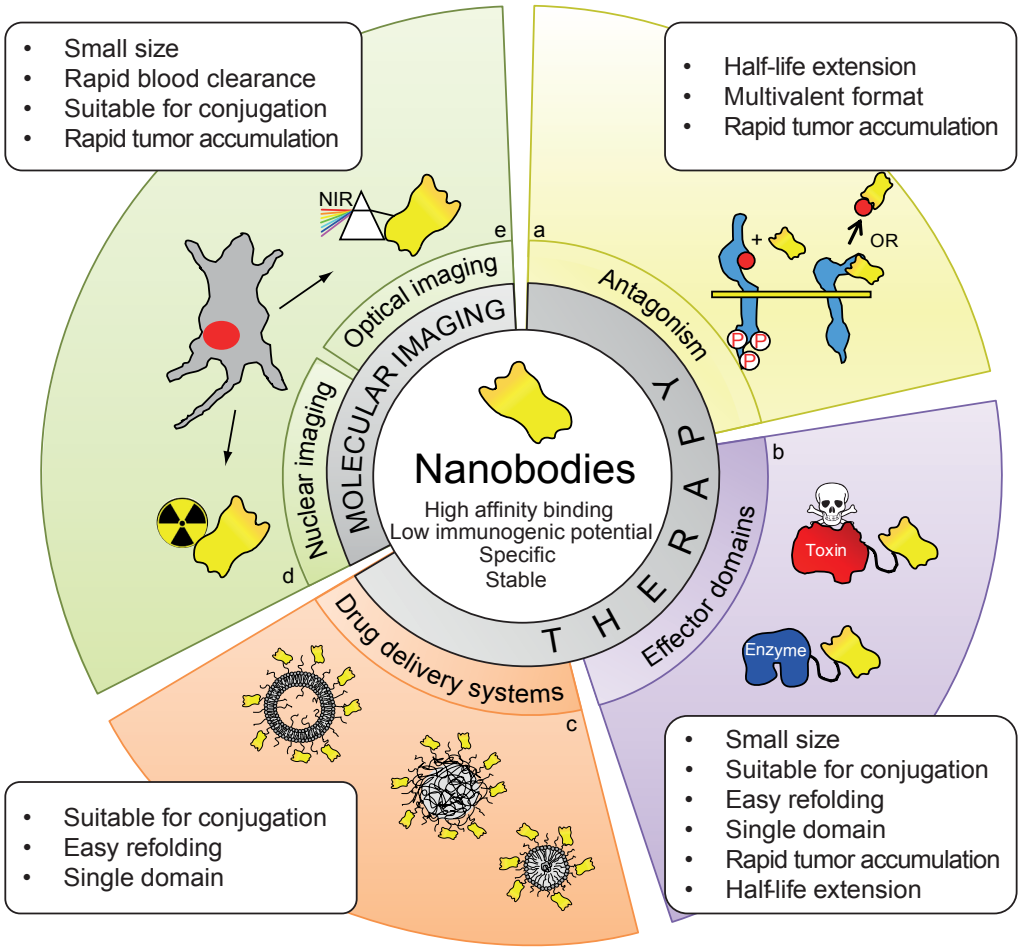

Figure 4. *Properties of nanobodies and pre-requisites for their applications. Schematic representation of the applications of nanobodies in cancer therapy: (a) preventing receptor phosphorylation/activation by competing with the ligand for binding to the receptor or by binding to the ligand; (b) targeting effector domains such as toxins or enzymes; and (c) as targeting moieties on the surface of drug delivery systems such as liposomes, polymeric micelles or albumin nanoparticles. Nanobodies have also been employed in molecular imaging of cancer, such as in (d) nuclear imaging where nanobodies are conjugated to radioligands, or in (e) optical imaging where near-infrared (NIR) fluorophores are conjugated to nanobodies. In addition, some of the pre-requisites for these applications are listed, which in fact correspond to the properties of nanobodies.*

is currently at the stage where multidisciplinarity is required in order to move forward and allow clinical translation of these novel and potent strategies that employ nanobodies for cancer therapy. Furthermore, we are convinced that newer approaches will be more focused on achieving complete eradication of cancer cells, rather than inhibition of tumor cell proliferation. In this context, the small dimensions of nanobodies are of particular interest as they can reach all cells within a tumor. In fact, the size and format of the drug or drug delivery system is very important and dictates its accumulation at the tumor [109]. Molecules that circulate long in the bloodstream have a greater chance of accumulating at the tumor, though at later time points. On the other hand, very small molecules need to have very high affinities so that they can bind to the target faster than they are cleared from the bloodstream. Nanobodies have given sufficient proof of being capable of binding tightly enough to their targets in vivo, allowing relatively high tumor uptakes [43, 99, 105]. Overall, using nanobodies as targeting moieties for effector domains seems to be the most promising avenue to reach complete tumor regression and novel studies in this context are eagerly awaited.

In this review we have described the most important advances in the field of nanobodies, going through different strategies for therapeutic applications. Nevertheless, there are various possibilities to further develop and improve the nanobody-mediated therapy. It is also important to find the right tumor markers for the highest selectivity of nanobodies. In the foreseeable future, more markers and their corresponding nanobodies will be characterized. Also, ongoing research will clarify the extent to which nanobodies will be valuable in the clinic. Yet, what should have become clear for the reader with the studies referred in this review is that nanobodies are very versatile and have become very potent tools for a variety of clinically relevant applications.

2.6. References

[1] A.M. Scott, J.D. Wolchok, L.J. Old, Antibody therapy of cancer. Nature Reviews Cancer 12(4) (2012) 278-287.

[2] A. Elbakri, P.N. Nelson, R.O. Abu-Odeh, The state of antibody therapy. Hum Immunol 71(12) (2010) 1243-1250.

[3] R.K. Oldham, R. Dillman, Monoclonal antibodies in cancer therapy: 25 years of progress. J Clin Oncol 26(11) (2008) 1774-1777.

[4] E. Mishani, A. Hagooly, Strategies for molecular imaging of epidermal growth factor receptor tyrosine kinase in cancer. J Nucl Med 50(8) (2009) 1199-1202.

[5] H. Zhao, K. Cui, A. Muschenborn, S.T.C. Wong, Progress of engineered antibody-targeted molecular imaging for solid tumors Molecular Medicine Reports 1 (2008) 131-134.

[6] T. Olafsen, A.M. Wu, Antibody vectors for imaging. Semin Nucl Med 40(3) (2010) 167-181.

[7] F. Fay, C.J. Scott, Antibody-targeted nanoparticles for cancer therapy. Immunotherapy 3(3) (2011) 381-394.

[8] V.R. Sarma, E.W. Silverton, D.R. Davies, W.D. Terry, The three-dimensional structure at 6 A resolution of a human gamma Gl immunoglobulin molecule. J Biol Chem 246(11) (1971) 3753-3759.

[9] K. Fujimori, D.G. Covell, J.E. Fletcher, J.N. Weinstein, A modeling analysis of monoclonal antibody percolation through tumors: a binding-site barrier. J Nucl Med 31(7) (1990) 1191-1198.

[10] R. Gong, W. Chen, D.S. Dimitrov, Expression, purification, and characterization of engineered antibody CH2 and VH domains.

Methods Mol Biol 899 (2012) 85-102.
[11] I. Altintas, R.J. Kok, R.M. Schiffelers, Targeting epidermal growth factor receptor in tumors: from conventional monoclonal antibodies via heavy chain-only antibodies to nanobodies. Eur J Pharm Sci 45(4) (2012) 399-407.
[12] K.R. Miller, A. Koide, B. Leung, J. Fitzsimmons, B. Yoder, H. Yuan, M. Jay, S.S. Sidhu, S. Koide, E.J. Collins, T cell receptor-like recognition of tumor in vivo by synthetic antibody fragment. PLoS One 7(8) (2012) e43746.
[13] A. Bell, Z.J. Wang, M. Arbabi-Ghahroudi, T.A. Chang, Y. Durocher, U. Trojahn, J. Baardsnes, M.L. Jaramillo, S. Li, T.N. Baral, M. O'Connor-McCourt, R. Mackenzie, J. Zhang, Differential tumor-targeting abilities of three single-domain antibody formats. Cancer Lett 289(1) (2010) 81-90.
[14] S. Hu, L. Shively, A. Raubitschek, M. Sherman, L.E. Williams, J.Y. Wong, J.E. Shively, A.M. Wu, Minibody: A novel engineered anti-carcinoembryonic antigen antibody fragment (single-chain Fv-CH3) which exhibits rapid, high-level targeting of xenografts. Cancer Res 56(13) (1996) 3055-3061.
[15] A. Orlova, V. Tolmachev, R. Pehrson, M. Lindborg, T. Tran, M. Sandström, F.Y. Nilsson, A. Wennborg, L. Abrahmsén, J. Feldwisch, Synthetic affibody molecules: a novel class of affinity ligands for molecular imaging of HER2-expressing malignant tumors. Cancer Res 67(5) (2007) 2178-2186.
[16] M.T. Stumpp, H.K. Binz, P. Amstutz, DARPins: a new generation of protein therapeutics. Drug Discov Today 13(15-16) (2008) 695-701.
[17] Y.L. Boersma, A. Plückthun, DARPins and other repeat protein scaffolds: advances in engineering and applications. Curr Opin Biotechnol 22(6) (2011) 849-857.
[18] C. Hamers-Casterman, T. Atarhouch, S. Muyldermans, G. Robinson, C. Hamers, E.B. Songa, N. Bendahman, R. Hamers, Naturally occurring antibodies devoid of light chains. Nature 363(6428) (1993) 446-448.
[19] K.E. Conrath, U. Wernery, S. Muyldermans, V.K. Nguyen, Emergence and evolution of functional heavy-chain antibodies in Camelidae. Dev Comp Immunol 27(2) (2003) 87-103.
[20] A.S. Greenberg, D. Avila, M. Hughes, A. Hughes, E.C. McKinney, M.F. Flajnik, A new antigen receptor gene family that undergoes rearrangement and extensive somatic diversification in sharks. Nature 374(6518) (1995) 168-173.
[21] J.P. Rast, C.T. Amemiya, R.T. Litman, S.J. Strong, G.W. Litman, Distinct patterns of IgH structure and organization in a divergent lineage of chrondrichthyan fishes. Immunogenetics 47(3) (1998) 234-245.
[22] S. Muyldermans, T. Atarhouch, J. Saldanha, J.A. Barbosa, R. Hamers, Sequence and structure of VH domain from naturally occurring camel heavy chain immunoglobulins lacking light chains. Protein Eng 7(9) (1994) 1129-1135.
[23] J.A. Kolkman, D.A. Law, Nanobodies - from llamas to therapeutic proteins. Drug Discovery Today: Technologies 7(2) (2010) e139-e146.
[24] H. Revets, P.D. Baetselier, S. Muyldermans, Nanobodies as novel agents for cancer therapy. Expert Opin Biol Ther 5(1) (2005) 111-124.
[25] S. Muyldermans, Nanobodies: Natural Single-Domain Antibodies. Annu Rev Biochem (2013).
[26] M. Arbabi-Ghahroudi, A. Desmyter, L. Wyns, R. Hamers, S. Muyldermans, Selection and identification of single domain antibody fragments from camel heavy-chain antibodies. FEBS Lett 414(3) (1997) 521-526.
[27] V. Cortez-Retamozo, M. Lauwereys, G.G. Hassanzadeh, M. Gobert, K. Conrath, S. Muyldermans, P. De Baetselier, H. Revets, Efficient tumor targeting by single-domain antibody fragments of camels. Int J Cancer 98(3) (2002) 456-462.
[28] F. Van Bockstaele, J.B. Holz, H. Revets, The development of nanobodies for therapeutic applications. Curr Opin Investig Drugs 10(11) (2009) 1212-1224.
[29] J. Bartunek, E. Barbato, G. Heyndrickx, M. Vanderheyden, W. Wijns, J.B. Holz, Novel antiplatelet agents: ALX-0081, a Nanobody directed towards von Willebrand factor. J Cardiovasc Transl Res 6(3) (2013) 355-363.
[30] C. Vincke, R. Loris, D. Saerens, S. Martinez-Rodriguez, S. Muyldermans, K. Conrath, General strategy to humanize a camelid single-domain antibody and identification of a universal humanized

nanobody scaffold. J Biol Chem 284(5) (2009) 3273-3284.
[31] T.T. Wu, G. Johnson, E.A. Kabat, Length distribution of CDRH3 in antibodies. Proteins 16(1) (1993) 1-7.
[32] J. Wesolowski, V. Alzogaray, J. Reyelt, M. Unger, K. Juarez, M. Urrutia, A. Cauerhff, W. Danquah, B. Rissiek, F. Scheuplein, N. Schwarz, S. Adriouch, O. Boyer, M. Seman, A. Licea, D.V. Serreze, F.A. Goldbaum, F. Haag, F. Koch-Nolte, Single domain antibodies: promising experimental and therapeutic tools in infection and immunity. Med Microbiol Immunol 198(3) (2009) 157-174.
[33] K.R. Schmitz, A. Bagchi, R.C. Roovers, P.M.P. van Bergen en Henegouwen, K.M. Ferguson, Structural evaluation of EGFR inhibition mechanisms for nanobodies/VHH domains. Structure *in press* (2013).
[34] A. Desmyter, T.R. Transue, M.A. Ghahroudi, M.H. Thi, F. Poortmans, R. Hamers, S. Muyldermans, L. Wyns, Crystal structure of a camel single-domain VH antibody fragment in complex with lysozyme. Nat Struct Biol 3(9) (1996) 803-811.
[35] E. Dolk, C. van Vliet, J.M. Perez, G. Vriend, H. Darbon, G. Ferrat, C. Cambillau, L.G. Frenken, T. Verrips, Induced refolding of a temperature denatured llama heavy-chain antibody fragment by its antigen. Proteins 59(3) (2005) 555-564.
[36] M.M. Harmsen, H.J. De Haard, Properties, production, and applications of camelid single-domain antibody fragments. Appl Microbiol Biotechnol 77(1) (2007) 13-22.
[37] M. Dumoulin, K. Conrath, A. Van Meirhaeghe, F. Meersman, K. Heremans, L.G. Frenken, S. Muyldermans, L. Wyns, A. Matagne, Single-domain antibody fragments with high conformational stability. Protein Sci 11(3) (2002) 500-515.
[38] R.C. Roovers, G.A. van Dongen, P.M. van Bergen en Henegouwen, Nanobodies in therapeutic applications. Curr Opin Mol Ther 9(4) (2007) 327-335.
[39] I. Vaneycken, M. D'huyvetter, S. Hernot, J.D. Vos, C. Xavier, N. Devoogdt, V. Caveliers, T. Lahoutte, Immuno-imaging using nanobodies. Curr Opin Biotechnol 22(6) (2011) 877-881.
[40] M.M. Kijanka, F.J. Warnders, M. El Khattabi, M. Lub-de-Hooge, G.M. van Dam, V. Ntziachristos, E.G.E. de Vries, S. Oliveira, P.M.P. van Bergen en Henegouwen, Rapid optical imaging of human breast tumor xenografts using anti-HER2 VHHs site-directly conjugated to IRDye800CW for image-guided surgery. Eur J Nucl Med Mol Imaging *in press* (2013).
[41] A. Sukhanova, K. Even-Desrumeaux, A. Kisserli, T. Tabary, B. Reveil, J.M. Millot, P. Chames, D. Baty, M. Artemyev, V. Oleinikov, M. Pluot, J.H. Cohen, I. Nabiev, Oriented conjugates of single-domain antibodies and quantum dots: toward a new generation of ultrasmall diagnostic nanoprobes. Nanomedicine 8(4) (2012) 516-525.
[42] L. Huang, L.O. Gainkam, V. Caveliers, C. Vanhove, M. Keyaerts, P. De Baetselier, A. Bossuyt, H. Revets, T. Lahoutte, SPECT imaging with 99mTc-labeled EGFR-specific nanobody for in vivo monitoring of EGFR expression. Mol Imaging Biol 10(3) (2008) 167-175.
[43] L.O. Gainkam, L. Huang, V. Caveliers, M. Keyaerts, S. Hernot, I. Vaneycken, C. Vanhove, H. Revets, P. De Baetselier, T. Lahoutte, Comparison of the biodistribution and tumor targeting of two 99mTc-labeled anti-EGFR nanobodies in mice, using pinhole SPECT/micro-CT. J Nucl Med 49(5) (2008) 788-795.
[44a] L,.Coppieters, T. Dreier, K. Silence, H. de Haard, M. Lauwereys, P. Casteels, E. Beirnaert, H. Jonckheere, C. Van de Wiele, L. Staelens, J. Hostens, H. Revets, E. Remaut, D. Elewaut, and P. Rottiers. 2006. Formatted anti-tumor necrosis factor alpha VHH proteins derived from camelids show superior potency and targeting to inflamed joints in a murine model of collagen-induced arthritis. Arthritis Rheum. 541856-1866.
[44b] B. Tijink, T. Laeremans, M. Budde, M.S. Walsum, T. Dreier, H.J. de Haard, C.R. Leemans, G.A. van Dongen, Improved tumor targeting of anti-epidermal growth factor receptor nanobodies through albumin binding: taking advantage of modular Nanobody technology. Mol Cancer Ther 7(8) (2008) 2288-2297.
[45] R.C. Roovers, T. Laeremans, L. Huang, S.D. Taeye, A.J. Verkleij, H. Revets, H.J. de Haard, P.M.P. van Bergen en Henegouwen, Efficient inhibition of EGFR signalling and of tumour growth by antagonistic anti-EGFR Nanobodies. Cancer Immunol Immunother 56(3) (2007) 303–317.

[46] R.C. Roovers, M.J. Vosjan, T. Laeremans, R. el Khoulati, R.C. de Bruin, K.M. Ferguson, A.J. Verkleij, G.A. van Dongen, P.M.P. van Bergen en Henegouwen, A biparatopic anti-EGFR nanobody efficiently inhibits solid tumour growth. Int J Cancer 129(8) (2011) 2013-2024.
[47] T. Peters-Jr, 5 - Metabolism: Albumin in the Body, In All About Albumin, 1995.
[48] D. Sleep, J. Cameron, L.R. Evans, Albumin as a versatile platform for drug half-life extension. Biochim Biophys Acta (2013).
[49] S.Y. Wang, G. Weiner, Complement and cellular cytotoxicity in antibody therapy of cancer. Expert Opin Biol Ther 8(6) (2008) 759-768.
[50] G. Richard, A.J. Meyers, M.D. McLean, M. Arbabi-Ghahroudi, R. Mackenzie, J.C. Hall, In Vivo Neutralization of α-Cobratoxin with High-Affinity Llama Single-Domain Antibodies (VHHs) and a VHH-Fc Antibody. PLoS One 8(7) (2013) e69495.
[51] S. De Buck, J. Nolf, T. De Meyer, V. Virdi, K. De Wilde, E. Van Lerberge, B. Van Droogenbroeck, A. Depicker, Fusion of an Fc chain to a VHH boosts the accumulation levels in Arabidopsis seeds. Plant Biotechnol J (2013).
[52] L. Naldini, E. Vigna, R.P. Narsimhan, G. Gaudino, R. Zarnegar, G.K. Michalopoulos, P.M. Comoglio, Hepatocyte growth factor (HGF) stimulates the tyrosine kinase activity of the receptor encoded by the proto-oncogene c-MET. Oncogene 6(4) (1991) 501-504.
[53] D.P. Bottaro, J.S. Rubin, D.L. Faletto, A.M. Chan, T.E. Kmiecik, G.F. Vande Woude, S.A. Aaronson, Identification of the hepatocyte growth factor receptor as the c-met proto-oncogene product. Science 251(4995) (1991) 802-804.
[54] C. Boccaccio, P.M. Comoglio, Invasive growth: a MET-driven genetic programme for cancer and stem cells. Nat Rev Cancer 6(8) (2006) 637-645.
[55] P.Y. Wen, D. Schiff, T.F. Cloughesy, J.J. Raizer, J. Laterra, M. Smitt, M. Wolf, K.S. Oliner, A. Anderson, M. Zhu, E. Loh, D.A. Reardon, A phase II study evaluating the efficacy and safety of AMG 102 (rilotumumab) in patients with recurrent glioblastoma. Neuro Oncol 13(4) (2011) 437-446.
[56] W. Okamoto, I. Okamoto, K. Tanaka, E. Hatashita, Y. Yamada, K. Kuwata, H. Yamaguchi, T. Arao, K. Nishio, M. Fukuoka, P.A. Jänne, K. Nakagawa, TAK-701, a humanized monoclonal antibody to hepatocyte growth factor, reverses gefitinib resistance induced by tumor-derived HGF in non-small cell lung cancer with an EGFR mutation. Mol Cancer Ther 9(10) (2010) 2785-2792.
[57] M.J. Vosjan, J. Vercammen, J.A. Kolkman, M. Stigter-van Walsum, H. Revets, G.A. van Dongen, Nanobodies targeting the hepatocyte growth factor: potential new drugs for molecular cancer therapy. Mol Cancer Ther 11(4) (2012) 1017-1025.
[58] K. Holmes, O.L. Roberts, A.M. Thomas, M.J. Cross, Vascular endothelial growth factor receptor-2: structure, function, intracellular signalling and therapeutic inhibition. Cell Signal 19(10) (2007) 2003-2012.
[59] E. Stuttfeld, K. Ballmer-Hofer, Structure and function of VEGF receptors. IUBMB Life 61(9) (2009) 915-922.
[60] A.K. Olsson, A. Dimberg, J. Kreuger, L. Claesson-Welsh, VEGF receptor signalling - in control of vascular function. Nat Rev Mol Cell Biol 7(5) (2006) 359-371.
[61] J.L. Spratlin, R.B. Cohen, M. Eadens, L. Gore, D.R. Camidge, S. Diab, S. Leong, C. O'Bryant, L.Q. Chow, N.J. Serkova, N.J. Meropol, N.L. Lewis, E.G. Chiorean, F. Fox, H. Youssoufian, E.K. Rowinsky, S.G. Eckhardt, Phase I pharmacologic and biologic study of ramucirumab (IMC-1121B), a fully human immunoglobulin G1 monoclonal antibody targeting the vascular endothelial growth factor receptor-2. J Clin Oncol 28(5) (2010) 780-787.
[62] M. Behdani, S. Zeinali, H. Khanahmad, M. Karimipour, N. Asadzadeh, K. Azadmanesh, A. Khabiri, S. Schoonooghe, M. Habibi-Anbouhi, G. Hassanzadeh-Ghassabeh, S. Muyldermans, Generation and characterization of a functional Nanobody against the vascular endothelial growth factor receptor-2; angiogenesis cell receptor. Mol Immunol 50(1-2) (2012) 35-41.
[63] S. Oliveira, P.M.P. van Bergen en Henegouwen, G. Storm, R.M. Schiffelers, Molecular biology of epidermal growth factor receptor inhibition for cancer therapy. Expert Opin Biol Ther 6(6) (2006) 605-617.
[64] L. Vecchione, B. Jacobs, N. Normanno, F. Ciardiello, S. Tejpar, EGFR-targeted therapy. Exp Cell Res 317(19) (2011) 2765-2771.

[65] L.B. Saltz, N.J. Meropol, P.J.S. Loehrer, M.N. Needle, J. Kopit, R.J. Mayer, Phase II trial of cetuximab in patients with refractory colorectal cancer that expresses the epidermal growth factor receptor. J Clin Oncol 22(7) (2004) 1201-1208.
[66] R.S. Herbst, M. Arquette, D.M. Shin, K. Dicke, E.E. Vokes, N. Azarnia, W.K. Hong, M.S. Kies, Phase II multicenter study of the epidermal growth factor receptor antibody cetuximab and cisplatin for recurrent and refractory squamous cell carcinoma of the head and neck. J Clin Oncol 23(24) (2005) 5578-5587.
[67] E. Van Cutsem, M. Peeters, S. Siena, Y. Humblet, A. Hendlisz, B. Neyns, J.L. Canon, J.L. Van Laethem, J. Maurel, G. Richardson, M. Wolf, R.G. Amado, Open-label phase III trial of panitumumab plus best supportive care compared with best supportive care alone in patients with chemotherapy-refractory metastatic colorectal cancer. J Clin Oncol 25(13) (2007) 1658-1664.
[68] D.K. Patel, Clinical use of anti-epidermal growth factor receptor monoclonal antibodies in metastatic colorectal cancer. Pharmacotherapy 28(11 Pt 2) (2008) 31S-41S.
[69] A. Harandi, A.S. Zaidi, A.M. Stocker, D.A. Laber, Clinical Efficacy and Toxicity of Anti-EGFR Therapy in Common Cancers. J Oncol 2009(567486) (2009).
[70] M.A. Pantaleo, M. Nannini, S. Fanti, S. Boschi, P.L. Lollini, G. Biasco, Molecular imaging of EGFR: it's time to go beyond receptor expression. J Nucl Med 50(7) (2009) 1195-1196.
[71] V. Tolmachev, Molecular Imaging of EGFR: It's Time to Go Beyond Receptor Expression. J Nucl Med 50(7) (2009) 1196.
[72] T.Y. Lee, R.M. Tjin-Tham-Sjin, S. Movahedi, B. Ahmed, E.A. Pravda, K.M. Lo, S.D. Gillies, J. Folkman, K. Javaherian, Linking antibody Fc domain to endostatin significantly improves endostatin half-life and efficacy. Clin Cancer Res 14(5) (2008) 1487-1493.
[73] S. Mohseni-Nodehi, R. Repp, C. Kellner, J. Bräutigam, M. Staudinger, N. Schub, M. Peipp, M. Gramatzki, A. Humpe, Enhanced ADCC activity of affinity maturated and Fc-engineered mini-antibodies directed against the AML stem cell antigen CD96. PLoS One 7(8) (2012) e42426.
[74] T.M. Allen, Ligand-targeted therapeutics in anticancer therapy. Nat Rev Cancer 2(10) (2002) 750-763.
[75] V. Cortez-Retamozo, N. Backmann, P.D. Senter, U. Wernery, P. De Baetselier, S. Muyldermans, H. Revets, Efficient cancer therapy with a nanobody-based conjugate. Cancer Res 64(8) (2004) 2853-2857.
[76] M. Behdani, S. Zeinali, M. Karimipour, H. Khanahmad, S. Schoonooghe, A. Aslemarz, N. Seyed, R. Moazami-Godarzi, F. Baniahmad, M. Habibi-Anbouhi, G. Hassanzadeh-Ghassabeh, S. Muyldermans, Development of VEGFR2-specific Nanobody Pseudomonas exotoxin A conjugated to provide efficient inhibition of tumor cell growth. N Biotechnol 30(2) (2013) 205-209.
[77] G.N. John, J.N. Giannios, P. Lambrinos, N. Alexandropoulos, Bispecific nanobody targeting DNMT1 and SHH conjugated to vinorelbine inhibit DNA methylation, hedgehog-patched (PCTH) receptor signaling protein smoothened and hTERT expression leading to re-expression of apoptotic tumor suppressor genes and induction. 2007 Prostate Cancer Symposium 2007.
[78] J.A. van de Water, T. Bagci-Onder, A.S. Agarwal, H. Wakimoto, R.C. Roovers, Y. Zhu, R. Kasmieh, D. Bhere, P.M.P. van Bergen en Henegouwen, K. Shah, Therapeutic stem cells expressing variants of EGFR-specific nanobodies have antitumor effects. Proc Natl Acad Sci U S A 109(41) (2012) 16642-16647.
[79] W.C. Zamboni, V. Torchilin, A.K. Patri, J. Hrkach, S. Stern, R. Lee, A. Nel, N.J. Panaro, P. Grodzinski, Best practices in cancer nanotechnology: perspective from NCI nanotechnology alliance. Clin Cancer Res 18(12) (2012) 3229-3241.
[80] A.M. Hillery, A.W. Lloyd, J. Swarbrick, Drug delivery and targeting for pharmacists and pharmaceutical scientists London, New York: Taylor & Francis, 2001.
[81] C. Mamot, D.C. Drummond, C.O. Noble, V. Kallab, Z. Guo, K. Hong, D.B. Kirpotin, J.W. Park, Epidermal growth factor receptor-targeted immunoliposomes significantly enhance the efficacy of multiple anticancer drugs in vivo. Cancer Res 65(24) (2005) 11631-11638.
[82] C. Mamot, R. Ritschard, W. Küng, J.W. Park, R. Herrmann, C.F. Rochlitz, EGFR-targeted immunoliposomes derived from the monoclonal antibody EMD72000 mediate

specific and efficient drug delivery to a variety of colorectal cancer cells. Drug Target 14(4) (2006) 215-223.
[83] K. Maruyama, PEG-immunoliposome. Biosci Rep 22(2) (2002) 251-266.
[84] C. Lourenco, M. Teixeira, S. Simoes, R. Gaspar, Steric stabilization of nanoparticles: size and surface properties. International Journal of Pharmaceutics 138(1) (1996) 1-12.
[85] H. Maeda, J. Wu, T. Sawa, Y. Matsumura, K. Hori, Tumor vascular permeability and the EPR effect in macromolecular therapeutics: a review. J Control Release 65(1-2) (2000) 271-284.
[86] H. Maeda, The enhanced permeability and retention (EPR) effect in tumor vasculature: the key role of tumor-selective macromolecular drug targeting. Adv Enzyme Regul 41 (2001) 189-207.
[87] S. Oliveira, R.M. Schiffelers, J. van der Veeken, R. van der Meel, R. Vongpromek, P.M. van Bergen en Henegouwen, G. Storm, R.C. Roovers, Downregulation of EGFR by a novel multivalent nanobody-liposome platform. J Control Release 145(2) (2010) 165-175.
[88] R. van der Meel, S. Oliveira, I. Altintas, R. Haselberg, J. van der Veeken, R.C. Roovers, P.M.P. van Bergen en Henegouwen, G. Storm, W.E. Hennink, R.M. Schiffelers, R.J. Kok, Tumor-targeted Nanobullets: Anti-EGFR nanobody-liposomes loaded with anti-IGF-1R kinase inhibitor for cancer treatment. J Control Release 159(2) (2012) 281-289.
[89] J. van der Veeken, S. Oliveira, R.M. Schiffelers, G. Storm, P.M.P. van Bergen en Henegouwen, R.C. Roovers, Crosstalk between epidermal growth factor receptor- and insulin-like growth factor-1 receptor signaling: implications for cancer therapy. Curr Cancer Drug Targets 9(6) (2009) 748-760.
[90] R. van der Meel, S. Oliveira, I. Altintas, R. Heukers, E.H. Pieters, P.M.P. van Bergen en Henegouwen, G. Storm, W.E. Hennink, R.J. Kok, R.M. Schiffelers, Inhibition of tumor growth by targeted anti-EGFR/IGF-1R Nanobullets depends on efficient blocking of cell survival pathways. Mol Pharm *in press* (2013).
[91] C. Mamot, R. Ritschard, A. Wicki, G. Stehle, T. Dieterle, L. Bubendorf, C. Hilker, S. Deuster, R. Herrmann, C. Rochlitz, Tolerability, safety, pharmacokinetics, and efficacy of doxorubicin-loaded anti-EGFR immunoliposomes in advanced solid tumours: a phase 1 dose-escalation study. Lancet Oncol 13(12) (2012) 1234-1241.
[92] M. Talelli, M. Iman, A.K. Varkouhi, C.J. Rijcken, R.M. Schiffelers, T. Etrych, K. Ulbrich, C.F. van Nostrum, T. Lammers, G. Storm, W.E. Hennink, Core-crosslinked polymeric micelles with controlled release of covalently entrapped doxorubicin. Biomaterials 31(30) (2010) 7797-7804.
[93] M. Talelli, R.J. Rijcken, S. Oliveira, R. van der Meel, P.M. van Bergen en Henegouwen, T. Lammers, C.F. van Nostrum, G. Storm, W.E. Hennink, Nanobody-shell functionalized thermosensitive core-crosslinked polymeric micelles for active drug targeting. J Control Release 151(2) (2011) 183-192.
[94] M. Talelli, S. Oliveira, R.J. Rijcken, E.H. Pieters, T. Etrych, K. Ulbrich, R.C. van Nostrum, G. Storm, W.E. Hennink, T. Lammers, Intrinsically active nanobody-modified polymeric micelles for tumor-targeted combination therapy. Biomaterials 34(4) (2013) 1255-1260.
[95] B.G. Müller, H. Leuenberger, T. Kissel, Albumin nanospheres as carriers for passive drug targeting: an optimized manufacturing technique. Pharm Res 13(1) (1996) 32-37.
[96] A.O. Elzoghby, W.M. Samy, N.A. Elgindy, Albumin-based nanoparticles as potential controlled release drug delivery systems. J Control Release 157(2) (2012) 168-182.
[97] I. Altintas, R. Heukers, R. van der Meel, M. Lacombe, M. Amidi, P.M.P. van Bergen en Henegouwen, W.E. Hennink, R.M. Schiffelers, R.J. Kok, Nanobody-albumin nanoparticles (NANAPs) for the delivery of a multikinase inhibitor 17864 to EGFR overexpressing tumor cells. J Control Release 165(2) (2013) 110-118.
[98] S.W. Reulen, I. van Baal, J.M. Raats, M. Merkx, Efficient, chemoselective synthesis of immunomicelles using single-domain antibodies with a C-terminal thioester. BMC Biotechnol 9(66) (2009).
[99] S. Oliveira, G.A. van Dongen, M. Stigter-van Walsum, R.C. Roovers, J.C. Stam, W. Mali, P.J. van Diest, P.M.P. van Bergen en Henegouwen, Rapid visualization of human tumor xenografts through optical imaging with a near-infrared fluorescent anti-epidermal

growth factor receptor nanobody. Mol Imaging 11(1) (2012) 33-46.
[100] R. Weissleder, U. Mahmood, Molecular imaging. Radiology 219(2) (2001) 316-333.
[101] S.A. Hilderbrand, R. Weissleder, Near-infrared fluorescence: application to in vivo molecular imaging. Curr Opin Chem Biol 14(1) (2010) 71-79.
[102] L.O. Gainkam, M. Keyaerts, V. Caveliers, N. Devoogdt, C. Vanhove, L. Van Grunsven, S. Muyldermans, T. Lahoutte, Correlation between epidermal growth factor receptor-specific nanobody uptake and tumor burden: a tool for noninvasive monitoring of tumor response to therapy. Mol Imaging Biol 13(5) (2011) 940-948.
[103] M. D'Huyvetter, A. Aerts, C. Xavier, I. Vaneycken, N. Devoogdt, M. Gijs, N. Impens, S. Baatout, B. Ponsard, S. Muyldermans, V. Caveliers, T. Lahoutte, Development of 177Lu-nanobodies for radioimmunotherapy of HER2-positive breast cancer: evaluation of different bifunctional chelators. Contrast Media Mol Imaging 7(2) (2012) 254-264.
[104] M. Fani, J.P. André, H.R. Maecke, 68Ga-PET: a powerful generator-based alternative to cyclotron-based PET radiopharmaceuticals. Contrast Media Mol Imaging 3(2) (2008) 67-77.
[105] M.J. Vosjan, L.R. Perk, R.C. Roovers, G.W. Visser, M. Stigter-van Walsum, P.M.P. van Bergen en Henegouwen, G.A. van Dongen, Facile labelling of an anti-epidermal growth factor receptor Nanobody with 68Ga via a novel bifunctional desferal chelate for immuno-PET. Eur J Nucl Med Mol Imaging 38(4) (2011) 753-763.
[106] I. Vaneycken, N. Devoogdt, N. Van Gassen, C. Vincke, C. Xavier, U. Wernery, S. Muyldermans, T. Lahoutte, V. Caveliers, Preclinical screening of anti-HER2 nanobodies for molecular imaging of breast cancer. FASEB J 25(7) (2011) 2433-2446.
[107] C. Xavier, I. Vaneycken, M. D'huyvetter, J. Heemskerk, M. Keyaerts, C. Vincke, N. Devoogdt, S. Muyldermans, T. Lahoutte, V. Caveliers, Synthesis, Preclinical Validation, Dosimetry, and Toxicity of 68Ga-NOTA-Anti-HER2 Nanobodies for iPET Imaging of HER2 Receptor Expression in Cancer. J Nucl Med (2013).
[108] S. Hernot, S. Unnikrishnan, Z. Du, T. Shevchenko, B. Cosyns, A. Broisat, J. Toczek, V. Caveliers, S. Muyldermans, T. Lahoutte, A.L. Klibanov, N. Devoogdt, Nanobody-coupled microbubbles as novel molecular tracer. J Control Release 158(2) (2012) 346-353.
[109] M.M. Schmidt, K.D. Wittrup, A modeling analysis of the effects of molecular size and binding affinity on tumor targeting. Mol Cancer Ther 8(10) (2009) 2861-2871.

Chapter 3

EGFR endocytosis requires its kinase activity and N-terminal transmembrane dimerization motif

Raimond Heukers[1], Jeroen F. Vermeulen[1], Farzad Fereidouni[2], Arjen N. Bader[2,†], Jarno Voortman[1], Rob C. Roovers[1,‡], Hans C. Gerritsen[2], and Paul M. P. van Bergen en Henegouwen[1]

[1] Cell Biology, Department of Biology, Utrecht University, Utrecht, The Netherlands
[2] Molecular Biophysics, Utrecht University, Utrecht, The Netherlands

† Present address: Wageningen University, 6703 HA Wageningen, The Netherlands
‡ Present address: Merus Biopharmaceuticals, 3584 CH Utrecht, The Netherlands

Journal of Cell Science. 2013 Nov 1;126(Pt 21):4900-12.

Abstract

EGFR signaling is attenuated by endocytosis and degradation of receptor/ligand complexes in lysosomes. Endocytosis of EGFR is known to be regulated by multiple posttranslational modifications. The observation that prevention of these modifications does not block endocytosis completely, suggests the involvement of other mechanism(s). Recently, receptor clustering has been suggested to induce internalization of multiple types of membrane receptors. However, the mechanism of clustering-induced internalization remains unknown. We have used biparatopic antibody fragments from llama (VHHs) to induce EGFR clustering without stimulating tyrosine kinase activity. Using this approach, we have found an essential role for the N-terminal GG4-like dimerization motif in the transmembrane domain (TMD) for clustering-induced internalization. Moreover, conventional EGF-induced receptor internalization depends exclusively on the N-terminal TMD dimerization motif and kinase activity. Mutations in this dimerization motif eventually lead to reduced EGFR degradation and sustained signaling. We propose a novel role for the TMD dimerization motif in the negative feedback control of EGFR. The widely conserved nature of GG4-like dimerization motifs in transmembrane proteins suggests a general role for these motifs in clustering-induced internalization.

3.1. Introduction

The receptor for the epidermal growth factor (EGFR, HER1 or ErbB1) is a receptor tyrosine kinase that, together with its family members HER2, 3, and 4 belongs to the ErbB-family of growth factor receptors [1]. This family of receptor tyrosine kinases is involved in the growth regulation of many different cancers, e.g. brain, breast, and head and neck tumors. In resting cells, the different members of the ErbB family are present in the plasma membrane as inactive monomers or as inactive homo- and hetero-dimers (predimers). EGF-binding induces the formation of additional dimers, tetramers and further higher order oligomers [2-7]. In addition, EGF initiates several structural rearrangements in the ecto- and intracellular domain which releases its auto-inhibitory state resulting in kinase activation and trans-phosphorylation of C-terminal tyrosine residues [8, 9]. The phosphorylated tyrosines serve subsequently as docking sites for various adaptor proteins involved in signal transduction of proliferative and anti-apoptotic pathways [10, 11].

The ErbB receptors are all composed of similar building blocks such as the extracellular domain consisting of subdomains I-IV, the trans- and juxtamembrane domains, the tyrosine kinase and the substrate domain [11]. The structural interactions required for receptor oligomerization are less well described, but crystal data from liganded ectodomains show different head to head interactions, which may be involved in cluster formation [5, 12, 13]. Recent data also suggest a role for signaling in receptor clustering as inhibition of receptor kinase activity or phospholipase D activity prevented EGFR clustering [4, 7, 14]. Dimerization of EGFR may also be regulated by two Sternberg-Gullick (GxxxG- or GG4-like) dimerization motifs within the transmembrane domain (TMD). Disulfide crosslinking experiments indicated EGF-induced association of the N-terminal GG4 motif [15]. Interestingly, mutations in the TMD of EGFR are frequently found in relation with different types of diseases [16] .

One of the most important negative feedback mechanisms of EGFR signaling is receptor downregulation, which is initiated by clathrin-mediated (CME) and/or clathrin-independent endocytosis [17, 18]. After their internalization, active receptor-ligand complexes are transported by multi-vesicular vesicles to lysosomes where receptor-ligand complexes are degraded [19]. Ligand binding induces a large increase in the internalization rate, which is regulated at different levels [18]. Although post-translational modifications like tyrosine an serine/threonine phosphorylation, ubiquitination and acetylation all play a role in regulating receptor endocytosis, blocking these modifications does not inhibit EGFR internalization completely, suggesting the existence of other as yet undefined mechanism(s) [20-22]. Recently, different antibody combinations or multitopic constructs showed a reduction in surface-expressed EGFR as a result of the kinase-independent internalization of EGFR, suggesting an involvement of EGFR clustering in EGFR internalization [23-26].

In this study we have investigated the role of receptor clustering in the internalization of EGFR by using biparatopic VHHs. VHHs or Nanobodies consist of the variable domain of the heavy-chain from heavy chain-only antibodies from *Llama glama* [27-29]. Biparatopic VHHs are bivalent anti-EGFR VHHs that are binding to two different, non-overlapping epitopes on the extracellular domain of EGFR [30, 31]. Anisotropy studies presented here show that biparatopic VHHs stimulate EGFR clustering to a similar extent as EGF without stimulating kinase activity. Clustering-induced internalization of EGFR was clathrin-mediated and depended entirely on its N-terminal TMD dimerization motif. Moreover, EGF-induced internalization of EGFR was completely blocked by a mutation in the N-terminal TMD dimerization motif in combination with a mutation inactivating the kinase. Mutations in the TMD reduced EGF-induced degradation of both EGFR and EGF, resulting in sustained signaling. We propose a model in which ligand-induced CME is regulated by receptor clustering in synergy with CME-involved adaptor proteins that are recruited to the post-translationally modified EGFR C-terminal tail.

3.2. Materials and Methods

3.2.1. Plasmids and constructs

EGFR-K721A, and EGFR-9Y-F, mRFP-Clathrin, Eps15-ΔI and HA-tagged Dynamin2 K44A were kindly provided by respectively Sara Sigismund (IFOM- FIRC Institute of Molecular Oncology, Milan, Italy), Klemens Rottner (Helmholtz Centre for Infection Research, Braunschweig, Germany), Alexandre Benmerah (Institut Cochin, Paris, France) [39] and Sandra Schmid [63]. The EGFR mutants were created by Quickchange mutagenesis using Phusion polymerase (Finnzymes, Finland). Primers sequences are available upon request. All mutants were sequence verified and cloned into pcDNA5-EF1α-IRES-Zeo.

3.2.2. Cell lines

The murine fibroblast cell lines NIH 3T3 clone 2.2 and HER14 were described previously [36]. The tumor cell line UM-SCC-14C was kindly provided by Prof. Dr. G.A.M.S. van Dongen (Department of Otolaryngology, VU University Medical Center, Amsterdam, The Netherlands) and A431 and HeLa were both obtained from ATCC (LGC Standards, Germany). HeLa cells expressing a temperature sensitive variant of the dynamin-K44A mutant were described previously and were kindly provided by Willem Stoorvogel (Department of Veterinary medicine, Utrecht University, Utrecht, The Netherlands) [44, 64, 65]. All cell lines were cultured as described previously [30]. Stable cell lines expressing the EGFR-mutants were generated as described by Hofman et al. [7]. Zeocin resistant cells were FACS-sorted for comparable EGFR-levels as HER14 cells ($3 \cdot 10^5$ receptors/cell [36]).

3.2.3. Immunofluorescence

Immunofluorescence stainings were performed as described previously [66]. $EGF^{Alexa488}$, $Trf^{Alexa546}$, $CTB^{Alexa546}$ and Alexa Fluor® 488 5-TFP were obtained from Invitrogen. In case of the alcohol treatments, cells were pretreated with 1% 1-butanol or 2-propanol for 1 min before the assay. Images were obtained using a Zeiss Axiovert 200M confocal microscope (Carl Zeiss Microscopy GmbH, Germany) equipped with a 63x water immersion objective (NA 1.2) or a Zeiss LSM700 confocal microscope (Carl Zeiss Microscopy GmbH, Germany) with a 63x oil immersion objective (NA 1.4). Pearson colocalization coefficient was determined using the ZEN 2011 software.

3.2.4. Homo-FRET anisotropy measurements

A detailed description of our confocal anisotropy imaging setup and homo-FRET method was published previously [7, 67, 68]. Briefly, a 473 nm solid state diode laser (Becker & Hickl, BDL-473-SMC) with a pulse repetition rate of 80 MHz polarized by a linear polarizer (Meadowlark,Frederick, CO, USA) was coupled into a confocal microscope (Nikon C1, Japan). The laser light is focused on the sample by a 60x water immersion objective (1.2 N.A., Nikon). Depolarization of excitation light due to high NA of the objective was reduced by under-filling its back aperture. Since the pinhole is located in the emission path only, the resolution was not affected. The emission is detected by a 515/30 nm band pass filter and a broadband polarizing beam splitter cube (PBS, OptoSigma, Santa Ana, CA, USA) was used to split the emission in a parallel and a perpendicular channel with respect to the excitation light. The signal was detected with two high quantum efficiency PMTs (Hamamatsu H7422P-40). Calibration of the system was preformed with GFP in 50% v/v glycerol/ buffer and an aqueous Fluorescein solution.

3.2.5. ^{125}I-labeling and internalization

VHHs and EGF were labeled according to the IODO-GEN method, as described by Salacinski et al. [69]. Internalization assays using ^{125}I-labeled protein were performed as described before [34]. Radioactivity of both surface bound fraction and internalized fraction were determined using the gamma counter and the ratio internalized:bound was plotted against time to determine specific internalization rate constants.

3.2.6. TIRF-M

Live cell imaging by dual color total internal reflection fluorescence microscopy (TIRF-M) was performed on an inverted microscope (Eclipse Ti-E, Nikon) with a Perfect Focus System (Nikon), equipped with an Apo CFI Apo TIRF 100×/1.49 N.A. oil objective (Nikon). The system was also equipped with a stage-top incubator (INUG2E-ZILCS, Tokai Hit) and cells were imaged in the phenol red free culture medium (Gibco) at 37°C and 5% CO_2. For excitation, a mercury lamp

HBO-103W/2 (Osram) or 491nm 100mW Calypso (Cobolt) and 561nm 100mW Jive (Cobolt) lasers were used. Emitted light was separated using an OptoSplit III image splitter (CAIRN Research Ltd, UK) equipped with an eGFP/mCherry filter cube (59022, Chroma). Movies were collected for up to 50 seconds (10 frames/sec), using a Photometrics Evolve 512 Back-illuminated EMCCD camera (Roper Scientific) that was controlled by MetaMorph 7.7.5 software (Molecular Devices). The 16-bit images were projected onto the CCD chip with intermediate 2.5x lens at a magnification of 0.063 μm/pixel.

3.2.7. RNA interference

Small interfering RNAs (siRNA) knock down was performed like described by Motley et al. [70]. The siRNAs against CHC, AP2 alpha subunit, and a scrambled negative control were adapted from Motley et al. [70] or Fallon et al. [71] and obtained as Stealth® siRNAs from Invitrogen. The following siRNAs were used: 5′-CCAUCUUCUUAACCCUGAGUGGUUA-3′ for clathrin heavy chain (CHC; starting from nucleotide 252), 5'-CCUGGAGAGCAUGUGCACGCUGGCC-3' for the alpha subunit of the AP2 complex, 5'-AACAAACAAGAAUUCUUUGUUGCUU-3' for Eps15/Eps15R and 5′-CCUUGACGUCAUAGUCAUUUGUGGA-3′ as a scrambled negative control. Knock down efficiency was checked on blot with antibodies against CHC (BD Biosciences), AP2 alpha (Sigma-Aldrich) and Eps15 (RF99, [72]. Dynasore was obtained from Sigma-Aldrich and used as described previously [43].

3.2.8. Downregulation and phosphorylation assays

Phosphorylation assays were performed by western blotting as described elsewhere [73]. Phosphorylation of EGFR and total EGFR was respectively checked with anti-pEGFR (Tyr 1068) (Cell Signaling Technology, Danvers, Massachusetts) anti-EGFR (c74B9, Cell Signaling Technology) antibodies. MAPK and phospho-MAPK was respectively checked with anti-MAP Kinase 2/Erk2 (1B3B9, Millipore Corporation, Bedford, Massachusetts) and anti-phospho-p44/42 MAPK (Erk1/2) (Thr202/Tyr204) (Cell Signaling Technology). Equal loading was checked with anti-actin (ICN Immunobiologicals, Irvine, California) or anti-tubulin (DM1A, Millipore). Antibody binding to blots was detected with IRDye680 and IRDye800 conjugated secondary antibodies (LI-COR Biosciences, Lincoln, Nebraska) and an Odyssey Infrared Imager (LI-COR Biosciences). EGF degradation was determined with ^{125}I-labeled EGF. Cells were pulsed with EGF in DMEM with 2% BSA, after which the medium was refreshed. After 4 hr at 37°C, the amount of free label in the medium was determined after protein precipitation in 10% TCA. Degraded EGF was plotted as the percentage free label compared to the total EGF uptake.

3.3. Results

3.3.1. Generation and characterization of biparatopic VHHs against EGFR ectodomain

To study the role of receptor clustering in EGFR internalization we aimed to induce receptor clustering by using biparatopic nanobodies that are binding intermolecularly to EGFRs without stimulating kinase activity. As building blocks for the biparatopic nanobodies, different anti-EGFR VHH constructs were used (Mono1-4) (Fig. 1A). The selection of the antagonistic monomeric VHHs 7D12 (Mono1), and 9G8 (Mono2) was previously described [30]. These nanobodies are binding to domain III, both compete for EGF-binding and in addition compete for binding of either cetuximab (7D12) or matuzumab (9G8). In another biparatopic construct, two non-EGF competing anti-EGFR nanobodies were used: the previously described EGb4 (Mono3) [32] and EGc9 (Mono4). The latter VHH was obtained from a new selection performed on bacterially expressed, recombinant EGFR domain I. Binding of these VHHs to recombinant EGFR ectodomain was shown by phage ELISA. As negative control a phage expressing a non-relevant VHH (NR-VHH) was used, which did not show any binding (Fig. 1B). A phage ELISA was also used to demonstrate binding of Mono 3 and Mono4 to EGFR domain I (Fig. 1C).

From these four building blocks two biparatopic VHHs were generated, of which the different VHH building blocks bind to non-overlapping epitopes on the ectodomain (Fig. 1A). To demonstrate this, cross-competition studies with monovalent VHHs and VHH-expressing phages were performed. Mono2-expressing phages were successfully displaced by a 100 fold excess of Mono2 protein, while binding was unaffected by the presence of a 100 fold excess of Mono1 (Fig. 1D, left). In a similar experiment we show that Mono3 and Mono4 are also binding to non-overlapping epitopes (Fig. 1D, right). These monovalent VHHs were subsequently fused into either the bivalent, mono-specific Bival1 (Mono1-Mono1), biparatopic Bipar1 (Mono1 and 2) or biparatopic Bipar2 (Mono2 and 3) using a 10 residues glycine-serine-linker (Fig. 1A). A cross-competition assay on HER14 cells shows that the two biparatopic VHHs are not competing with each other for EGFR binding (Fig. 1E). Recent X-ray data with Mono1 and 2 (7D12 and 9G8) showed that the 10 amino acid linker is too short for intramolecular binding of the two epitope-binding domains to a single EGFR [31]. In agreement with this is the result obtained with a sedimentation velocity analytical ultracentrifugation (SV-AUC) experiment showed that Bipar1 binds to EGFR with a 1:2 (VHH:EGFR) stoichiometry. This intermolecular binding would enable Bipar1 to stimulate higher order EGFR clusters on cells.

Since activation of EGFR is accompanied with EGFR oligomerization, we first checked whether the biparatopic VHHs are non-agonistic. While EGF treatment resulted in a clear phosphorylation of EGFR, the VHH-constructs lacked agonistic activity (Fig. 1F). In conclusion, we have generated two non-agonistic biparatopic VHHs, which both consist of two

non-overlapping epitope binding nanobodies, one is interacting with domain III (Bipar1) and the other with domain I (Bipar2).

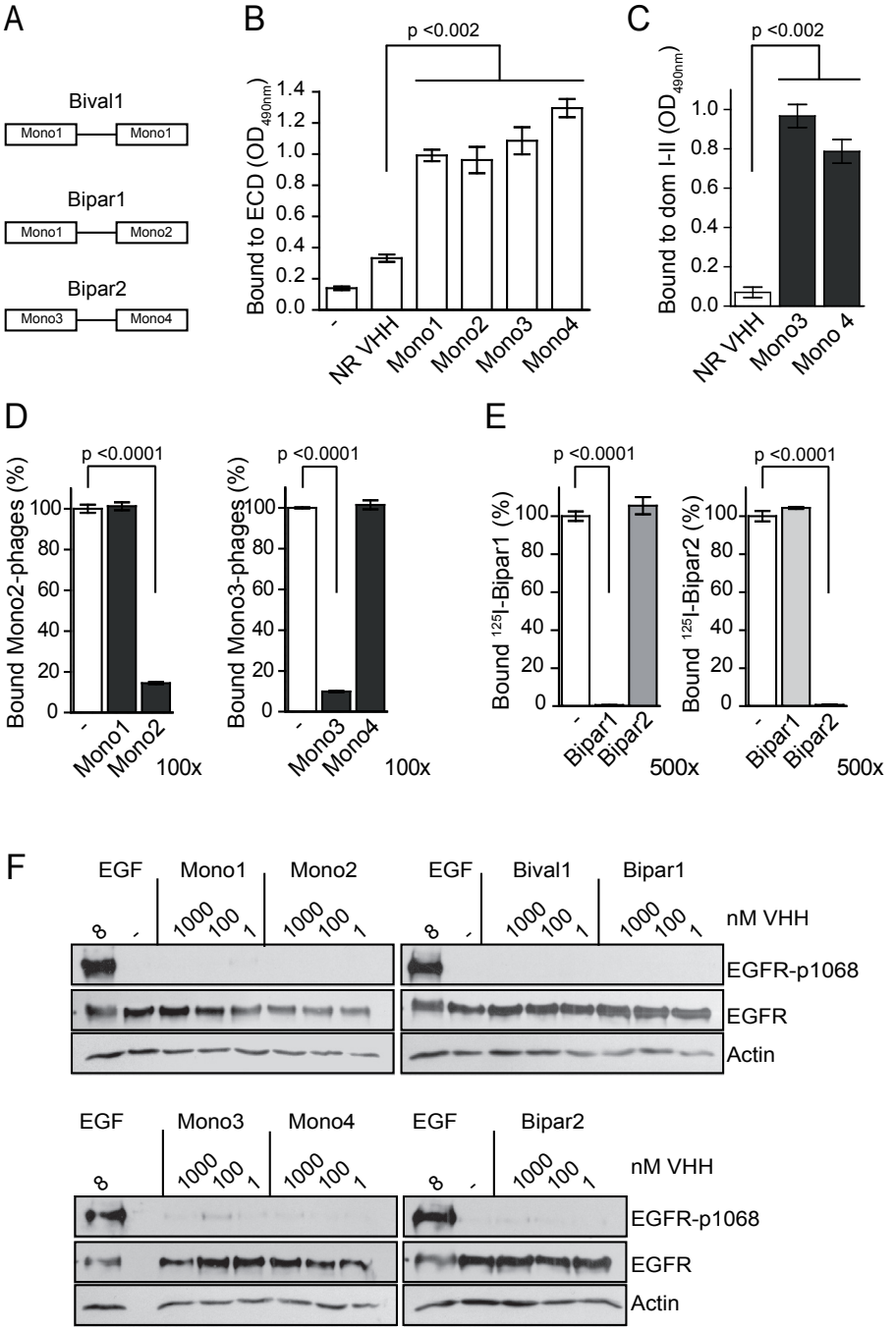

Figure 1. *Selected VHHs bind at non-overlapping sites on EGFR ectodomain. (A) Schematic presentation of used nanobody constructs. Phages expressing the indicated VHHs or a non-relevant VHH were bound to EGFR extracellular domain (B) or domain I+II of the EGFR extracellular domain (C) for 1 hr at RT. Bound phages in the ELISAwere detected with anti-M13 antibodies and OPD/H_2O_2. (D) Cross-competition of phages expressing Mono2 or Mono3 for binding to EGFR extracellular domain with an excess of indicated VHHs. Bound phages were detected as indicated in A. (E) Cross-competition ^{125}I-labeled Bipar1 (left) or Bipar2 (right) by 500-fold molar excess of unlabeled VHHs on HER14 cells. Cells were incubated with VHHs for 2 hrs on ice after which radioactivity was quantified. (F) HER14 cells were serum starved for 4 hr and treated for 10 min with either 8 nM of EGF or a concentration range of VHHs. Phosphorylated EGFR and total EGFR was detected on blot using anti-pEGFR (pY1068) and anti-EGFR antibodies. Actin was used as loading control. Error bars represent SEM.*

3.3.2. Biparatopic VHHs induce EGFR-clustering

To investigate whether the anti-EGFR VHHs induce receptor clustering, we have used homo-Förster Resonance Energy Transfer (homo-FRET) [33]. In this assay, clustering of EGFR is analyzed on NIH 3T3 cells expressing EGFR fused to monomeric GFP (mGFP) by confocal time-resolved fluorescence anisotropy imaging microscopy. Homo-FRET between EGFR-mGFP molecules causes a reduction in fluorescence anisotropy, which is used as a measure for EGFR clustering (Fig. 2). Both biparatopic VHHs are able to induce similar changes in anisotropy as EGF, indicating that biparatopic VHHs generate higher order clusters of EGFR similar to EGF (Fig. 2A). In contrast to biparatopic VHHs, binding of either monovalent or bivalent VHHs does not induce EGFR clustering (Fig. 2A). This VHH-induced clustering of EGFR was concentration dependent (Fig. 2B). Moreover, Bipar1-induced receptor clustering was lost upon addition of a 100 fold molar excess of either one of the two monovalent VHHs, Mono 1 or Mono 2 (Fig. 2C), demonstrating the importance of the binding of both EGFR-binding domains for EGFR clustering.

3.3.3. Clustering VHHs induce EGFR-internalization

As the biparatopic VHHs were shown to induce receptor clustering, they were subsequently tested for their capacity to induce receptor internalization. Internalization rate constants (k_e) were determined following the previously described method [34]. Uptake of non-agonistic monovalent VHHs is being considered as pinocytosis (k_e = 0.0025 min^{-1}). Activation of EGFR by EGF stimulates internalization up to 40 times (k_e = 0.14 min^{-1}) as compared to the pinocytosis (Fig. 3A).

The bivalent monospecific VHHs stimulated EGFR internalization slightly (Fig, 3B). However, a three times increase in EGFR internalization was observed with the biparatopic construct ($k_{e, mono}$ = 0.003 min^{-1}, $k_{e, bivalent}$ = 0.005 min^{-1} and $k_{e, Bipar1}$ = 0.009 min^{-1}) (Fig. 3B). Although directed against different epitopes, both biparatopic VHHs internalized at a similar internalization rate. Since the two biparatopic VHHs bind non-overlapping epitopes themselves, we aimed for

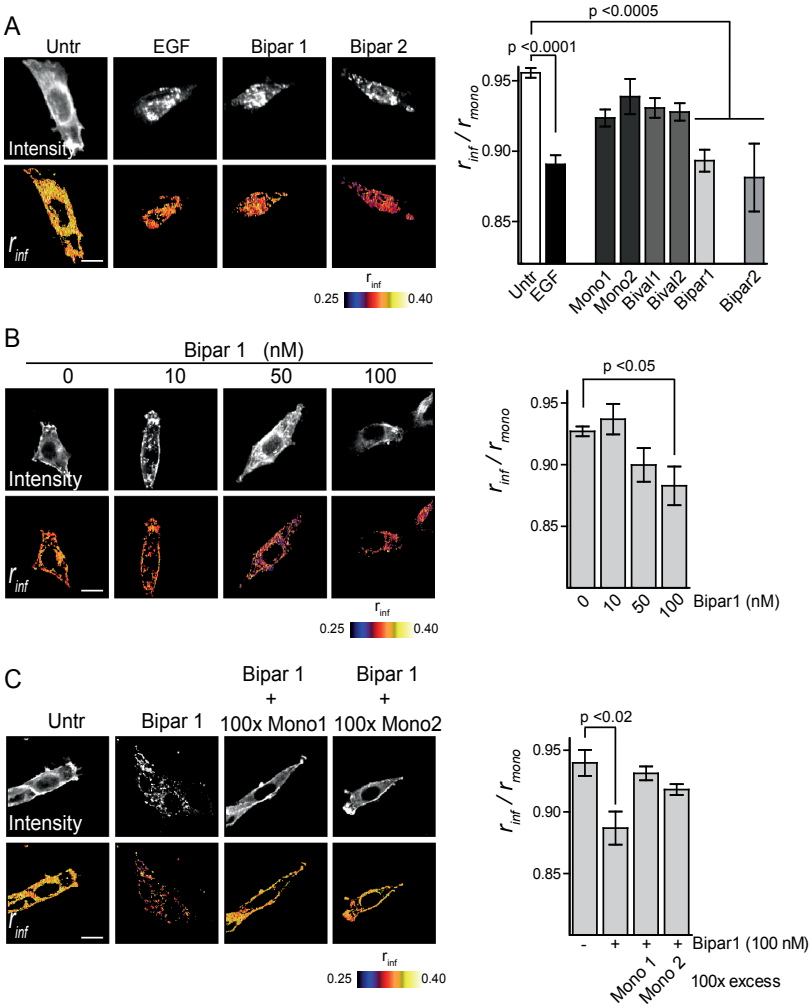

Figure 2. *Biparatopic VHHs cluster EGFR to same extend as EGF. (A) Confocal time-resolved fluorescence anisotropy imaging microscopy (CTR-FAIM) analysis of receptor clustering. NIH 3T3 2.2 cells expressing EGFR-mGFP, were seeded on glass cover slips and allowed to adhere overnight. Cells were treated with 50 nM of the indicated VHHs for 20 min or 8 nM of EGF for 10 min at 37°C and subsequently PFA-fixed. Changes in anisotropy values, due to homo-FRET, were determined as described in Materials and methods and presented in false colors. Limiting anisotropy values (r_{inf}) of EGFR-mGFP were plotted as fraction of the anisotropy value of mGFP (r_{mono}). (B) Bipar1-induced EGFR clustering is concentration dependent. EGFR-mGFP expressing cells were treated with indicated concentrations of Bipar1 for 20 min and anisotropy values were determined. (C) VHH-induced clustering of EGFR depends on binding of both epitope-binding domains. EGFR-mGFP expressing cells were treated with 100 nM Bipar1 with or without a 100-fold excess or either Mono1 or Mono2 for 20 min and anisotropy values were determined. Scale bars represent 20 µm. Error bars represent SEM with n>5.*

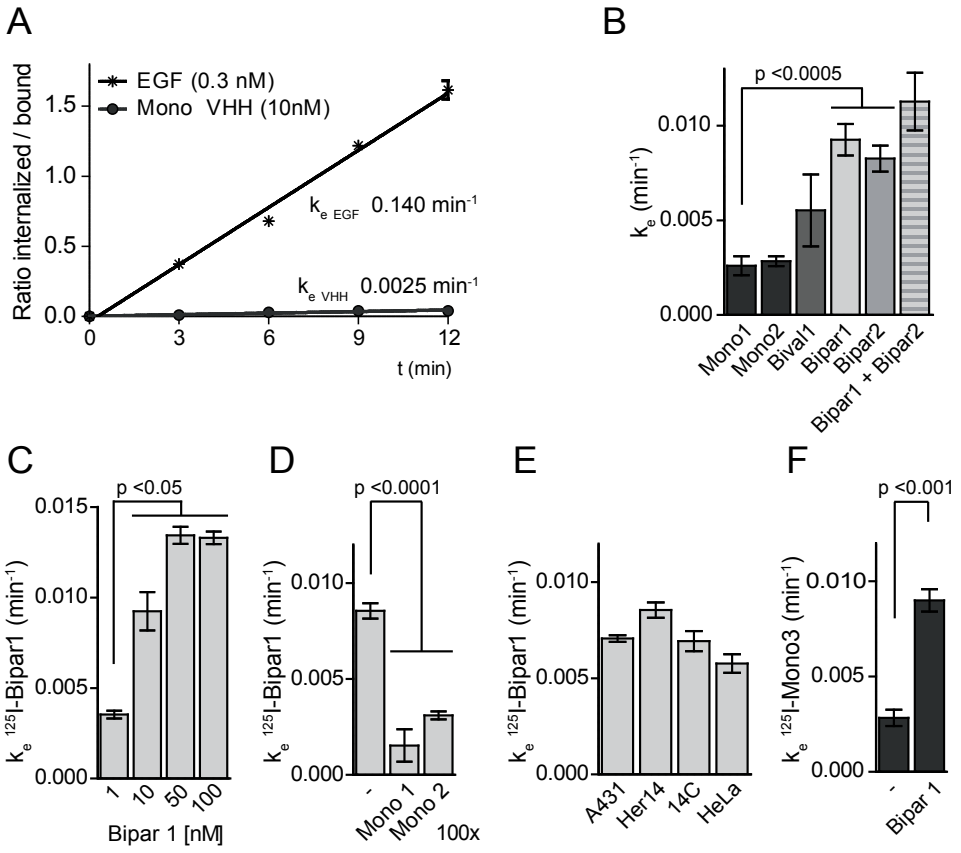

Figure 3. *EGFR clustering by biparatopic VHHs induces internalization of both receptor and VHH.(A) EGF induces rapid EGFR internalization. 10 nM of ^{125}I-labeled monovalent VHH or 0.3 nM of EGF was allowed to internalize for 3, 6, 9 and 12 minutes. Cells were stripped (bound fraction) and lysed in 1M NaOH (internalized fraction). Internalized/bound fractions were plotted in time. This data was used to determine the internalization rate constants (k_e). (B) Biparatopic VHHs internalize faster than monovalent ones. 10 nM of ^{125}I-labeled VHHs were allowed to internalize into HER14 cells for up to 12 min. In case of treatment with Bipar1 and Bipar2, a mixture of 10 nM unlabeled Bipar2 and 10 nM ^{125}I-labeled Bipar1 was used. (C) Bipar1-induced internalization rate is concentration dependent up to 50 nM. (D) Induction of internalization by biparatopic VHHs requires both EGFR binding domains. Internalization rate constants of ^{125}I-labeled Bipar1 were determined with or without 100-fold molar excess of Mono1 or Mono2. (E) The k_e of Bipar1 is independent of EGFR expression levels. Internalization rates using 10 nM of ^{125}I-labeled Bipar1 were determined in A431, HER14, 14C and HeLa cells. (F) Upon treatment with biparatopic VHHs, EGFR is internalized with a similar rate as the VHHs. The k_e of EGFR was determined with ^{125}I-EGb4 by co-incubation with 10 nM of unlabeled Mono1 or Bipar1. Error bars represent SEM.*

even faster internalization by a treatment of cells with Bipar1 and Bipar2 simultaneously. This combination did not significantly enhance the internalization rate as compared to biparatopic VHHs alone (k_e = 0.011 min^{-1}, Fig. 3B). Furthermore, internalization rate constants of Bipar1 were concentration dependent up to 50 nM, resulting in a maximum internalization rate constant of 0.013 min^{-1} (Fig. 3C). This is more than a 4 fold increase in internalization as compared to pinocytosis. Excess of either Mono1 or Mono2, which prevented clustering, similarly reduced the internalization rate constant of Bipar1 back to that of pinocytosis (Fig. 3D). This observation demonstrates that the intermolecular interactions of biparatopic VHHs are essential for biparatopic VHH-induced EGFR internalization. Moreover, rate constants of Bipar1-induced internalization were similar for cells expressing different numbers of EGFR: for high EGFR expression levels we used A431 (2.6 x 10^6 receptors/cell [35]), moderate expression levels UM-SCC-14C and HER14 (3 x 10^5 receptors/cell [36]), and low expression levels HeLa cells (5 x 10^4 receptors/cell [37]). This shows that Bipar1-induced internalization occurs irrespective of EGFR expression levels (Fig. 3E).

We so far determined internalization rate constants of the ligands. To test whether the internalization rate constants determined for the ligands corresponds to the rate constants of the EGFR itself, we used ^{125}I-labeled Mono3 (or EGb4), a non-agonistic anti-EGFR VHH that does not compete with the binding of EGF or Bipar1. Treatment with 10 nM of unlabeled Bipar1 indeed induced internalization of EGb4 with a similar rate as the ^{125}I-labeled biparatopic VHHs (Fig. 3F). This suggests that the measured internalization rate constant of Bipar-1 indeed reflects the internalization rate of the receptor itself. Taken together, these data demonstrate that extracellular clustering of EGFR by biparatopic VHHs stimulates EGFR internalization up to four times as compared to pinocytosis. This effect was seen regardless the binding specificity of the two biparatopic VHHs.

3.3.4. Clustering-induced internalization occurs via clathrin-mediated endocytosis

EGF-induced endocytosis of EGFR occurs via clathrin-mediated and clathrin-independent pathways. To determine which of these pathways is used by the VHH-induced EGFR internalization we analyzed whether we could detect any colocalization of EGFR with clathrin on the cell membrane by live cell, dual-color total internal reflection fluorescence microscopy (TIRFM). Therefore, Bipar1 or EGF was labeled with Alexa488 and applied to HER14 cells expressing RFP-clathrin. After addition of fluorescent ligand, internalization was monitored for several minutes (Fig. 4A top, Fig. S1, S2 and Movies S1 and S2). EGF clusters internalize via pre-existing clathrin coated lattices or sheets, which is in agreement with a previous publication [38]. Also the Bipar1-induced EGFR clusters internalized via pre-existing clathrin sheets. Furthermore, at the onset of colocalization with pre-existing clathrin-coated sheets, a dynamic reorganization

and accumulation of clathrin was observed (Movie S2). These data show that EGFR clusters accumulate at pre-existing clathrin-coated sheets where coated pits and vesicles are formed and then pinch off from the plasma membrane.

More evidence for a role of clathrin-mediated endoctosis (CME) in clustering-induced internalization of EGFR was obtained by over-expression of a dominant negative version of Eps15 lacking the EH-domains (Eps15ΔI). This mutant is unable to bind EGFR and instead blocks clathrin-mediated endocytosis by sequestering AP2 and CHC [39]. Over-expression of Eps15ΔI strongly inhibited Bipar1 internalization, but had no effect on internalization of EGF (Fig. 4B). This indicates that Bipar1 induced internalization completely depends on the clathrin-mediated route while an alternative clathrin-independent route exists for EGF [40, 41]. To obtain more evidence for the clathrin dependence of Bipar-induced EGFR internalization, we blocked CME by the inhibition of phosphatidylinositol 4,5-bisphosphate (PIP2) production with primary alcohols [42]. PIP2 recruits various adaptor proteins of the CME machinery. Internalization of Bipar1, Transferrin (Trf) and Cholera Toxin B (CTB) was assessed in the presence of the primary alcohol 1-butanol. While the clathrin-mediated uptake of both Bipar1 and Trf was blocked, CTB was internalized normally (Fig. S3). In contrast, the secondary alcohol 2-propanol had no effect on the internalization of either of these ligands. Furthermore, disruption of caveolin-mediated endocytosis by fillipin, completely inhibited CTB uptake, but had no effect on endocytosis of both Bipar1 and Trf, which excludes a role for caveolin in clustering-induced EGFR endocytosis (Fig. S3).

The involvement of clathrin in the Bipar-induced EGFR internalization was furthermore checked by siRNA knock downs of clathrin heavy chain (CHC), the α-subunit of adaptor protein-2 (AP2) complex and Eps15. Knock down efficiency was determined by western blotting (Fig. 4C). While knocking down CHC reduced the internalization of Bipar1 to the level of a monovalent VHH, it did not affect internalization of monovalent VHH (Fig. 4D). Furthermore, siRNA knockdown of the α-subunit of AP2 also significantly reduced the internalization rate constant of Bipar1. However, knock down of Eps15 had no effect on Bipar1 internalization, which was expected since Eps15 is involved in the ubiquitin-regulated endocytosis of EGFR (Sigismund et al., 2005). Finally, treatment of the cells with 80 nM of Dynasore, a dynamin inhibitor, also significantly inhibited the internalization of Bipar1 (Fig. 4D) [43]. This was confirmed by determining the internalization rate constant of Bipar1 and immunofluorescnce studies of Bipar1in HeLa cells stably expressing the thermosensitive mutant of dynamin, Dyn-K44A [44](Fig. 4E,F). Taken together, our experiments show that the clustering-induced internalization of EGFR occurs via the clathrin-, AP2- and dynamin-mediated internalization route. This phenomenon is referred to as clustering-induced clathrin-mediated endocytosis (CIC-ME).

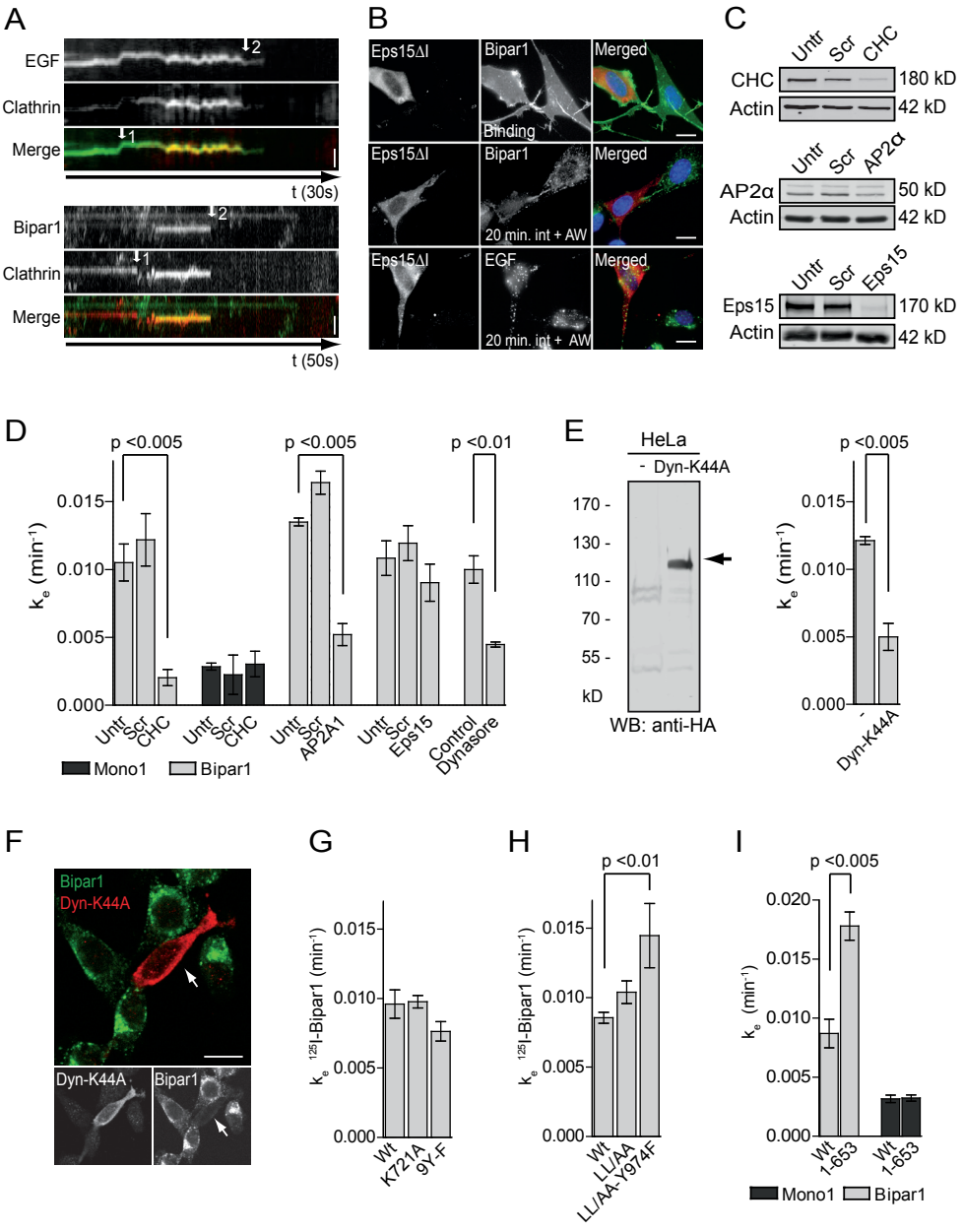
A
EGF
Clathrin
Merge
t (30s)
Bipar1
Clathrin
Merge
t (50s)
B
Eps15ΔI
Bipar1
Merged
Binding
20 min. int + AW
EGF
C
Untr
Scr
CHC
CHC
Actin
180 kD
42 kD
AP2α
50 kD
Eps15
170 kD
D
p <0.005
p <0.01
ke (min-1)
Mono1
Bipar1
Dynasore
E
HeLa
- Dyn-K44A
kD
WB: anti-HA
F
Bipar1
Dyn-K44A
G
ke 125I-Bipar1 (min-1)
Wt
K721A
9Y-F
H
LL/AA
LL/AA-Y974F
I
1-653

***Figure 4**. Clustering-induced EGFR internalization occurs via clathrin-dependent endocytosis. (A) Live cell, dual-color TIRF-M shows colocalization (arrow 1) of internalizing EGFR clusters (arrow 2) with dynamic clathrin-coated pits. Internalization of either $EGF^{Alexa488}$ or $Bipar1^{Alexa488}$ was assessed in HER14 cells expressing mRFP-Clathrin. Movies were collected in TIRF-mode for 50 seconds at 10 frames/sec. Bars represent 1 µm. (B) Clustering-induced internalization is inhibited by over expression of Eps15-ΔI. 10 nM of $Bipar1^{Alexa488}$ or 40 nM of $EGF^{Alexa488}$ was allowed to internalize for 20 min at 37°C in HER14 cells over expressing Flag-tagged Eps15-ΔI. Cells were stripped and permeabilized with saponin. Eps15-ΔI was detected with anti-Flag and Alexa555-coupled secondary antibodies. Bars represent 15 µm. (C, D) Clustering-induced internalization is clathrin, AP2 and dynamin dependent. HER14 cells were left untreated or were transfected with scrambled siRNA or siRNA against CHC, AP2α or Eps15. (C) Knock down efficiency was checked by Western blotting and actin was used as loading control. (D) The k_e of ^{125}I-Mono1 or ^{125}I-Bipar1 was determined in siRNA treated cells described in C. To test the role of dynamin, k_e of Bipar1 was determined in HER14 cells, in the presence and pretreated for 30 min with 80 µM Dynasore or DMSO. (E) Internalization rate constant of Bipar1 was determined in HeLa cells overexpressing dynamin-K44A mutant (right). Expression of dynamin-K44A was checked by western blotting (left). The overexpression of dynamin-K44A is indicated with an arrow. (F) Internalization of $Bipar1^{Alexa488}$ in cells expressing dynamin-K44A (arrow). Cells were treated as in B and dynamin-K44A was detected with anti-HA antibodies (red). Bars represent 15 µm. (G-I) The k_e of Bipar1 was determined in NIH-3T3 2.2 cells stably expressing: the kinase dead mutant (K721A) or a mutant in which 9 phospho-tyrosines were mutated into phenylalanines (9Y-F) (G), mutants lacking either one (EGFR-LL/AA) or both (EGFR-LL/AA-Y974F) AP2-binding domains (H) or a mutant lacking the complete intracellular part (EGFR 1-653) (I). Error bars represent SEM.*

3.3.5. Intracellular domain is not required for clustering-induced internalization

Activated EGFRs interact directly and indirectly with the different adaptor proteins of the CME pathway via their phosphorylated tyrosines, ubiquitinated or acetylated lysines, or other specific docking sites. Since the VHHs are not agonistic, it is unlikely that clustering-induced internalization of EGFR is dependent on kinase activity or phospho-tyrosines in the intracellular domain. To test this, internalization of Bipar1 was analyzed in NIH 3T3 2.2 cells stably expressing an EGFR mutant with an inactive tyrosine kinase domain (EGFR-K721A), or with a mutant lacking nine (phospho) tyrosine kinase substrate residues in the C-terminal tail (EGFR 9YF) (Fig. 4G). The internalization rate constants of Bipar1 in cells stably expressing these mutants were similar to those observed in cells expressing wild type EGFR, indicating that clustering-induced internalization of EGFR is independent of its kinase activity.

Besides the phospho-tyrosine mediated interactions, the AP2-complex can also bind to EGFR directly via two AP2-binding domains: a double leucine motif (LL1010/1011) and a tyrosine based motif at position 974 (YRAL) [45]. To determine whether Bipar-induced CME depends on these AP2-binding domains we tested CME of EGFR mutated at these sites. Bipar1 was still internalized in NIH 3T3 2.2 cells expressing either EGFR LL/AA or the double EGFR LL/AA-Y974F mutant (Fig. 4H). More surprisingly, Bipar1 was even internalized in cells expressing a mutant that lacked almost the complete intracellular part of EGFR (EGFR 1-653, Fig. 4I). No change in uptake of Mono1 was observed, indicating that the pinocytosis was not

affected. Taken together, these experiments show that clustering-induced CME of EGFR does not require its intracellular domain for internalization.

3.3.6. Transmembrane GG4 dimerization motif is crucial for clustering-induced endocytosis

The observations that clustering-induced internalization is independent of the intracellular part of EGFR might indicate a possible role for the transmembrane domain (TMD). To test this hypothesis, we replaced the complete TMD of EGFR by a leucine-alanine repeat (EGFR-LALA) that favors an α-helical conformation (Fig. 5A, B). In cells stably expressing the EGFR-LALA mutant, the internalization rate of Bipar1 was reduced back to that of pinocytosis (Fig. 5B). In contrast, pinocytosis, as measured with Mono1, remained unchanged. This indicates that indeed the TMD is essential for regulating clustering-induced endocytosis.

ErbB receptors have two (small)xxx(small) motifs (also called Sternberg-Gullick, GxxxG or GG4 motifs) in their TMD, indicated as the N-terminal or C-terminal TMD-dimerization motif. Such motifs form a 'groove', which stabilize TMD dimers by forming a well-packed interface through van der Waals interactions [46]. To investigate the role for the N-terminal TMD-dimerization motif in clustering-induced EGFR internalization, we replaced the two small residues (glycines) in this motif by either isoleucine (G625I) or valine (G628V) (Fig. 5A and C). Both mutations where described previously to disrupt the dimerization of TMDs [47, 48]. To test whether the C-terminal TMD-dimerization motif is also involved in this internalization, this was also mutated (A637I) or valine (G641V) (Fig. 5A and C). Cell lines stably expressing these mutant EGFRs were made and sorted for similar expression levels (Table S1). Interestingly, both TMD point mutations of the N-terminal dimerization motif completely blocked the internalization of Bipar1 (Fig. 5C). In these cells, the residual internalization rate was comparable to pinocytosis, as measured with uptake of Mono1. The C-terminal TMD mutation also affected the internalization rate of Bipar1, but not to the same extend as mutation of the N-terminal motif. Control experiments show that binding of Bipar1 to wild type EGFR or the TMD mutants (G625I, G628V) cannot be competed off by the monovalent VHHs, demonstrating biparatopic binding (Fig. S4A). Moreover, control anisotropy experiments showed that these mutants could still be clustered by either EGF or Bipar1, similar as wild type EGFR (Fig. S4A, B). Based on these results, we conclude that the TMD and more specifically, the N-terminal GG4 motif of EGFR-TMD, is crucial for clustering-induced internalization.

3.3.7. A role for the TMD GG4 motif in EGF-induced receptor internalization

If single point mutations in the TMD of EGFR have such drastic effects on clustering-induced internalization, we questioned their role in EGF-induced endocytosis of EGFR. To this end, the above described replacement of the TMD for a LALA repeat and the different point mutations

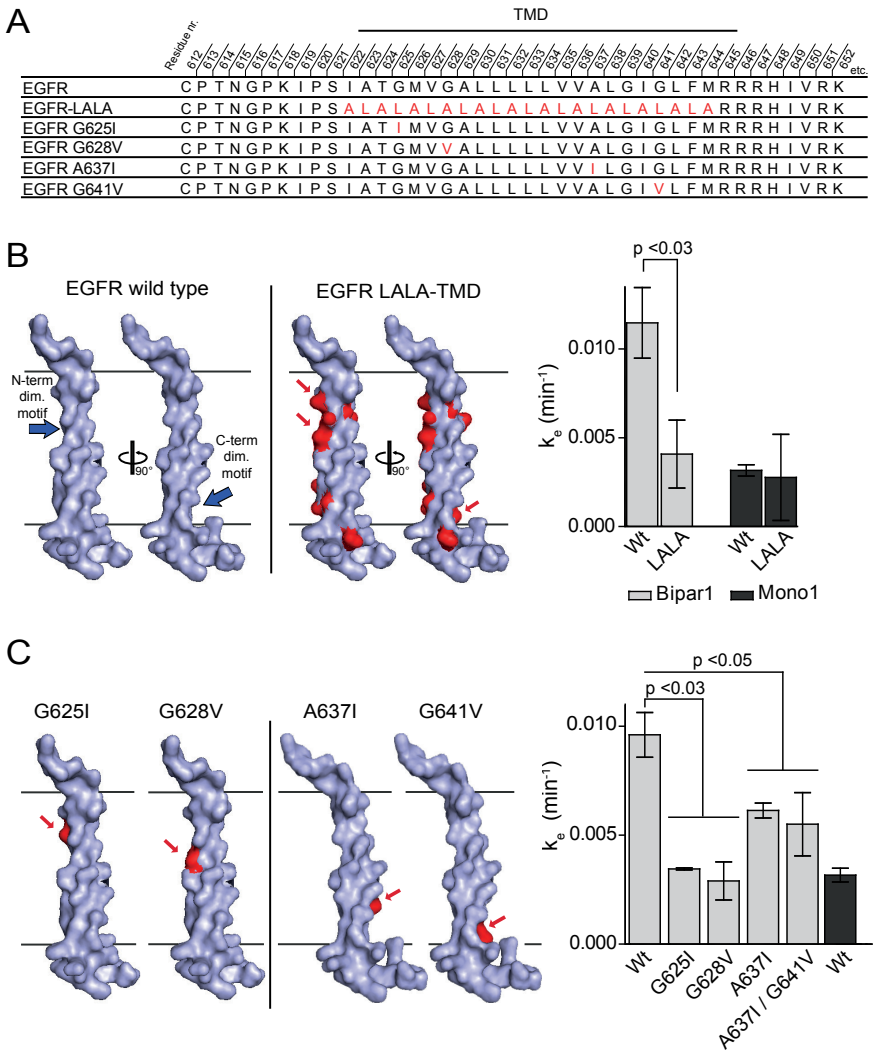

Figure 5. *Clustering-induced endocytosis is regulated by N-terminal TMD dimerization motif. (A) TMD and flanking sequences of EGFR and its LALA (TMD of a Leucine-Alanine repeat), G625I (numbering is excluding signal sequence), G628V, A637I and G641V mutants. Mutated residues are indicated in red. (B) Model of the TMD of EGFR and the LALA mutant (left). The blue arrows indicate the N-terminal and C-terminal GG4 dimerization motifs. The red arrows indicate the mutated residues (red) that fill up this groove. Domain structures were modeled using SWISS-MODEL automated homology-based modeling and PyMOL. The k_e of Mono1 or Bipar1 was determined in NIH-3T3 2.2 cells stably expressing wild type EGFR or its LALA mutant (right). (C) Models of EGFR TMDs containing the G625I, G628V, G637I and G641V mutations (left). The k_e of Mono1 or Bipar1 was determined in NIH-3T3 2.2 cells stably expressing wild type EGFR or the G625I, G628V, A637I and A637I/G641V mutants (right). Error bars represent SEM.*

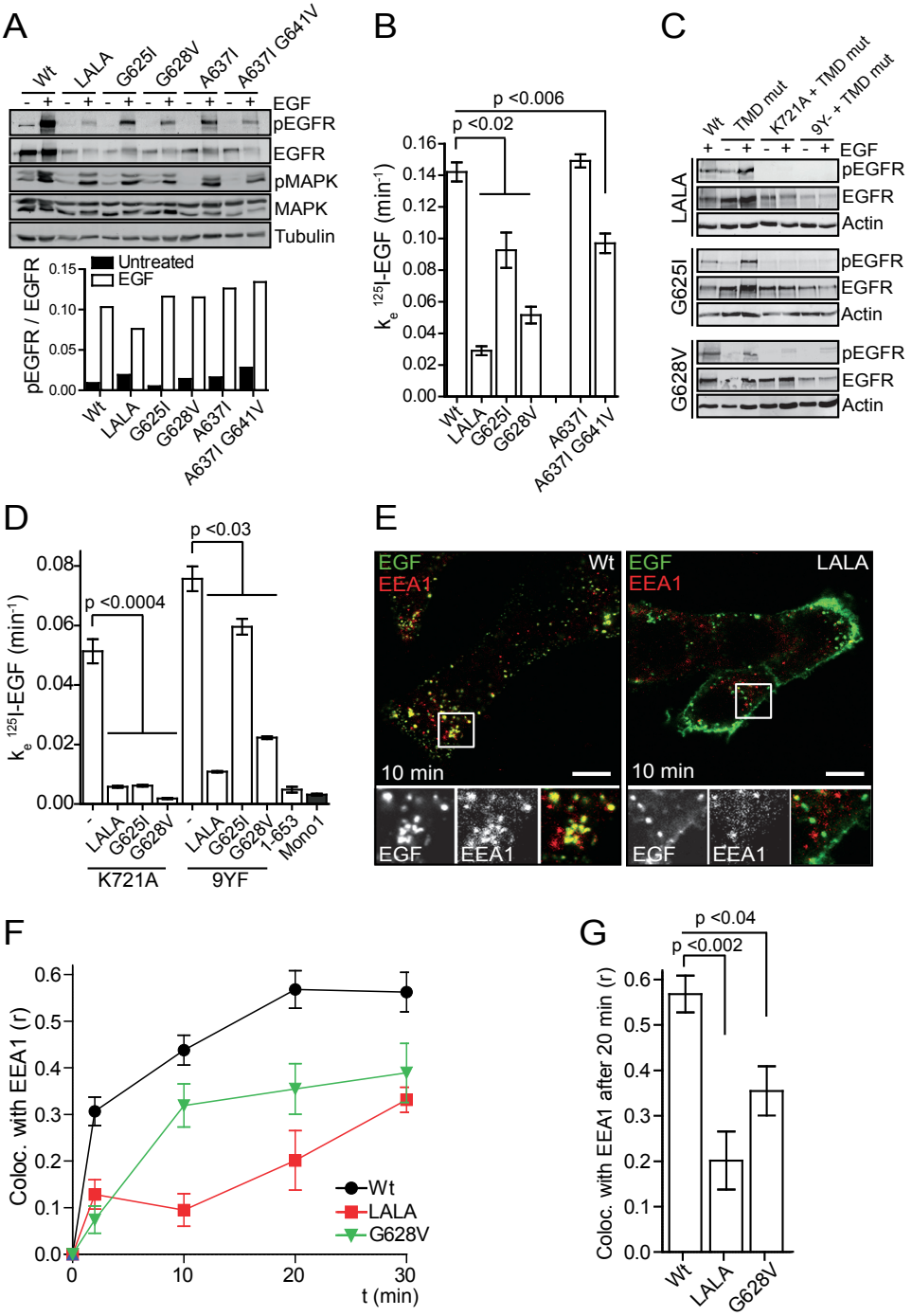
A
Wt
LALA
G625I
G628V
A637I
A637I G641V
EGF
pEGFR
EGFR
pMAPK
MAPK
Tubulin
Untreated
EGF
pEGFR / EGFR
B
p <0.006
p <0.02
k_e ^{125}I-EGF (min^{-1})
C
Wt
TMD mut
K721A + TMD mut
9Y- + TMD mut
EGF
LALA
G625I
G628V
pEGFR
EGFR
Actin
D
p <0.03
p <0.0004
k_e ^{125}I-EGF (min^{-1})
K721A
9YF
1-653
Mono1
E
EGF
EEA1
Wt
LALA
10 min
F
Coloc. with EEA1 (r)
t (min)
Wt
LALA
G628V
G
p <0.04
p <0.002
Coloc. with EEA1 after 20 min (r)

Figure 6. *Ligan-induced endocytosis is mediated by TMD dimerization and kinase activity. (A) Mutations in the TMD of EGFR do not influence EGF-induced receptor activation. NIH-3T3 2.2 cells stably expressing the indicated mutants were serum starved for 4 hr and treated with 8 nM of EGF for 10 min. Phosphorylated EGFR, total EGFR expression and α-tubulin was detected by western blotting. (B) EGF internalization is dependent on the N-terminal TMD dimerization motif. The k_e of 80 pM (0.5 ng/ml) of ^{125}I-EGF was determined in the cell lines shown in A. (C) Lack of kinase activity or phosphotyrosines were tested by western blotting. NIH-3T3 2.2 cells stably expressing either EGFR-K721A or EGFR-9Y-F mutants or variants containing the TMD mutations were treated as in A. (D) The k_e of 80 pM of ^{125}I-EGF was determined in the cell lines shown in C. Surface expression levels of these EGFR mutants are shown in Table S1. (E) Colocalization of EGF^{ALEXA488} with EEA1 after 10 minutes of treatment. Bars represent 15 μm. (F) Quantification of colocalization of EGF and EEA1 in time as determined with the Pearson coefficient. (G) Quantification of colocalization of EGF and EEA1 after 20 min. Error bars represent SEM.*

were used to investigate the internalization of EGF. None of the different TMD mutations affected EGF-induced kinase activation and downstream MAPK signaling (Fig. 6A), which is in agreement with observations that the TMD is not essential for kinase activation [15]. However, a significant reduction in the internalization rate constant of EGF was observed for the LALA-TMD and the G628V mutation (Fig. 6B). The effect of the G625I mutation was less severe although still apparent and significant. In contrast, mutations in the C-terminal TMD-dimerization motif did not affect internalization at all (A637I) or to a minor extend (A6371I/G641V) (Fig 6B). These results demonstrate a prominent role for the N-terminal TMD-dimerization motif in EGF-induced EGFR internalization and a minor role for the C-terminal TMD-dimerization motif.

In contrast to the observations for clustering-induced endocytosis, alterations in the TMD dimerization motifs did not reduce EGF-induced uptake to the level of pinocytosis. This residual internalization could very well be regulated by EGF-induced kinase activation. To test this hypothesis, we introduced the previously described TMD mutations into the EGFR kinase dead mutant (K721A), and in an EGFR mutant lacking nine tyrosine residues in the intracellular domain (9YF). Since the N-terminal mutations had the biggest effect on EGF internalization, only those were added to the K721A and 9YF mutants. Absence of tyrosine phosphorylation of these mutants was evident from Western blotting (Fig. 6C). When the TMD-mutations were combined with a kinase-inactivating mutation (K721A), a complete block of EGF-induced internalization was observed (Fig. 6D). The TMD mutations in the 9YF mutant did not completely abolish the EGF-induced internalization. This was observed with both glycine mutations of the GG4 motif. The observation that the 9YF mutant was still incompletely inhibited might suggest that additional internalization signals other than phospho-tyrosine sites become activated. These findings show that EGF-induced internalization of EGFR critically depends on both the N-terminal GG4 TMD dimerization motif and a functional kinase domain. Furthermore, we conclude that factors that are not activated by phospho-tyrosine residues are also involved in EGFR internalization.

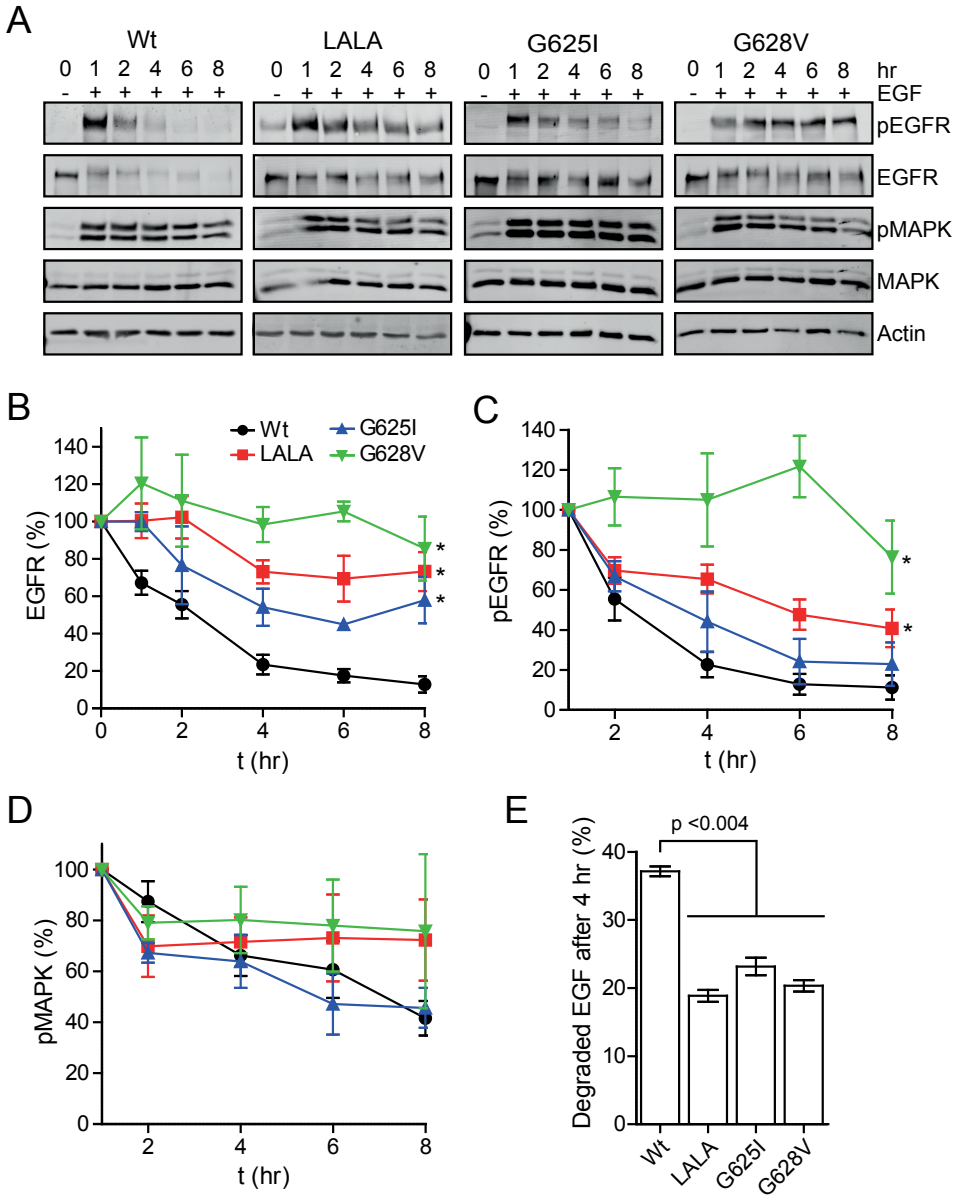
A
Wt
LALA
G625I
G628V
0 1 2 4 6 8
- + + + + +
hr
EGF
pEGFR
EGFR
pMAPK
MAPK
Actin
B
Wt
LALA
G625I
G628V
EGFR (%)
t (hr)
C
pEGFR (%)
t (hr)
D
pMAPK (%)
t (hr)
E
p <0.004
Degraded EGF after 4 hr (%)
Wt
LALA
G625I
G628V

Figure 7. *Mutation of the N-term TMD dimerization motif affects EGFR degradation and signaling. (A) NIH-3T3 2.2 cells stably expressing the indicated mutants were serum starved for 4 hr in 0% FCS and treated with 8 nM of EGF for the indicated time periods. Phosphorylated EGFR, total EGFR, phosphorylated MAPK, MAPK and α-tubulin were detected on blot as described in Figure 6. (B-D) Quantification of the blots shown in A. The total EGFR (B) and phosphorylated EGFR (C) signals were corrected for equal loading as determined with α-tubulin. The signal of phosphorylated MAPK (D) was corrected for total MAPK expression. (D) EGF degradation is inhibited in the TMD mutants. ^{125}I-labeled EGF was allowed to internalize into NIH-3T3 2.2 cells stably expressing the indicated mutants for 15 minutes, after which the medium was replaced. After 4 hr, the amount of free label was measured and plotted as a percentage of the total. Error bars represent SEM.*

So far, the effects of mutations in the TMD dimerization motifs were only detected within the first 12 minutes of endocytosis. To study the effects of these mutations on a longer term, localization of EGF to the early endosomes was assessed over time (Fig. 6E-G). In case of wild type EGFR, EGF was clearly internalized and mostly localized into EEA1 positive vesicles after 10 min (Fig. 6E). However, in cells expressing the EGFR-LALA mutant, EGF was still located on the cell surface after 10 minutes and did not colocalize with EEA1. The EGFR-LALA and EGFR-G628V mutants showed a clear delay in localization of EGF into early endosomes compared to wild type EGFR (Fig. 6F). After 20 minutes, localization of EGF into EEA1 endosomes in significantly reduced in the EGFR-LALA and EGFR-G628V mutants compared to wild type EGFR (Fig. 6G). Taken together, our experiments reveal a role for TMD dimerization motifs in the EGF-induced internalization of EGFR.

3.3.8. The N-terminal TMD dimerization motif in EGFR is required for EGF-induced negative feedback mechanism

To assess whether mutations in the TMD dimerization motif would also affect the EGF-induced downregulation, cells expressing either wild type or the TMD mutants were treated for up to 8 hr with EGF. Subsequently, the effect on total EGFR levels and downstream signaling was measured (Fig. 7). In wild type EGFR, EGF-induced activation of EGFR and downstream MAPK signaling was rapidly attenuated in time as a result of downregulation of ligand (Fig. 7E) and receptor (Fig. 7A, left panel). However, in case of the three TMD mutants, EGF-induced degradation of EGFR was significantly inhibited (Fig. 7B). More importantly, this inhibited degradation in the EGFR-LALA and G628V mutants also resulted in persistent EGFR activation and signaling towards MAPK (Fig. 7D and E). These data demonstrate that the TMD is not only important in the initial process of EGF-induced endocytosis, but also affects the subsequent events of the ligand-induced negative feedback loop. In conclusion, our experiments reveal for the first time a role for the TMD dimerization motifs of EGFR in ligand-induced endocytosis and as a consequence also in its negative feedback mechanism.

3.4. Discussion

Receptor downregulation is an important negative-feedback control mechanism for EGFR signaling. Mutations in EGFR that are related to an impaired downregulation are considered as hotspots in the induction of cancer [49, 50]. The internalization of EGFR is regulated by multiple redundant and interdependent mechanisms [22]. Binding of EGF induces several post-translational modifications of the intracellular EGFR domain, i.e. Ser/Thr phosphorylation, ubiquitination and acetylation [22, 51]. It is not surprising that many publications have addressed the involvement of these modifications in the regulation of EGFR endocytosis. However, blocking these modifications never completely prevented EGFR endocytosis suggesting the existence of other mechanism(s) involved in internalization. As EGF also induces receptor clustering, we decided to investigate a possible role for receptor clustering in the internalization process by making use of the unique properties of VHHs.

By using non-agonistic, monovalent anti-EGFR VHHs (Mono1 and Mono2) we found that in resting cells, EGFR is internalized at a very low rate via pinocytosis (Fig. 3). This occurs at a rate of 0.0025 min^{-1}, meaning that 0.25% of the initial total surface-located EGFR population is internalized per minute, requiring more than 400 min for a complete internalization of the initial surface located EGFR population ($t½ > 200$ min). This rate constant is much lower than the previously described fluid phase uptake rate of EGFR, which was determined with bivalent anti-EGFR constructs (MoAb 528), (Sunada et al., 1986; Herbst et al., 1994; Wiley et al., 1991). As shown here, receptor dimerization by bivalent constructs stimulate EGFR internalization, which may explain the higher rate of fluid phase uptake of previous studies. On the other hand, rate constants of activated EGFR are quite similar to previously published internalization rate constants (Sorkin and Goh, 2008; Wiley, 2003). As a consequence, the stimulation of internalization of active EGFRs is much larger than previously thought. Activated EGFRs are internalized at a rate >40 faster ($ke = 0.10$ min^{-1}) than the pinocytosis of EGFR, and as a result all active EGFRs are internalized within 10 min ($t½ \approx 5$ min).

By using biparatopic nanobodies we could induce EGFR clustering to a similar extend as observed with EGF but without stimulating EGFR kinase activity (Fig. 4). Clustering of EGFR using the biparatopic nanobodies resulted in EGFR internalization with internalization rate constants that were four times higher than the pinocytosis: ~1% of surface located EGFR was internalized per minute ($t½ \approx 50$ min). Interestingly, internalization rate constants of EGF-induced internalization of the kinase dead EGFR (Fig. 6D) is still five times higher than the Bipar1-induced internalization of wild type EGFR. As EGF, in contrast to the VHHs, induces more than just clustering (e.g. intra- and extra-cellular conformational changes), other ligand-induced processes might further contribute to the observed internalization. Clustering-induced internalization was recently also observed with transferrin receptors. In that study, biotinylated

receptors were expressed and extracellularly clustered using multivalent streptavidin [52]. This suggests that clustering might potentially play a more general role in the internalization of transmembrane receptors.

With different approaches we demonstrated that the clustering-induced internalization of EGFR occurs exclusively via the clathrin-, AP2 and dynamin-mediated pathway (Fig. 5). This is in contrast with a previous study showing that antibody-induced internalization of EGFR is not affected by clathrin knockdown [53]. In this study, EGFR internalization was induced by an antibody combination of anti-EGFR (C225) and donkey-anti human IgG. This may result in the formation of very large complexes that are unable to internalize via coated vesicles. In case of Bipar1-induced internalization, deletion of the intracellular domain of EGFR revealed a function for the transmembrane domain, more particular the GG4-like dimerization motifs. This motif was first described by Sternberg and Gullick and is present in the transmembrane domain of many growth factor receptors [54, 55]. The small residues of the GG4-like motif (blue arrows in Fig. 6) form 'grooves' that interact and stabilize TMD-dimers by Van der Waals interactions [56]. Interestingly, mutations in such TMD dimerization motifs have been found in relationship with the development of different diseases [16]. So far, the function of these GG4 motifs has been investigated in relation to receptor activation [15, 56, 57]. However, systematic mutagenesis of this TMD, as performed in our study and in studies from others, does not indicate a role for the TMD dimerization motif in receptor activation. In contrast, a clear function for this motif was found in the clustering-induced internalization of EGFR.

Having determined a novel role for TMD dimerization motifs in CIC-ME, we subsequently investigated whether this motif is also involved in EGF-induced internalization. Although less complete, a clear reduction in the EGF-induced receptor internalization was observed in cells expressing EGFR with the entire TMD mutated or when either of the two glycine residues of the N-terminal motif were replaced by a larger residue (isoleucine or valine) (Fig. 6). Only one additional point mutation in the kinase domain (K721A) reduced EGF-induced receptor internalization back to the level of pinocytosis (Fig. 6). This suggests that EGFR internalization is regulated at two levels. One level involves predominantly the N-terminal dimerization motif in the TMD and the other involves its kinase activity and post-translational modifications. In the wild type EGFR both clustering and kinase activity may act synergistically in stimulating the uptake of EGF.

An interesting question is how these two systems cooperate in stimulating the CME of EGFR. EGFR internalization is activated by different interdependent but also redundant internalization signals [22]. Following this idea, we suggest that internalization signals are already present in non-activated receptors, and can become active by receptor clustering. One of these signals may be found in the four positively charged amino acids at the C-terminal site just next

to its TMD: three arginines, and one histidine. Clustering of EGFR and thereby also their TMD's provides a positively charged patch just below the membrane that may function as a sink for negatively charged lipids as phosphatidylinositol 4,5-bisphosphate (PIP_2). Several papers show the requirement for PIP_2 in the formation of the clathrin-coat, for instance by binding to the AP2 subunit μ2 [58]. Secondly, ErbB receptors have two TMD dimerization motifs and disulfide crosslinking and NMR studies showed that ErbB TMDs predominantly interact via their N-terminal GG4-like motif. Interestingly, since this dimerization occurs in an angle of 46 ± 5°, such dimers might create a wedge-like structure in the plasma membrane [15, 59]. Clustering of such wedge-like structures could potentially induce a concave membrane curvature. The observations that especially the N-terminal TMD dimerization motif plays the biggest role in EGF internalization, supports this curvature hypothesis. The mechanically induced curvature can subsequently be sensed by BAR- (Bin/Amphiphysin/Rvs) domain containing proteins. As these proteins often contain interaction domains with CME adaptor proteins, recruitment of BAR-proteins to the bended membrane domain may induce local recruitment of the CME machinery. An example of such a BAR-protein is the recently identified F-BAR domain-containing Fer/Cip4 homology domain-only proteins 1 and 2 (FCHo1/2), of which involvement in the initiation of EGFR internalization has recently been suggested [60]. Taken together, different mechanisms may be activated by receptor clustering, which all could contribute to the recruitment and binding of AP2-complexes, subsequently resulting in the formation of a clathrin coat. Further post-translational modifications of the EGFR intracellular domain may provide for additional interactions with components from the CME machinery, collectively contributing to the 40 times acceleration of EGFR internalization.

Finally, the importance of the TMD dimerization motif was demonstrated for receptor down regulation. Because this mechanism is an important feature of the negative feedback mechanism, mutation of the dimerization domain results in sustained signaling. As such, mutations in the TMD may contribute to malfunctioning of all receptors containing such TMD dimerization motifs. Several mutations have been described for the Fibroblast Growth Factor Receptor (FGFR), including a G380R mutation of FGFR3 that inhibits receptor down regulation and a G388R mutation of FGFR4, which is associated with accelerated tumor progression [61, 62].
In summary, our experiments have demonstrated a novel role for the TMD dimerization motif in clustering-induced receptor internalization. Since many other receptors contain such dimerization motifs, it is interesting to investigate the role of TMD dimerization motifs in the internalization of a broader spectrum of receptors.

3.5. Acknowledgements

We would like to thank Casper Hoogenraad, Anna Akhmanova, and Ilya Grigoriev for their support. Ger Arkesteijn is acknowledged for his help with the cell-sorting and Cilia de Heus, Rachid El Khoulati, Wang Li Ching, Mohamed Kaplan and Nivard Kagie for their contribution to this work. This study was funded by the Focus & Massa project of the Utrecht University, The Netherlands, and by a grant from arGEN-X, Gent, Belgium.

3.6. References

1. Yarden, Y. The EGFR family and its ligands in human cancer. signalling mechanisms and therapeutic opportunities. *Eur. J. Cancer* 37 Suppl 4, S3-8 (2001).
2. Whitson, K. B., Beechem, J. M., Beth, A. H. & Staros, J. V. Preparation and characterization of Alexa Fluor 594-labeled epidermal growth factor for fluorescence resonance energy transfer studies: application to the epidermal growth factor receptor. *Anal. Biochem.* 324, 227-236 (2004).
3. Clayton, A. H. *et al*. Ligand-induced dimer-tetramer transition during the activation of the cell surface epidermal growth factor receptor-A multidimensional microscopy analysis. *J. Biol. Chem.* 280, 30392-30399 (2005).
4. Clayton, A. H., Tavarnesi, M. L. & Johns, T. G. Unligated epidermal growth factor receptor forms higher order oligomers within microclusters on A431 cells that are sensitive to tyrosine kinase inhibitor binding. *Biochemistry* 46, 4589-4597 (2007).
5. Clayton, A. H., Orchard, S. G., Nice, E. C., Posner, R. G. & Burgess, A. W. Predominance of activated EGFR higher-order oligomers on the cell surface. *Growth Factors* 26, 316-324 (2008).
6. Saffarian, S., Li, Y., Elson, E. L. & Pike, L. J. Oligomerization of the EGF receptor investigated by live cell fluorescence intensity distribution analysis. *Biophys. J.* 93, 1021-1031 (2007).
7. Hofman, E. G. *et al*. Ligand-induced EGF receptor oligomerization is kinase-dependent and enhances internalization. *J. Biol. Chem.* 285, 39481-39489 (2010).
8. Jura, N. *et al*. Mechanism for activation of the EGF receptor catalytic domain by the juxtamembrane segment. *Cell* 137, 1293-1307 (2009).
9. Thiel, K. W. & Carpenter, G. Epidermal growth factor receptor juxtamembrane region regulates allosteric tyrosine kinase activation. *Proc. Natl. Acad. Sci. U. S. A.* 104, 19238-19243 (2007).
10. Citri, A. & Yarden, Y. EGF-ERBB signalling: towards the systems level. *Nat. Rev. Mol. Cell Biol.* 7, 505-516 (2006).
11. Burgess, A. W. EGFR family: structure physiology signalling and therapeutic targets. *Growth Factors* 26, 263-274 (2008).
12. Garrett, T. P. *et al*. Crystal structure of a truncated epidermal growth factor receptor extracellular domain bound to transforming growth factor alpha. *Cell* 110, 763-773 (2002).
13. Groenen, L. C., Walker, F., Burgess, A. W. & Treutlein, H. R. A model for the activation of the epidermal growth factor receptor kinase involvement of an asymmetric dimer? *Biochemistry* 36, 3826-3836 (1997).
14. Ariotti, N. *et al*. Epidermal growth factor receptor activation remodels the plasma membrane lipid environment to induce nanocluster formation. *Mol. Cell. Biol.* 30, 3795-3804 (2010).
15. Lu, C. *et al*. Structural evidence for loose linkage between ligand binding and kinase activation in the epidermal growth factor receptor. *Mol. Cell. Biol.* 30, 5432-5443 (2010).
16. Li, E. & Hristova, K. Role of receptor tyrosine kinase transmembrane domains in cell signaling and human pathologies. *Biochemistry* 45, 6241-6251 (2006).
17. Madshus, I. H. & Stang, E. Internalization and intracellular sorting of the EGF receptor: a model for understanding the mechanisms of receptor trafficking. *J. Cell. Sci.* 122, 3433-3439 (2009).
18. Sorkin, A. & Goh, L. K. Endocytosis and intracellular trafficking of ErbBs. *Exp. Cell Res.* 314, 3093-3106 (2008).

19. Lai, W. H. *et al*. Ligand-mediated internalization, recycling, and downregulation of the epidermal growth factor receptor in vivo. *J. Cell Biol.* 109, 2741-2749 (1989).
20. Wang, Q., Zhu, F. & Wang, Z. Identification of EGF receptor C-terminal sequences 1005-1017 and di-leucine motif 1010LL1011 as essential in EGF receptor endocytosis. *Exp. Cell Res.* 313, 3349-3363 (2007).
21. Huang, F., Goh, L. K. & Sorkin, A. EGF receptor ubiquitination is not necessary for its internalization. *Proc. Natl. Acad. Sci. U. S. A.* 104, 16904-16909 (2007).
22. Goh, L. K., Huang, F., Kim, W., Gygi, S. & Sorkin, A. Multiple mechanisms collectively regulate clathrin-mediated endocytosis of the epidermal growth factor receptor. *J. Cell Biol.* 189, 871-883 (2010).
23. Boersma, Y. L., Chao, G., Steiner, D., Wittrup, K. D. & Pluckthun, A. Bispecific designed ankyrin repeat proteins (DARPins) targeting epidermal growth factor receptor inhibit A431 cell proliferation and receptor recycling. *J. Biol. Chem.* 286, 41273-41285 (2011).
24. Hackel, B. J., Neil, J. R., White, F. M. & Wittrup, K. D. Epidermal growth factor receptor downregulation by small heterodimeric binding proteins. *Protein Eng. Des. Sel.* 25, 47-57 (2012).
25. Friedman, L. M. *et al*. Synergistic down-regulation of receptor tyrosine kinases by combinations of mAbs: implications for cancer immunotherapy. *Proc. Natl. Acad. Sci. U. S. A.* 102, 1915-1920 (2005).
26. Spangler, J. B. *et al*. Combination antibody treatment down-regulates epidermal growth factor receptor by inhibiting endosomal recycling. *Proc. Natl. Acad. Sci. U. S. A.* 107, 13252-13257 (2010).
27. Roovers, R. C., van Dongen, G. A. & van Bergen en Henegouwen, P. M. Nanobodies in therapeutic applications. *Curr. Opin. Mol. Ther.* 9, 327-335 (2007).
28. Van Bockstaele, F., Holz, J. B. & Revets, H. The development of nanobodies for therapeutic applications. *Curr. Opin. Investig Drugs* 10, 1212-1224 (2009).
29. Muyldermans, S., Atarhouch, T., Saldanha, J., Barbosa, J. A. & Hamers, R. Sequence and structure of VH domain from naturally occurring camel heavy chain immunoglobulins lacking light chains. *Protein Eng.* 7, 1129-1135 (1994).
30. Roovers, R. C. *et al*. A bi-paratopic anti-EGFR nanobody efficiently inhibits solid tumour growth. *Int. J. Cancer* (2011).
31. Schmitz, K. R., Bagchi, A., Roovers, R. C., van Bergen En Henegouwen, P. M. & Ferguson, K. M. Structural Evaluation of EGFR Inhibition Mechanisms for Nanobodies/VHH Domains. *Structure* (2013).
32. Hofman, E. G. *et al*. EGF induces coalescence of different lipid rafts. *J. Cell. Sci.* 121, 2519-2528 (2008).
33. Bader, A. N. *et al*. Homo-FRET imaging as a tool to quantify protein and lipid clustering. *Chemphyschem* 12, 475-483 (2011).
34. Wiley, H. S. & Cunningham, D. D. The endocytotic rate constant. A cellular parameter for quantitating receptor-mediated endocytosis. *J. Biol. Chem.* 257, 4222-4229 (1982).
35. Haigler, H., Ash, J. F., Singer, S. J. & Cohen, S. Visualization by fluorescence of the binding and internalization of epidermal growth factor in human carcinoma cells A-431. *Proc. Natl. Acad. Sci. U. S. A.* 75, 3317-3321 (1978).
36. Honegger, A. M. *et al*. A mutant epidermal growth factor receptor with defective protein tyrosine kinase is unable to stimulate proto-oncogene expression and DNA synthesis. *Mol. Cell. Biol.* 7, 4568-4571 (1987).
37. Berkers, J. A., van Bergen en Henegouwen, P. M. & Boonstra, J. Three classes of epidermal growth factor receptors on HeLa cells. *J. Biol. Chem.* 266, 922-927 (1991).
38. Rappoport, J. Z. & Simon, S. M. Endocytic trafficking of activated EGFR is AP-2 dependent and occurs through preformed clathrin spots. *J. Cell. Sci.* 122, 1301-1305 (2009).
39. Benmerah, A., Bayrou, M., Cerf-Bensussan, N. & Dautry-Varsat, A. Inhibition of clathrin-coated pit assembly by an Eps15 mutant. *J. Cell. Sci.* 112 (Pt 9), 1303-1311 (1999).
40. Huang, F., Khvorova, A., Marshall, W. & Sorkin, A. Analysis of clathrin-mediated endocytosis of epidermal growth factor receptor by RNA interference. *J. Biol. Chem.* 279, 16657-16661 (2004).
41. Sigismund, S. *et al*. Clathrin-independent endocytosis of ubiquitinated cargos. *Proc. Natl. Acad. Sci. U. S. A.* 102, 2760-2765 (2005).
42. Boucrot, E., Saffarian, S., Massol, R., Kirchhausen, T. & Ehrlich, M. Role of lipids and actin in the formation of clathrin-coated pits. *Exp. Cell Res.* 312, 4036-4048 (2006).
43. Kirchhausen, T., Macia, E. & Pelish, H. E.

Use of dynasore, the small molecule inhibitor of dynamin, in the regulation of endocytosis. *Methods Enzymol.* 438, 77-93 (2008).
44. Altschuler, Y. *et al*. Redundant and distinct functions for dynamin-1 and dynamin-2 isoforms. *J. Cell Biol.* 143, 1871-1881 (1998).
45. Huang, F., Jiang, X. & Sorkin, A. Tyrosine phosphorylation of the beta2 subunit of clathrin adaptor complex AP-2 reveals the role of a di-leucine motif in the epidermal growth factor receptor trafficking. *J. Biol. Chem.* 278, 43411-43417 (2003).
46. MacKenzie, K. R., Prestegard, J. H. & Engelman, D. M. A transmembrane helix dimer: structure and implications. *Science* 276, 131-133 (1997).
47. Escher, C., Cymer, F. & Schneider, D. Two GxxxG-like motifs facilitate promiscuous interactions of the human ErbB transmembrane domains. *J. Mol. Biol.* 389, 10-16 (2009).
48. Mendrola, J. M., Berger, M. B., King, M. C. & Lemmon, M. A. The single transmembrane domains of ErbB receptors self-associate in cell membranes. *J. Biol. Chem.* 277, 4704-4712 (2002).
49. Pines, G., Kostler, W. J. & Yarden, Y. Oncogenic mutant forms of EGFR: lessons in signal transduction and targets for cancer therapy. *FEBS Lett.* 584, 2699-2706 (2010).
50. Polo, S. & Di Fiore, P. P. Endocytosis conducts the cell signaling orchestra *Cell* 124, 897-900 (2006).
51. Heisermann, G. J. & Gill, G. N. Epidermal growth factor receptor threonine and serine residues phosphorylated in vivo. *J. Biol. Chem.* 263, 13152-13158 (1988).
52. Liu, A. P., Aguet, F., Danuser, G. & Schmid, S. L. Local clustering of transferrin receptors promotes clathrin-coated pit initiation. *J. Cell Biol.* 191, 1381-1393 (2010).
53. Berger, C., Madshus, I. H. & Stang, E. Cetuximab in combination with anti-human IgG antibodies efficiently down-regulates the EGF receptor by macropinocytosis. *Exp. Cell Res.* 318, 2578-2591 (2012).
54. Sternberg, M. J. & Gullick, W. J. Neu receptor dimerization. *Nature* 339, 587 (1989).
55. Sternberg, M. J. & Gullick, W. J. A sequence motif in the transmembrane region of growth factor receptors with tyrosine kinase activity mediates dimerization. *Protein Eng.* 3, 245-248 (1990).
56. Cymer, F. & Schneider, D. Transmembrane helix-helix interactions involved in ErbB receptor signaling. *Cell. Adh Migr.* 4, 299-312 (2010).
57. Endres, N. F. *et al*. Conformational coupling across the plasma membrane in activation of the EGF receptor. *Cell* 152, 543-556 (2013).
58. Jost, M., Simpson, F., Kavran, J. M., Lemmon, M. A. & Schmid, S. L. Phosphatidylinositol-4,5-bisphosphate is required for endocytic coated vesicle formation. *Curr. Biol.* 8, 1399-1402 (1998).
59. Mineev, K. S. *et al*. Spatial structure of the transmembrane domain heterodimer of ErbB1 and ErbB2 receptor tyrosine kinases. *J. Mol. Biol.* 400, 231-243 (2010).
60. Henne, W. M. *et al*. FCHo proteins are nucleators of clathrin-mediated endocytosis. *Science* 328, 1281-1284 (2010).
61. Jezequel, P. *et al*. G388R mutation of the FGFR4 gene is not relevant to breast cancer prognosis. *Br. J. Cancer* 90, 189-193 (2004).
62. Monsonego-Ornan, E., Adar, R., Feferman, T., Segev, O. & Yayon, A. The transmembrane mutation G380R in fibroblast growth factor receptor 3 uncouples ligand-mediated receptor activation from down-regulation. *Mol. Cell. Biol.* 20, 516-522 (2000).
63. Damke, H., Baba, T., Warnock, D. E. & Schmid, S. L. Induction of mutant dynamin specifically blocks endocytic coated vesicle formation. *J. Cell Biol.* 127, 915-934 (1994).
64. Damke, H., Baba, T., van der Bliek, A. M. & Schmid, S. L. Clathrin-independent pinocytosis is induced in cells overexpressing a temperature-sensitive mutant of dynamin. *J. Cell Biol.* 131, 69-80 (1995).
65. van Dam, E. M. & Stoorvogel, W. Dynamin-dependent transferrin receptor recycling by endosome-derived clathrin-coated vesicles. *Mol. Biol. Cell* 13, 169-182 (2002).
66. Stoorvogel, W. *et al*. Sorting of ligand-activated epidermal growth factor receptor to lysosomes requires its actin-binding domain. *J. Biol. Chem.* 279, 11562-11569 (2004).
67. Bader, A. N., Hofman, E. G., van Bergen En Henegouwen, P. M. & Gerritsen, H. C. Imaging of protein cluster sizes by means of confocal time-gated fluorescence anisotropy microscopy. *Opt. Express* 15, 6934-6945 (2007).
68. Bader, A. N., Hofman, E. G., Voortman, J., en Henegouwen, P. M. & Gerritsen, H. C. Homo-FRET imaging enables quantification of protein cluster sizes with subcellular resolution. *Biophys. J.* 97, 2613-2622 (2009).

69. Salacinski, P. R., McLean, C., Sykes, J. E., Clement-Jones, V. V. & Lowry, P. J. Iodination of proteins, glycoproteins, and peptides using a solid-phase oxidizing agent, 1,3,4,6-tetrachloro-3 alpha,6 alpha-diphenyl glycoluril (Iodogen). *Anal. Biochem.* 117, 136-146 (1981).
70. Motley, A., Bright, N. A., Seaman, M. N. & Robinson, M. S. Clathrin-mediated endocytosis in AP-2-depleted cells. *J. Cell Biol.* 162, 909-918 (2003).
71. Fallon, L. *et al*. A regulated interaction with the UIM protein Eps15 implicates parkin in EGF receptor trafficking and PI(3)K-Akt signalling. *Nat. Cell Biol.* 8, 834-842 (2006).
72. Schumacher, C. *et al*. The SH3 domain of Crk binds specifically to a conserved proline-rich motif in Eps15 and Eps15R. *J. Biol. Chem.* 270, 15341-15347 (1995).
73. Roovers, R. C. *et al*. Efficient inhibition of EGFR signaling and of tumour growth by antagonistic anti-EFGR Nanobodies. *Cancer Immunol. Immunother.* 56, 303-317 (2007).

3.7. Supplementary information

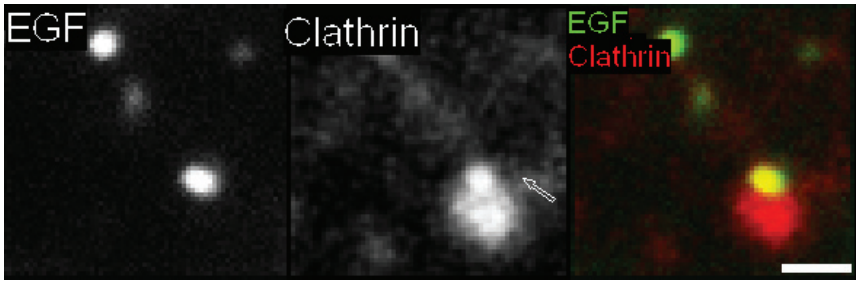

Movie S1. *Internalization of EGF via a clathrin-coated pit. Internalization of EGF-Alexa488 (green) was analyzed in HER14 cells expressing mRFP-clathrin (red). Movie was collected in TIRF mode for 30 sec at 10 frames/sec. Bar is 1µm.*

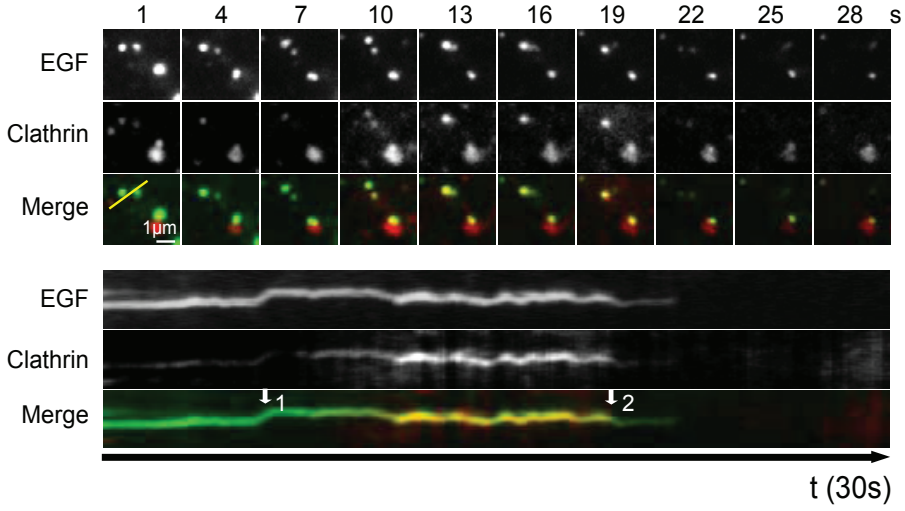

Figure S1. *Analysis of EGF internalization via coated pit. Screen shots of TIRF-M Movie 1 showing internalization of EGF. The bottom panel shows the kymographs of the indicated area (yellow line) generated for both channels separately and merged. Kymographs were generated using MetaMorph 7.7.5 software (Molecular Devices). Arrow1 indicates colocalization of EGF with clathrin and arrow 2 indicates pinching off from the plasma membrane.*

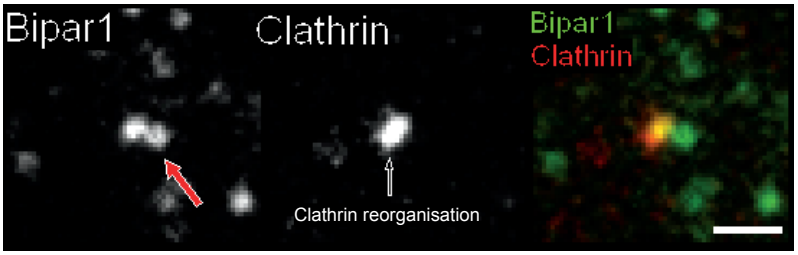

Movie 2. *Internalization of Bipar1 via a clathrin-coated pit. Internalization of Bipar1-Alexa488 (green) was analyzed in HER14 cells expressing mRFP-clathrin (red). Movie was collected in TIRF mode for 50 sec at 10 frames/sec. Bar is 1µm.*

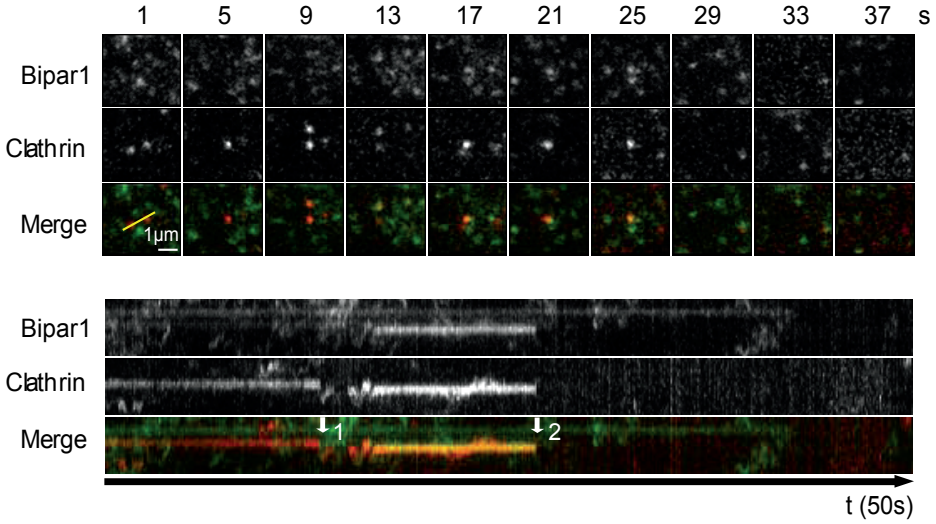

Figure S2. *Analysis of Bipar1 internalization via coated pit. Screen shots of TIRF-M Movie2 showing internalization of Bipar1. The bottom panel shows the kymographs of the indicated area (yellow line) generated for both channels separately and merged. Kymographs were generated using MetaMorph 7.7.5 software (Molecular Devices).*

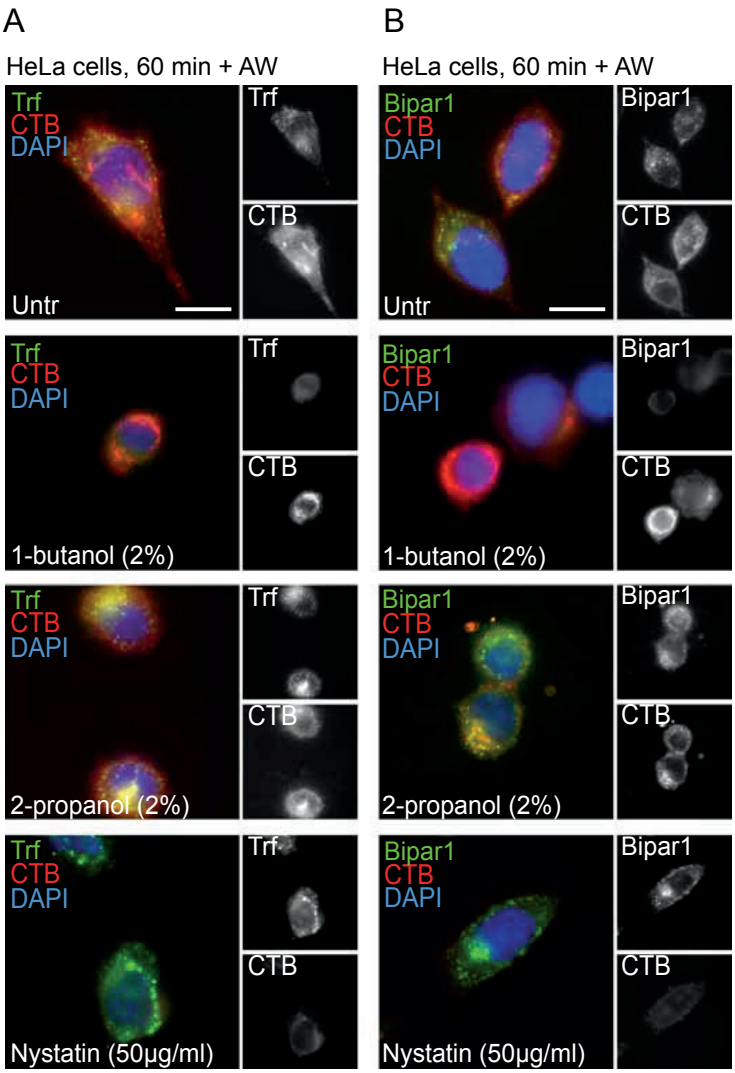

Figure S3. *Bipar1 internalization is dependent on PIP2 but independent of caveolin. PIP2 production and thereby clathrin-mediated endocytosis was blocked by pre-treatment with 2% 1-butanol for 2 min. As controls, cells were either left untreated or were treated with 2% 2-propanol. For inhibition of caveolin-mediated endocytosis, 14C cells were pre-treated with 50 µg/ml Nystatin for 2 min. Bipar1-Alexa488 or Transferrin-Alexa488 (Trf) were prebound together with Cholera toxin B-Alexa555 (CTB) to cells on ice and were allowed to internalize in the presence of 1-butanol, 2-propanol or Nystatin for 60 min. Bound ligands were removed by acid wash and cells were fixed in 4% PFA. Bar is 15 µm.*

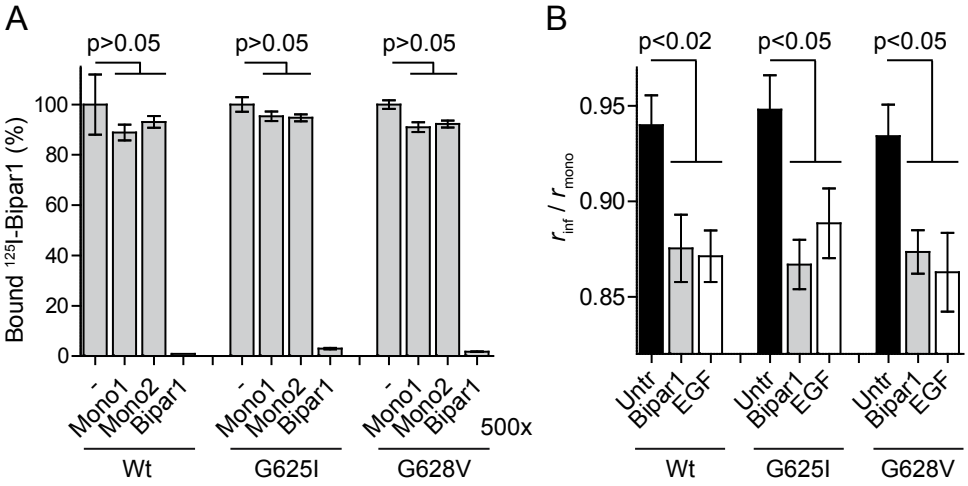

Figure S4. *Bipar1 and EGF induces clustering of EGFR TMD mutants. A. Bipar1 binds to EGFR TMD mutants with both epitope-binding domains. 125I-Bipar1 with or without a 500x excess of unlabeled Mono1, Mono2 or Bipar1 was allowed to bind cells stably expressing EGFR wt or the TMD mutants for 2h on ice. Note that competition is only obtained with excess Bipar1.B. Both Bipar1 and EGF induce clustering of EGFR TMD mutants. Cells expressing mGFP-tagged EGFR wt or TMD mutants were incubated with 10 nM of Bipar1 for 20 min and subsequently fixed in 4% PFA. The limiting average anisotropy (rinf) was determined as described in the Materials and methods and was plotted as fraction of the anisotropy value of mGFP (rmono). Error bars represent SEM with n>5.*

Table S2

	molecules/cell	SD
HER14	2.7E+05	7.3E+03
LALA	1.8E+05	3.9E+04
1-653 LALA	3.2E+05	6.6E+03
K721A LALA	1.3E+05	2.6E+03
9Y LALA	1.0E+05	7.6E+03
G625I	2.8E+05	6.1E+03
1-653 G625I	3.9E+05	8.5E+03
K721A G625I	5.8E+05	1.1E+05
9Y G625I	2.3E+05	1.0E+04
G628V	5.4E+05	3.2E+04
1-653 G628V	4.2E+05	1.6E+04
K721A G628V	5.1E+05	1.3E+04
9Y G628V	2.5E+05	6.9E+03

Chapter 4

EGFR clustering induces clathrin-mediated endocytosis followed by ubiquitin-independent lysosomal degradation

Raimond Heukers[1], Cilia de Heus[1], Ian Kercher[1], Farzad Fereidouni[2†], Arjen Bader[2‡], Hans Gerritsen[2], Paul M. P. van Bergen en Henegouwen[1]

[1] Cell Biology, Department of Biology, Utrecht University, Utrecht, The Netherlands
[2] Molecular Biophysics, Utrecht University, Utrecht, The Netherlands

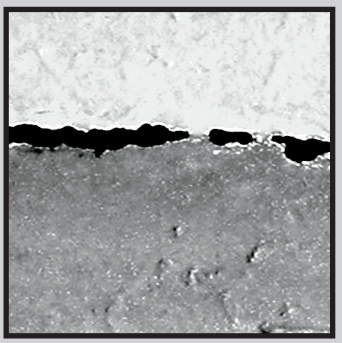

Abstract

The epidermal growth factor receptor (EGFR) is overexpressed on a variety of cancers and is therefore a good target for cancer therapy. Recently, antibody combinations and biparatopic or triepitopic antibody constructs have been introduced to inhibit cancer cell proliferation by stimulating EGFR downregulation. We have previously shown that biparatopic nanobodies induce EGFR clustering leading to clustering-induced clathrin-mediated endocytosis (CIC-ME), requiring transmembrane (TMD) dimerization motifs of EGFR. In the present study, we addressed the molecular mechanism behind triepitopic antibody-induced EGFR downregulation. Our results show that triepitopic constructs induce EGFR clustering to a similar extent as EGF. Antibody-induced EGFR clustering induces CIC-ME, independently of kinase activity but completely dependent on the TMD of EGFR. CIC-ME subsequently resulted in lysosomal degradation of the receptor, which occurred in the absence of receptor phosphorylation or ubiquitination. Our data reveals a novel mechanism for receptor sorting to lysosomes, which is regulated by EGFR clustering.

4.1. Introduction

The epidermal growth factor receptor (EGFR, HER1 or ErbB1) is a transmembrane receptor tyrosine kinase that, together with its family members HER2, HER3, and HER4 belongs to the ErbB-family [1]. Activation of EGFR results in signaling towards proliferative and anti-apoptotic pathways [2-4]. This ligand-induced signaling is immediately counteracted by a negative feedback mechanism consisting of rapid internalization via clathrin-dependent and independent endocytosis followed by lysosomal degradation of the receptor/ligand complex [5-8]. The receptors of the ErbB family are found overexpressed or deregulated in various types of cancer and this is correlated with poor prognosis [9]. Besides small molecule inhibitors, several monoclonal antibodies against ErbB receptors have been developed in the last decades and some have already found their way into the clinic (i.e. Cetuximab and Panitumumab) [10]. However, results obtained with such therapies are not always successful and leave opportunities for improvements.

One such improvement is based on the observation that receptor downregulation from the plasma membrane by combinations of antibodies and multi-epitopic constructs like biparatopic or triepitopic antibody-fibronectin fusion constructs enhances the anti-tumor efficacy [11-14]. This antibody-induced receptor downregulation is already observed with receptors like EGFR, HER2 and transferrin receptor (TfR) [11-13, 15-17]. In addition, crosslinking of cetuximab by anti-human IgG antibodies also efficiently induced EGFR downregulation [18]. In case of EGFR, most of these approaches induce a rapid internalization of the receptor without activating its kinase. This means that other, kinase independent mechanisms are responsible for the observed downregulation of EGFR from the membrane. Currently, the mechanism behind antibody-induced receptor downregulation is unclear, but is thought to involve receptor clustering on the plasma membrane followed by an intracellular block of receptor recycling [12, 13, 15, 16].

Previously, we have studied the effect of extracellular clustering on EGFR endocytosis by using biparatopic antibody-formats constructed from llama antibody fragments (VHHs or Nanobodies) [19]. EGFR clustering, as detected by fluorescence anisotropy imaging, induced EGFR internalization up to 4-fold. Clustering-induced internalization occurred via clathrin-mediated endocytosis (CIC-ME) and was completely dependent on the transmembrane domain (TMD) of EGFR. The TMD of all the members of the ErbB family of receptors contain two dimerization motifs, also known as GG4-like, GxxxG or Sternberg-Gullick motifs [20-22]. In EGFR, these motifs are designated as the N-terminal (Gly625 to Gly628) and the C-terminal (Ala637 to Gly 641) TMD dimerization motif [23]. CIC-ME via biparatopic VHHs was previously shown to be particularly dependent on the N-terminal dimerization motif. This correlates well with cysteine cross-linking data showing that during the first steps of ligand-induced internalization (within the first 5 min), mainly the N-terminal motifs of EGFR TMDs interact [24].

Here, we have investigated the mechanism of antibody-induced downregulation of

EGFR in more detail by using the previously published triepitopic antibody-fusion constructs [13]. These constructs very efficiently induce receptor sequestering from the plasma membrane without activating the kinase of EGFR. The ability of the triepitopic constructs to induce receptor clustering was assessed by determining limiting anisotropy levels (r_{inf}) by confocal homo-FRET imaging. Clustering-induced internalization of EGFR and the involvement of its kinase activity, clathrin-mediated endocytosis and the TMD dimerization motifs in this process were tested by confocal immunofluorescence microscopy. In order to study the intracellular fate of the receptor upon clustering-induced internalization, the sub-cellular localization, total protein and post-translational modifications of EGFR were determined. We demonstrate that clustering-induced EGFR downregulation is independent of receptor phosphorylation or ubiquitination, which suggests a novel mechanism for EGFR sorting.

4.2. Materials and methods

4.2.1. Cell lines

The EGFR negative murine fibroblast cell line NIH 3T3 clone 2.2 was obtained from ATCC (LGC Standards, Germany). The HER14 cells that stably express human EGFR are derived from NIH 3T3 clone 2.2 [25]. All cell lines were cultured in Dulbecco's modified Eagle's medium (DMEM) (Gibco, Invitrogen, United Kingdom) supplemented with 8% FCS (v/v), 100 U/ml penicillin, 100 µg/ml streptomycin, and 2 mM L-glutamine (PAA, Germany) at 37°C in a 5% CO_2- and under a humidified atmosphere. NIH 3T3 2.2 cells stable expressing the different EGFR-mutants (EGFR-K721A, EGFR-9Y-, EGFR-G628V and EGFR-A637I) or EGFR-mGFP were described previously [19, 26].

4.2.2. Antibodies

The triepitopic antibody constructs directed against the ectodomain of EGFR were constructed, described and kindly provided by Jamie B. Spangler and Dane K. Wittrup (Department of Biological Engineering, Massachusetts Institute of Technology, Cambridge, MA, USA) [13].

4.2.3. DNA Constructs

Dynamin2-K44A construct was kindly provided by respectively Alexandre Benmerah (Institut Cochin, Paris, France) and Sandra Schmid (UT Southwestern Medical Center, Dallas, Texas). Overexpression of the non-functioning Dynamin2-K44A mutant, blocks the pinching off of vesicles from the plasma membrane [27]. HER14 cells were transfected with Fugene HD (Roche Diagnostics, The Netherlands) according to the manufacturer's protocol and cells were used for assays 48 h after transfection.

4.2.4. Homo-FRET anisotropy measurements

The confocal time resolved anisotropy imaging setup and homo-FRET method that was used here were published previously [28, 29]. In short, a 473 nm solid state diode laser (Becker & Hickl, BDL-473-SMC) with a pulse repetition rate of 80 MHz polarized by a linear polarizer (Meadowlark,Frederick, CO, USA) was coupled into a confocal microscope (Nikon C1, Japan). The light was focused on the sample by a 60x water immersion objective (NA = 1.2, Nikon, Japan). Depolarization of excitation light due to high NA of the objective was reduced by under-filling its back aperture. Since the pinhole is located in the emission path only, the resolution was not affected. The emission is detected by a 515/30 nm band pass filter and a broadband polarizing beam splitter cube (PBS, OptoSigma, Santa Ana, CA, USA) was used to split the emission in a parallel and a perpendicular channel with respect to the excitation light. The signal was detected with two high quantum efficiency PMTs (Hamamatsu H7422P-40). Calibration of the system was preformed with GFP in 50/50 glycerol/ buffer and an aqueous Fluorescein solution, as described previously.

4.2.5. Immunofluorescence

$EGF^{Alexa488}$ was obtained from Invitrogen. One day before the assay, cells were seeded on cover slips and allowed to adhere overnight. Cells were serum starved for 4 hr in 0% FCS and incubated with 8nM of $EGF^{Alexa488}$ or 25 nM of triepitopic constructs for the indicated time at 37ºC. Cells were washed and fixed in 4% paraformaldehyde and autofluorescence was quenched with 50 mM NH_4Cl. Bound/internalized antibodies were stained after permeabilization in 0.1% Triton-X100 by incubation with Alexa488-conjugated rabbit-anti-human IgG antibodies (Invitrogen). Late endosomes and lysosomes were stained with Lysotracker Red (Invitrogen) according to the manufacturer's protocol. Nuclear staining was performed with DAPI (Roche, The Netherlands) and samples were mounted in Slowfade (Invitrogen). Chlorpromazine (CPZ) was kindly provided by Marcel A.G. van der Heyden (Medical Physiology, Division of Heart and Lungs, UMC Utrecht, The Netherlands). Images were obtained using a Zeiss LSM700 confocal microscope (Carl Zeiss Microscopy GmbH, Germany) equipped with and 63x oil immersion objective (NA 1.4).

4.2.6. EGFR phosphorylation and degradation

Phosphorylation of EGFR was determined by western blotting as described previously [30]. In short, for the phosphorylation assay, cells were serum starved overnight in 0% FCS in DMEM and subsequently treated with 8 nM of EGF or 25 nM of the triepitopic constructs for 10 min at 37˚C. For the degradation assay, cells were treated with EGF or the triepitopic constructs in complete medium for 4 hr. After the treatments, the cells were lysed in reducing sample buffer (50 mM Tris-HCl, pH 6.8, 10% glycerol, 100 mM DTT, 2% SDS and 0.01% bromophenol

blue) and the samples were subjected to SDS-PAGE (BioRad) and western blotting to PVDF membrane. Phosphorylation of EGFR was detected with anti-pEGFR (against phosphorylated tyrosine 1068) antibodies (Cell Signaling Technology, Danvers, Massachusetts) and total EGFR levels were determined with anti-EGFR (clone c74B9, Cell Signaling Technology). Equal loading was checked with anti-tubulin (DM1A, Millipore). Antibody binding to blot was detected with IRDye680- or IRDye800-conjugated secondary antibodies (LI-COR Biosciences, Lincoln, Nebraska) followed by quantification on an Odyssey Infrared Imager (LI-COR Biosciences).

4.2.7. Ubiquitination

One day before the assay, cells were seeded in a 6-wells plate after which they were serum starved o/n in 0% FCS /DMEM/P/S. Cells were stimulated with either 8 nM of EGF or 25 nM of HND+LCA construct for 15 min at 37°C. Then the cells were washed with ice cold PBS and lysed in mild TX-100 lysis buffer (50 mM Tris-HCl pH 7.5, 150 mM NaCl, 1% Triton-X100, supplemented with complete protease inhibitor (Roche) and 10 mM of N-ethylmaleimide) for 10 min on ice. The cells were scrapped and the nuclear fraction was spun down. For capturing the EGFR, the supernatant was pre-incubated with 1 µg of HND+LCA construct for 2 hr at 4°C followed by incubation with sepharose-A beads for 1 hr at 4˚C. The beads were washed with lysis buffer and re-suspended in reducing sample buffer. The samples were boiled for 5 minutes and then used for western blotting as described above. Ubiquitinated proteins were detected on blot using mouse-anti-ubiquitin (clone P4D1, Santa Cruz Biotechnology).

4.3. Results

4.3.1. Triepitopic constructs cluster EGFR and internalize without activating the receptor

In order to gain more insight in the mechanism behind antibody-induced EGFR internalization and degradation, we studied the uptake and degradation route of EGFR using four variants of recently published triepitopic antibody-fibronectin fusion constructs (Fig. 1A) [13]. These constructs consist of an anti-EGFR IgG backbone (C225/Cetuximab) to which different anti-EGFR fibronectin subunits (called A, B and D) were fused to the N-terminus of the heavy chain and the C-terminus of the light chain. These antibody-fibronectin fusion constructs contain 6 epitope-binding domains, which are able to bind to different epitopes of the extracellular domain of EGFR.

The ability of these multi-epitopic antibody constructs to induce clustering of EGFR was tested by using the previously published homo-FRET or anisotropy assay [28, 29]. As a control for EGFR clustering, the limiting fluorescence anisotropy (r_{inf}) was determined in cells expressing EGFR-mGFP treated with 8 nM of EGF (Fig. 2) [26, 31]. The higher order clustering of the receptor,

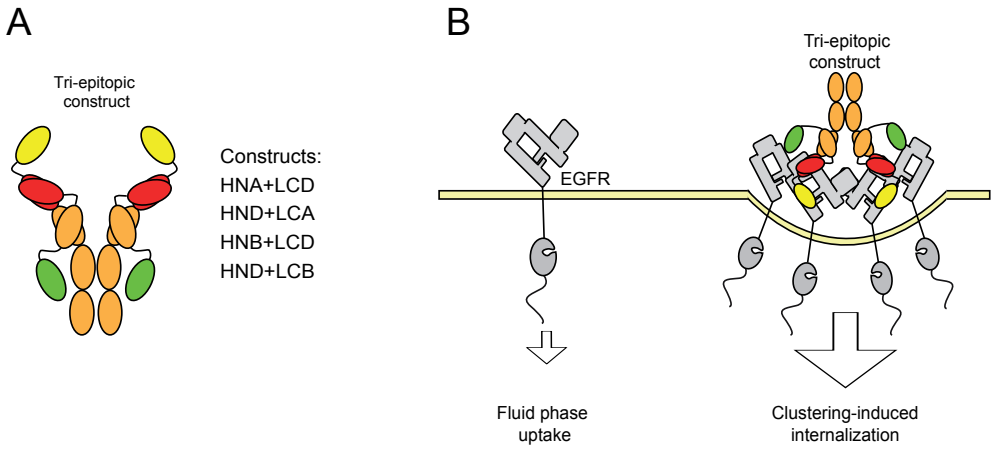

Figure 1. *Graphical representation of clustering-induced endocytosis of EGFR by the triepitopic antibody fusion construct. A. The triepitopic antibody fusion constructs consists of a C225 (Cetuximab) of which the backbone is indicated in orange and the epitope-binding domains in red, to which three types of fibronectin domains directed against EGFR (designated as A, B or D, indicated in green or yellow) were fused to either the N-terminus of the heavy chain or the C-terminus of the light chain. B. The multi-epitopic nature of the triepitopic construct enables the formation of EGFR clusters at the plasma membrane, leading to its internalization.*

as induced by EGF, is indicated by a decrease in relative anisotropy from ~0.97 to ~0.89 (r_{inf}/ $r_{mono,}$ Fig. 2B). Treatment of these cells with a concentration range of the triepitopic constructs also resulted in a decrease in limiting anisotropy. Upon treatment with three of the four constructs (HNA+LCD, HND+LCA and HNB+LCD), this decrease was comparable to that observed with EGF, indicating a similar level of higher order clustering. In contrast, HND+LCB was not that potent in clustering EGFR and only resulted in a small decrease of the relative fluorescence anisotropy to 0.93 (r/r_{mono}). This data indicates that most of the triepitopic constructs are indeed able to cluster EGFR and to a similar extend as observed with EGF.

To test whether EGFR clustering was associated by enhanced endocytosis of EGFR, we studied the internalization by confocal immunofluorescence microscopy, like was done previously by Berger et al. (Fig. 3A) [18]. The natural ligand of EGFR, EGF, was internalized very efficiently at 37°C, which was determined by the appearance of an intracellular endosomal staining pattern. In contrast, at 4°C, no internalization was observed. Similarly to what was observed with EGF, all four triepitopic constructs induced the formation of fluorescently stained endosomes after 40 minutes of incubation.

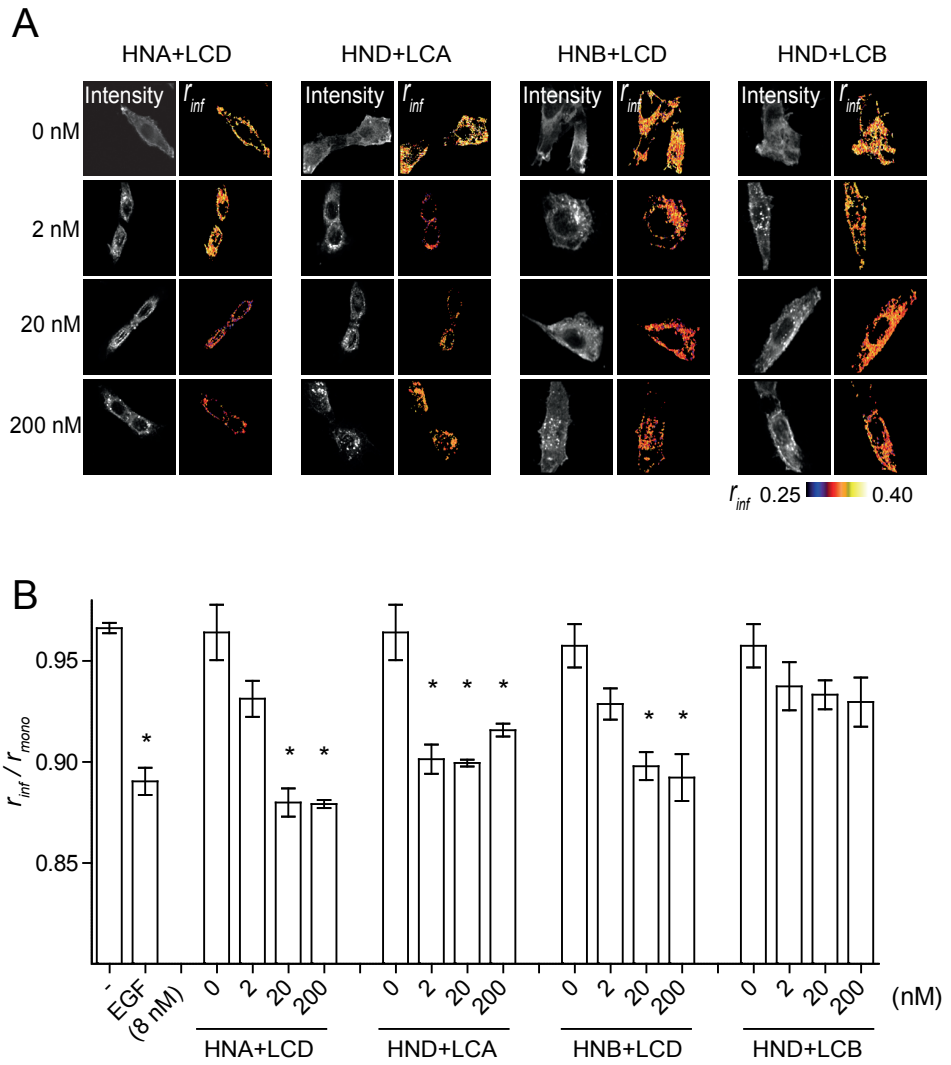

Figure 2. *Triepitopic antibody-fusions induce EGFR clustering. A. Confocal time-resolved fluorescence anisotropy imaging microscopy (CTR-FAIM) analysis of receptor clustering. NIH 3T3 2.2 cells expressing EGFR-mGFP, were seeded on glass cover slips and allowed to adhere overnight. Cells were treated with the indicated concentration of the triepitopic constructs for 20 min or 8nM of EGF for 10 min at 37°C and subsequently washed with PBS and PFA-fixed. Anisotropy values, due to homo-FRET, were determined as described in materials and methods and presented in false colors. B. Anisotropy values (r_{inf}) of EGFR-mGFP were plotted as fraction of that of monomeric mGFP (r_{mono}). * indicates $p<0.001$. Error bars represent SEM, where n=4.*

Previously, the triepitopic constructs showed strong EGFR downregulation capacity without being agonistic [13]. To confirm whether the observed receptor clustering and internalization takes place without receptor activation, phosphorylation of EGFR was assessed by western blotting (Fig. 3B). Compared to the strong EGFR activating effect of EGF, the triepitopic antibody constructs induced no or only minor receptor phosphorylation. Treatment of the cells with the antibody constructs was confirmed by the appearance of antibody bands on western blot when incubated with anti-IgG antibodies. Taken together, the triepitopic constructs are indeed capable of clustering EGFR very efficiently and inducing its internalization without being agonistic. Therefore, these constructs are considered to be useful as tools to study the molecular determinants for antibody-induced receptor downregulation.

4.3.2. Receptor clustering via triepitopic antibodies induces TMD-dependent CIC-ME

As a first step in studying the mechanistic requirements for antibody-induced clustering-induced receptor downregulation, internalization of one of the triepitopic constructs (HNA+LCD) was tested in cells expressing either the kinase dead EGFR mutant (K721A) or the mutant in which the 9 phospho-tyrosines were mutated to phenylalanines (9Y-F) (Fig. 3C). In both cases, a clear uptake of HNA+LCD was observed, suggesting a trivial role for the kinase or the phosphotyrosines. This is in good correlation with the lack of agonistic properties of these constructs. To test whether clustering-induced, kinase-independent internalization was clathrin-mediated, uptake of HNA+LCD was assessed in HER14 cells treated with an inhibitor of clathrin-mediated endocytosis, chlorpromazine (CPZ) (Fig. 3D). CPZ stabilizes clathrin coats on intracellular endosomes and thereby prevents the formation of new clathrin-coated vesicles at the plasma membrane [32]. Inhibition of clathrin-mediated endocytosis markedly reduced the uptake of HNA+LCD, as indicated by the absence of an intracellular endosomal staining pattern. To test the role of dynamin in this process, uptake was also assessed in cells overexpressing a non-functioning dynamin mutant (dynamin-K44A, Fig. 3E). A reduced uptake of HNA+LCD was observed in cells expressing the dynamin mutant, compared to the normal uptake in the non-transfected cells. Taken together, these data show that the triepitopic constructs internalize kinase-independently via clathrin- and dynamin- mediated endocytosis.

Previous work already demonstrated an essential role for the TMD dimerization motif in kinase-independent, clustering-induced internalization of EGFR [19]. To test whether the TMD of EGFR is also involved in internalization induced by the large clusters that are putatively induced by the triepitopic constructs, internalization was assessed in two cells lines stably expressing EGFR TMD mutants EGFR-G628V and EGFR-A637I (Fig. 3F). In case of the EGFR-G628V mutant the “groove” of the N-terminal TMD dimerization motif was filled by replacing the small glycine by the larger amino acid valine. Similarly, in the A637I mutant, the C-terminal

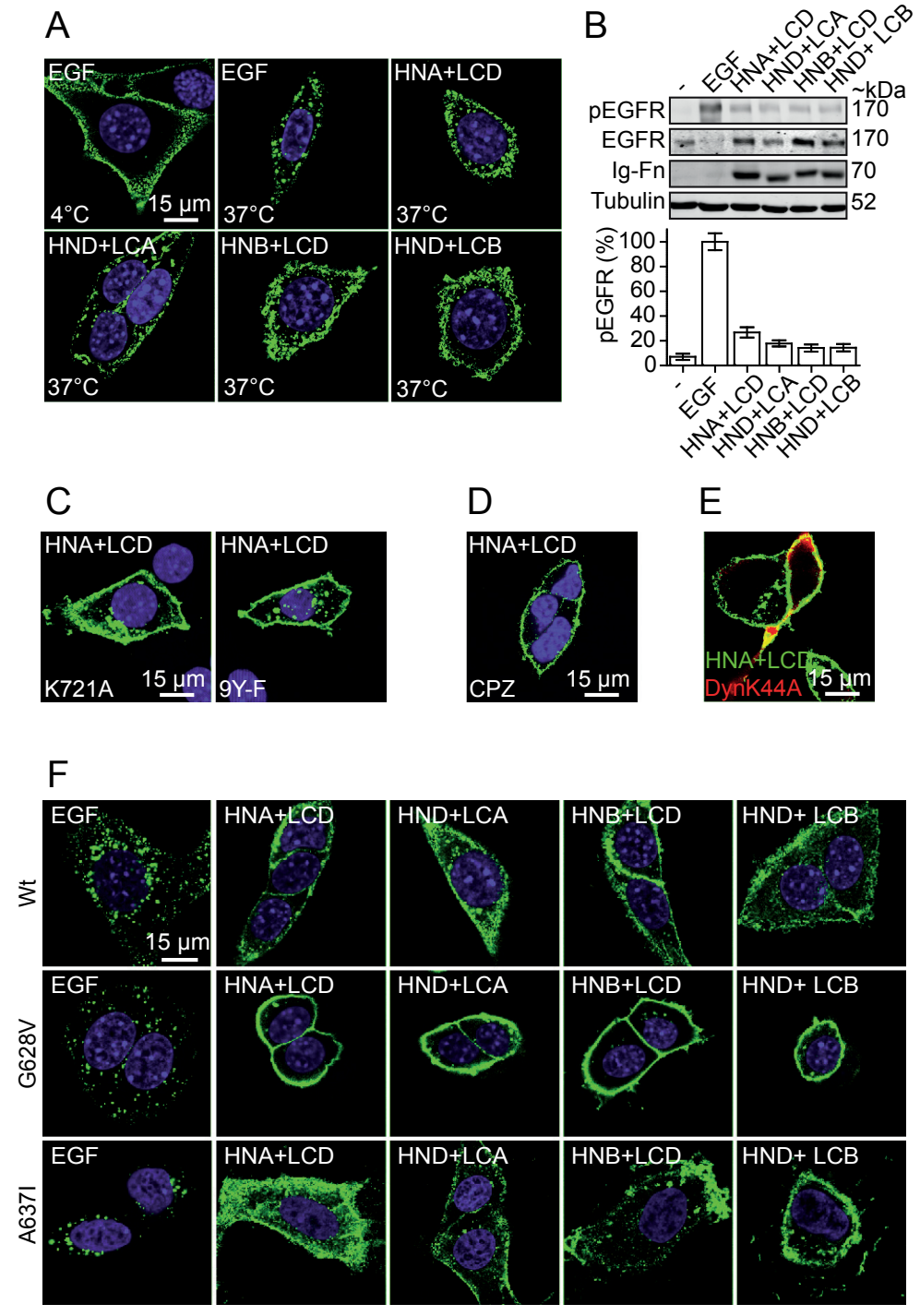
A
EGF
4°C
15 µm
EGF
37°C
HNA+LCD
37°C
HND+LCA
37°C
HNB+LCD
37°C
HND+LCB
37°C
B
-
EGF
HNA+LCD
HND+LCA
HNB+LCD
HND+ LCB
~kDa
pEGFR
170
EGFR
170
Ig-Fn
70
Tubulin
52
pEGFR (%)
100
80
60
40
20
0
C
HNA+LCD
K721A
15 µm
HNA+LCD
9Y-F
D
HNA+LCD
CPZ
15 µm
E
HNA+LCD
DynK44A
15 µm
F
Wt
G628V
A637I
EGF
HNA+LCD
HND+LCA
HNB+LCD
HND+ LCB
15 µm

Figure 3. *Triepitopic fusions induce EGFR internalization without activating its kinase. A. Internalization of $EGF^{Alexa488}$ or the four triepitopic constructs in HER14 cells. Serum starved cells were incubated with 8nM of $EGF^{Alexa488}$ or 25nM of the triepitopic constructs for 40 min at 37°C and subsequently washed with PBS and PFA-fixed. After permeabilization in 0.1% Triton-X100, internalized triepitopic constructs were detected with Alexa488-conjugated goat anti-human IgG. B. The triepitopic constructs are not agonistic. Serum starved HER14 cells were treated with either 8 nM of EGF or 25nM of the triepitopic constructs. Phosphorylated EGFR was detected on blot using anti-pEGFR (pY1068) antibodies. Total EGFR expression was checked with anti-EGFR antibodies and tubulin was used as loading control. The triepitopic constructs were detected with anti-human IgG antibodies. Error bars represent SEM, where n=3. C. Antibody-induced internalization is kinase independent. Internalization of HNA+LCD was assessed in cells expressing either wild type EGFR, the kinase dead EGFR mutant (EGFR-K721A) or the EGFR mutant lacking the 9 phosphotyrosines (EGFR-9Y-F). D. Antibody-induced internalization dependents on clathrin. Internalization of HNA+LCD was assessed in HER14 cells pre-treated with chlorpromazine (CPZ) for 30 min. E. Antibody-induced internalization is dependent on dynamin. Internalization of HNA+LCD (green) was assessed in cells overexpressing the non-functioning dynamin-K44A mutant (red). F. N-terminal TMD is necessary for antibody-induced endocytosis. Internalization of HNA+LCD was assessed in cells expressing either wild type EGFR or the TMD mutants (EGFR-G628V and EGFR-A637I). Nuclei were stained with DAPI (blue).*

TMD dimerization motif was filled up by replacing the alanine by an isoleucine. Both mutations are known to disrupt TMD dimerization [22, 23]. As indicated by the endosomal staining, EGF was clearly internalized in both TMD mutants. In contrast, the triepitopic antibodies were not internalized in the N-terminal EGFR mutant G628V, indicated by the green linear pattern around the cell membrane (Fig. 3F). In case of the C-terminal TMD mutant, the triepitopic antibody constructs internalized normally, resulting in a similar endosomal staining pattern as with wild type EGFR. Taken together, this data shows the involvement of the TMD of EGFR in clustering-induced internalization by triepitopic antibodies and suggests a crucial role for the N-terminal TMD dimerization motif in this process.

4.3.3. Triepitopic constructs induce lysosomal degradation of EGFR

Antibody-induced internalization of EGFR is often assessed by studying surface receptor levels and characterized as a persistent sequestering of EGFR from the plasma membrane [11-13, 15, 16]. This long term removal of EGFR from the plasma membrane could be an effect of inhibited recycling and intracellular accumulation of the receptor. Alternatively, internalized receptors could be targeted for degradation, by an endosomal sorting process. Therefore, EGFR degradation upon triepitopic antibody-induced internalization was assessed in HER14 cells (Fig. 4A, top blot and white bars in the histogram). As a control, a 4h of incubation with EGF resulted in an efficient 70% reduction of EGFR protein on western blot. Interestingly, all four triepitopic constructs induced a similar level of EGFR down-regulation as EGF (60-90% decrease in total EGFR protein). The antibody constructs induced a similar 75-90% downregulation of the C-terminal TMD mutant A637I (middle blot and dark gray bars). In contrast, EGFR degradation was significantly

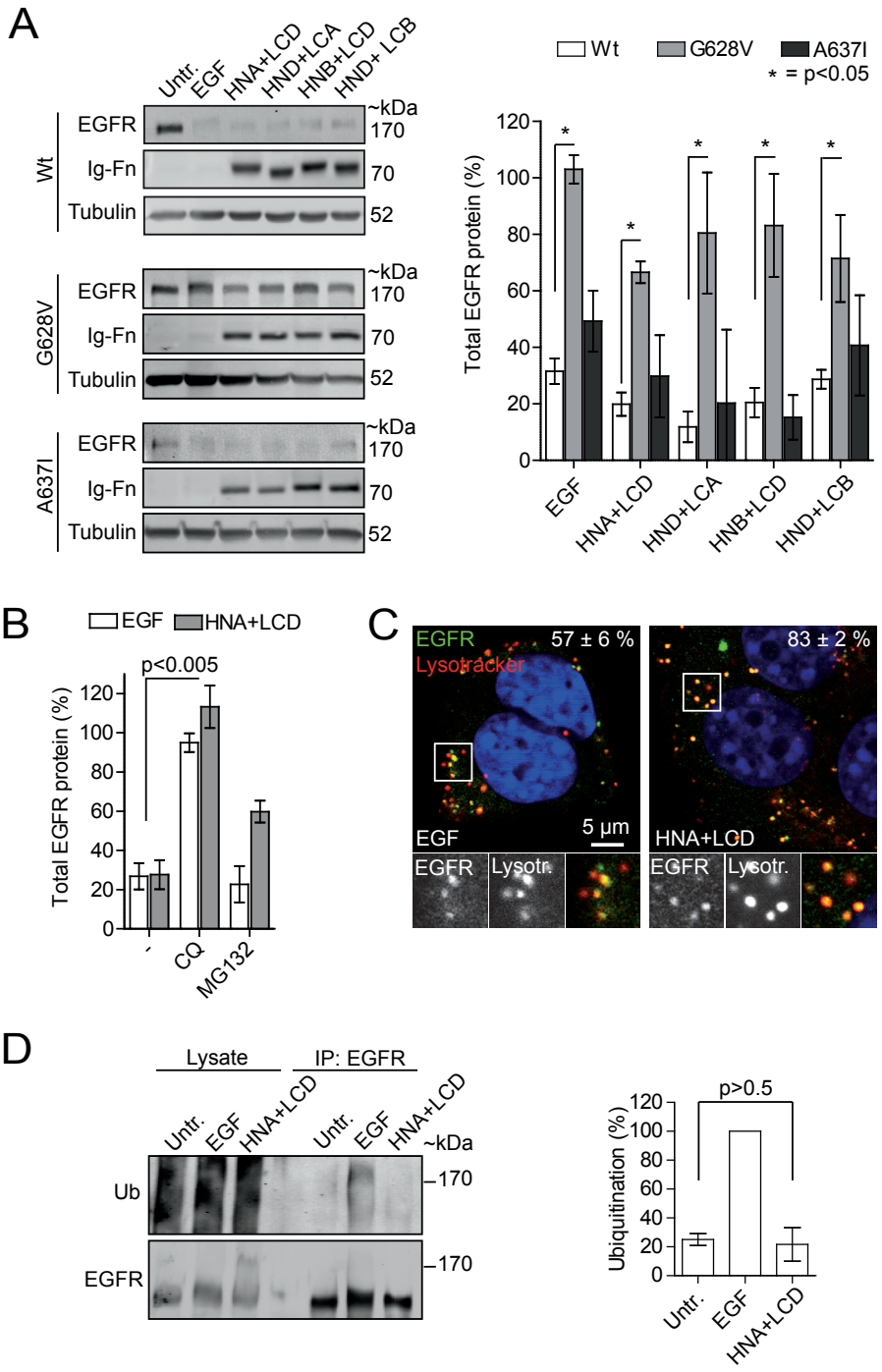
A
Untr.
EGF
HNA+LCD
HND+LCA
HNB+LCD
HND+ LCB
Wt
EGFR
Ig-Fn
Tubulin
~kDa
170
70
52
G628V
A637I
Wt
G628V
A637I
* = p<0.05
Total EGFR protein (%)
EGF
HNA+LCD
HND+LCA
HNB+LCD
HND+LCB
B
EGF
HNA+LCD
p<0.005
Total EGFR protein (%)
-
CQ
MG132
C
EGFR
Lysotracker
57 ± 6 %
83 ± 2 %
EGF
HNA+LCD
5 µm
EGFR
Lysotr.
D
Lysate
IP: EGFR
Untr.
EGF
HNA+LCD
~kDa
Ub
EGFR
170
p>0.5
Ubiquitination (%)

Figure 4. *Triepitopic constructs cause ubiquitin-independent degradation of EGFR in lysosomes. A. Down-regulation assay showing EGFR downregulation in HER14 cells or the mutant cell lines expressing EGFR-G628V and EGFR-A637I upon 4h treatment with 8nM of EGF or 25nM of the different triepitopic fusion constructs (left). The triepitopic antibodies and tubulin are stained as controls. Band were quantified using the Odyssey Infrared scanner (right) and plotted as percentage of untreated. B. EGF- and HNA+LCD-induced down-regulation of EGFR in HER14 cells treated with lysosomes inhibitor chloroquin (CQ) or proteasomal inhibitor MG132. C. Internalization of EGFR-mGFP (green) and co-localization with lysotracker 548 (red) upon 4h treatment with EGF or HNA+LCD. Nuclei were stained with DAPI (blue) D. HNA+LCD does not induce ubiquitination of EGFR. Cells were incubated with EGF or the triepitopic construct HNA+LCD and ubiquitination of total cell lysates or immunoprecipitated EGFR was determined by western blotting. Error bars represent SEM, where n=3.*

inhibited in case of the N-terminal TMD mutant G628V, indicating the requirement for receptor internalization (bottom blot) in this process. Quantification showed that the N-terminal TMD mutant G628V showed no or little reduction of EGFR (light grey bars show 0% degradation for EGF and 0-45% for the antibody constructs, $p<0.05$).

To determine whether the triepitopic constructs induce EGFR degradation in lysosomes, EGFR downregulation was assessed in cells in which lysosomal and proteasomal degradation was respectively inhibited with chloroquine (CQ) and MG132 (Fig. 4B). While cells without inhibitor showed an 80% downregulation of EGFR both upon treatment with EGF and HNA+LCD, inhibition of lysosomal degradation by CQ completely blocked the degradation of EGFR upon both these treatments. In contrast, inhibition of the proteasome by MG132 only partially blocked HNA+LCD-induced EGFR degradation. To further confirm the role of lysosomes in antibody-induced downregulation of EGFR, co-localization of EGFR with late endosomal/lysosomal compartment was studied (Fig. 4C). After 4 hours of incubation, a clear co-localization of EGFR with late endosomes/lysosomes was observed both in cells incubated with EGF (57 ± 6%) or HNA+LCD (83 ± 2%), as indicated by the yellow overlay of the green EGFR-GFP and the red late endosomes or lysosomes. These data suggest lysosomal trafficking of EGFR upon clustering-induced internalization via the triepitopic constructs and indicate an important role for the lysosomes in antibody-induced degradation of EGFR.

Sorting of EGFR to the degradation route occurs at the early endosomes and involves ubiquitin-mediated interactions with ESCRT1-3 complexes. Ligand-induced ubiquitination of EGFR is regulated by the binding of Cbl to the phosphorylated intracellular domain of the receptor. The antibody-induced downregulation of EGFR occurred independently of kinase activity. To see whether antibody-induced EGFR downregulation is controlled by ubiquitination or EGFR, the ubiquitination level of EGFR was tested in HER14 cells by immunoprecipitation of the receptor from total cell lysate (Fig. 4D). Treatment of the cell with EGF resulted in a clear ubiquitination of EGFR in the immunoprecipitated fraction, as indicated by an increase in molecular weight of EGFR and the positive staining with anti-ubiquitin. In contrast, treatment

of these cells with the HNA+LCD did not result in detectable receptor ubiquitination. As a control, the total lysates clearly show other ubiquitinated proteins in this sample. Taken together, clustering and internalization of EGFR via the triepitopic antibody constructs results in a fast, ubiquitination-independent trafficking towards late endosomal/lysosomal compartments, which eventually leads to lysosomal degradation of the receptor.

4.4. Discussion

Antibody therapies directed against growth factor receptors like EGFR or HER2 are generally designed to block their activation and thereby inhibit the downstream signaling toward proliferation. Even though this tends to reduce tumor growth, more aggressive approaches are often required for a complete therapy. Therefore, antibodies like cetuximab are commonly used in combination with other types of therapy, such as chemo- or radiotherapy [33, 34]. Recently, the anti-tumor efficacy of immunotherapy was improved by inducing the internalization of overexpressed receptors and thereby removing them from the plasma membrane. This phenomenon is observed with combinations of antibodies and multiepitopic formats against EGFR, TfR and HER2 and is thought to be mediated by receptor clustering [11, 12, 17, 18, 35]. For example, a mixture of two non-competitive anti-EGFR antibodies, Sym004, was shown to induce EGFR internalization and degradation, resulting in an excellent growth inhibiting properties and is currently in a clinical trial [14, 36]. However, the exact mechanism behind this antibody-induced receptor downregulation remains unclear.

Receptor clustering of different receptors like EGFR and TfR was recently shown to induce kinase-independent internalization. By using confocal fluorescence anisotropy imaging microscopy, which is based on homo-FRET between adjacent mGFP molecules, we first showed that the triepitopic constructs were very efficient in inducing clustering of EGFR-mGFPs. Actually, the decrease in limiting anisotropy (r_{inf}) induced by the triepitopic constructs was comparable to that observed with EGF. Many studies were already dedicated to determine the actual cluster size of these EGF-induced EGFR clusters [26, 29, 31, 37, 38, 38, 39, 39]. Since current techniques for determining cluster size do not discriminate between clusters of 4 proteins or more, an exact cluster size for activated EGFR is still under debate. Nevertheless, activated EGFR oligomerizes on the plasma membrane with >4 receptors/cluster, which are therefore referred to as higher order clusters.

In general, membrane proteins like EGFR are constitutively internalized via pinocytosis and subsequently recycled back to the plasma membrane [40-42]. As a consequence, surface expression levels of EGFR are a result of a delicate balance between internalization and recycling. Recycling of EGFR can occur via two different pathways. Upon internalization, vesicles that have fused with early endosomes can either recycle back to the plasma membrane immediately (fast recycling) or via subsequent sorting into perinuclear sorting compartments (slow recycling).

Clustering-induced sequestering of EGFR was previously suggested to be a result of a blocked recycling [12, 13, 15, 16]. We have recently shown that EGFR clustering enhances the internalization rate constant of EGFR by 4 times, as a result of the induction of clathrin-mediated endocytosis [19]. With confocal microscopy we have shown that the EGFR clustering by the trieptopic constructs results in receptor internalization. We propose that EGFR clustering by the triepitopic constructs stimulates both internalization via CIC-ME and a block in the slow recycling of internalized EGFR. Interestingly, the mechanical, extracellular clustering of EGFR by the triepitopic constructs is insufficient to activate the receptor. This suggests that this clustering does not induce a similar conformational change in EGFR that is known to be involved in ligand-induced receptor activation [43]. Furthermore, the absence of receptor activation also indicates that the observed receptor internalization is the direct result of the higher order receptor clusters.

An interesting question is how receptor clusters can have such an effect on receptor internalization. We previously observed that clustering of EGFR by biparatopic nanobodies induces CIC-ME, which depends entirely on the N-terminal TMD dimerization motif. We now show that the same mechanism applies for the larger clusters here. Antibody-induced internalization was absent in cells expressing EGFR with a mutated N-terminal TMD dimerization motif. No effect was found with EGFR mutated in their C-terminal TMD dimerization motif. This might point to an important role for the induction of plasma membrane curvature in the process of antibody-induced CIC-ME. Molecular models, simulations and NMR data revealed that N-terminally linked dimerization motifs of EGFR or HER2 form a wedge-shaped dimer at an angle of 46 ± 5° [44, 45]. Higher order clustering of EGFR, and thereby the clustering of the wedge-shaped TMDs, might bend the membrane slightly inwards, locally lowering the energy threshold and providing the first step for internalization. This inward-curvature hypothesis is supported by the observation that especially the N-terminal TMD dimerization motif interacts upon EGF treatment and plays a role in internalization [19, 24]. This clustering-induced remodeling of the membrane should be studied more carefully, for example by molecular dynamics simulations [46, 47] in giant unilamellar vesicles (GUVs) [48]. Upon curvature, curvature sensing adaptor proteins such as BAR (Bin/Amphiphysin/Rvs) domain containing proteins could subsequently interact with mediators of the CME machinery [49-51].

The triepitopic antibody constructs also resulted in intracellular trafficking of EGFR towards late endosomal/lysosomal compartments and in lysosomal degradation of the receptor. In the conventional, ligand-induced, negative feedback mechanism of EGFR, posttranslational modifications on the cytoplasmic tail of EGFR like phosphorylation and ubiquitination regulate intracellular sorting of activated receptors towards degradation [7, 52, 53]. While c-Cbl induced monoubiquitination of multiple lysine residues of EGFR promotes lysosomal degradation, c-Cbl independent polyubiquitination of lysines in the kinase domain is also observed and was found

to drive proteasomal degradation of the receptor [54-56]. Despite the very efficient downregulation of EGFR by the triepitopic constructs, no posttranslational modification of the receptor (neither phosphorylation nor ubiquitination) could be detected. This is in good correlation with the antibody-induced receptor downregulation of EGFR by a combination of antibodies [11]. However, more recent work did show ubiquitination upon clustering of EGFR via an anti-EGFR antibody combination or a complex of C225 and anti-human IgG [18, 57]. This however, was accompanied by kinase activation, which might actually have resulted in the ubiquitination. If EGFR clustering via triepitopic antibodies induces lysosomal trafficking and degradation without posttranslational modifications, other sorting signals might be responsible.

Besides that the endosomal cargo as such might serve as a trafficking signal, it is possible that clustering by itself is a lysosomal targeting signal. Clustering-mediated trafficking of vesicles is already observed with GPCRs, which require dimerization or oligomerization to traffic from the ER to the plasma membrane [58]. Similarly, a correlation between higher order oligomerization and trafficking is observed in polarized cells. For example, complexes of polymeric IgA receptor (pIgA-R) and transferrin (TfR) are increasingly clustered upon trafficking from the basolateral sides of polarized cells to perinuclear endosomes [59]. Our anisotropy data shows that the triepitopic constructs result in persistent clustering of EGFR in endosomal compartments (Fig. S1). This might create protein and lipid domains that pack low affinity interacting proteins involved in trafficking, similarly as observed for internalization. This process might include activation-independent sorting signals like the two dileucine motifs (LL-679/680 and LL-1010/1011) in EGFR that are associated with receptor degradation [60, 61] or alternative sorting machineries like the sorting nexins [62, 63]. Furthermore, similar as to the plasma membrane, early endosomes have also been shown to contain clathrin-coated sheets. Receptor clusters inside endosomes might therefore be sufficient to drive effective downstream sorting, invagination and formation of multi-vesicular vesicles.

In conclusion, we show that triepitopic anti-EGFR antibodies cluster EGFRs to the same extent as the natural ligand EGF and thereby induce kinase-independent internalization via clathrin-mediated endocytosis. The mechanism behind this antibody-induced internalization of EGFR involves the N-terminal TMD domain and upon internalization, the triepitopic constructs cause an EGF-like lysosomal degradation of EGFR. Lysosomal sorting of EGFR induced by the tri-epitopic antibody constructs does not require phosphorylation or ubiquitination but might involve other lysosomal trafficking signals originating from receptor oligomerization.

4.5. References

1. Yarden, Y. The EGFR family and its ligands in human cancer. signalling mechanisms and therapeutic opportunities. *Eur. J. Cancer* **37 Suppl 4**, S3-8 (2001).
2. Jorissen, R. N. *et al*. Epidermal growth factor receptor: mechanisms of activation and signalling. *Exp. Cell Res.* **284**, 31-53 (2003).
3. Burgess, A. W. EGFR family: structure physiology signalling and therapeutic targets. *Growth Factors* **26**, 263-274 (2008).
4. Citri, A. & Yarden, Y. EGF-ERBB signalling: towards the systems level. *Nat. Rev. Mol. Cell Biol.* **7**, 505-516 (2006).
5. Sorkin, A. & von Zastrow, M. Endocytosis and signalling: intertwining molecular networks. *Nat. Rev. Mol. Cell Biol.* **10**, 609-622 (2009).
6. Lai, W. H. *et al*. Ligand-mediated internalization, recycling, and downregulation of the epidermal growth factor receptor in vivo. *J. Cell Biol.* **109**, 2741-2749 (1989).
7. Madshus, I. H. & Stang, E. Internalization and intracellular sorting of the EGF receptor: a model for understanding the mechanisms of receptor trafficking. *J. Cell. Sci.* **122**, 3433-3439 (2009).
8. Goh, L. K., Huang, F., Kim, W., Gygi, S. & Sorkin, A. Multiple mechanisms collectively regulate clathrin-mediated endocytosis of the epidermal growth factor receptor. *J. Cell Biol.* **189**, 871-883 (2010).
9. Uberall, I., Kolar, Z., Trojanec, R., Berkovcova, J. & Hajduch, M. The status and role of ErbB receptors in human cancer. *Exp. Mol. Pathol.* **84**, 79-89 (2008).
10. Patel, D. K. Clinical use of anti-epidermal growth factor receptor monoclonal antibodies in metastatic colorectal cancer. *Pharmacotherapy* **28**, 31S-41S (2008).
11. Friedman, L. M. *et al*. Synergistic down-regulation of receptor tyrosine kinases by combinations of mAbs: implications for cancer immunotherapy. *Proc. Natl. Acad. Sci. U. S. A.* **102**, 1915-1920 (2005).
12. Spangler, J. B. *et al*. Combination antibody treatment down-regulates epidermal growth factor receptor by inhibiting endosomal recycling. *Proc. Natl. Acad. Sci. U. S. A.* **107**, 13252-13257 (2010).
13. Spangler, J. B., Manzari, M. T., Rosalia, E. K., Chen, T. F. & Wittrup, K. D. Triepitopic antibody fusions inhibit cetuximab-resistant BRAF and KRAS mutant tumors via EGFR signal repression. *J. Mol. Biol.* **422**, 532-544 (2012).
14. Pedersen, M. W. *et al*. Sym004: a novel synergistic anti-epidermal growth factor receptor antibody mixture with superior anticancer efficacy. *Cancer Res.* **70**, 588-597 (2010).
15. Boersma, Y. L., Chao, G., Steiner, D., Wittrup, K. D. & Pluckthun, A. Bispecific designed ankyrin repeat proteins (DARPins) targeting epidermal growth factor receptor inhibit A431 cell proliferation and receptor recycling. *J. Biol. Chem.* **286**, 41273-41285 (2011).
16. Hackel, B. J., Neil, J. R., White, F. M. & Wittrup, K. D. Epidermal growth factor receptor downregulation by small heterodimeric binding proteins. *Protein Eng. Des. Sel.* **25**, 47-57 (2012).
17. Liu, A. P., Aguet, F., Danuser, G. & Schmid, S. L. Local clustering of transferrin receptors promotes clathrin-coated pit initiation. *J. Cell Biol.* **191**, 1381-1393 (2010).
18. Berger, C., Madshus, I. H. & Stang, E. Cetuximab in combination with anti-human IgG antibodies efficiently down-regulates the EGF receptor by macropinocytosis. *Exp. Cell Res.* **318**, 2578-2591 (2012).
19. Heukers, R. *et al*. EGFR endocytosis requires its kinase activity and N-terminal transmembrane dimerization motif. *J. Cell. Sci.* (*in press*).
20. Sternberg, M. J. & Gullick, W. J. A sequence motif in the transmembrane region of growth factor receptors with tyrosine kinase activity mediates dimerization. *Protein Eng.* **3**, 245-248 (1990).
21. Cymer, F. & Schneider, D. Transmembrane helix-helix interactions involved in ErbB receptor signaling. *Cell. Adh Migr.* **4**, 299-312 (2010).
22. Mendrola, J. M., Berger, M. B., King, M. C. & Lemmon, M. A. The single transmembrane domains of ErbB receptors self-associate in cell membranes. *J. Biol. Chem.* **277**, 4704-4712 (2002).
23. Escher, C., Cymer, F. & Schneider, D. Two GxxxG-like motifs facilitate promiscuous interactions of the human ErbB transmembrane domains. *J. Mol. Biol.* **389**, 10-16 (2009).
24. Lu, C. *et al*. Structural evidence for loose linkage between ligand binding and kinase activation in the epidermal growth factor

receptor. *Mol. Cell. Biol.* **30**, 5432-5443 (2010).
25. Honegger, A. M. *et al*. A mutant epidermal growth factor receptor with defective protein tyrosine kinase is unable to stimulate proto-oncogene expression and DNA synthesis. *Mol. Cell. Biol.* **7**, 4568-4571 (1987).
26. Hofman, E. G. *et al*. Ligand-induced EGF receptor oligomerization is kinase-dependent and enhances internalization. *J. Biol. Chem.* **285**, 39481-39489 (2010).
27. Damke, H., Baba, T., Warnock, D. E. & Schmid, S. L. Induction of mutant dynamin specifically blocks endocytic coated vesicle formation. *J. Cell Biol.* **127**, 915-934 (1994).
28. Bader, A. N., Hofman, E. G., van Bergen En Henegouwen, P. M. & Gerritsen, H. C. Imaging of protein cluster sizes by means of confocal time-gated fluorescence anisotropy microscopy. *Opt. Express* **15**, 6934-6945 (2007).
29. Bader, A. N., Hofman, E. G., Voortman, J., en Henegouwen, P. M. & Gerritsen, H. C. Homo-FRET imaging enables quantification of protein cluster sizes with subcellular resolution. *Biophys. J.* **97**, 2613-2622 (2009).
30. Roovers, R. C. *et al*. Efficient inhibition of EGFR signaling and of tumour growth by antagonistic anti-EFGR Nanobodies. *Cancer Immunol. Immunother.* **56**, 303-317 (2007).
31. Clayton, A. H. *et al*. Ligand-induced dimer-tetramer transition during the activation of the cell surface epidermal growth factor receptor-A multidimensional microscopy analysis. *J. Biol. Chem.* **280**, 30392-30399 (2005).
32. Wang, L. H., Rothberg, K. G. & Anderson, R. G. Mis-assembly of clathrin lattices on endosomes reveals a regulatory switch for coated pit formation. *J. Cell Biol.* **123**, 1107-1117 (1993).
33. Gerber, D. E. & Choy, H. Cetuximab in combination therapy: from bench to clinic. *Cancer Metastasis Rev.* **29**, 171-180 (2010).
34. Nieder, C., Pawinski, A., Dalhaug, A. & Andratschke, N. A review of clinical trials of cetuximab combined with radiotherapy for non-small cell lung cancer. *Radiat. Oncol.* **7**, 3-717X-7-3 (2012).
35. Perera, R. M. *et al*. Treatment of human tumor xenografts with monoclonal antibody 806 in combination with a prototypical epidermal growth factor receptor-specific antibody generates enhanced antitumor activity. *Clin. Cancer Res.* **11**, 6390-6399 (2005).
36. Koefoed, K. *et al*. Rational identification of an optimal antibody mixture for targeting the epidermal growth factor receptor. *MAbs* **3**, 584-595 (2011).
37. Clayton, A. H., Tavarnesi, M. L. & Johns, T. G. Unligated epidermal growth factor receptor forms higher order oligomers within microclusters on A431 cells that are sensitive to tyrosine kinase inhibitor binding. *Biochemistry* **46**, 4589-4597 (2007).
38. Clayton, A. H., Orchard, S. G., Nice, E. C., Posner, R. G. & Burgess, A. W. Predominance of activated EGFR higher-order oligomers on the cell surface. *Growth Factors* **26**, 316-324 (2008).
39. Saffarian, S., Li, Y., Elson, E. L. & Pike, L. J. Oligomerization of the EGF receptor investigated by live cell fluorescence intensity distribution analysis. *Biophys. J.* **93**, 1021-1031 (2007).
40. Steinman, R. M., Mellman, I. S., Muller, W. A. & Cohn, Z. A. Endocytosis and the recycling of plasma membrane. *J. Cell Biol.* **96**, 1-27 (1983).
41. Herbst, J. J., Opresko, L. K., Walsh, B. J., Lauffenburger, D. A. & Wiley, H. S. Regulation of postendocytic trafficking of the epidermal growth factor receptor through endosomal retention. *J. Biol. Chem.* **269**, 12865-12873 (1994).
42. Wiley, H. S. *et al*. The role of tyrosine kinase activity in endocytosis, compartmentation, and down-regulation of the epidermal growth factor receptor. *J. Biol. Chem.* **266**, 11083-11094 (1991).
43. Jura, N. *et al*. Mechanism for activation of the EGF receptor catalytic domain by the juxtamembrane segment. *Cell* **137**, 1293-1307 (2009).
44. Mineev, K. S. *et al*. Spatial structure of the transmembrane domain heterodimer of ErbB1 and ErbB2 receptor tyrosine kinases. *J. Mol. Biol.* **400**, 231-243 (2010).
45. Endres, N. F. *et al*. Conformational coupling across the plasma membrane in activation of the EGF receptor. *Cell* **152**, 543-556 (2013).
46. Yin, Y., Arkhipov, A. & Schulten, K. Simulations of membrane tubulation by lattices of amphiphysin N-BAR domains. *Structure* **17**, 882-892 (2009).
47. Arkhipov, A. *et al*. Architecture and membrane interactions of the EGF receptor. *Cell* **152**, 557-569 (2013).
48. Sezgin, E. *et al*. Elucidating membrane

structure and protein behavior using giant plasma membrane vesicles. *Nat. Protoc.* **7**, 1042-1051 (2012).
49. Henne, W. M. *et al*. FCHo proteins are nucleators of clathrin-mediated endocytosis. *Science* **328**, 1281-1284 (2010).
50. Doherty, G. J. & McMahon, H. T. Mechanisms of endocytosis. *Annu. Rev. Biochem.* **78**, 857-902 (2009).
51. McMahon, H. T., Kozlov, M. M. & Martens, S. Membrane curvature in synaptic vesicle fusion and beyond. *Cell* **140**, 601-605 (2010).
52. Sorkin, A. & Goh, L. K. Endocytosis and intracellular trafficking of ErbBs. *Exp. Cell Res.* **315**, 683-696 (2009).
53. Rappoport, J. Z. & Simon, S. M. Endocytic trafficking of activated EGFR is AP-2 dependent and occurs through preformed clathrin spots. *J. Cell. Sci.* **122**, 1301-1305 (2009).
54. Huang, F., Kirkpatrick, D., Jiang, X., Gygi, S. & Sorkin, A. Differential regulation of EGF receptor internalization and degradation by multiubiquitination within the kinase domain. *Mol. Cell* **21**, 737-748 (2006).
55. Umebayashi, K., Stenmark, H. & Yoshimori, T. Ubc4/5 and c-Cbl continue to ubiquitinate EGF receptor after internalization to facilitate polyubiquitination and degradation. *Mol. Biol. Cell* **19**, 3454-3462 (2008).
56. Zhou, L. & Yang, H. The von Hippel-Lindau tumor suppressor protein promotes c-Cbl-independent poly-ubiquitylation and degradation of the activated EGFR. *PLoS One* **6**, e23936 (2011).
57. Ferraro, D. A. *et al*. Inhibition of triple-negative breast cancer models by combinations of antibodies to EGFR. *Proc. Natl. Acad. Sci. U. S. A.* **110**, 1815-1820 (2013).
58. Canals, M., Lopez-Gimenez, J. F. & Milligan, G. Cell surface delivery and structural re-organization by pharmacological chaperones of an oligomerization-defective alpha(1b)-adrenoceptor mutant demonstrates membrane targeting of GPCR oligomers. *Biochem. J.* **417**, 161-172 (2009).
59. Wallrabe, H., Bonamy, G., Periasamy, A. & Barroso, M. Receptor complexes cotransported via polarized endocytic pathways form clusters with distinct organizations. *Mol. Biol. Cell* **18**, 2226-2243 (2007).
60. Huang, F., Jiang, X. & Sorkin, A. Tyrosine phosphorylation of the beta2 subunit of clathrin adaptor complex AP-2 reveals the role of a di-leucine motif in the epidermal growth factor receptor trafficking. *J. Biol. Chem.* **278**, 43411-43417 (2003).
61. Tsacoumangos, A., Kil, S. J., Ma, L., Sonnichsen, F. D. & Carlin, C. A novel dileucine lysosomal-sorting-signal mediates intracellular EGF-receptor retention independently of protein ubiquitylation. *J. Cell. Sci.* **118**, 3959-3971 (2005).
62. Gullapalli, A. *et al*. A role for sorting nexin 2 in epidermal growth factor receptor down-regulation: evidence for distinct functions of sorting nexin 1 and 2 in protein trafficking. *Mol. Biol. Cell* **15**, 2143-2155 (2004).
63. Kurten, R. C., Cadena, D. L. & Gill, G. N. Enhanced degradation of EGF receptors by a sorting nexin, SNX1. *Science* **272**, 1008-1010 (1996).

4.6. Supplementary information

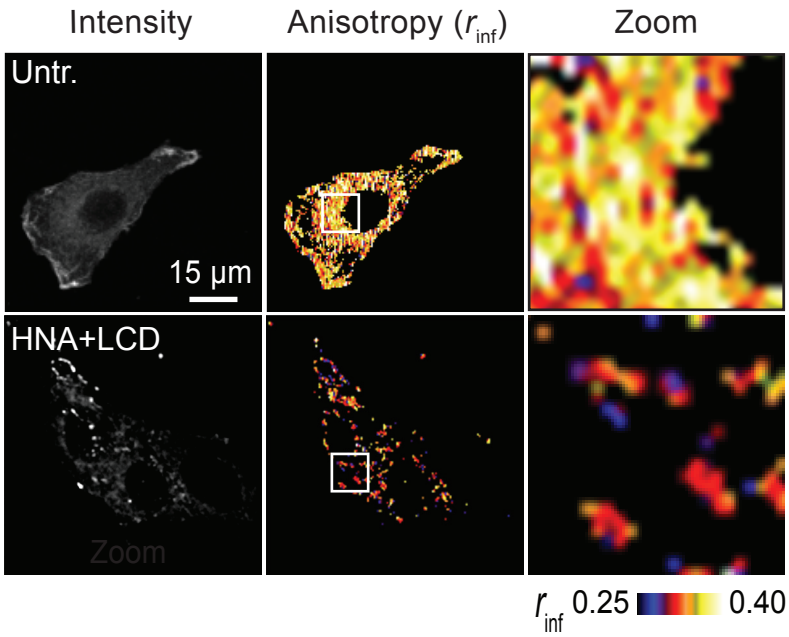

Figure S1. *Triepitopic fusion constructs cluster EGFR in endocytic vesicles. Confocal time-resolved fluorescence anisotropy imaging microscopy (CTR-FAIM) analysis of receptor clustering in cells that were treated with 200 nM of the triepitopic constructs for 20 min. Anisotropy values, due to homo-FRET, were determined as described in materials and methods and presented in false colors.*

Chapter 5

Nanobody-albumin nanoparticles (NANAPs) for the delivery of a multikinase inhibitor 17864 to EGFR overexpressing tumor cells

Isil Altintas[1], Raimond Heukers[2], Roy van der Meel[1], Marie Lacombe[3], Maryam Amidi[1], Paul M.P. van Bergen en Henegouwen[2], Wim E. Hennink[1], Raymond M. Schiffelers[4] and Robbert J. Kok[1]

[1] Department of Pharmaceutics, Utrecht Institute for Pharmaceutical Sciences, Utrecht University, Utrecht, The Netherlands
[2] Cell Biology, Department of Biology, Utrecht University, Utrecht, The Netherlands
[3] Linxis, Breda, The Netherlands
[4] Laboratory of Clinical Chemistry and Haematology, UMC Utrecht, Utrecht, The Netherlands

Journal of Controlled Release, 2013, 165:110-8.

Abstract

A novel, EGFR-targeted nanomedicine has been developed in the current study. Glutaraldehyde crosslinked albumin nanoparticles with a size of approximately 100nm were loaded with the multikinase inhibitor 17864-L_x—a platinum-bound sunitinib analogue—which couples the drug to methionine residues of albumin and is released in a reductive environment. Albumin nanoparticles were surface-coated with bifunctional polyethylene glycol 3500 (PEG) and a nanobody—the single variable domain of an antibody—(EGa1) against the epidermal growth factor receptor (EGFR). EGa1-PEG functionalized nanoparticles showed a 40-fold higher binding to EGFR-positive 14C squamous head and neck cancer cells in comparison to PEGylated nanoparticles. 17864-L_x loaded EGa1-PEG nanoparticles were internalized by clathrin-mediated endocytosis and ultimately digested in lysosomes. The intracellular routing of EGa1 targeted nanoparticles leads to a successful release of the kinase inhibitor in the cell and inhibition of proliferation whereas the non-targeted formulations had no antiproliferative effects on 14C cells. The drug loaded targeted nanoparticles were as effective as the free drug *in vitro*. These results demonstrate that multikinase inhibitor loaded albumin nanoparticles are interesting nanomedicines for the treatment of EGFR-positive cancers.

5.1. Introduction

One of the improvements of nanomedicine formulations is to increase the therapeutic index of highly potent drugs that often show severe side effects. Targeted delivery of these drugs to tumor tissues can increase antitumor efficacy and reduce toxicity by avoidance of normal tissues. Well known examples of nanoparticulate carriers are liposomes [1,2], polymeric nanoparticles [3] and micelles [4]. Recently, albumin nanoparticles have gained attention [5-10] especially after the success of albumin-based formulations such as Abraxane® [11]. These formulations take advantage of the properties of albumin, which is nature's own carrier for binding and transporting drugs within the body [12]. In recent years, albumin nanoparticles have been further functionalized by coupling tumor-directed monoclonal antibodies (i.e., trastuzumab, cetuximab, anti-CD3) [13-19] and other targeting ligands (i.e. folate, RGD, apolipoproteins) [20-25] onto their surface in order to increase their uptake by tumor cells.

In the present study, a novel type of decorated nanobody-albumin nanoparticles, (abbreviated as NANAPs) is described. These nanoparticles are functionalized with anti-EGFR nanobody (EGa1) attached to the distal end of surface coated PEG chains (Fig. **1**). Nanobodies are low molecular weight proteins (~15 kDa) that are derived from heavy chain-only antibodies as found in camels, llamas and dromedaries [26]. The antigen recognition domain of this type of antibodies is expressed in a single chain, in contrast to conventional antibodies which encode the antigen recognition loops in two separate heavy and light chains. Consequently, the recombinant production of nanobodies is easier than that of conventional antibodies, while they contain several other advantageous features such as high affinity to the target and the absence of an Fc domain [27-29]. Particularly in the case of antibody coupled nanoparticles, the presence of an Fc domain could lead to the recognition of the nanoparticles by the immune system, resulting in their fast clearance from the blood circulation [30]. Furthermore, compared to monoclonal antibodies, the single domain format of nanobodies facilitates easy selection from phage libraries [31]. As a result, nanobodies have been rapidly developed for many applications, i.e., imaging, cancer immunotherapy, blocking blood clotting and resins for immuno-affinity purification [32].

In this study, we explored the loading of a kinase inhibitor to albumin nanoparticles via chemical conjugation to the albumin backbone. The multikinase inhibitor 17864 used in this study targets several growth-factor signaling pathways and is structurally closely related to sunitinib [33]. Multikinase inhibitors inhibit the activity of several receptor tyrosine kinases by competitive inhibition of ATP binding, and thus are able to intervene in proliferation and survival of tumor cells and angiogenesis. Although the activity versus multiple molecular targets is attractive from efficacy point-of-view, this is also associated with lack of selectivity and hence greater risk for side effects [34]. Therefore, to enhance the accumulation of 17864 in tumor cells and prevent the exposure of healthy cells to the inhibitor, in the present study we developed

a targeted nanomedicine that can guide the multikinase inhibitor to tumor cells. 17864 can be coupled to albumin nanoparticles by the use of a platinum based linker that coordinates the drug at its pyridyl moiety and albumin at methionine and cysteine residues. As such, the presently developed NANAPs that can accumulate in EGFR-expressing tumor cells and upon intracellular degradation will release the conjugated multikinase inhibitor into the reductive environment of the cytosol, where the 17864 is released from the platinum linker [35]. Both 17864 and the 17864-L_x adducts inhibit several important tumor associated pathways like PDGFR and c-Kit [33]. The present study explores the potential of 17864-albumin nanoparticles as EGFR-directed targeted nanomedicine. The enzymatic degradability of the developed nanoparticles and cellular uptake and intracellular routing, as well as antiproliferative activity on EGFR positive human head and neck squamous cell carcinoma (HNSCC) UM-SCC-14C (14C) are studied.

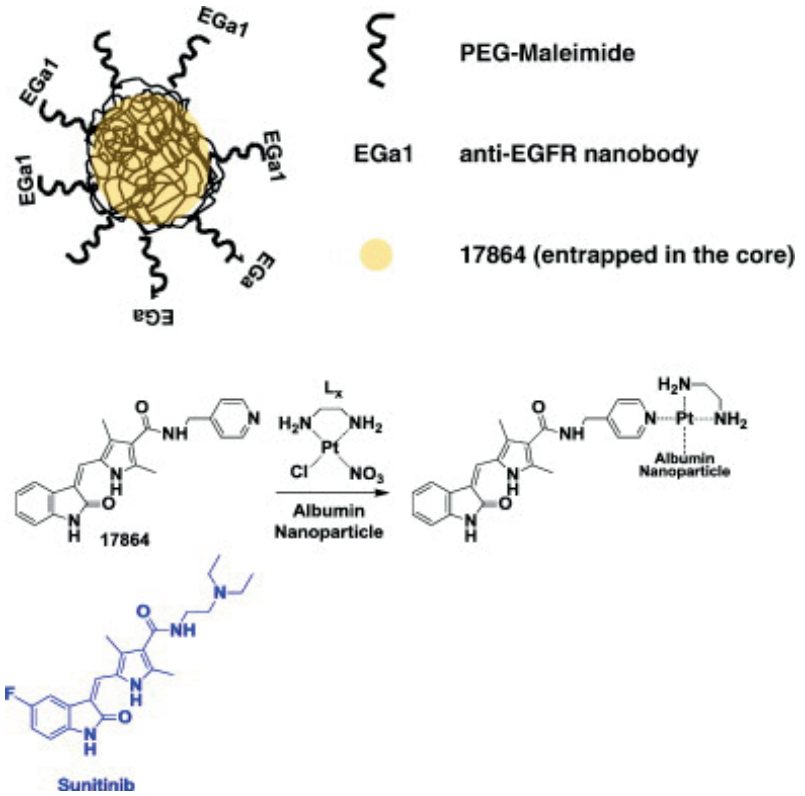

Figure 1. *Schematic representation of targeted nanobody-albumin nanoparticles (NANAPs) which consists of a glutaraldehyde crosslinked albumin core that has been surface modified with EGa1-PEG tethers. The multikinase inhibitor 17864 has been loaded into the core of the nanoparticles and is retained into the particles via L_x based platinum coordinative linkage. 17864 is an analogue of sunitinib.*

5.2. Materials and methods

5.2.1. Chemicals

Albumin, human fraction V powder and glutaraldehyde, 8% aqueous solution, grade I, were purchased from Sigma Aldrich. NHS-PEG3500- maleimide was obtained from Jenkem Technology (Beijing, China). Sunitinib-malate was purchased from LC Laboratories, Germany. 17864 was obtained from Vichem chemie (Budapest, Hungary) and linked to L_x as described previously [33]. Rhodamine-L_x was obtained from Kreatech (Amsterdam, The Netherlands). Trypsin (5 mg/ml) from porcine supplemented with EDTA and fetal calf serum was obtained from PAA, GE Healthcare.

5.2.2. Preparation of nanoparticles

Nanoparticles were prepared by a desolvation technique according to Langer et al., with some modifications [36]. Briefly, 50 mg of HSA was dissolved in 1 ml deionized water, pH was adjusted to 8.3 by addition of 0.1 M NaOH and the solution was filtered through a 0.2 µm filter. Nanoparticles were formed by adding 4 ml of 92% ethanol to 1 ml of the HSA solution drop wise under constant stirring at 450 rpm. Immediately after ethanol addition, the formed particles were crosslinked with 8% glutaraldehyde (GA) and reacted overnight at room temperature (RT) under stirring. 18, 29 or 59 µl 8% glutaraldehyde (corresponding to 18:1, 30:1, 60:1 GA:HSA mol/mol ratios) was added to obtain low, medium and high crosslinked nanoparticles, respectively. The nanoparticles were purified by two-step centrifugation, once at 1000 g for 5 min and once at 35,000 g three times for 1 h at 4 °C in deionized water. After centrifugation, the nanoparticles were sonicated for 4 min and stored in deionized water at 4 °C. The yield of nanoparticles was calculated from the dry weight of the nanoparticle suspensions after evaporation of the carrier solvent from 100 µl aliquots in a thermographic analyzer (TGA Q50™ instrument, USA). Aliquots of the suspensions corresponding to 6 µg albumin were loaded onto an SDS gel (4–12% crosslinked, Invitrogen, Breda, Netherlands) under reducing conditions to check for the possible presence of albumin and soluble multimers by Coomassie blue staining.

5.2.3. Loading of kinase inhibitors into albumin nanoparticles

Loading of sunitinib into albumin nanoparticles with different cross-link densities is described in the supplemental information. Coupling of 17864-L_x was performed according to Harmsen et al. [33] with minor modifications. In brief, 12 mg of low crosslinked nanoparticles (0.07 mg/ml in water) was incubated with 1.2 mg of 17864-L_x (10:1 mol/mol, 17864-L_x:HSA) in 20 mM tricine/NaNO3 pH 8.5 buffer overnight at 37 °C. To prevent flocculation, SDS was added (final concentration 0.008% (v/v)). 17864-L_x loaded nanoparticles were purified by centrifugation

and stored as described above. The 17864 content of the nanoparticles was determined after cleavage of the 17864-L_x coordinative bond by an overnight incubation with 0.5 M KSCN at 80 °C, followed by extraction with ACN (2:1, v/v) [37]. Released 17864 was determined with ultra-high performance liquid chromatography (Acquity UPLC®) on an Acquity UPLC® BEH C18 1.7 µm, 2.1×50 mm column (Waters, Ireland). 17864 was eluted with a water/ACN/TFA gradient starting from 100% eluent A (95% H2O, 5% ACN, 0.1% TFA) and going up to 100% eluent B (5% H2O, 95% ACN, 0.1% TFA) in 7 min at a flow rate of 1 ml/min. 17864 was detected at 425 nm and eluted at 2.2 min. 17864-L_x was injected as a reference and eluted at 2.7 min.

5.2.4. Preparation of labeled nanoparticles for imaging

For cellular uptake and intracellular routing, three types of fluorescently labeled nanoparticles were prepared. Rhodamine was linked to the nanoparticles via the same linkage approach as 17864, using a rhodamine-L_x adduct (Rho-L_x). In detail, 12 mg of nanoparticles (3 mg/ml) was labeled with 144 µg of Rho-L_x (from a 4 mg/ml water stock), (1:1, mol/mol, Rho-L_x:HSA). Alexa-488 labeled nanoparticles were prepared by reacting 10 mg of nanoparticles (3 mg/ml) with 33.9 nmol of Alexa488-NHS (Invitrogen, 0.2:1 mol/mol, Alexa488-NHS: HSA) in 0.1 M phosphate buffer (PB), pH 8 for 2 h at RT. For lysosomal degradation studies, nanoparticles were labeled with the near-infrared dye IRDye800 (Westburg, Leusden, The Netherlands). 18 mg of nanoparticles (3 mg/ml) was labeled with 85.5 nmol of IRDye800 CW NHS (0.3:1 mol/mol, IRDye800:HSA) in 0.1 M PB, pH 8 for 2 h at RT. Labeled nanoparticles were purified as described in Section 2.2 and resuspended in 0.1 M PB pH 7.4 prior to use.

5.2.5. Preparation of NANAPs

Production of the anti-EGFR-1 nanobody (EGa1) was done as described by Roovers et al., with minor modifications [31]. Briefly, *Escherichia coli* BL21-CodonPlus(DE3)-RIL cells (Agilent Technologies, Inc., Santa Clara, CA, USA) transformed with pET28-nanobody plasmid were grown overnight at 37 °C in 2× TY medium containing 2% glucose and supplemented with 100 µg/ml kanamycin and chloramphenicol. Next, 400 ml of 2× TY (tryptone/yeast extract) medium containing 0.2% glucose and 100 µg/ml kanamycin and chloramphenicol was inoculated with bacteria from an overnight culture with an OD600 of 0.1. This bacterial culture was incubated at 37 °C at 250 rpm until it reached an OD600 of 0.6. Subsequently, 0.5 mM IPTG was added to the bacterial culture to induce EGa1 expression and the culture was further incubated at 25 °C for 6 h. Cells were spun down at 4500 rpm and at 4 °C for 15 min and the pellet was resuspended in 6.4 ml (per 400 ml culture) ice cold TES (200 mM Tris-HCl, 0.5 mM EDTA, 500 mM sucrose, pH 8). To this suspension 10 ml of diluted ice cold TES (1:3 in water) was added and incubated on ice for 30 min. The bacteria were spun down at 4 °C for 15 min at 4500 rpm and the supernatant

was collected. The pellet was resuspended in 10 ml ice cold TES, 120 µl 1 M magnesium sulfate was added and the mixture was incubated on ice for 30 min. The suspension was spun down at 4 °C for 15 min at 4500 rpm and the supernatant was added to the previously collected supernatant. Purification was performed on an ÄKTA purifier 10 (GE 7 Healthcare Europe GmbH, Munich, Germany) using a HisTrap™ Column (GE Healthcare) according to the manufacturer's protocol. Nanobodies were eluted with an imidazole gradient (10–500 mM in 50 mM sodium phosphate, 300 mM NaCl, pH 8 buffer) and the collected fractions were dialyzed overnight against PBS pH 7.4 and stored at 4 °C. This procedure yielded 10 mg EGa1/1L bacterial culture, as was determined by a Micro BCA protein assay (Pierce Biotechnology, Rockford, IL, USA). EGa1 nanobody (18.3 kDa) was modified with an 8-fold molar excess of N-succinimidyl-S-acetylthioacetate (SATA) (Pierce Biotechnology, Rockford, IL, USA) as described in [38]. The introduced sulfhydryl groups were deacetylated for 30 min at RT by a deprotection buffer (0.5 M Hepes, 0.5 M hydroxylamine-HCl, 0.25 mM EDTA, pH 7) prior to addition of SATA-EGa1 to freshly prepared maleimidiyl-PEG nanoparticles. 12 mg of drug-loaded or empty nanoparticles (3 mg/ml) was reacted with 6.3 mg of NHS-PEG3500-maleimide (10:1, mol/mol, PEG:HSA) in 0.1 M phosphate buffer, pH 8 for 1 h at RT on a roller bench. PEGylated nanoparticles were isolated by centrifugation and resuspended in 0.1 M PB, pH 7 and immediately reacted with SATA-modified EGa1 (46 µg EGa1/mg nanoparticle, 0.2 nmol EGa1/nmol albumin) for 2 h at RT. The depletion of the free EGa1 in the coupling reaction was confirmed by loading an aliquot of the reaction mixture to a gel after 2 h. Control batches of PEGylated nanoparticles not-bearing EGa1 were prepared by overnight quenching of maleimidyl groups in 0.1 M sodium carbonate buffer, pH 9. Final products were centrifuged, washed, and resuspended in 0.1 M PB, pH 7 prior to use. Coupling of EGa1 to nanoparticles was studied by dot-blot immunodetection of EGa1 by spotting 2 µg of NANAPs onto a nitrocellulose membrane, followed by anti-EGa1 western blotting. The membrane was blocked with 5% BSA in Tris-buffered saline with 0.1% Tween-20, pH 7.5 (TBS-T) at 4 °C overnight and incubated with rabbit polyclonal anti-VHH serum (antiserum raised to llama heavy chain only variable domain, diluted 1:5000 in 5% BSA in TBS-T) for 2 h and subsequently with goat anti-rabbit peroxidase-conjugated secondary antibody (1:1000 dilution in 5% BSA TBS-T, Thermo Fisher Scientific, Rockford, IL, USA) for 1 h at RT. The signal was detected by using the SuperSignal West Femto Maximum Sensitivity Substrate (Thermo Fisher Scientific, Perbio Science Nerderland B.V) and chemiluminescence was visualized by a ChemiDoc XRS system (Bio-Rad Laboratories, Inc, USA).

5.2.6. Characterization of NANAPs

Size distribution and polydispersity of the NANAPs were determined by dynamic light scattering (DLS) on a Malvern ALV CGS-3 (Malvern Instruments, Malvern, UK) containing a He\Ne laser

source (λ=632.8 nm, 22 mW output power) under an angle of 90°. The zeta potential of the nanoparticles was determined using a Malvern zetasizer Nano-Z (Malvern Instruments, Malvern, UK). The measurements were performed in 5 mM phosphate buffer, pH 7.4 at 25 °C. The morphology and size of the nanoparticles were visualized by transmission electron microscopy (TEM). Briefly, samples (0.1 mg/ml in water) were soaked onto carbon coated copper grids for 2 min and excess liquid was removed by a filter paper. The grids were negatively stained with 2% uranyl acetate (Merck) for 45 s and dried for 10 min at RT before acquisition of TEM images (Tecnai 10, Philips, The Netherlands).

5.2.7. Release of 17864 from NANAPs

Release studies with 17864-loaded NANAPs (0.7 mg/ml) were conducted in PBS, 5 mM DTT in PBS and PBS supplemented with 10% fetal calf serum. At indicated time points samples were collected and diluted with 2 volumes of ACN to extract the released drug from the nanoparticles. Samples were spun down and the supernatants were analyzed by UPLC as described in Section 2.3. Measurements were performed in triplicate.

5.2.8. Cell experiments

Cell experiments were performed with the EGFR-positive head and neck squamous cell carcinoma cell line UM-SCC-14C (abbreviated as 14C, developed by Dr. T.E. Carey, Ann Arbor, MI, USA). The cells were cultured in Dulbecco's Modified Eagle's Medium (DMEM, PAA, Pasching, Austria) containing 3.7 g/l sodium bicarbonate, 4.5 g/l L-glucose, 2 mM L-glutamine and supplemented with 5% (v/v) fetal calf serum, penicillin (100 IU/ml), streptomycin (100 µg/ml), and amphotericin B (0.25 µg/ml) at 37 °C in a humidified atmosphere containing 5% CO2. The tests for mycoplasma infection were performed every 3 months and the cells were found to be mycoplasma free.

5.2.9. Binding and intracellular routing of NANAPs

Cellular binding of NANAPs was studied using Rho-L_x labeled nanoparticles. 14C cells were trypsinized and seeded at 50,000 cells/well in round bottom 96-well plates (Becton & Dickinson, Mountain View, CA, USA) on ice to prevent adherence. Next, the cells were incubated at 4 °C with Rho-L_x labeled nanoparticles at concentrations ranging from 0.0625 to 2 mg/ml in culture medium. Incubations were performed for 1 h in culture medium in the dark after which the cells were washed three times with 0.3% BSA in PBS and fixed with 10% formalin. The mean fluorescence intensity was determined with a BD FACSCanto II and analyzed with BD FACSDiva™ software (Becton & Dickinson, USA). Each experiment was performed in triplicate. To demonstrate the involvement of EGa1/EGFR-1 in the interaction of nanoparticles with the

cells, incubations were performed in the presence of an excess of free (100 µg) EGa1 nanobody (corresponding to 22-fold molar excess for 1 mg/ml Ega1-PEG-NP).

Internalization of NANAPs was studied with Alexa-488 labeled nanoparticles. 14C cells were seeded at 50,000 cells/well in 12 well plates and adhered overnight at 37 °C. 14C cells were pre-incubated with 2% of either 1-butanol or 2-propanol in serum free culture medium for 1 min. Subsequently, Alexa-488-conjugated nanoparticles (0.5 mg/ml) were allowed to internalize for 30 min in complete culture medium containing 2% of either 1-butanol or 2-propanol at 37 °C. After incubation, cells were put on ice and washed with ice-cold PBS to stop the internalization. Surface bound nanoparticles were removed by an acid wash (250 mM NaCl, 100 mM glycine, pH 2.5), performed two times for 10 min on ice followed by fixation of cells with 4% PFA (paraformaldehyde). Formalin-induced auto-fluorescence was quenched with 100 mM glycine in PBS for 15 min. Nuclei were stained with DAPI (Roche), 1 µg/ml in PBS for 5 min at RT. Images were taken with a wide field Olympus AX70 microscope, attached to a CCD camera (Nikon DXM1200) using a 60× objective oil immersion (NA 1.25/PlanFl).

Lysosomal colocalization of NANAPs was studied with Alexa-488 labeled nanoparticles. 14C cells were seeded at 50.000 cells/well in 12 well plates containing uncoated 12 mm glass cover slips and were allowed to adhere overnight. Cells were incubated with Alexa-488 conjugated nanoparticle formulations (0.5 mg/ml) in culture medium for 2 h at 37 °C. As a positive control for lysosomal uptake, Alexa-488 conjugated EGF (Invitrogen, 1 ng/ml) was allowed to internalize for 15 min and was chased for an additional 45 min at 37 °C. Late endosomes and lysosomes were stained by adding Lysotracker-Red DND-99 (Invitrogen, 65 nM in culture medium containing 2% Marvel) 90 min before fixation. Subsequently, cells were washed with PBS and fixed with 4% PFA for 30 min on ice and autofluorescence was quenched with 100 mM glycine for 15 min. Nuclei were stained with DAPI. Images were taken with a Zeiss Axiovert 200M confocal microscope equipped with a 63× oil immersion objective (NA 1.4).

Lysosomal degradation of NANAPs was studied with IRdye800 labeled nanoparticles. After cellular internalization and digestion of these NPs, the IRDye800 metabolites will not diffuse out of the cells due to the hydrophilic and charged nature of this label [39]. 14C cells were seeded at 50,000 cells/well in 12-well plates (Becton & Dickinson, Mountain View, CA, USA) and were allowed to adhere overnight. Cells were pulsed with 0.5 mg/ml IRdye800 labeled NPs, PEG-NPs and EGa1-PEG-NPs for 2 h at 37 °C. The medium was replaced by fresh incubation medium supplemented with or without 10 µM of chloroquine (CQ) and cells were incubated for an additional 48 h at 37 °C. Cells were washed with PBS and lysed in 40 µl of reducing sample buffer (50 mM Tris-HCl, pH 6.8, 10% glycerol, 100 mM DTT, 2% SDS and 0.01% bromophenol blue). High and low molecular weight IRDye800 peptidic fragments were separated by SDS-PAGE and quantified using an Odyssey Infrared Imager ® (LI-COR Biosciences).

5.2.10. Inhibition of tumor cell proliferation

Antiproliferative effects of 17864 loaded NANAPs were determined by a BrdU assay performed according to the supplier's instruction (Roche Diagnostics, Mannheim, Germany). 14C cells were seeded (4000 cells/well) in 96-well plates and allowed to adhere overnight. Cells were incubated with nanoparticles diluted in culture medium to concentrations ranging from 25 to 800 μg/ml (albumin concentration), corresponding to 3–100 μM conjugated 17864. In addition, cells were incubated with solutions of 2.5–60 μM of free 17864 and 17864-Lx for comparison with the nanoparticle formulations. After incubation for 48 h, the medium was replaced with BrdU (10 μM) containing complete medium and cells were incubated overnight at 37 °C. BrdU incorporation into the DNA was determined according to the supplier's protocol and measured on a SPECTROstarNano (BMG Labtech, Germany) at 450 nm with a reference wavelength of 690 nm. Cell proliferation is expressed relative to control cells not treated with nanoparticles.

5.3. Results and discussion

5.3.1. Preparation of albumin nanoparticles

The nanoparticles were prepared by ethanol desolvation of albumin followed by crosslinking with GA [17,18,36]. As shown in Table **1**, a subsequent two-step centrifugation yielded well-defined 100 nm nanoparticles with a narrow size-distribution. At pH 7.4 the nanoparticles have a negative zeta-potential (as expected; the pI of the native albumin is 4.5 [40]). The zeta potentials became more negative with increasing GA crosslinking, which is in agreement with the depletion of primary amino groups upon increased GA crosslinking. The yield of the nanoparticles can be increased by increasing the ethanol volume fraction, however this also leads to the unwanted formation of bigger aggregates.

Table 1. *Characteristics of nanoparticles*

Crosslink density	**Low**	**Medium**	**High**
Size (nm)	98 ± 10	97 ± 2	94 ± 3
PDI	0.07 ± 0.03	0.08 ± 0.04	0.1 ± 0.03
Zeta Potential (mV)	-29 ± 1.5	-36.5 ± 1.4	-38.5 ± 1.2
Yield (mg, %)	24 ± 3, 48	24 ± 2, 48	27 ± 1, 54

PDI: polydispersity index (n=3)

5.3.2. Loading of multikinase inhibitors and preparation of NANAPs

Nanoparticles loaded with the clinically approved multikinase inhibitor sunitinib were prepared by either pre-loading or post-loading of the drug into albumin nanoparticles (see supplemental information). *In vitro* release studies, however, demonstrated a very rapid release of sunitinib from the nanoparticles, independent of the crosslink density, in the presence of 1% or 4% albumin in the release buffer (100% of the loaded amount was released in less than 30 min most likely due to interaction with soluble albumin; data not shown). Therefore, the studies were continued with the 17864-L_x compound which was conjugated to the albumin nanoparticles via a coordinative linkage [35]. Only low cross-linked nanoparticles were used for the following studies, since a better degradability and PEGylation efficiency were anticipated, as compared to higher crosslinked nanoparticles. Upon coupling of 17864-L_x, size, zeta potential and PDI of drug loaded nanoparticles were similar as those of unloaded nanoparticles (see Tables **1** and **2**). 17864-loaded nanoparticles were surface modified with the bifunctional NHS-PEG3500-maleimide polymer and finally with SATA-EGa1 to yield NANAPs. PEGylation shielded the surface of the nanoparticles, as intended, since surface charge was slightly decreased from −26 to −21 mV after PEGylation (Table **2**). Importantly, the coupling of EGa1 to NANAPs was confirmed by a nanobody dot-blot analysis (Fig. **2A**). There was no free nanobody detectable 2 h after the coupling reaction with EGa1 observed by running an aliquot of the reaction mixture on a gel (results not shown). The final drug loaded NANAPs had a size of 138 nm, a narrow size distribution (PDI=0.13) and slightly negative zeta potential of −21 mV. The size and morphology of the NANAPs were visualized by TEM (Fig. **2B**), confirming their spherical shape. The observed size of the NANAPs (~100 nm) was in agreement with the DLS measurements.

Table 2. *Properties of nanoparticles after drug loading and surface functionalization*

Samples	EE%	LC%	LR (drug:HSA)	Size (nm)	PDI	Zeta Pot. (mV)
D-NP (17864-L_x-NP)	72 ± 5	4.0 ± 0.3	7.2 ± 0.5:1	100 ± 8	0.05 ± 0.02	-26 ± 2
PEG-D-NP				142 ± 5	0.17 ± 0.03	-21 ± 1
EGa1-PEG-D-NP (NANAPs)				138 ± 4	0.14 ± 0.04	-21 ± 2
PEG-NP	-	-	-	140 ± 2	0.11 ± 0.02	-23 ± 3
EGa1-PEG-NP	-	-	-	141 ± 3	0.13 ± 0.02	-23 ± 2

EE: encapsulation efficiency, LC: loading capacity, LR: loading ratio (mol/mol), PDI: polydispersity index, Zeta Pot: zeta potential, D-NP: Drug loaded nanoparticle, NP: nanoparticle, PEG: polyethylene glycol 3500.

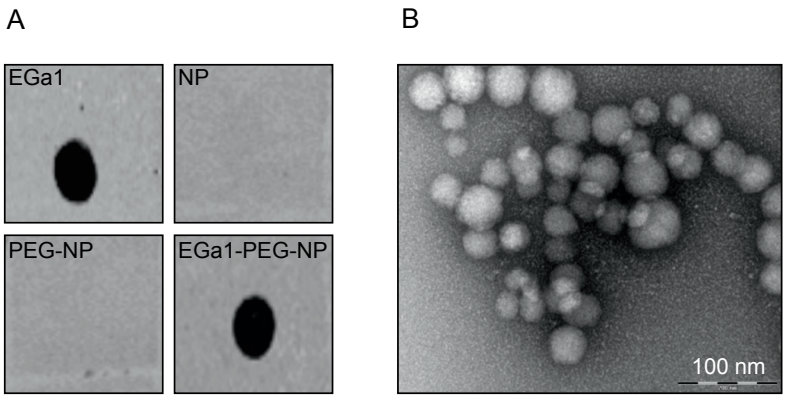

Figure 2. *(**A**) Dot blot analysis of free EGa1, nanoaprticles (NP), PEGylated nanoparticles (PEG-NP), EGa1 coupled PEGylated nanoparticles (EGa1-PEG-NP) and (**B**) Transmission electron microscopy image of 17864 loaded EGa1-PEG-NP.*

5.3.3. 17864 release and degradation of NANAPs

The 17864-Lx kinase inhibitor was conjugated to the albumin nanoparticles via a Pt(II) coordinative bond at sulfur containing side chain residues as methionine or cysteine. Previous studies with a drug-Lx conjugate have shown that the Lx linker is stable in plasma or serum [41], but that drug can be released via competitive displacement with thiol containing molecules [35]. As shown in Fig. **3**, less than 10% of the bound 17864 was released within 48 h in PBS or serum supplemented PBS. In the presence of DTT, however, the release of 17864 increased to 55% in 48 h. Of note, only the free 17864 was detected and not the 17864-Lx drug-platinum adduct. These results are in agreement with previous data obtained from Lx release [35]. Total release of the drug was obtained by competitive displacement with an excess of a platinum ligand at higher temperatures (see Section 2.3). One of the advantages of albumin nanoparticles over polymeric particles is their susceptibility of the core material to enzymatic digestion. Modification of the albumin by cross-linking and attachment of drug and PEG may however hamper its biodegradability. The influence of extent of crosslinking on degradability was studied by using trypsin as a model enzyme. As expected and also observed by Langer et al. [42] an increased crosslink density caused a decrease in degradation rate (Fig. **S1**). In addition, PEGylation and drug coupling both reduced the degradation rate of NPs (Fig. **S2A**). However, degradation was still observed for the three types of nanoparticles as determined by SDS-PAGE analysis (Fig. **S2B**) of the tryptic digests obtained after 6 h. Intact nanoparticles (lanes 1, 3, 5) were not able to enter the polyacrylamide gel and were retained in the slots at the top part of the gel. All digested samples (lanes 2, 4, 6) showed small peptidic fragments, indicating that nanoparticles had been degraded to fragments smaller than 10 kDa.

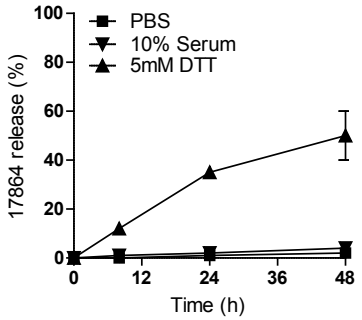

Figure 3. *The release of 17864 from NANAPs in PBS, PBS with 10% serum and 5 mM DTT at pH 7.4, 37 °C.*

5.3.4. Binding and intracellular routing of NANAPs

The binding of NANAPs by EGFR expressing 14C tumor cells was investigated using Rho-Lx labeled nanoparticles. Fig. **4A** shows that after incubation for 1 h at 4 °C, NPs bound non-specifically to 14C cells, however after PEGylation this non-specific binding was completely prevented. Importantly, when PEG-NPs were functionalized with the targeting ligand EGa1, total binding increased 5-fold in comparison to bare NPs. Moreover, at the highest dose EGa1 PEG-NPs bound over 40-fold more efficiently than PEGylated NPs without EGa1, clearly showing the potential of EGFR directed targeting for this type of head-and-neck carcinoma. To further demonstrate the interaction of EGa1-decorated nanoparticles with the target EGFR receptor, the binding of these nanoparticles was studied after preincubation of the cells with an excess of free EGa1. Fig. **4B** shows that binding of the EGa1 nanoparticles was indeed strongly inhibited by free nanobody, demonstrating the specificity of the interaction.

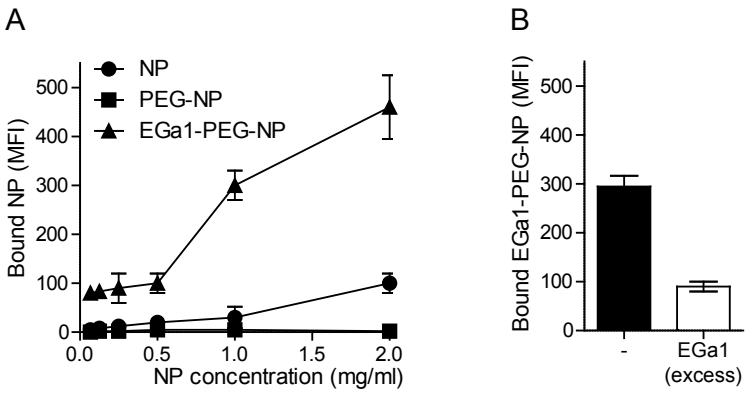

Figure 4. *Fluorescence activated cell sorting analysis of binding of Rho-L$_x$ labeled (A) EGa1-PEG-NP, NP, PEG NP and (B) EGa1-PEG-NP with and without free EGa1 (100 µg) at 4 °C for 1 h on 14C cells (MFI; mean fluorescence intensity).*

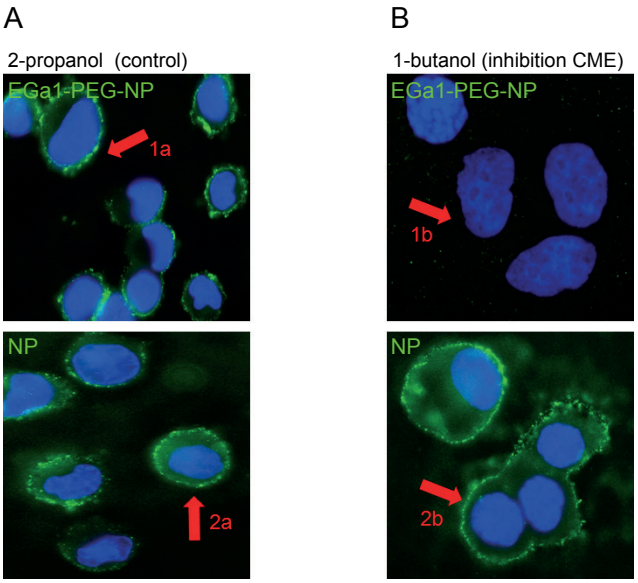

Figure 5. *A) Internalization of nanoparticle formulations by 14C cells pre-incubated with either 2-propanol or B) 1-butanol for 30 min at 37 °C. Nanoparticles were labeled with Alexa-488 (green) and the nucleus was stained with DAPI (blue). Arrow 1a: EGa1-PEG-NPs are taken up. Arrow 2a: NPs are taken up. Arrow 1b: EGa1-PEG-NP uptake is clathrin-dependent. Arrow 2b: NP uptake is clathrin-independent.*

To study the uptake as well as the pathway of endocytosis and lysosomal colocalizations of the nanoparticles, 14C cells were incubated with Alexa-488 labeled nanoparticles at 37 °C. To allow visualization of internalized nanoparticles only, i.e. without interference of surface located nanoparticles, the cells were stripped by a mild acid-wash procedure after the incubations. Activated EGF receptors are internalized into cells by both clathrin-mediated (CME) (at physiological plasma concentration of EGF; 1 ng/ml) and non-clathrin-mediated endocytosis (high EGF concentration) [43]. We investigated which of these trafficking routes is involved in the uptake of the EGFR targeted nanoparticles by studying their uptake in the presence of 1-butanol. Phospholipids play an important role in CME, especially during the formation of the clathrin coated vesicles that bud off from the cell membrane. While the vesicles are forming, adaptor proteins involved in clathrin-mediated endocytosis interact with the phospholipid, phosphoinositide-4,5-biphosphate (PIP2) in the membrane [44]. 1-Butanol, inhibits the formation of PIP2, resulting in the removal of PIP2 from the membrane, consequently blocking CME [45]. EGa1-PEG-NPs were internalized in the presence of 2-propanol (which does not interfere with CME) as shown in Fig. **5A**. In contrast, EGa1-PEG-NPs were not internalized in the presence of 1-butanol (Fig. **5B**). From this result, it is concluded that EGa1-PEG-NPs are taken up specifically via CME. In contrast, non-PEGylated

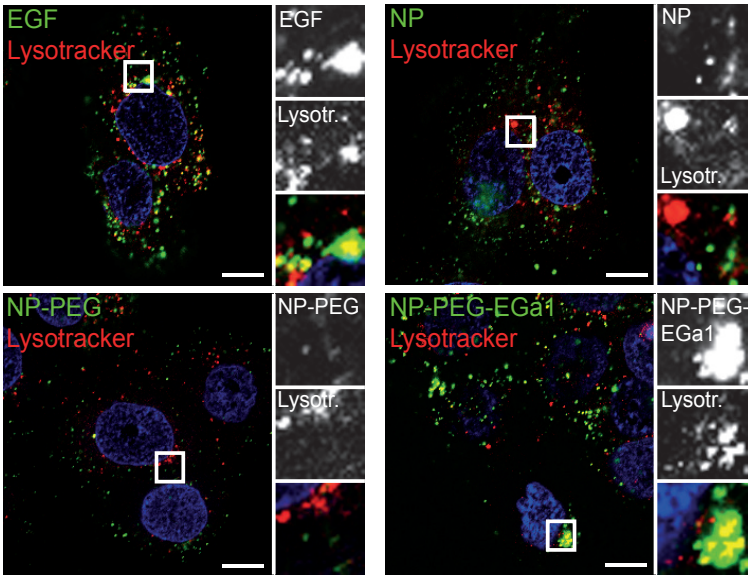

***Figure 6**. Co-localization of EGF, NPs, PEG-NPs and EGa1-PEG-NPs (green) with Lysotracker Red (lysosome marker) on 14C cells after 24 h. Nuclei were stained with DAPI (blue). Boxed areas were enlarged.*

NPs without EGa1 were internalized via clathrin-independent mechanisms, as addition of 1-butanol did not affect their uptake (Fig. **5A–B**, arrows **2a** and **2b**). To investigate whether the internalized NPs were transported to lysosomes, co-localization of Alexa-488 nanoparticles was studied with lysotracker-red. EGF was used as a positive control for lysosomal targeting. Both EGF and EGa1-PEG-NPs accumulated in the lysosomal compartment, as demonstrated by co-localization of the green labeled nanoparticle with the red lysotracker, resulting in yellow perinuclear staining (Fig. **6**). In contrast, NPs were internalized via a different type of endocytic vesicles and did not co-localize with lysotracker.

5.3.5. Lysosomal uptake and degradation of NANAPs

Lysosomal degradation of the particles after their uptake by 14C cells was studied with IRDye800 labeled nanoparticles. IRDye800 remains entrapped inside the cells due to the hydrophilic and charged nature of this label [39]. 14C cells that were incubated with nanoparticles for 24 h were lysed and the cell lysates were loaded onto a gel. SDS-PAGE analysis showed the intracellular degradation of the internalized EGa1-PEG-NPs, PEG-NPs and NPs into small fragments (Fig. **7A**). PEG-NPs showed a low extent of internalization resulting in only minor degradation products. The degradation of NPs was 5 times less than the EGa1-PEG-NPs (Fig.

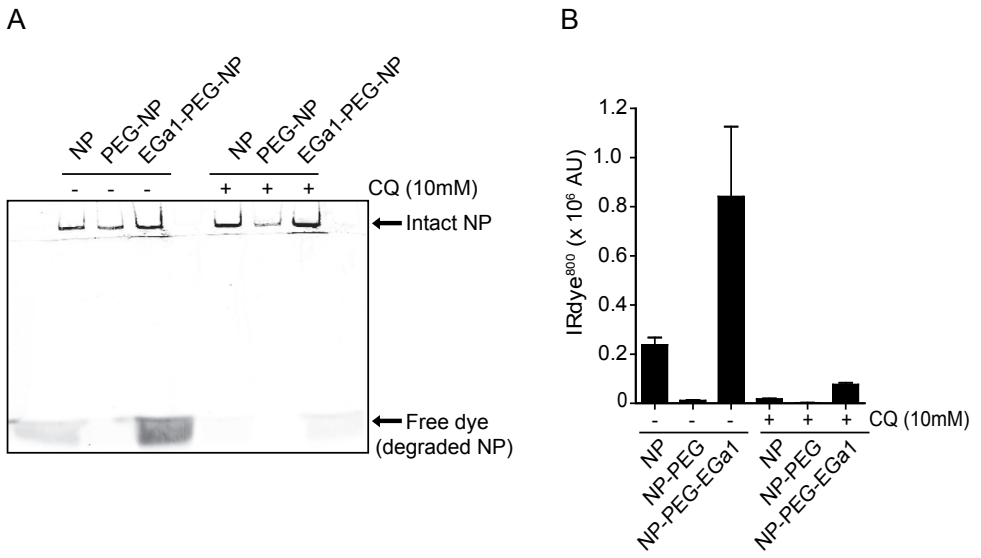

***Figure** 7. Quantification of lysosomal degradation of NANAPS with and without chloroquine treatment. Cells were lysed and the lysates were loaded on an SDS-PAGE gel to visualize the IRdye800 after 24 h incubation with 14C cells at 37 °C. Band intensities of degraded nanoparticles were quantified (n=3).*

5

7B). To demonstrate that this degradation occurs in lysosomes, chloroquine was added which impairs endocytosis, exocytosis and lysosomal degradation. As a weak base it can enter low pH endosomal and lysosomal compartments. Its accumulation results in an increase in pH and osmotic pressure thereby inhibiting the lysosomal degradation and endosomal trafficking inside the cells [46]. EGa1-PEG-NPs and NPs that were localized in lysosomes were affected from CQ treatment similarly. As such, the inhibition of lysosomal activity resulted in a 10-fold decrease in degradation in the presence of CQ (Fig. **7B**).

5.3.6. Inhibition of tumor cell proliferation

17864 inhibits multiple tyrosine kinases involved in tumor cell proliferation. The anti-proliferation activity of 17864-loaded nanoparticles was studied using a BrdU proliferation assay, after 48 h of incubation with 14C cells. NANAPs efficiently inhibited tumor cell proliferation, with an IC_{50} of 40 μM (Fig. **8A**), which is 2.8 times higher than the IC_{50} of free 17864 and 17864-L_x (Fig. **8B**, 14 μM for both compounds). As discussed in previous sections, EGa1-decorated nanoparticles enter cells via CME and require lysosomal processing before 17864 can be released. In contrast, small molecule inhibitors diffuse across the cellular membranes without prior activation steps, which often render small molecules more effective than their nanomedicine counterpart in experiments

with *in vitro* cultured cells [47]. The *in vitro* experiments in Fig. **8** demonstrate the importance of active targeting in the intracellular accumulation and activation of albumin nanoparticles. Non-targeted PEGylated nanoparticles with 17864 did not inhibit proliferation of 14C tumor cells, which can be ascribed to the very low cellular uptake of these particles. But even bare nanoparticles loaded with 17864, which are internalized and degraded to some extent, were not capable of reaching the IC_{50} at the tested concentration range (Fig. **8C**). EGa1 nanobody in itself is a blocker of EGFR phosphorylation and may therefore inhibit proliferation of EGFR-positive 14C cells. Previous studies with EGa1 decorated liposomes have shown that such nanoparticles, due to multimerization of the nanobody, are even stronger inhibitors of EGFR phosphorylation than free nanobody [38]. However, the inhibitory effect of multivalent EGa1-liposomes is not sufficient to completely prevent tumor cell proliferation and only resulted in significant growth inhibition of 14C cells when the liposomes were loaded with an antiproliferative drug [48]. Our results are in line with such observations, as we only see profound inhibitory effects of the combined coupling of EGa1 and 17864 to albumin nanoparticles (Fig. **8D**).

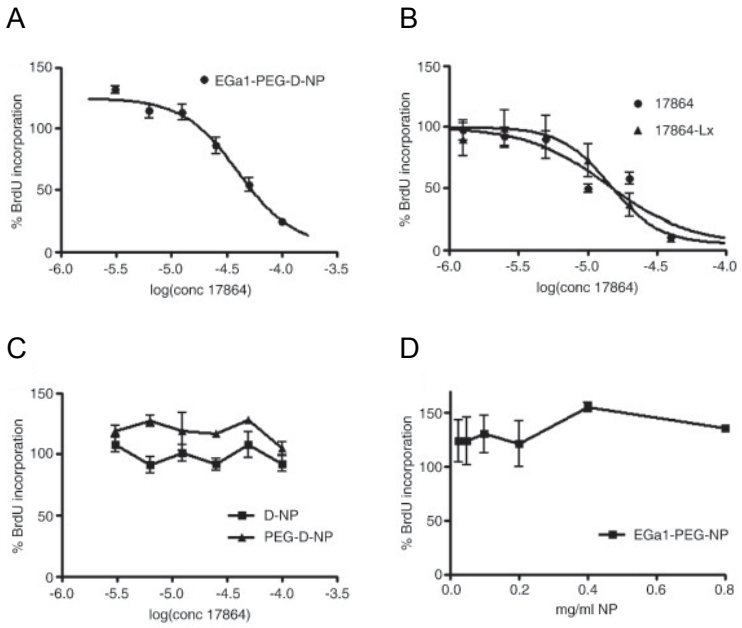

Figure 8. *Inhibition of 14C cell proliferation with different types of NPs and drug treatments after 48 h incubation at 37 °C. A) Incubation with 17864-L_x loaded EGa1-PEG-NPs (0.025– 0.8 mg/ml NP; equivalent to 3–100 μM 17864); B) Incubation with free 17864 and 17864-L_x; (equivalent to 1–40 μM 17864); C) Incubation with 17864-L_x loaded PEG-NP and NPs (0.025–0.8 mg/ml NP; equivalent to 3–100 μM 17864); and D) Incubation with EGa1-PEG-NPs not loaded with 17864-L_x (0.025–0.8 mg/ml NP).*

5.4. Conclusion

In conclusion, we have developed a novel drug carrier system loaded with the multikinase inhibitor 17864 conjugated to the albumin backbone via a platinum based linker (L_x). PEGylation of nanoparticles successfully inhibited the aspecific binding of the nanoparticles to cells. Further functionalization with EGa1 resulted in nanoparticles that were internalized in an EGFR-dependent manner. The pathway of uptake and compartmentalization in the lysosomes was crucial for the intracellular release of 17864 from L_x. The tunable characteristics of the NANAPs make them promising new materials favorable for *in vivo* use as targeted nanomedicines in the treatment EGFR positive cancers.

5.5. Acknowledgments

We thank Öznur Akbal from Hacettepe University for her assistance in the experiments and Vichem Chemie for the production of 17864. This project is supported by the Utrecht University Focus and Massa program Nanobullets: The next generation in drug targeting.

5.6. References

[1] A. Abu Lila, T. Ishida, H. Kiwada, Targeting anticancer drugs to tumor vasculature using cationic liposomes, Pharm Res. 27 (2010) 1171-1183.
[2] F. Yang, C. Jin, Y. Jiang, J. Li, Y. Di, Q. Ni, D. Fu, Liposome based delivery systems in pancreatic cancer treatment: From bench to bedside, Cancer Treat. Rev. 37 (2011) 633-642.
[3] S. Parveen, S.K. Sahoo, Polymeric nanoparticles for cancer therapy, J. Drug Target. 16 (2008) 108-123.
[4] U. Kedar, P. Phutane, S. Shidhaye, V. Kadam, Advances in polymeric micelles for drug delivery and tumor targeting, Nanomedicine: Nanotechnology, Biology and Medicine. 6 (2010) 714-729.
[5] F. Kratz, Albumin as a drug carrier: Design of prodrugs, drug conjugates and nanoparticles, J. Controlled Release. 132 (2008) 171-183.
[6] H. Jeong, M. Huh, S. Lee, H. Koo, I. Kwon, S. Jeong, K. Kim, Photosensitizer-conjugate human serum albumin nanoparticles for effective photodynamic therapy, Theranostics. 6 (2011) 230-239.
[7] S. Dreis, F. Rothweiler, M. Michaelis, J. Cinatl Jr., J. Kreuter, K. Langer, Preparation, characterisation and maintenance of drug efficacy of doxorubicin-loaded human serum albumin (HSA) nanoparticles, Int. J. Pharm. 341 (2007) 207-214.
[8] S. Rhaese, H. von Briesen, H. Rübsamen-Waigmann, J. Kreuter, K. Langer, Human serum albumin–polyethylenimine nanoparticles for gene delivery, J. Controlled Release. 92 (2003) 199-208.
[9] A.P. Retnakumari, P.L. Hanumanthu, Malarvizhi. G.L., R. Prabhu, N. Sidharthan, M.V. Thampi, D. Menon, U. Mony, K. Menon, P. Keechilat, S. Nair, M. Koyakutty, Rationally Designed Aberrant Kinase-Targeted Endogenous Protein Nanomedicine against Oncogene Mutated/Amplified Refractory Chronic Myeloid Leukemia, Molecular Pharmaceutics. (2012) PMID:22971013.
[10] K. Ulbrich, M. Michaelis, F. Rothweiler, T. Knobloch, P. Sithisarn, J. Cinatl, J. Kreuter, Interaction of folate-conjugated human serum albumin (HSA) nanoparticles with tumour cells, Int. J. Pharm. 406 (2011) 128-134.
[11] F. Petrelli, K. Borgonovo, S. Barni, Targeted delivery for breast cancer therapy: the history of nanoparticle-albumin-bound paclitaxel, Expert Opin. Pharmacother. 11 (2010) 1413-1432.
[12] F. Kratz, B. Elsadek, Clinical impact of serum proteins on drug delivery, J. Controlled Release. 161 (2012) 429-445.
[13] K. Löw, M. Wacker, S. Wagner, K. Langer, H. von Briesen, Targeted human serum albumin nanoparticles for specific uptake in

EGFR-Expressing colon carcinoma cells, Nanomedicine: Nanotechnology, Biology and Medicine. 7 (2011) 454-463.
[14] M. Anhorn, S. Wagner, J. Kreuter, K. Langer, H. von Briesen, Specific targeting of HER2 overexpressing breast cancer cells with doxorubicin-loaded trastuzumab-modified human serum albumin nanoparticles, Bioconjug Chem. 19 (2008) 2321-2331.
[15] I. Steinhauser, B. Spänkuch, K. Strebhardt, K. Langer, Trastuzumab-modified nanoparticles: Optimisation of preparation and uptake in cancer cells, Biomaterials. 27 (2006) 4975-4983.
[16] I.M. Steinhauser, K. Langer, K.M. Strebhardt, B. Spänkuch, Effect of trastuzumab-modified antisense oligonucleotide-loaded human serum albumin nanoparticles prepared by heat denaturation, Biomaterials. 29 (2008) 4022-4028.
[17] H. Wartlick, K. Michaelis, S. Balthasar, K. Strebhardt, J. Kreuter, K. Langer, Highly Specific HER2-mediated Cellular Uptake of Antibody-modified Nanoparticles in Tumour Cells, J. Drug Target. 12 (2004) 461-471.
[18] S. Wagner, F. Rothweiler, M.G. Anhorn, D. Sauer, I. Riemann, E.C. Weiss, A. Katsen-Globa, M. Michaelis, J. Cinatl Jr., D. Schwartz, J. Kreuter, H. von Briesen, K. Langer, Enhanced drug targeting by attachment of an anti αv integrin antibody to doxorubicin loaded human serum albumin nanoparticles, Biomaterials. 31 (2010) 2388-2398.
[19] N. Dinauer, S. Balthasar, C. Weber, J. Kreuter, K. Langer, H. von Briesen, Selective targeting of antibody-conjugated nanoparticles to leukemic cells and primary T-lymphocytes, Biomaterials. 26 (2005) 5898-5906.
[20] L. Zhang, S. Hou, S. Mao, D. Wei, X. Song, Y. Lu, Uptake of folate-conjugated albumin nanoparticles to the SKOV3 cells, Int. J. Pharm. 287 (2004) 155-162.
[21] D. Zhao, X. Zhao, Y. Zu, J. Li, Y. Zhang, R. Jiang, Z. Zhang, Preparation, characterization and in vitro targeted delivery of folate-decorated paclitaxel-loaded bovine serum albumin nanoparticles, Int J Nanomedicine. 20 (2010) 669-677.
[22] Q. Li, C. Liu, X. Zhao, Y. Zu, Y. Wang, B. Zhang, D. Zhao, Q. Zhao, L. Su, Y. Gao, B. Sun, Preparation, characterization and targeting of micronized 10-hydroxycamptothecin-loaded folate-conjugated human serum albumin nanoparticles to cancer cells, Int J Nanomedicine. 6 (2011) 397-405.
[23] J. Kreuter, T. Hekmatara, S. Dreis, T. Vogel, S. Gelperina, K. Langer, Covalent attachment of apolipoprotein A-I and apolipoprotein B-100 to albumin nanoparticles enables drug transport into the brain, J. Controlled Release. 118 (2007) 54-58.
[24] P.K. Dubey, D. Singodia, R.K. Verma, S.P. Vyas, RGD modified albumin nanospheres for tumour vasculature targeting, J. Pharm. Pharmacol. 63 (2011) 33-40.
[25] X. Qu, C. Yang, J. Zhang, N. Ding, Y. Lu, L. Huang, G. Xiang, In vitro evaluation of a Folate-bovine serum albumin-doxorubicin conjugate, J. Drug Target. 18 (2010) 351-361.
[26] S. Muyldermans, M. Lauwereys, Unique single-domain antigen binding fragments derived from naturally occurring camel heavy-chain antibodies, Journal of Molecular Recognition. 12 (1999) 131-140.
[27] V. Joosten, M.S. Roelofs, N. van den Dries, T. Goosen, C.T. Verrips, C.A.M.J.J. van den Hondel, B.C. Lokman, Production of bifunctional proteins by Aspergillus awamori: Llama variable heavy chain antibody fragment (VHH) R9 coupled to Arthromyces ramosus peroxidase (ARP), J. Biotechnol. 120 (2005) 347-359.
[28] P.A. Barthelemy, H. Raab, B.A. Appleton, C.J. Bond, P. Wu, C. Wiesmann, S.S. Sidhu, Comprehensive Analysis of the Factors Contributing to the Stability and Solubility of Autonomous Human VH Domains, Journal of Biological Chemistry. 283 (2008) 3639-3654.
[29] I. Vaneycken, J. Govaert, C. Vincke, V. Caveliers, T. Lahoutte, P. De Baetselier, G. Raes, A. Bossuyt, S. Muyldermans, N. Devoogdt, In vitro analysis and in vivo tumor targeting of a humanized, grafted nanobody in mice using pinhole SPECT/Micro-CT, J Nucl Med. 51 (2010) 1099-1106.
[30] A.M. Eisenbeis, S.J. Grau, Monoclonal antibodies and Fc fragments for treating solid tumors, Biologics. 6 (2012) 13-20.
[31] R. Roovers, P. Henderikx, W. Helfrich, E. van der Linden, A. Reurs, A. de Bruïne, J. Arends, L. de Leij, H. Hoogenboom, High-affinity recombinant phage antibodies to the pan-carcinoma marker epithelial glycoprotein-2 for tumour targeting, Br. J Cancer. 78 (1998) 1407-1416.
[32] F. Rahbarizadeh, D. Ahmadvand, Z. Sharifzadeh, Nanobody; an Old Concept and New Vehicle for Immunotargeting, Immunol.

Invest. 40 (2011) 299-338.
[33] S. Harmsen, M. Dolman, Z. Nemes, M. Lacombe, B. Szokol, J. Pató, G. Kéri, L. Orfi, G. Storm, W. Hennink, R. Kok, Development of a cell-selective and intrinsically active multikinase inhibitor bioconjugate, Bioconjug Chem. 22 (2011) 540-545.
[34] D. Berz, H. Wanebo, Targeting the growth factors and angiogenesis pathways: Small molecules in solid tumors, J. Surg. Oncol. 103 (2011) 574-586.
[35] K. Temming, M. Lacombe, P. van der Hoeven, J. Prakash, T. Gonzalo, E. Dijkers, L. Orfi, G. Kéri, K. Poelstra, G. Molema, R. Kok, Delivery of the p38 MAPkinase inhibitor SB202190 to angiogenic endothelial cells: development of novel RGD-equipped and PEGylated drug-albumin conjugates using platinum(II)-based drug linker technology, Bioconjug Chem. 17 (2006) 1246-1255.
[36] K. Langer, S. Balthasar, V. Vogel, N. Dinauer, H. von Briesen, D. Schubert, Optimization of the preparation process for human serum albumin (HSA) nanoparticles, Int. J. Pharm. 257 (2003) 169-180.
[37] M.M. Fretz, M.E.(.M. Dolman, M. Lacombe, J. Prakash, T.Q. Nguyen, R. Goldschmeding, J. Pato, G. Storm, W.E. Hennink, R.J. Kok, Intervention in growth factor activated signaling pathways by renally targeted kinase inhibitors, J. Controlled Release. 132 (2008) 200-207.
[38] S. Oliveira, R.M. Schiffelers, J. van der Veeken, R. van der Meel, R. Vongpromek, van Bergen en Henegouwen,Paul M.P., G. Storm, R.C. Roovers, Downregulation of EGFR by a novel multivalent nanobody-liposome platform, J. Controlled Release. 145 (2010) 165-175.
[39] S. Oliveira, R. Cohen, M. Stigter-van Walsum, G.A. van Dongen, S.G. Elias, P.J. van Diest, W. Mali, van Bergen en Henegouwen, P.M., A novel method to quantify IRDye800CW fluorescent antibody probes ex vivo in tissue distribution studies, EJNMMI Research. 2 (2012).
[40] A.O. Elzoghby, W.M. Samy, N.A. Elgindy, Albumin-based nanoparticles as potential controlled release drug delivery systems, J. Controlled Release. 157 (2012) 168-182.
[41] J. Prakash, M. Sandovici, V. Saluja, M. Lacombe, R.Q.J. Schaapveld, M.H. de Borst, H. van Goor, R.H. Henning, J.H. Proost, F. Moolenaar, G. Këri, D.K.F. Meijer, K. Poelstra, R.J. Kok, Intracellular Delivery of the p38 Mitogen-Activated Protein Kinase Inhibitor SB202190 [4-(4-Fluorophenyl)-2-(4-hydroxyphenyl)-5-(4-pyridyl)1H-imidazole] in Renal Tubular Cells: A Novel Strategy to Treat Renal Fibrosis, Journal of Pharmacology and Experimental Therapeutics. 319 (2006) 8-19.
[42] K. Langer, M.G. Anhorn, I. Steinhauser, S. Dreis, D. Celebi, N. Schrickel, S. Faust, V. Vogel, Human serum albumin (HSA) nanoparticles: Reproducibility of preparation process and kinetics of enzymatic degradation, Int. J. Pharm. 347 (2008) 109-117.
[43] A. Sorkin, L.K. Goh, Endocytosis and intracellular trafficking of ErbBs, Exp Cell Res. 314 (2008) 3093-3106.
[44] E. Boucrot, S. Saffarian, R. Massol, T. Kirchhausen, M. Ehrlich, Role of lipids and actin in the formation of clathrin-coated pits, Exp. Cell Res. 312 (2006) 4036-4048.
[45] C. Antonescu, G. Danuser, S. Schmid, Phosphatidic acid plays a regulatory role in clathrin-mediated endocytosis, Mol Biol Cell. 21 (2010) 2944-2952.
[46] J.L. Ambroso, C. Harris, Chloroquine accumulation and alterations of proteolysis and pinocytosis in the rat conceptus in vitro, Biochem. Pharmacol. 47 (1994) 679-688.
[47] M. Talelli, M. Iman, A.K. Varkouhi, C.J.F. Rijcken, R.M. Schiffelers, T. Etrych, K. Ulbrich, C.F. van Nostrum, T. Lammers, G. Storm, W.E. Hennink, Core-crosslinked polymeric micelles with controlled release of covalently entrapped doxorubicin, Biomaterials. 31 (2010) 7797-7804.
[48] R. van der Meel, S. Oliveira, I. Altintas, R. Haselberg, J. van der Veeken, R.C. Roovers, van Bergen en Henegouwen,Paul M.P., G. Storm, W.E. Hennink, R.M. Schiffelers, R.J. Kok, Tumor-targeted Nanobullets: Anti-EGFR nanobody-liposomes loaded with anti-IGF-1R kinase inhibitor for cancer treatment, J. Controlled Release. 159 (2012) 281-289.

5.7. Supplementary information

Methods

Loading of albumin nanoparticles with sunitinib

Two approaches were followed to load the multikinase inhibitor sunitinib in albumin nanoparticles: a pre-loading method in which sunitinib was added to the albumin solution before formation of nanoparticles and post-loading, by loading already formed nanoparticles with sunitinib.

Pre-loading method

50 mg of human serum albumin (50 mg/ml in deionized water, pH adjusted to 8.3) was mixed with 1.3 mg of sunitinib malate (3.2: 1, mol:mol, sunitinib: albumin). 2.8 ml of 92% ethanol was added drop wise and albumin was crosslinked with 18, 29, 59 µl of 8% glutaraldehyde to obtain low, medium and high crosslinked nanoparticles. Nanoparticles were purified by two-step centrifugation, once at 1000 g for 5 min and later at 35000 g three times for 1h at 4 ºC in deionized water. After centrifugation, nanoparticles were sonicated for 4 min and stored in deionized water at 4 ºC . The yield was determined by thermographic analysis by measuring the dry weight of a 100 µl nanoparticle suspension. To determine sunitinib loading, nanoparticles were treated with acetonitrile (2:1 (v/v); ACN: nanoparticle suspension) at room temperature overnight to extract sunitinib from the nanoparticles. After centrifugation and two additional extractions with ACN, the combined supernatants were analyzed by ultra performance liquid chromatography (Acquity UPLC®) on an Acquity UPLC® BEH C18 1.7 µm, 2.1 x 50 mm column (Waters, Ireland). Sunitinib was eluted with a water/ACN/TFA gradient starting from 100% eluent A (95% H_2O, 5% ACN, 0.1% TFA) and going up to 100% eluent B (5% H_2O, 95% ACN, 0.1% TFA) in 3.5 min at a flow rate of 1 ml/min. Sunitinib was detected at 425 nm and eluted at 1.2 min.

Post-loading method

12 mg of low crosslinked nanoparticles (2 mg/ml in deionized water) was incubated with 0.72 mg of sunitinib (10:1, mol/mol, sunitinib: albumin) in deionized water overnight at room temperature. 0.008 % (v/v) SDS was added to the reaction mixture to prevent flocculation. After 16 h, particles were purified and stored as mentioned above. Sunitinib loading was determined by UPLC as mentioned above.

Trypsin digestion albumin nanoparticles

Nanoparticles (3 mg/ml in PBS) were incubated with trypsin (85 µg/ml in PBS) at 37 ºC under constant shaking. At different time intervals, the turbidity was measured at 550 nm with a UV

spectrophotometer (UVmini 1240 CE, UV-VIS spectrophotometer, Shimadzu) and correlated to a calibration curve made 0.6-2.2 mg/ml drug-free nanoparticles in PBS (r^2 = 0.9955). Trypsin digested samples were analyzed by SDS-PAGE electrophoresis (NuPAGE Novex Bis-Tris mini gel, 4-12% gradient, 1 mm, Invitrogen, Breda, The Netherlands) and stained with Coomassie blue.

Results and Discussion

Loading of albumin nanoparticles with sunitinib

Table 1S. *Properties of sunitinib loaded albumin nanoparticles*

Drug	Loading method	NP Crosslink (CL) density	EE%	LR (drug: HSA)	Size (nm)	PDI	Zeta Pot. (mV)
Sunitinib	Pre	Low	29 ± 2	2.6 ± 0.2:1	130 ± 4	0.12 ± 0.02	-24 ± 1
		Medium	26 ± 1	2.7 ± 0.1:1	133 ± 7	0.06 ± 0.01	-22 ± 2
		High	23 ± 2	2.8 ± 0.1:1	132 ± 4	0.07 ± 0.03	-23 ± 3
	Post	Low	80 ± 6	8.0 ± 0.6:1	131 ± 3	0.09 ± 0.03	-22 ± 1

EE: encapsulation efficiency, LR: loading ratio (mol:mol), PDI: polydispersity index, Zeta Pot: zeta potential

The clear difference in encapsulation efficiencies of post and pre-loaded nanoparticles can be attributed to the difference of the reaction buffers. The pre-loading was performed in 75% ethanol whereas the post-loading was performed in fully aqueous conditions. Therefore, the partitioning of sunitinib to albumin nanoparticles is higher in post-loading in comparison to pre-loading.

Trypsin digestion of low, medium and high crosslinked albumin nanoparticles

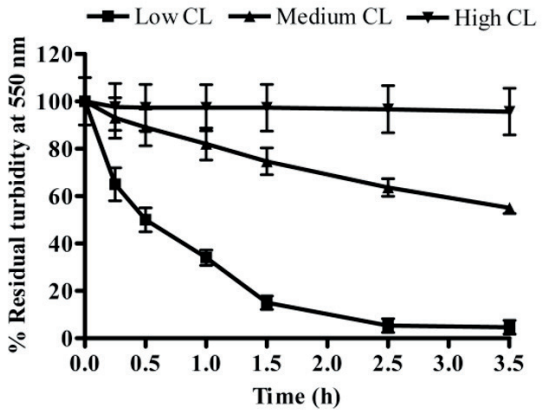

Figure S1. *Percentage of residual turbidity of Low, Medium and High crosslinked (CL) nanoparticles after treatment with trypsin in PBS, pH 7.4, 37 ºC measured at 550 nm (n=3).*

Trypsin digestion of 17864 loaded albumin nanoparticles

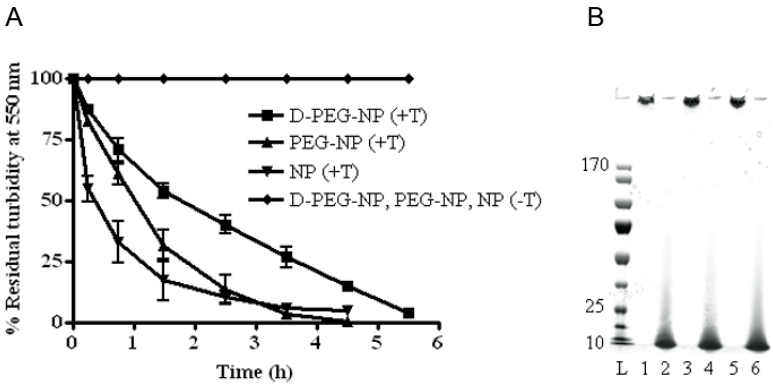

Figure S2. *A) Percentage of residual turbidity of NP, PEG-NP and 17864-L$_x$ (D) PEG-NP after incubation with (+T) and without (-T) trypsin in PBS, pH 7.4, 37 ºC measured at 550 nm (n=3). B) Gel image of trypsin digested fragments. Lane L: protein ladder, 1: intact NP (-T), 2: digested NP, 3: intact PEG-NP (-T), 4: digested PEG-NP, 5: intact D-PEG-NP (-T), 6: digested D-PEG-NP.*

Chapter 6

Targeting hepatocyte growth factor receptor (Met) positive tumor cells using internalizing nanobody-decorated albumin nanoparticles

Raimond Heukers[1†], Isil Altintas[2†], Smiriti Raghoenath[1], Erica de Zan[2], Richard Pepermans[1], Rob C. Roovers[1,‡], Rob Haselberg[3], Wim E. Hennink[2], Raymond M. Schiffelers[2,4], Robbert J. Kok[2], and Paul M.P. van Bergen en Henegouwen[1]*

[1] Cell Biology, Department of Biology, Utrecht University, Utrecht, The Netherlands
[2] Department of Pharmaceutics, Utrecht Institute for Pharmaceutical Sciences, Utrecht University, Utrecht, The Netherlands
[3] Division of BioAnalytical Chemistry, AIMMS research group BioMolecular Analysis, VU University Amsterdam, Amsterdam, The Netherlands
[4] Laboratory Clinical Chemistry and Haematology, UMC Utrecht, Utrecht, The Netherlands

† Authors contributed equally
‡ Current address: Merus BV, Utrecht, The Netherlands

Biomaterials. 2014 Jan;35(1):601-10

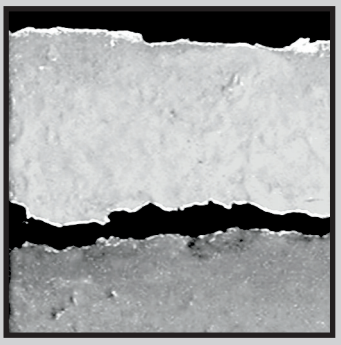

Abstract

The hepatocyte growth factor receptor (HGFR, c-Met or Met), is a receptor tyrosine kinase that is involved in embryogenesis, tissue regeneration and wound healing. Abnormal activation of this proto-oncogene product is implicated in the development, progression and metastasis of many cancers. Current therapies directed against Met, such as ligand- or, dimerization-blocking antibodies or kinase inhibitors, reduce tumor growth but hardly eradicate the tumor. In order to improve anti-Met therapy, we have designed a novel drug delivery system consisting of cross linked albumin nanoparticles decorated with newly selected anti-Met nanobodies (anti-Met-NANAP). The anti-Met NANAPs bound specifically to and were specifically taken up by Met-expressing cells and transported to lysosomes for degradation. Treatment of tumor cells with anti-Met NANAPs also resulted in down regulation of the total Met protein. This study shows that anti-Met NANAPs offer a potential system for lysosomal delivery of drugs into Met-positive tumor cells.

6.1. Introduction

The hepatocyte growth factor (HGF) receptor (HGFR, c-Met or Met), is a receptor tyrosine kinase (RTK) that is primarily expressed on epithelial cells. HGF is the only known, high affinity ligand for this receptor (1). Binding of HGF to Met activates the receptor, resulting in tyrosine phosphorylation of the receptor and the activation of several downstream signal transduction pathways such as MAPK, STAT and PI3kinase/Akt (1-4). Met/HGF signaling is important for embryogenesis and also for tissue regeneration and wound healing in the adult life (5-7). Deregulated Met signaling is implicated in the development, progression and metastasis of a wide variety of human cancers (8,9). This can be due to either mutational activation, receptor/ligand overexpression, autocrine activation or ligand-independent activation of Met. Met is therefore an attractive target for anticancer therapy and several agents interfering with the Met/HGF pathway are under development such as, Met/HGF signaling small molecule inhibitors, antibodies and decoy receptors (10,11). However, to improve on these existing therapies, it can be expected that the efficacy of anti-Met therapies can be further augmented by combining them with chemotherapeutic drugs, especially when these are combined in a targeted drug delivery system (12).

Like most RTKs, ligand binding and activation of the Met tyrosine kinase initiates internalization of the receptor-ligand complexes, which is followed by intracellular trafficking and degradation of both receptor and ligand in lysosomes (11-15). This internalization and lysosomal trafficking can be used for targeted delivery and release of drugs inside tumor cells. Previously, we designed anti-EGFR Nanobody-Albumin Nanoparticles (NANAPs) which are albumin-based nanoparticles decorated with nanobodies that target the epidermal growth factor receptor (EGFR). NANAPs were shown to bind to and internalize into EGFR-expressing cells and were found to be suitable for targeted delivery of anti-cancer drugs into cells (16). A nanobody (or VHH) is the antigen-binding domain of heavy-chain-only antibodies found in members of the *camelidae* family. Despite their small (~15 kDa) size, their binding affinity is similar to that of monoclonal antibodies (17). Due to their small size and less complex structure nanobodies can be easily produced in prokaryotic systems giving them advantage over monoclonal antibodies or antibody fragments (18). Nanobody-coupled liposomal and polymeric nanoparticles have already been shown to induce tumor regression in mice bearing head and neck squamous carcinoma tumors (19,20).

In this study we have developed a NANAP system that specifically targets the Met receptor. Met binding nanobodies were selected by phage display technology and their binding capacity and agonistic/antagonistic properties were characterized. We then designed anti-Met NANAPs by using the nanobody with the highest binding affinity to Met to decorate the albumin-based nanoparticles. We showed that the anti-Met NANAPs stimulate the down regulation of

Met in human, Met-expressing gastric cancer (MKN45) and lung carcinoma (A549) cell lines. Our data demonstrate that anti-Met NANAPs constitute a nanocarrier for the treatment of Met expressing cancer cells.

6.2. Materials and Methods

6.2.1. Cell culture and cell lines

The human ovarian carcinoma cell line TOV-112D (cat nr. CRL-11731), human lung carcinoma cell line A549 (cat.nr. CCL-185) and the human epidermoid squamous carcinoma cell line A431 (cat. nr. CRL-1555) were all obtained from American Tissue Culture Collection (ATCC, LGC Standards GmbH, Wesel, Germany) and the human gastric cancer cell line MKN45 (cat. nr. ACC-409) was obtained from the Deutsche Sammlung von Mikroorganismen und Zellkulturen (DSMZ, Braunschweig, Germany). TOV-112D and A431 cells were cultured in Dulbecco's Modification of Eagle Medium (DMEM: Gibco, Invitrogen, Breda, The Netherlands) supplemented with 100 units/ml streptomycin, 0.1 mg/ml penicillin, 2 mM L-glutamine and 10% fetal calf serum (FCS) at 37°C and 5% CO_2. MKN45 cells were cultured in RPMI 1640 (Life Technologies Inc., Invitrogen) supplemented with 100 units/ml streptomycin, 0.1 mg/ml penicillin, 2 mM L-glutamine and 20% FCS. A549 cells were cultured in Ham's F12 (Life Technologies, Inc., Invitrogen) supplemented with streptomycin, penicillin, L-glutamine and 10% FCS under the previously mentioned conditions. Met expression of cells seeded for one or two days was determined by western blotting using mouse-anti-HGFR (MAB3581, R&D Systems Europe Ltd, Abingdon, UK) followed by goat-anti-mouse^{Alexa488} (Invitrogen) incubation. For the generation of the stable TOV+Met cell line, human Met-encoding cDNA (kindly provided by Dr. Morag Park, McGill University, Montreal, Canada) was first transferred from the pXM vector into a pMX-IRES-Zeo vector (generated from the pMX-SupF vector kindly provided by prof. Garry P. Nolan, Stanford University School of Medicine, Stanford, California, USA) via XhoI-XhoI digestion (Thermo Scientific, Breda, The Netherlands) and ligation (T4 ligase, Promega, Madison, USA). TOV-112D cells were transfected with this pMX-Met-IRES-Zeo using Fugene HD (Roche, Mannheim, Germany) and grown under selection pressure using 200 µg/ml of Zeocin (Invitrogen) for 8 weeks. Single clones were tested for Met-expression by western blotting.

6.2.2. Nanobody selection

Nanobodies directed against Met were selected using phage display technology from an'immune' phage antibody library that was made from *Llama Glama* immunized with A431 membrane vesicles, as previously described (21). For selections, Maxisorp 96-wells plates (Nunc, Roskilde, Denmark) were coated overnight with rabbit-anti-hIgG in PBS (1:2000, Dako, Glostrup,

Denmark) at 4°C. Next day, non-specific binding was blocked with 2% skimmed milk (Marvel) in PBS (MPBS) for an hour at RT. Subsequently, 1 µg of Met-Fc fusion protein diluted in MPBS (R&D systems) per well was captured for 1h at room temperature (RT). After three washes with PBS, captured antigen was incubated with phages (blocked in 2% MPBS) for 2h at RT. After washing, bound phages were detached by 100 mM triethylamine (TEA) elution. For phage ELISA, Maxisorp plates were coated with rabbit-anti-hIgG as described above and 50 ng/well of Met ectodomain-Fc fusion protein (R&D Systems) was captured for 1h at RT in 2% MPBS. Single clone phages were incubated for 2h at RT, washed extensively and bound phage was detected with mouse-anti-$M13^{HRP}$ (1:10,000), followed by o-phenylenediamine (OPD) development. The reaction was stopped by the addition of 3M H_2SO_4 and OD was read at 450nm. The cDNAs of the selected clones were sequenced and then re-cloned into a pET28a vector containing C-terminal Myc-6-His tags and which allows the purification of nanobodies from the periplasmic space of *E.coli*.

6.2.3. Production and purification of Nanobodies

Nanobodies were produced as described before (16), but with minor modifications. Briefly, *E. coli BL*-21 Codon Plus (DE3)-RIL (Agilent Technologies Inc., Santa Clara, CA, USA) cells were transformed with pET28-derived nanobody-encoding plasmid and a single antibiotic-resistant colony was picked. Production was performed by growing these bacteria in 2xTY medium containing 2% (w/v) glucose and 100 µg/ml ampicillin at 37°C overnight. Four hundred milliliters of 2xTY medium (supplemented with 100 µg/ml ampicillin and 0.2% (w/v) glucose) was inoculated with the bacteria from the overnight culture with an OD_{600} of 0.1. This bacterial culture was subsequently incubated at 37 °C at 250 rpm until it reached an OD_{600} of 0.6. Subsequently, 0.5 mM IPTG was added to the bacterial culture to induce nanobody expression and the culture was further incubated at 37°C for 3.5 h. After 3.5 h, cells were spun down (5000 rpm, 15 min, 4°C) and the obtained pellet was stored over night at -20°C. The following day, periplasmic fractions were made by incubating the pellet in 6.4 ml ice cold TES (200 mM Tris-HCl, 0.5 mM EDTA, 500 mM sucrose, pH 8.0). To this suspension, 10 ml of diluted ice cold TES (1:3 in water) was added and incubated on ice for 30 min. The bacteria were spun down at 4 °C for 15 min at 5000 rpm and the supernatant was collected. The pellet was resuspended in 10 ml ice cold TES, 120 µl 1 M $MgSO_4$ was added and the mixture was incubated on ice for 30 min. The suspension was spun down at 4 °C for 15 min at 5000 rpm and the supernatant containing the nanobody was added to the previously collected supernatant. The his-tagged nanobodies were purified by means of immobilized metal ion affinity chromatography (IMAC) on TALON resin (Clontech, Palo Alto, CA, USA) according to the manufacturer's protocol (Batch/Gravity-Flow), except 50 mM NaH_2PO_4, 300 mM NaCl, 20 mM imidazole, pH 8.0 was used for all washing steps

and elution was performed with the same wash buffer but containing 300 mM imidazole, pH 8.0 buffer. Imidazole was removed by means of dialysis against PBS overnight at 4°C. Finally, protein fractions and purity were analyzed by SDS polyacrylamide gel electrophoresis (SDS-PAGE). Protein concentrations were determined using a Micro BCA assay (ThermoScientific).

6.2.4. FACS analysis

For FACS analysis of binding of the anti-Met nanobodies, Met-expressing A431 cells were trypsinized, blocked and incubated with anti-Met VHHs (developed in house) or $EGF^{Alexa488}$ (Invitrogen) on ice for 2 h. The cells were washed three times with PBS and fixed in 4% paraformaldehyde (PFA). Auto-fluorescence was quenched with 100 mM glycine in PBS for 15 min and VHHs were detected with Prot-G purified rabbit-anti-VHH (developed in house), followed by goat-anti-$rabbit^{Alexa488}$ (Invitrogen) incubation. FACS analysis was performed on a BD analyzer (BD Biosciences, Breda, The Netherlands).

6.2.5. Binding and affinity determination of nanobodies

TOV-112D, TOV+Met (1.5 x 10^4 per well) or MKN45 cells (6 x 10^4 per well) were seeded in a 96-wells plates (Nunc) one day before the assay. The cells were pre-incubated with binding medium (2% BSA in CO_2-independent medium (Gibco) for 10 min on ice after which the cells were incubated in binding medium supplemented with or without nanobodies (0.005-1000 nM) for 2h on ice. After three washes with ice cold PBS, cells were fixed in 4% PFA and fixative was subsequently quenched with 100 mM glycine in PBS for 15 min. Bound nanobody was detected with rabbit-anti-VHH (1:1000) in PBS containing 2% BSA (PBA) followed by goat-anti-rabbit IRDye800CW (Li-COR Biosciences, UK, 1:500 in PBA) incubation for 1h at RT each. Finally, cells were washed twice with PBA and fluorescence was measured using the Odyssey Infrared Imager. Binding affinity (K_D) for one site specific binding was determined by curve fitting using GraphPad Prism 5.02 for Windows (GraphPad Software, San Diego, CA).

6.2.6. HGF competition

HGF was labeled with ^{125}I (Perkin Elmer, USA) according to the IODO-GEN (Sigma-Aldrich) method as described previously (22). The specific activity of I^{125}-HGF was measured at ~30,000 CPM/µg. Maxisorp 96-well ELISA plates (Nunc) were coated with rabbit anti-human IgG (Dako, Glostrup, Denmark; 4 µg/mL in PBS). The next day, wells were washed with PBS, blocked with 1% MPBS and subsequently incubated with 0.1 µg/mL of Met-ECD-Fc. After washing with PBS, the wells were incubated with 1 nM of ^{125}I-HGF in the presence or absence of 1000 nM of nanobodies for 1h. Wells were washed four times with PBS and bound I^{125}-HGF was collected after 5 min incubation with 1 M NaOH; radioactivity was measured using a gamma counter

(Wallac Wizard, Perkin Elmer). Results were analyzed using GraphPad Prism version 5.02 for Windows, GraphPad Software (San Diego, CA).

6.2.7. Preparation of albumin nanoparticles

Nanoparticles were prepared by the ethanolic desolvation technique as described previously (16,23) with minor modifications. Briefly, human serum albumin (HSA, 50 mg/ml) was dissolved in deionized water after which the pH was adjusted to 8.3 by addition of 0.1 M NaOH and the solution was filtered through a 0.2 μm filter (Minisart® syringe filters, Sartorius-stedim, Germany). Nanoparticles were formed by adding 92% ethanol drop wise under constant stirring. The formed particles were crosslinked with 8% glutaraldehyde (GA) overnight at RT. The nanoparticles were purified by centrifugation first at 1,000 g for 5 min (pellet discarded, supernatant collected) and three times at 45,000 g for 1 h at 4ºC in deionized water. Nanoparticles were stored in deionized water at 4ºC. Nanoparticle yield was determined by measuring the dry weight by thermogravimetric analysis. The absence of soluble albumin and multimers was checked by SDS-PAGE (4-12% crosslinked, Invitrogen) under reducing conditions followed by Coomassie blue staining. For enabling detection of nanoparticles in fluorescence microscopy or quantification on the Odyssey Infrared Imager, nanoparticles were labeled with either Alexa488-NHS (Invitrogen) or IRDye800CW-NHS (Li-COR) as described before (16).

6.2.8. PEGylation and G2 coupling to albumin nanoparticles

The anti-Met nanobody G2 was modified with either a 2-,4- or 8-fold molar excess of N-succinimidyl-S-acetylthioacetate (SATA) (Pierce Biotechnology, Rockford, IL, USA) as described in (19). Briefly, the introduced sulfhydryl groups were deacetylated for 30 min at RT prior to addition of SATA-G2 to freshly prepared maleimidiyl-PEG nanoparticles. 18 mg of nanoparticles (4 mg/ml) were reacted with 14 mg of NHS-PEG3500-maleimide (15:1, mol/mol, PEG:HSA) in 0.1 M phosphate buffer (PB), pH 8 for 1 h at RT on a roller bench. PEGylated nanoparticles were collected by centrifugation and resuspended in 0.1 M PB, pH 7 and immediately reacted with SATA-modified G2 (0.1 mg G2 / mg nanoparticle, 0.4 nmol G2 / nmol albumin) for 2 h at RT. G2-PEG-NP were characterized for G2 coupling with dot-blot immunodetection of G2 (16).

6.2.9. Characterization of nanoparticles

Size distribution and polydispersity of the nanoparticles were determined by dynamic light scattering (DLS) on a Malvern ALV CGS-3 (Malvern Instruments, Malvern, UK) containing a He\Ne laser source (λ=632.8 nm, 22 mW output power) under an angle of 90°. The zeta potential of the nanoparticles was determined using a Malvern zetasizer Nano-Z (Malvern Instruments,

Malvern, UK). The measurements were performed in 5 mMPB, pH 7.4 at 25 °C.

6.2.10. G2-SATA characterization by capillary electrophoresis

The degree of SATA labeling on G2 was measured by means of capillary electrophoresis (CE) experiments which were carried out on a P/ACE MDQ™ CE instrument (Beckman Coulter, Brea, CA, USA). The separation voltage was − 30 kV and the capillary temperature was 20 °C. Fused-silica capillaries (total length, 85 cm; inner diameter, 50 μm, outer diameter, 360 μm) were obtained from Polymicro (Phoenix, AZ, USA). The capillaries were coated with a triple layer Polybrene-dextran sulfate-Polybrene (PB-DS-PB) coating as described previously (24-26). The background electrolyte (BGE) was 100 mM acetic acid (pH 2.8). Nanobody was hydrodynamically injected for 14 s at 1 psi (equal to 1% of the capillary volume). MS detection was performed using a micrOTOFQ orthogonal-accelerated time-of-flight (TOF) mass spectrometer (Bruker Daltonics, Bremen, Germany). Transfer parameters were optimized by direct infusion of an electrospray ionization (ESI) tuning mix (Agilent Technologies, Waldbronn, Germany). CE-MS coupling was realized by a co-axial sheath liquid interface (Agilent Technologies, Waldbronn, Germany). A sheath liquid of isopropanol-BGE (75/25, v/v) at a flow rate of 3 μL/min was used. The following optimized spray conditions were used: dry gas temperature, 180°C; nitrogen flow, 4 L/min; and nebulizer pressure, 0.4 bar. Electrospray in positive ionization mode was achieved using an ESI voltage of −4.5 kV. CE-MS data were analyzed using Bruker Daltonics DataAnalysis software. For the determination of peak areas, extracted-ion electropherograms (EIEs) were constructed for the respective protein species from their most abundant m/z signals ($[M + nH]^{n+;}$ n=12-15). Protein charge assignment and molecular weight determinations were performed using the 'charge deconvolution' utility of the DataAnalysis software.

6.2.11. Cellular binding and internalization of nanoparticles

To test the binding of the NANAP's to Met-expressing cells, TOV-112D, TOV+Met, A549 (20.000 cells/ well) and MKN45 (60.000 cells/ well) were seed into 96-wells plates (Nunc), one day before the assay. Cells were pre-incubated with binding medium for 10 min on ice and subsequently incubated with IRDye800-labeled nanoparticles (0.06-0.5 mg/ml) for 2h on ice. Cells were washed for 10 min with 2% Marvel in binding medium, followed by PBS, after which binding of nanoparticles was quantified with the Odyssey Infrared Imager.

For fluorescence microscopy imaging, the cells were seeded in chamber slide (Lab-Tek, Nunc) one day before the experiment. Cells were incubated with 0.25 mg/ml of Alexa488-conjugated nanoparticles in binding medium for 2h on ice. For internalization, the nanoparticles were allowed to internalize for 2h at 37°C. Cells were washed with binding medium and PBS extensively and fixed in 4% PFA. PFA-induced autofluorescence was quenched by incubation

with 100 mM glycine in PBS for 15 min at RT and slides were mounted using SlowFade (Invitrogen). Fluorescent pictures were taken using a Zeiss LSM700 confocal microscope (Carl Zeiss Microscopy GmbH, Germany) equipped with and 63x oil immersion objective (NA 1.4).

6.2.12. Nanoparticle lysosomal degradation assay

Lysosomal processing of nanoparticles was studied with IRdye800-labeled nanoparticles as described previously (16). Cells were seeded (200.000 cells/well for A549 and 600.000 cells/well for MKN45) in 12-well plates (Becton & Dickinson, Mountain View, CA, USA) one day before the experiment. Cells were pulsed with 0.25 mg/ml IRDye800-labeled nanoparticles for 2 h at 37ºC. The medium was replaced by fresh medium supplemented with or without 10 µM of chloroquine (CQ, an inhibitor of lysosomal degradation, Sigma Aldrich) or lactacystin (LC, an inhibitor of proteasomal degradation, kindly provided by Dr. Marcel A.G. van der Heijden, Division of Heart and Lungs, UMC Utrecht, The Netherlands) and cells were incubated for an additional 16 h at 37 ºC. Cells were washed with PBS and lysed in 30 µl of reducing sample buffer (50 mM Tris-HCl, pH 6.8, 10% glycerol, 100 mM DTT, 2% SDS and 0.01% bromophenol blue). IRDye800 peptide fragments were separated by SDS-PAGE and quantified using the Odyssey Infrared Imager. Mean and SEM of the intensity of the peptide bands obtained from three independent experiments were calculated.

6.2.13. Phosphorylation and downregulation of Met

Agonistic or antagonistic properties of G2 (1nM, 1 µM), PEG-NP (0.5 mg/ml) and G2-PEG-NP (0.5 mg/ml) were studied using A549 and MKN45 cells that were seeded in 12 well plates (240.000 cells/well) and incubated overnight in 0.1% FBS. Formulations were diluted in 0.1% FBS medium and incubated with the cells for 30 min at 4°C. Subsequently, 50 ng/ml HGF (R&D system) was added and the cells were incubated for 10 min at 37°C. Cells were washed with PBS two times, lysed with RIPA buffer (Teknova) supplemented with Halt™ Protease & Phosphatase Inhibitor Cocktail (Thermo Scientific) and lysates were collected. For Met down-regulation experiments, A549 and MKN45 cells (200.000 and 400.000 cells/well) were seeded in 24 well plates and adhered overnight, followed by incubation with 100 nM G2, 0.5 mg/ml PEG-NP or G2-PEG-NP in (serum-containing) medium for 48h at 37°C. Next, cells were washed with PBS two times and lysed. The collected fractions were centrifuged at 15.000 g for 15 min at 4°C and the supernatant was collected and stored at 4°C. Quantification of total protein content was performed using a Micro BCA Kit (Thermo Scientific) and a fraction corresponding to 5 µg protein was loaded on a reducing SDS-PAGE gel (4-12% crosslinked, Invitrogen). Western Blot analysis was performed as previously described (16). Total and phosphorylated Met were detected by immunoblotting with rabbit anti-phospho-Met (pY1234/pY1235) and anti-Met antibody (Cell

Signaling, 1:1000 diluted) in 5% BSA-TBS-T for 2h on the roller bench at RT. Beta-actin rabbit antibody (Cell Signaling, 1:1000 diluted) was used as a loading control. Anti-rabbit IgG HRP-linked (Cell Signalling, 1:3000 diluted) secondary antibody was added to the membrane and proteins were visualized by chemoluminescence.

6.2.14. Scratch wound assay

The effect of G2 and G2-PEG-NP on cell migration was assessed by a scratch wound assay as described by Liang *et al*. with minor modifications (27). Briefly, cells were seeded in a 48 wells-plates and allowed to adhere overnight (120.000 cells/well for MKN45 and 45.000 cells/well for A549). The following day, cells were starved in 0.1% FBS medium for 2h and a vertical, uninterrupted wound was created in the cell monolayer using a sterile 200 µl pipette tip. Formulations were diluted in 0.1% FBS medium and incubated for 24h. Images of the wounded cell monolayer were taken using a Nikon Eclipse Te-2000-U microscope (40X magnification) at the start of the incubations and again after 24h. The surface of the scratch area (A) was measured using ImageJ software. Results are expressed as percentages of wound closure for each well using the formula: 100 x [1 - (A_{t24} / A_{t0})]. Statistical analysis was performed with GraphPad Prism software using a one-way analysis of variance (ANOVA) followed by Student's t-test.

6.3. Results

6.3.1. Selection and characterization of anti-Met nanobodies

To obtain nanobodies against the extracellular domain of Met, selections were performed from an in-house prepared phage nanobody library that was constructed using the immunoglobulin repertoire of peripheral blood lymphocytes of Llama immunized with vesicles from Met-expressing A431 cells (21). After a single round of selection on the Met ectodomain, followed by a non-specific elution, binding of Met-specific clones to the Met ectodomain was tested by phage-ELISA. Of all phages that bound Met, three clones were selected (C3, F5 and G2) based on their binding and DNA sequences and these were re-cloned into a bacterial production vector. Binding of these anti-Met nanobodies to Met-expressing cells was first tested on A431 cells by fluorescence activated cell sorting (FACS) analysis (Fig. **1A**). As compared to the untreated cells (indicated in red), all three nanobodies showed significant binding to A431 cells. Because A431 cells also express high numbers of EGFR, EGF-Alexa488 was taken as a control for binding. HGF was not a proper control for specific receptor binding, since this growth factor also interacts with heparin sulfates, which are present in the plasma membrane (28).

To test the specificity of the nanobodies towards Met, we used Met-positive and Met-negative cell lines. The expression of Met on TOV-112D cells was first tested and these cells

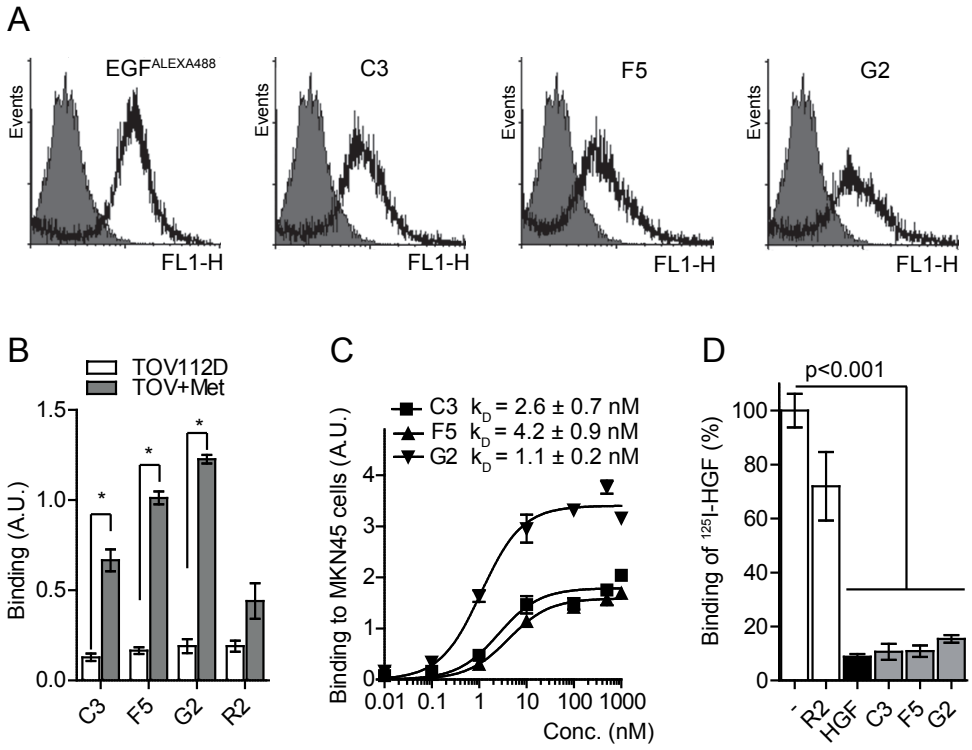

***Figure 1**. The three selected anti-Met nanobodies bind Met with low nM affinities on cells. A) Binding of anti-Met nanobody C3, F5 and G2 to A431 cells measured by FACS and compared to untreated cells (grey area). EGF-Alexa488 was used as a positive control for binding. B) Specific binding of C3, F5 and G2 to TOV+MET cells. R2 (non-relevant nanobody) was used as a negative control. C) Binding curves and affinities (K_D) of C3, F5 and G2 on high Met expressing cell line MKN45. D) Binding competition of ^{125}I-labeled HGF by anti-Met nanobodies. Maxisorp plates were coated with Met ectodomain and binding of 1 nM of ^{125}I-labeled HGF in the presence or absence of 1000 nM of nanobodies. Error bars represent SEM, where n>4.*

were confirmed to be Met-negative (Fig. **S1A**). Subsequently, a clone stably expressing Met was obtained by transient transfection and selection for antibiotic resistance. Stable Met-expression of different clones was determined by immunofluorescence and the cell line showing highest Met expression was selected as the Met-positive cell line, indicated as TOV+Met (Fig. **S1B**). All three anti-Met nanobodies showed significant binding to only the TOV+Met cells, but not to TOV-112D cells, indicating specificity towards the human Met receptor (Figure 1B). The control nanobody R2 (directed at the Azo Dye RR6 (29)) did not significantly bind to either cell line. Subsequently, binding of the nanobodies to Met was further characterized by determining their affinity (K_D) on MKN45 cells, which over-express Met on their cell surface (Fig. **1C**). All three

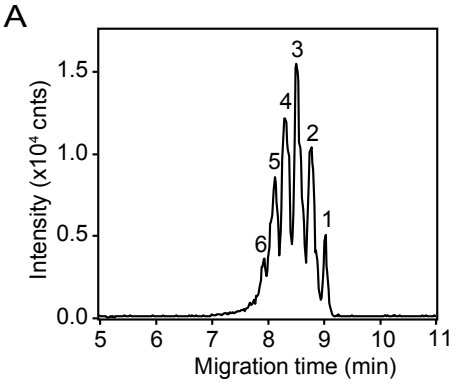

Peak no.	M_w	Rel. peak area (%)	Identity
1	17618	5.4	G2
2	17733	18.8	+1 SATA
3	17850	30.1	+2 SATA
4	17966	28.9	+3 SATA
5	18083	13.5	+4 SATA
6	18198	3.3	+5 SATA

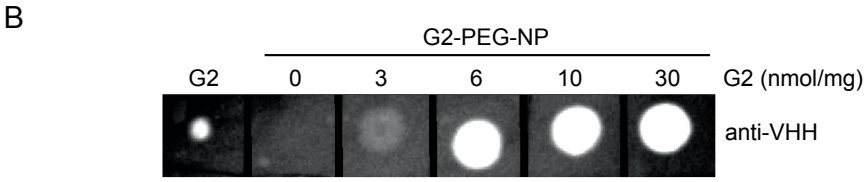

***Figure 2**. Generating anti-Met NANAPs using G2. A) G2-SATA (1:8 ratio) characterization by CE-TOF-MS. B) Dot-blot analysis of G2 coupled to PEGylated nanoparticles.*

6

nanobodies bound to MKN45 cells with low nanomolar affinities (2.6 ± 0.7 nM for C3, 4.2 ± 0.9 nM for F5 and 1.1 ± 0.2 nM for G2). To test whether the obtained nanobodies competed for ligand binding, a HGF competition assay was performed. As a control, an excess of unlabeled HGF was able to almost completely compete off the binding of ^{125}I-labeled HGF from coated Met ectodomain (Fig. **1D**). Similarly, all three anti-Met nanobodies clearly showed competition with the labeled HGF, while the non-relevant nanobody R2 did not show any effect.

6.3.2. Modification of anti-Met nanobodies

In order to obtain nanoparticles targeting Met expressing tumors, these particles should be decorated with the selected nanobodies. This coupling was achieved via SATA groups on lysine residues of the nanobodies and a maleimide-PEG linker on the nanoparticles. To test whether random SATA modifications would affect the integrity of the selected nanobodies, different amounts of SATA were allowed to react with C3, F5 and G2 and the effect of these modifications on binding affinity was studied on MKN45 cells (Fig. S**2A-C**). The introduction of SATA moieties to C3 and F5 did decrease their binding affinity to MKN45 cells by two fold, whereas G2, even with high modification ratios, was not affected (K_D of ~1 nM for all degrees of modification). The degree of SATA modification in G2, the average amount of SATA modifications per molecule,

was quantified by capillary electrophoresis followed by time-of-flight mass spectrometry (CE-TOF-MS) (Fig. **2A**). The molecular weight found for peak 1 (17.6 kDa) corresponded to the unconjugated G2 nanobody. The subsequent increases in molecular weight (peak 2-6) corresponded well with the calculated mass of the introduced SATA groups (116 Da). G2 carrying 1 to 4 SATA modifications accounted for more than 90% of the relative peak area and on average, a conjugation of approximately 2.4 SATA molecules per G2 nanobody was found.

6.3.3. Preparation and characterization of G2-coupled albumin nanoparticles

The SATA-modified G2 nanobody was coupled to the PEGylated nanoparticles (NP) to generate G2 decorated nanoparticles (G2-PEG-NP). The coupling efficiency of SATA-modified G2 to albumin nanoparticles was investigated by reacting increasing amounts of G2 with the PEGylated nanoparticles, followed by dot-blot analysis of the nanoparticles with anti-VHH antiserum. Nanobody coupling was found to be saturated at G2:NP ratios of 6 nmol/mg NP and higher (Fig. **2B**). The covalent attachment of G2 to the PEG anchor was confirmed by SDS-PAGE analysis of G2-PEG-NP, which showed the absence of unbound G2, indicating complete binding of G2 nanobodies to the nanoparticles (data not shown). Size determination of the nanoparticles showed that the G2-decorated nanoparticles were approximately 100 nm in size after PEGylation (polydispersity <0.1) and had a slightly negative zeta potential of -19 mV (Table **1**).

Table 1. *Characteristics of albumin nanoparticles*

Nanoparticles	Size (nm)	Zeta potential (mV)	PDI*
NP	87 ± 9	-30 ± 3	0.06 ± 0.02
PEG-NP	106 ± 5	-18 ± 2	0.10 ± 0.03
G2-PEG-NP**	102 ± 3	-19 ± 4	0.10 ± 0.02

*: Polydispersity index, **: 6 nmol G2/mg NP

6.3.4. The anti-Met NANAPs bind specifically to Met-expressing cells

The specificity of the G2-coupled nanoparticles was determined by studying the binding of IRDye800-conjugated PEG-NP and G2-PEG-NP to either Met negative TOV-112D cells or the TOV+Met variant (Fig. **3A-B, left**). Both non-targeted PEG-NP and targeted G2-PEG-NP showed some binding to the Met-negative cells. The linear fashion in which this binding was detected was considered to be indicative of non-specific low-affinity interactions. Importantly, G2-PEG-NP showed specific binding to TOV+Met cells with a half-maximal binding of approximately 0.15 mg/ml. Fluorescence microscopy imaging with Alexa488-labeled nanoparticles confirmed specific binding of G2-PEG-NP to TOV+Met cells and low background binding to Met-negative cells (Fig. **3A-B, right**). Similar results with respect to binding specificity were obtained with

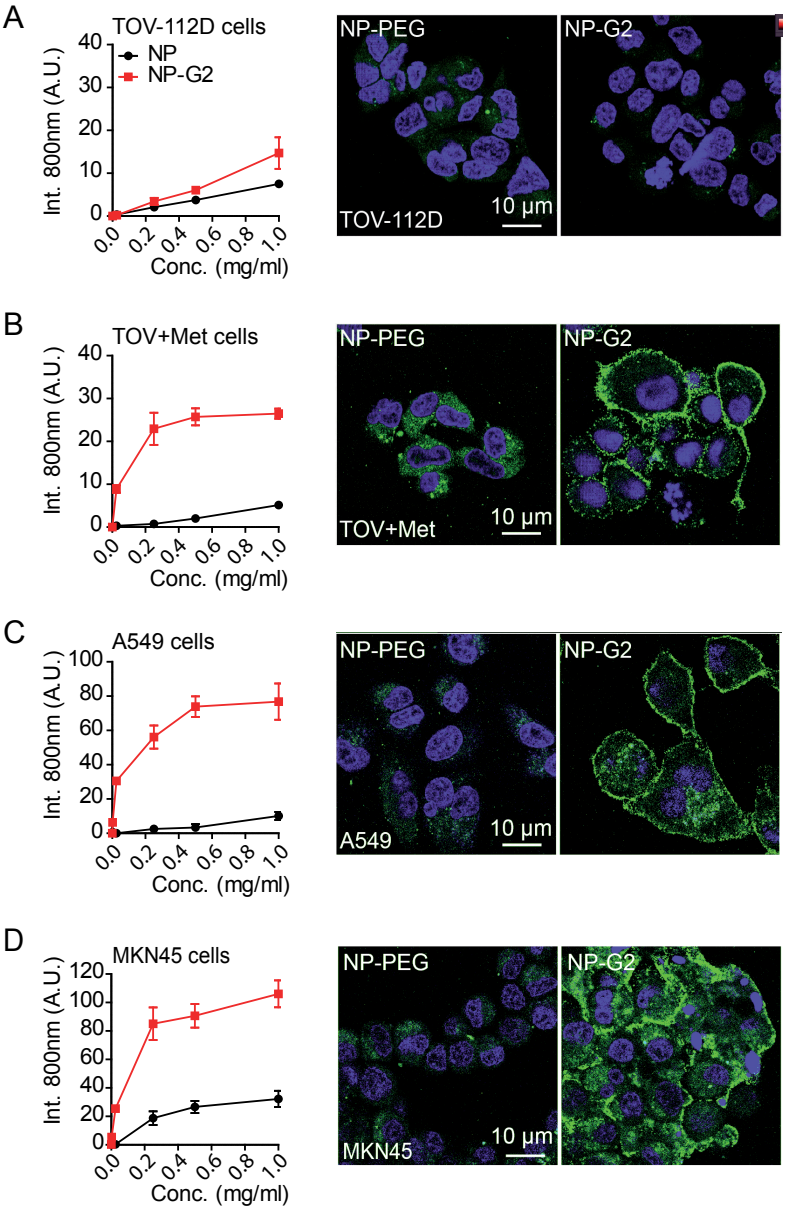

Figure 3. *G2-PEG-NPs bind specifically to Met expressing cells. A) TOV-112D, B) TOV+Met, C) A549, or D) MKN45 cells were incubated with fluorescently labeled PEG-NP or G2-PEG-NP. A concentration range of IRDye800-conjugated NANAPs were used for determining level of binding by the Odyssey Infrared Scanner (left) and 0.5mg/ml of Alexa488-conjugated NANAPs were used for detection by confocal fluorescence microscopy (right, indicated in green). Nuclei were stained with DAPI (blue). Error bars represent SEM, where n=3.*

the Met-expressing tumor cell lines, A549 and MKN45. Only G2-PEG-NP showed membrane binding to the Met-expressing tumor cell lines while untargeted PEG-NP showed only low (background) binding (Fig. **3C-D**).

6.3.5. NANAPs induce Met phosphorylation but no cell scattering

In order to study whether the observed nanoparticle uptake is accompanied by receptor activation, their agonistic/antagonistic properties were determined on A549 cells by western blotting (Fig. **4A**). The G2 nanobody alone did not stimulate Met activity at a low concentration (1 nM), but at higher concentration (1 μM) the Met receptor was clearly phosphorylated. As expected, PEG-NP did not result in Met activation, but the targeted G2-PEG-NP stimulated Met activity at all concentrations tested (Fig. **4A**). To test whether the nanobodies or nanoparticles would have an intrinsic therapeutic activity by blocking ligand binding, A549 cells were incubated with G2 or nanoparticles, in the presence and absence of HGF. None of the formulations blocked HGF-induced phosphorylation of Met (Fig**. 4B**). Also in the MKN45 cells, none of the formulations were able to reduce receptor activation of Met (Fig. **S3)**. To investigate whether the agonistic property of G2-PEG-NP as observed by Met activation would have an actual downstream effect, we performed a scratch wound assay (Fig. **4C**). For this experiment, A549 cells were used, since the constitutive activation of Met in MKN45 cells make them non-responsive to the ligand for Met. G2, PEG-NP or G2-PEG-NP did not induce wound closure; a complete closure of the scratch wound was only observed upon treatment with HGF. This means that, even though the G2-PEG-NP or G2 (only at 1 μM) are able to cause phosphorylation of Met, this is insufficient to induce scattering of A549 cells. A similar approach was chosen to investigate the downstream antagonistic effect of the anti-Met nanobodies or nanoparticles (Fig. **4D**). Here, the wound closing effect of HGF was partially blocked by a high concentration of G2 and by the G2-PEG-NPs. Despite inducing Met phosphorylation, the anti-Met NANAPs do inhibit cell scattering and thereby wound healing in A549 cells.

6.3.6. Internalization, lysosomal sorting and degradation of Met and G2-PEG-NP

Eventually, anti-Met NANAPs could function as a nanocarrier for the intracellular delivery of therapeutic agents. We therefore assessed whether the G2-PEG-NPs were internalized by Met expressing cells using confocal fluorescence microscopy. After 2h of incubation, specific uptake of only the G2-PEG-NP could be observed in both A549 and MKN45 cells, as indicated by an intracellular endosomal staining pattern (Fig. **5A**). Co-staining of the cells with early endosomal marker EEA-1 showed that the internalized nanoparticles were localized in early endosomes, which is apparent from the yellow color in the merged image with green-labeled nanoparticles and red-labeled-EEA-1 (Fig. **5B**). Nevertheless, not all G2-PEG-NP were located in early endosomes

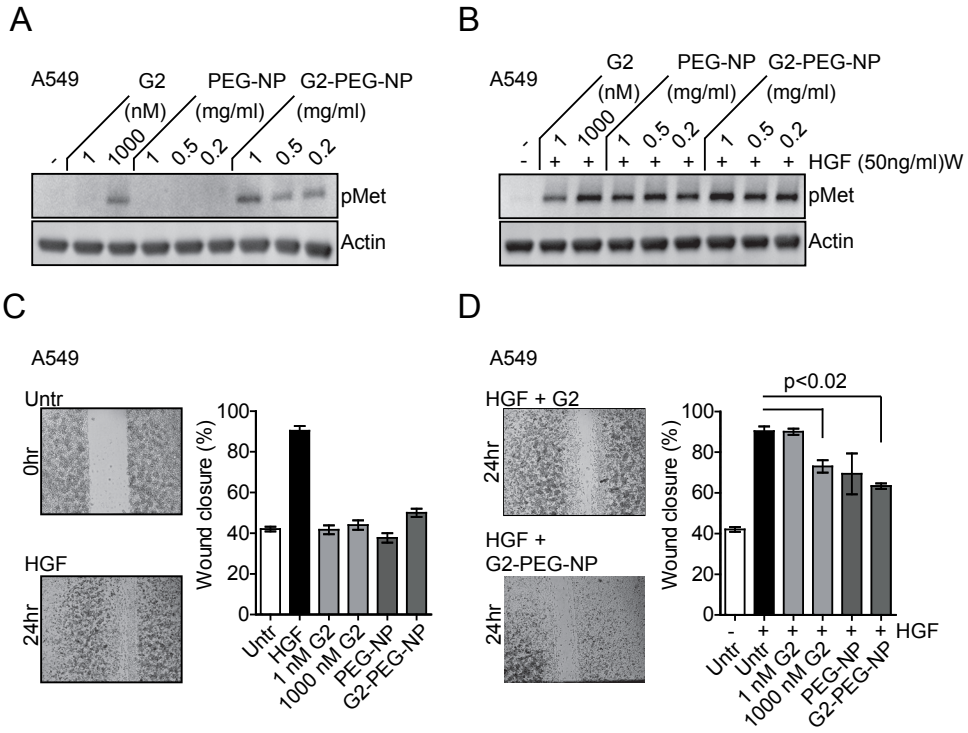

***Figure 4**. Agonistic and/or antagonistic activities of nanoparticles. A) Activation of Met expressed in A549 cells is assessed by western blotting using anti-phospho-Met. Actin is used as a loading control. Both G2 (only at 1000nM) and the G2-PEG-NP activate Met . B) Both G2 and G2-PEG-NP do not block HGF-induced Met phosphorylation. C-D) Scratch-wound assay in the absence (C) and presence (D) of HGF on A549 cells. None of the formulations tested induced a closure of the wound. Only G2-PEG-NP slightly reduces wound closure. Error bars represent SEM, where n=3.*

at this time point, which could be due to the highly dynamic nature of endocytic vesicles, in which cargo is rapidly transported to further downstream compartments like sorting and late endosomes and eventually lysosomes (30).

To investigate whether the nanoparticles were routed towards late endosomes or lysosomes, co-localization of Alexa488-labeled G2-PEG-NP with Lysotracker Red was studied in A549 and MKN45 cells by confocal fluorescence microscopy (Fig. **6A**). After 16h of incubation, the G2-PEG-NP co-localized almost completely with lysotracker Red, indicating that these NANAPs indeed end up in late-endosomal/lysosomal compartments. To check whether the nanoparticles were also degraded, a pulse-chase experiment was performed with IRDye800-labeled G2-PEG-NP or PEG-NP. After 16h, degradation of the nanoparticles was observed by

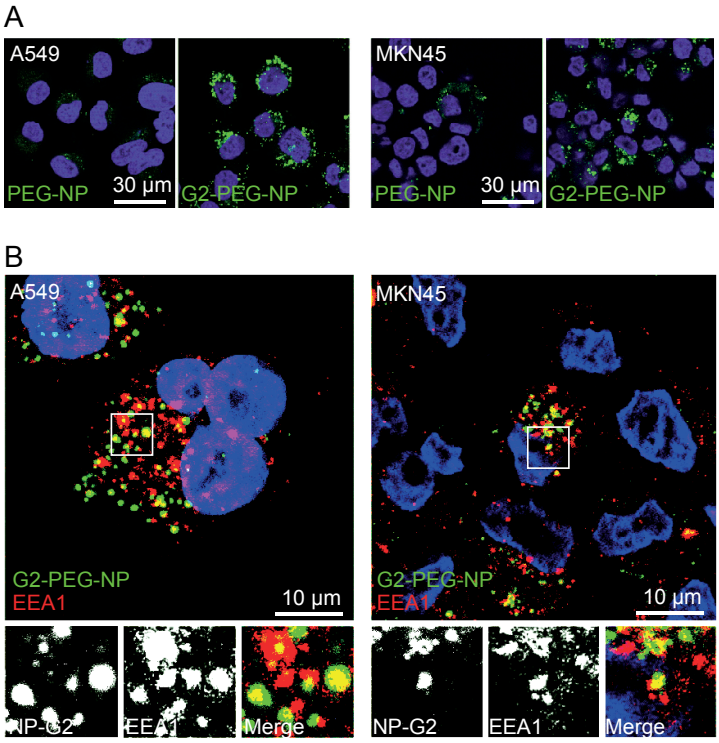

Figure 5. G2-PEG-NP internalize specifically into Met-expressing cells. A) A549 (left) and MKN45 (right) cells were incubated with Alexa488-conugated G2-PEG-NP or PEG-NP for 2h at 37˚C. B) Cells were incubated as in A and subsequently fixed and permeabilized. Early endosomes were stained with anti-EEA1 antibodies and nuclei were stained with DAPI (blue).

SDS-PAGE, which is apparent by the appearance of free IRDye800 at the bottom of the gel (Fig. **6B**). Only Met-targeted nanoparticles showed signs of degradation, which is in good correlation with the specific binding and internalization of the G2-PEG-NP mentioned above (Fig. 5A).

In general, protein degradation in cells is mediated by the proteasome complex and/or by the proteases in the endosomal/lysosomal system. Lysosomal degradation of Met plays an important role in the ligand-induced negative feedback mechanism of Met (15). In addition, it has been reported that ligand-induced degradation of Met is also regulated by proteasomal degradation (31). To study the nature of the observed degradation of the nanoparticles in more detail, we inhibited both lysosomal and proteasomal degradation with either the lysosome inhibitor chloroquine (CQ), and the proteasome inhibitor lactacystin (LC). In both A549 and MKN45 cells, co-incubation with 10 µM of CQ for 16h blocked the degradation of the G2-PEG-NP almost completely (Fig. **6C-D**). In contrast, LC had no effect on nanoparticle degradation in A549 cells and a minor effect in MKN45 cells.

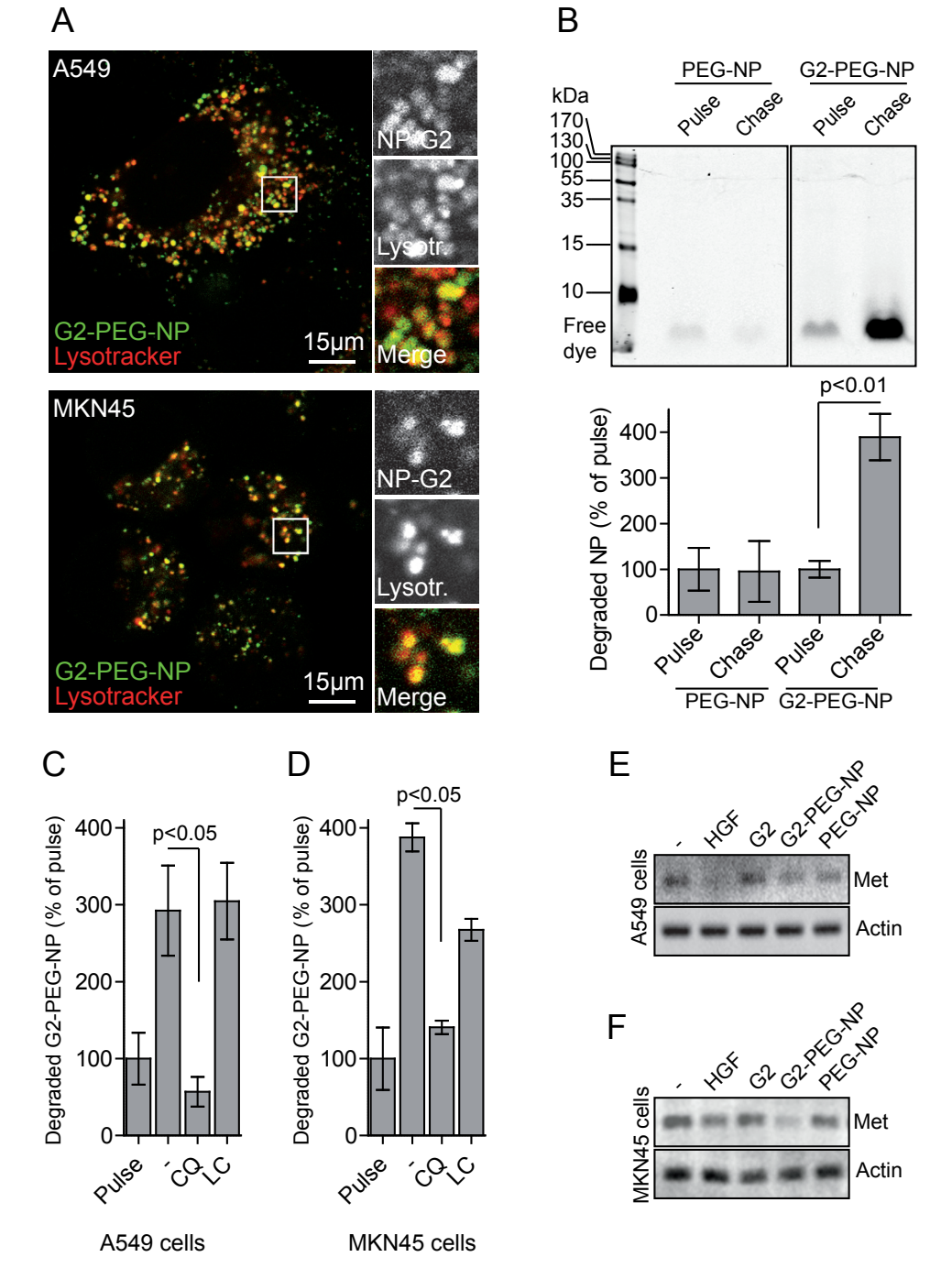
A
A549
NP-G2
Lysotr.
G2-PEG-NP
Lysotracker
15µm
Merge
MKN45
NP-G2
Lysotr.
G2-PEG-NP
Lysotracker
15µm
Merge
B
PEG-NP
G2-PEG-NP
kDa
170
130
100
55
35
15
10
Free dye
Pulse
Chase
Pulse
Chase
p<0.01
Degraded NP (% of pulse)
400
300
200
100
0
Pulse
Chase
Pulse
Chase
PEG-NP
G2-PEG-NP
C
Degraded G2-PEG-NP (% of pulse)
p<0.05
400
300
200
100
0
Pulse
-
CQ
LC
A549 cells
D
Degraded G2-PEG-NP (% of pulse)
p<0.05
400
300
200
100
0
Pulse
-
CQ
LC
MKN45 cells
E
-
HGF
G2
G2-PEG-NP
PEG-NP
A549 cells
Met
Actin
F
-
HGF
G2
G2-PEG-NP
PEG-NP
MKN45 cells
Met
Actin

***Figure 6**. Anti-Met NANAPs are degraded by lysosomes and induce receptor downregulation. A) A549 (top) and MKN45 (bottom) cells were incubated with Alexa488-conjugated G2-PEG-NP for 16h and fixed for confocal fluorescence imaging. Late endosomes and lysosomes were stained with Lysotracker-Red. B) MKN45 cells were pulsed for 2h with IRDye800-conjugated PEG-NP or G2-PEG-NP and chased for 16h. Cells were lysed and free dye was separated from intact nanoparticles by electrophoresis. Degradation of G2-PEG-NP is apparent as the appearance of free dye (green) at the bottom of the gel and was quantified using the Odyssey Infrared scanner (right panel). C) A549 cells or D) MKN45 cells were incubated with IRDye800-conjugated G2-PEG-NP in the absence or presence of the inhibitors chloroquine (CQ) and Lactacystin (LC) after which the appearance of free dye was quantified as in B. E, F) Met downregulation 48h after treatment with HGF (50 ng/ml), G2 (100 nM), PEG-NP (0.5 mg/ml) and G2-PEG-NP (0.5 mg/ml) on E) A549 and F) MKN45 cells. Error bars represent SEM where n=3.*

This lysosomal targeting makes the anti-Met NANAPs suitable for the intracellular delivery and release of therapeutic compounds. In addition, lysosomal trafficking of Met induced by the NANAPs could potentially lead to receptor downregulation in Met-overexpressing tumors. This is particularly interesting for tumors that highly overexpress Met and thereby induce constitutive activation of the receptor, as is the case with the MKN45 cell line (Fig. **S3**). To investigate whether lysosomal degradation of G2-PEG-NP is accompanied by receptor degradation, cells were incubated with G2, PEG-NP, G2-PEG-NP and HGF for 48h after which total Met protein levels were determined by western blotting (Figure 6**E-F**). While HGF most prominently induced Met downregulation in A549 cells, treatment with G2-PEG-NP downregulated total Met protein in both A549 and MKN45 cells. All together, these data indicate that anti-Met NANAPs are primarily translocated to late endosomes and lysosomes, which eventually results in lysosomal degradation of both the nanoparticles and Met receptors.

6.4. Discussion

Met overexpression is correlated with poor prognosis in most of the aggressive cancers, such as brain, liver, pancreatic cancers and gastric carcinoma (8). Targeted delivery of small-molecule drugs can contribute to selective inhibition or even killing of Met-expressing tumor cells. In this study, we performed phage display selections for nanobodies specifically binding to human Met and evaluated the applicability of an anti-Met nanobody for targeting albumin nanoparticles to Met expressing tumor cells. Previously, similar nanoparticles were used to retarget toxins like doxorubicin and fluorescent dyes like Cy5 using whole antibodies or peptides directed against avβ3-integrins, the chemokine receptor 4 (CXCR4), or somatostatin receptors (32-34). Recently, Lu *et al*. reported the selection of anti-Met single chain antibodies (scFv) that were used for targeting of quantum dots or doxorubicin loaded liposomes (35). The affinity of the reported scFv's was studied on isolated Met and was about 10-fold less than our anti-Met nanobodies, which were tested on Met-positive cells. A disadvantage of the nanobody is the possible effect of the conjugation of a chemical compound as SATA on the affinity. We have recently shown that

this can be circumvented by the site-directional conjugation to a cysteine residue located at the C-terminus of the nanobody (36). Here, the effect of SATA modification on the binding affinity of the selected anti-Met nanobodies was tested and revealed only a small effect for only one of the nanobodies. This indicates that the SATA groups probably do not bind to a region involved in the antigen recognition.

Besides binding Met with high affinity, the selected nanobodies could compete for HGF binding to recombinant Met ectodomain. However, this competition was not observed on cells. Although the contrast between these observations is quite evident, it might be explained by a mechanistic difference between binding of HGF to isolated and cellular Met. HGF binding to Met occurs via two interaction sites, the SEMA domain and the immunoglobulin-like region of Met (37,38). Binding of HGF to the SEMA domain is considered to induce a conformational change of the ectodomain, revealing the second binding position on the Ig-like regions. Possibly, the interaction of the radiolabeled HGF and the coated recombinant ectodomain only involved one of these binding domains and could therefore be disrupted easily via the selected nanobodies. On cells, the binding between HGF and Met is considered to be further stabilized by secondary interactions of HGF with heparin sulphate on the membranes (28). The fact that G2-PEG-NPs did not compete with HGF on cells also suggest that the potential therapeutic effects of the NANAP's *in vivo* would be independent of HGF levels.

The agonistic activity of G2-PEG-NP is possibly induced by receptor clustering via the multivalent anti-Met format of the nanoparticles. The fact that this was insufficient to induce cell migration, suggests that the NANAPs were unable to fully activate all downstream pathways of Met towards migration. Similar differential downstream signaling towards cell motility, invasion and proliferation was observed with different agonistic antibodies against Met (39). Possibly, the nanoparticles and antibodies induce only a minor activation of Met, which is insufficient to activate downstream pathways. A recent study with oral squamous carcinoma cells showed that, despite a clear phosphorylation of Met, scratch wound healing occurred dose-dependently and only above a certain threshold concentration of HGF (no wound healing at 3.7 ng/ml of HGF to a clear healing at 33 ng/ml) (40). These data suggest the existence of threshold of Met activation requires for the full range of biological responses. Since Met activation by either G2 or G2-PEG-NP did not result in a cellular response like cell migration, we consider their agonistic properties to be of little consequence for future use of the nanoparticles.

In general, the internalization of drug loaded and targeted nanocarriers greatly enhances the specific killing of the targeted cells. (12,41,42). The efficacy of antibodies or nanoparticles can be enhanced by employing receptor-mediated uptake which previously have shown that internalizing liposomes decorated with anti-EGFR nanobodies reduced total EGFR protein expression and inhibited cell growth more potently than a nanobody alone (19). The nanoparticles

in this study also internalized and were subsequently targeted to lysosomes where they were degraded. Internalization of these complexes might be initiated by complex formation of Met as previously suggested by the induced internalization of EGFR using anti-EGFR nanobodies bound to liposomes (19). The anti EGFR liposomes did not stimulate tyrosine kinase activity of EGFR, which is in contrast to the G2-PEG-NPs. While this activation did not result in cell scattering, it resulted in Met receptor internalization and eventually downregulation. This reduces the over-activation of this pathway, which could potentially contribute to the inhibition of tumor growth as we previously have shown for the EGFR (19). In a study by Petrelli et al., Met downregulation was shown to reduce tumor size regardless of receptor phosphorylation (43). As such, the G2-PEG-NP could therefore have an intrinsic anti-tumor activity, as observed in the scratch wound assay (Fig. S2), where G2-PEG-NPs inhibited wound healing in A549 cells.

6.5. Conclusion

We have generated nanobodies specifically binding to Met, which were used to target human albumin nanoparticles to Met expressing cells. Moreover, after binding, the NANAP-Met complexes were internalized and transported to lysosomes for degradation. We conclude that the nanoparticles designed and characterized in this paper are a good candidate for the selective delivery of chemotherapeutic drugs in the treatment of Met overexpressing tumors.

6.6. Acknowledgements

This study was funded by the Focus & Massa project of the Utrecht University, The Netherlands

6.7. References

(1) Naldini L, Vigna E, Narsimhan RP, Gaudino G, Zarnegar R, Michalopoulos GK, et al. Hepatocyte growth factor (HGF) stimulates the tyrosine kinase activity of the receptor encoded by the proto-oncogene c-MET. Oncogene 1991;6(4):501-504.
(2) Ferracini R, Longati P, Naldini L, Vigna E, Comoglio PM. Identification of the major autophosphorylation site of the Met/hepatocyte growth factor receptor tyrosine kinase. J Biol Chem 1991;266(29):19558-19564.
(3) Bussolino F, Di Renzo MF, Ziche M, Bocchietto E, Olivero M, Naldini L, et al. Hepatocyte growth factor is a potent angiogenic factor which stimulates endothelial cell motility and growth. J Cell Biol 1992;119(3):629-641.
(4) Xiao GH, Jeffers M, Bellacosa A, Mitsuuchi Y, Vande Woude GF, Testa JR. Anti-apoptotic signaling by hepatocyte growth factor/Met via the phosphatidylinositol 3-kinase/Akt and mitogen-activated protein kinase pathways. Proc Natl Acad Sci U S A 2001;98(1):247-252.
(5) Birchmeier C, Gherardi E. Developmental roles of HGF/SF and its receptor, the c-Met tyrosine kinase. Trends Cell Biol 1998;8(10):404-410.
(6) Chmielowiec J, Borowiak M, Morkel M, Stradal T, Munz B, Werner S, et al. c-Met is essential for wound healing in the skin. J Cell Biol 2007;177(1):151-162.
(7) Huh CG, Factor VM, Sanchez A, Uchida K, Conner EA, Thorgeirsson SS. Hepatocyte growth factor/c-met signaling pathway is required for efficient liver regeneration and repair. Proc Natl Acad Sci U S A 2004;101(13):4477-4482.
(8) Birchmeier C, Birchmeier W, Gherardi E, Vande Woude GF. Met, metastasis, motility and

more. Nat Rev Mol Cell Biol 2003;4(12):915-925.
(9) Corso S, Comoglio PM, Giordano S. Cancer therapy: can the challenge be MET? Trends Mol Med 2005;11(6):284-292.
(10) Knudsen BS, Vande Woude G. Showering c-MET-dependent cancers with drugs. Curr Opin Genet Dev 2008;18(1):87-96.
(11) Liu X, Newton RC, Scherle PA. Developing c-MET pathway inhibitors for cancer therapy: progress and challenges. Trends Mol Med 2010;16(1):37-45.
(12) Iyer U, Kadambi VJ. Antibody drug conjugates - Trojan horses in the war on cancer. J Pharmacol Toxicol Methods 2011c;64(3):207-212.
(13) Li N, Hill KS, Elferink LA. Analysis of receptor tyrosine kinase internalization using flow cytometry. Methods Mol Biol 2008;457:305-317.
(14) Eierhoff T, Hrincius ER, Rescher U, Ludwig S, Ehrhardt C. The epidermal growth factor receptor (EGFR) promotes uptake of influenza A viruses (IAV) into host cells. PLoS Pathog 2010;6(9):e1001099.
(15) Lefebvre J, Ancot F, Leroy C, Muharram G, Lemiere A, Tulasne D. Met degradation: more than one stone to shoot a receptor down. FASEB J 2012;26(4):1387-1399.
(16) Altintas I, Heukers R, van der Meel R, Lacombe M, Amidi M, van Bergen En Henegouwen PM, et al. Nanobody-albumin nanoparticles (NANAPs) for the delivery of a multikinase inhibitor 17864 to EGFR overexpressing tumor cells. J Control Release 2013;165(2):110-118.
(17) Hamers-Casterman C, Atarhouch T, Muyldermans S, Robinson G, Hamers C, Songa EB, et al. Naturally occurring antibodies devoid of light chains. Nature 1993;363(6428):446-448.
(18) Altintas I, Kok RJ, Schiffelers RM. Targeting epidermal growth factor receptor in tumors: from conventional monoclonal antibodies via heavy chain-only antibodies to nanobodies. Eur J Pharm Sci 2012;45(4):399-407.
(19) Oliveira S, Schiffelers RM, van der Veeken J, van der Meel R, Vongpromek R, van Bergen En Henegouwen PM, et al. Downregulation of EGFR by a novel multivalent nanobody-liposome platform. J Control Release 2010;145(2):165-175.
(20) Talelli M, Oliveira S, Rijcken CJ, Pieters EH, Etrych T, Ulbrich K, et al. Intrinsically active nanobody-modified polymeric micelles for tumor-targeted combination therapy. Biomaterials 2013;34(4):1255-1260.
(21) Hofman EG, Ruonala MO, Bader AN, van den Heuvel D, Voortman J, Roovers RC, et al. EGF induces coalescence of different lipid rafts. J Cell Sci 2008;121(Pt 15):2519-2528.
(22) Salacinski PR, McLean C, Sykes JE, Clement-Jones VV, Lowry PJ. Iodination of proteins, glycoproteins, and peptides using a solid-phase oxidizing agent, 1,3,4,6-tetrachloro-3 alpha,6 alpha-diphenyl glycoluril (Iodogen). Anal Biochem 1981;117(1):136-146.
(23) Langer K, Balthasar S, Vogel V, Dinauer N, von Briesen H, Schubert D. Optimization of the preparation process for human serum albumin (HSA) nanoparticles. Int J Pharm 2003;257(1-2):169-180.
(24) Haselberg R, de Jong GJ, Somsen GW. Capillary electrophoresis of intact basic proteins using noncovalently triple-layer coated capillaries. J Sep Sci 2009;32(14):2408-2415.
(25) Haselberg R, de Jong GJ, Somsen GW. Capillary electrophoresis-mass spectrometry of intact basic proteins using Polybrene-dextran sulfate-Polybrene-coated capillaries: system optimization and performance. Anal Chim Acta 2010;678(1):128-134.
(26) Haselberg R, Brinks V, Hawe A, de Jong GJ, Somsen GW. Capillary electrophoresis-mass spectrometry using noncovalently coated capillaries for the analysis of biopharmaceuticals. Anal Bioanal Chem 2011;400(1):295-303.
(27) Liang CC, Park AY, Guan JL. In vitro scratch assay: a convenient and inexpensive method for analysis of cell migration in vitro. Nat Protoc 2007;2(2):329-333.
(28) Lyon M, Deakin JA, Mizuno K, Nakamura T, Gallagher JT. Interaction of hepatocyte growth factor with heparan sulfate. Elucidation of the major heparan sulfate structural determinants. J Biol Chem 1994;269(15):11216-11223.
(29) Frenken LG, van der Linden RH, Hermans PW, Bos JW, Ruuls RC, de Geus B, et al. Isolation of antigen specific llama VHH antibody fragments and their high level secretion by Saccharomyces cerevisiae. J Biotechnol 2000;78(1):11-21.
(30) Gruenberg J. The endocytic pathway: a

mosaic of domains. Nat Rev Mol Cell Biol 2001;2(10):721-730.
(31) Hammond DE, Urbe S, Vande Woude GF, Clague MJ. Down-regulation of MET, the receptor for hepatocyte growth factor. Oncogene 2001;20(22):2761-2770.
(32) Wagner S, Rothweiler F, Anhorn MG, Sauer D, Riemann I, Weiss EC, et al. Enhanced drug targeting by attachment of an anti alphav integrin antibody to doxorubicin loaded human serum albumin nanoparticles. Biomaterials 2010 Mar;31(8):2388-2398.
(33) Bunschoten A, Buckle T, Kuil J, Luker GD, Luker KE, Nieweg OE, et al. Targeted non-covalent self-assembled nanoparticles based on human serum albumin. Biomaterials 2012;33(3):867-875.
(34) Bae S, Ma K, Kim TH, Lee ES, Oh KT, Park ES, et al. Doxorubicin-loaded human serum albumin nanoparticles surface-modified with TNF-related apoptosis-inducing ligand and transferrin for targeting multiple tumor types. Biomaterials 2012;33(5):1536-1546.
(35) Lu RM, Chang YL, Chen MS, Wu HC. Single chain anti-c-Met antibody conjugated nanoparticles for in vivo tumor-targeted imaging and drug delivery. Biomaterials 2011;32(12):3265-3274.
(36) Kijanka M, Warnders FJ, El Khattabi M, Lub-de Hooge M, van Dam GM, Ntziachristos V, et al. Rapid optical imaging of human breast tumour xenografts using anti-HER2 VHHs site-directly conjugated to IRDye 800CW for image-guided surgery. Eur J Nucl Med Mol Imaging 2013;*in press*.
(37) Stamos J, Lazarus RA, Yao X, Kirchhofer D, Wiesmann C. Crystal structure of the HGF beta-chain in complex with the Sema domain of the Met receptor. EMBO J 2004;23(12):2325-2335.
(38) Basilico C, Arnesano A, Galluzzo M, Comoglio PM, Michieli P. A high affinity hepatocyte growth factor-binding site in the immunoglobulin-like region of Met. J Biol Chem 2008;283(30):21267-21277.
(39) Prat M, Crepaldi T, Pennacchietti S, Bussolino F, Comoglio PM. Agonistic monoclonal antibodies against the Met receptor dissect the biological responses to HGF. J Cell Sci 1998;111 (Pt 2)(Pt 2):237-247.
(40) Brusevold IJ, Aasrum M, Bryne M, Christoffersen T. Migration induced by epidermal and hepatocyte growth factors in oral squamous carcinoma cells in vitro: role of MEK/ERK, p38 and PI-3 kinase/Akt. J Oral Pathol Med 2012;41(7):547-558.
(41) Sapra P, Allen TM. Internalizing antibodies are necessary for improved therapeutic efficacy of antibody-targeted liposomal drugs. Cancer Res 2002;62(24):7190-7194.
(42) Bai F, Wang C, Lu Q, Zhao M, Ban FQ, Yu DH, et al. Nanoparticle-mediated drug delivery to tumor neovasculature to combat P-gp expressing multidrug resistant cancer. Biomaterials 2013;34(26):6163-6174.
(43) Petrelli A, Circosta P, Granziero L, Mazzone M, Pisacane A, Fenoglio S, et al. Ab-induced ectodomain shedding mediates hepatocyte growth factor receptor down-regulation and hampers biological activity. Proc Natl Acad Sci U S A 2006;103(13):5090-5095.

6.8. Supplementary information

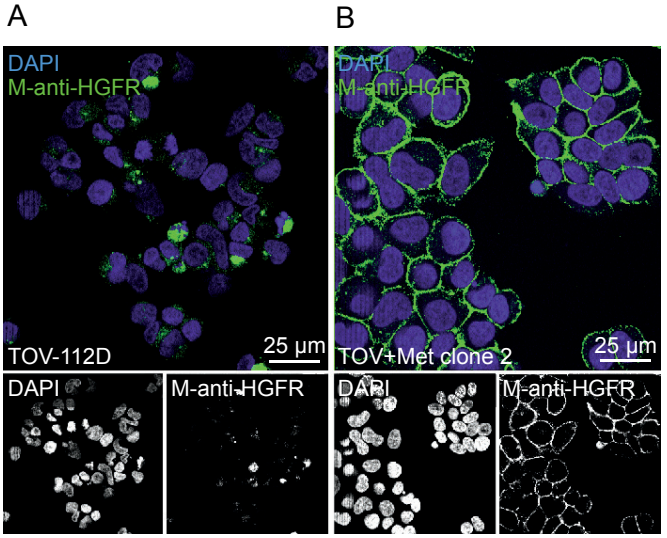

***Figure S1**. Establishment of TOV-112D cells stably expressing human Met. TOV-112D cells were stably transfected with cDNA encoding human Met. Expression of Met on the plasma membrane (green) of A) Met negative (TOV-112D) and B) Met positive (TOV+Met) cells was detected by incubating PFA-fixed cells with mouse anti-HGFR (M-anti-HGFR) followed by anti-mouse IgG coupled to Alexa488. Nuclei were stained with DAPI (blue). Cells were imaged using confocal microscopy.*

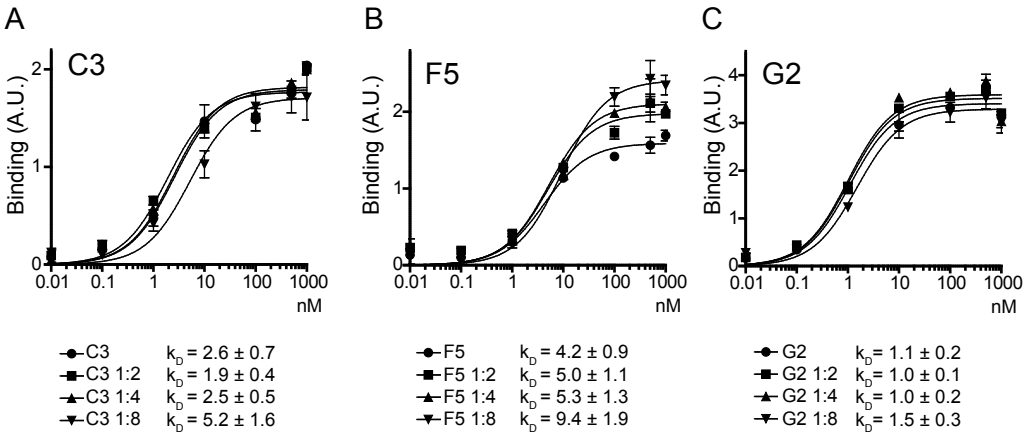

***Figure S2.** Binding studies of indicated SATA modified anti-Met VHHs using MKN45 cells and coupling to nanoparticles. A-C) Binding curves and affinities (K_D) of the anti-Met VHH C3 (A), F5 (B) and G2 (C), all modified with the indicated ratio's of 1:2, 1:4 and 1:8 VHH:SATA (mol/mol).*

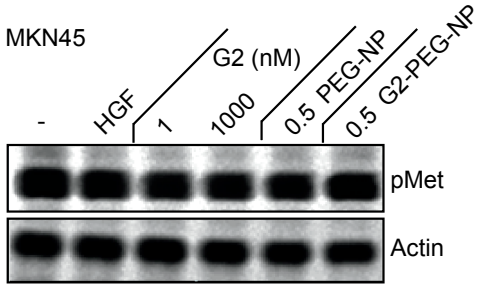

Figure S3. *MKN45 cells are constitutively active. Both G2 and G2-PEG-NP do not affect the phosphorylation status of Met.*

Chapter 7

Nanobody-photosensitizer conjugates for targeted photodynamic therapy

Raimond Heukers [1], Paul M. P. van Bergen en Henegouwen [1], Sabrina Oliveira [1]

[1] Cell Biology, Department of Biology, Utrecht University, Utrecht, The Netherlands

Nanomedicine, under revision

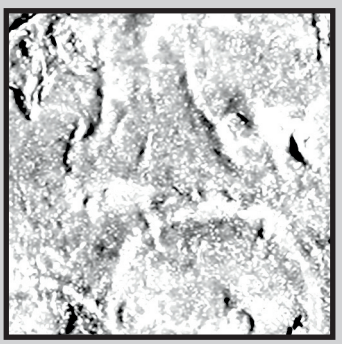

Abstract

Photodynamic therapy (PDT) induces cell death through light-activation of a photosensitizer (PS). Targeted delivery of PS via monoclonal antibodies has improved tumor selectivity. However, due to their size, these conjugates have relatively poor tumor penetration and a characteristic long half-life, leading to limited therapeutic efficacy and long photosensitivity for patients. To target PS homogenously through tumors and to accelerate PS clearance, we have developed new nanosized conjugates consisting of nanobodies targeting the epidermal growth factor receptor (EGFR) and a traceable PS (IRDye700DX). Results show that these conjugates specifically induce cell death of EGFR overexpressing cells with low IC50 values, while PS alone or the nanobody-PS conjugates in absence of light induce no toxicity. Intracellular delivery of nanobody-PS conjugates using biparatopic nanobodies leads to the strongest phototoxicity. Altogether, these EGFR targeted nanobody-PS conjugates are specific and potent nanomedicines, enabling the combination of molecular imaging with cancer therapy.

7.1. Introduction

Photodynamic therapy (PDT) makes use of three essential elements to induce cell death: a photosensitizer (PS), light of a particular wavelength, and oxygen. Since the first evidence of PDT-induced cell toxicity in the early 1900's[1-3], many reports have been published on the usage of PDT to treat cancers of the bladder, skin, head and neck and of the ovaries, among others[4-9]. In general, the PS is administrated intravenously and, after a period of time, light of a particular wavelength is applied to the diseased area. Activated PS often leads to type II photo-oxidative reactions, in which it reacts directly with oxygen to form the very toxic singlet oxygen ($^1O_2$) that damages lipids, proteins and/or nucleic acids[10]. Type I reactions can also occur, in which reactive oxygen species are formed via intermediate reaction of PS with substrates other than oxygen. As these transient oxygen species are short-lived molecules and have very short diffusion distances, their toxicity is confined to the PS localization upon light application[10]. Subsequently, cells die through necrosis and/or apoptosis and tumor destruction occurs through microvasculature damage and involvement of both immune and inflammatory systems[13, 14]. The most commonly used PS include haematoporphirin derivatives (e.g. Photofrin®), chlorins (e.g. Foscan®), and phthalocyanines[8, 9, 15].

The high degree of hydrophobicity and lack of specificity of the PS result in illumination times two to four days after PS administration, in some off-target toxicity, and in a rather long period of patients' photosensitivity after PDT treatment[8, 9, 15]. Therefore, efforts have been made to render PS more hydrophilic and to target these molecules more selectively to tumors, through chemical modifications, delivery systems, and/or targeting molecules[16-20]. In particular, photoimmunotherapy (PIT) refers to the use of antibodies for the targeting of PS in PDT[18]. Although promising results have been reported with mAb-PS conjugates, improvements can be made with respect of time needed for tumor accumulation, their tissue penetration within tumors, and the clearance of unbound conjugates. This has stimulated research on the usage of antibody fragments to target PS, but currently only a small number of such studies have been published[21-23]. To improve PDT application, we have developed a new nanomedicine, which combines a PS with nanobodies as targeting moieties. Nanobodies are the variable domain of a particular sort of antibodies, i.e. the heavy chain-only antibodies that were first discovered in dromedaries in 1993[24]. Importantly, although smaller than full-length antibodies (15 kDa and 2.5 nm x 4 nm[25, 26], compared to 150 kDa and 14.2 nm × 8.5 nm × 3.8 nm of mAbs[27]), nanobodies can bind very specifically and tightly to their antigens (low nanomolar affinities), for instance to the epidermal growth factor receptor (EGFR), which is overexpressed in many types of human cancers[28, 29]. Recently, we have demonstrated the advantages of nanobodies for optical molecular imaging of EGFR-positive tumors[30]. Nanobodies showed a faster accumulation at the tumor, a more homogeneous distribution within the tumor, and a more rapid clearance of unbound molecules.

In an attempt to translate these properties to the PDT context, we have conjugated the same anti-EGFR nanobody (7D12) to a PS. Furthermore, similarly to what was shown with internalizing mAbs[31-33], we aimed to improve the potency of the PDT even further by stimulating intracellular delivery of the PS. For that, we used a biparatopic nanobody (7D12-9G8) that is known to be internalized via clustering-induced endocytosis of EGFR (Chapter 3).

To further contribute to a more effective PDT, the PS used in this study is traceable through optical imaging which enables the light application at the most appropriate time and location. The idea of visualizing tumors through imaging of a PS dates back to the 1920's[34], but the exploration of this feature is still in its infancy[5], mainly due to the poor absorption of common PS in the near infrared range, which is the most effective range of wavelength to penetrate through human tissues[35]. The PS used in this study is the recently described, near infrared fluorescent PS, IRDye700DX. This phthalocyanine derivative has previously been conjugated to an EGFR targeted mAb and was shown to be phototoxic when bound to the cell membrane or after internalization[36]. Furthermore, tumor specific PDT was shown, where shrinkage of tumors was only observed in those overexpressing EGFR.

In this study, monovalent or biparatopic nanobodies targeting EGFR are conjugated to the traceable PS IRDye700DX. These conjugates are here characterized and their phototoxicity is evaluated *in vitro*. These new nanomedicines could have a significant impact on current PDT protocols, combining molecular imaging with therapy.

7.2. Methods

7.2.1. Production of nanobodies and PS conjugation

Nanobodies 7D12, R2, and 7D12-9G8 were produced as previously described[30, 37]. His-tagged nanobodies were produced in E. coli and purified from the periplasmic space by TALON affinity purification[38]. The photosensitizer IRDye700DX (here named PS) was purchased from LI-COR (LICOR Biosciences, Lincoln, Nebraska) as an N-hydroxysuccinimidine (NHS) ester. Conjugation of the PS to the nanobodies, purification and characterization of the nanobody-PS conjugates were performed as described in the Supplementary Materials.

7.2.2. Cell lines and culture conditions

The mouse fibroblast cell line NIH 3T3 2.2 (abbreviated 3T3 2.2) was described in[39]; the human head and neck squamous cell carcinoma cell line UM-SCC-14C (abbreviated 14C) was kindly provided by Prof. Dr. G.A.M.S. van Dongen, (VUMC, Amsterdam, The Netherlands); the human epithelial carcinoma cell line A431 (CRL-1555) and the human cervical carcinoma cell line HeLa (CCL-2) were both obtained from ATCC (LGC Standards, Wesel, Germany). All cell lines were

cultured as described in the Supplementary Materials.

7.2.3. Cell binding assay

To assess nanobody-PS conjugates specificity, binding assays were performed on all cell lines, as described in detail in the Supplementary Materials. For evaluation of the association kinetics, 14C cells were incubated with 25 nM of nanobody-PS at 37°C for up to 30 min. Thereafter, cells were washed twice and the fluorescence intensity of bound conjugates was detected with the Odyssey Infrared scanner, using the 700 nm channel.

7.2.4. *In vitro* PDT

One day after seeding 8000 cells per well of 96-wells plates (Greiner Bio-One, Alphen a/d Rijn, The Netherlands), cells are washed once with PDT medium (DMEM without phenol red supplemented with 8% FCS (v/v), 100 U/ml penicillin, 100 µg/ml streptomycin, and 2 mM L-glutamine). Then, a dilution range of nanobody-PS conjugates was added to the cells and incubated for 30 min at 37°C. After the incubation (also referred to as pulse), cells were washed twice with PDT medium. Immediately after, the fluorescence intensity of the conjugates bound to and/or internalized by the cells was detected with the Odyssey scanner and the cells were illuminated immediately after, unless otherwise mentioned. Plates were illuminated with ~ 4 mW/cm^2 fluence rate (measured with an Orion Laser power/energy monitor, Ophir Optronics LTD, Jerusalem, Israel), for a total light dose of 10 or 5 J/cm^2, using a device consisting of 96 LED lamps (670 ± 10 nm, 1 LED per well) described in[40, 41]. After illumination, cells were placed back into the incubator, unless mentioned otherwise. In all experiments, a number of wells were covered during illumination as internal negative control. Experiments were repeated at least twice.

7.2.5. Cell viability assay

After overnight incubation of the cells treated as described above, cells were incubated with the Alamar Blue reagent, according to the manufacturer's protocol (AbD Serotec, Oxford, United Kingdom) and as described in the Supplementary Materials. Results are expressed as cell viability in percentage (%), thus relatively to the untreated cells, and the half maximal inhibitory concentration (IC50) are determined with using the GraphPad Prism 5.02 software.

7.2.6. Internalization assay

Cells were pulsed with 25 nM of nanobody-PS conjugates for different time periods up to 30 min at 37°C in PDT-medium, after which the cells were washed and fresh PDT-medium was added to the cells. Pulsed nanobody-PS was then chased for 210 min (time point 240 min) at 37°C. At each time point, cells were washed twice and total fluorescence intensity was determined using

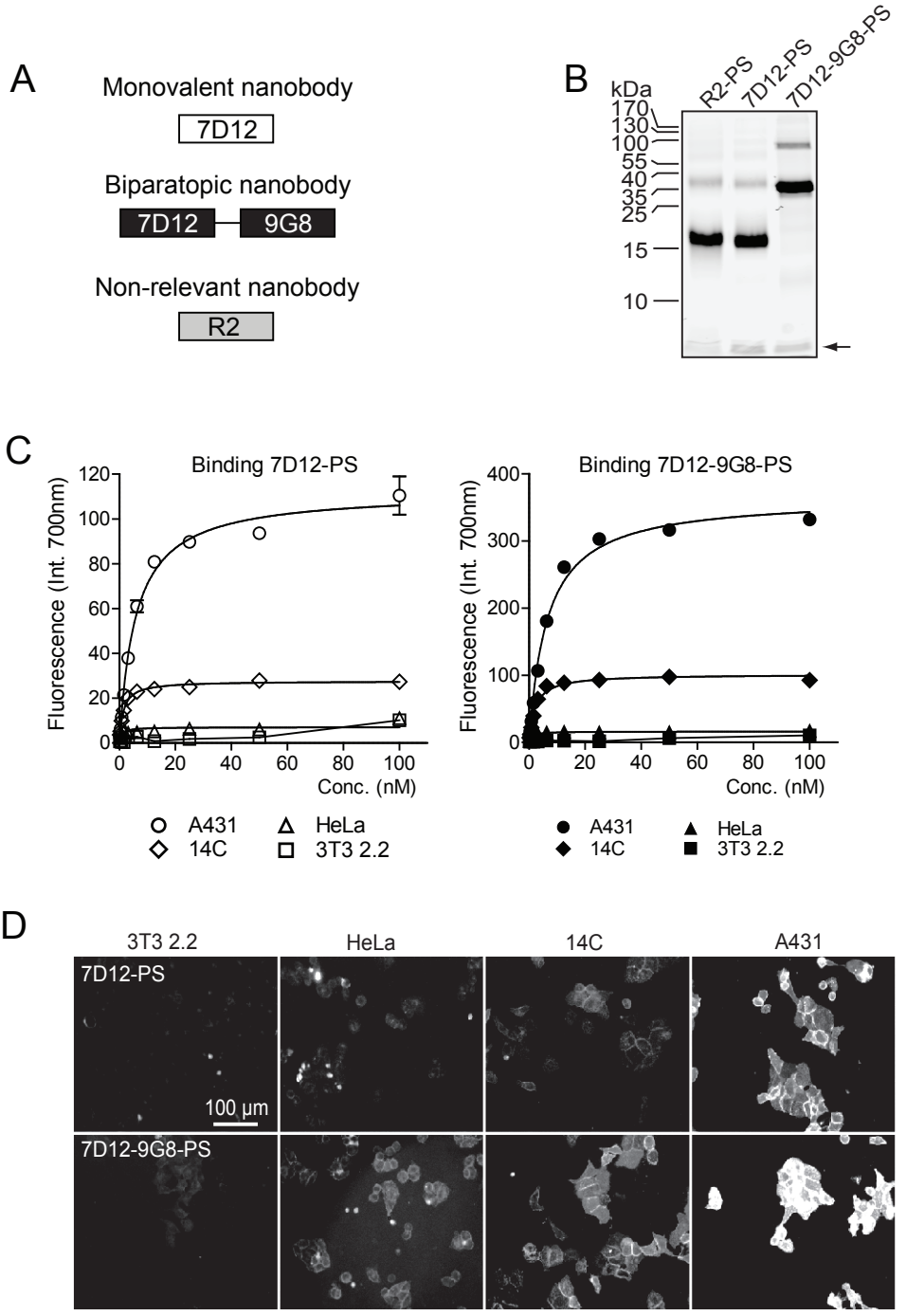
A
Monovalent nanobody
7D12
Biparatopic nanobody
7D12
9G8
Non-relevant nanobody
R2
B
kDa
R2-PS
7D12-PS
7D12-9G8-PS
170
130
100
55
40
35
25
15
10
C
Binding 7D12-PS
Fluorescence (Int. 700nm)
Conc. (nM)
A431
HeLa
14C
3T3 2.2
Binding 7D12-9G8-PS
Fluorescence (Int. 700nm)
Conc. (nM)
A431
HeLa
14C
3T3 2.2
D
3T3 2.2
HeLa
14C
A431
7D12-PS
100 µm
7D12-9G8-PS

Figure 1. *A. Schematic representation of the nanobodies targeting EGFR and of the negative control. B. Fluorescent nanobody-PS conjugates separated by SDS PAGE. Conjugates are identified as R2-PS, 7D12-PS and 7D12-9G8-PS. Free PS is observed at the gel front, indicated by the arrow. C. Nanobody-PS conjugates bind to the three cell lines according to their EGFR expression level: A431 > 14C > HeLa and not to 3T3 2.2 cells (no EGFR). D. Images of fluorescence microscopy obtained with an EVOS microscope.*

the Odyssey Infrared scanner. In order to study the internalized fraction, cells were incubated on ice and surface bound nanobody-PS was removed by an acid wash of pH 2.5 for 2 x 10 min after which the residual (internalized) fluorescence intensity was measured.

7.2.7. Co-culture assay

A mixture consisting of 50% of HeLa and 50% of 14C cell lines was seeded in 96-wells plates (Greiner), pulsed with 25 nM of nanobody-PS and followed by 10 or 5 J/cm^2 of light dose. Either immediately after the light treatment or after overnight incubation (~ 16 h), cells were incubated at room temperature with propidium iodide (Invitrogen) that is impermeable to live cells and with calcein AM (Invitrogen) that only stains living cells, according to the manufacturers' protocol. Cells were then imaged as described in the Supplementary Materials.

7.2.8. Statistics

Data was analyzed using the GraphPad Prism 5.02 software for Windows (GraphPad Software, San Diego, CA). Analysis of significance was performed by t-test and differences with p-values <0.05 were considered significant.

7.3. Results

7.3.1. Production and characterization of nanobody-PS conjugates

The EGFR specific nanobody 7D12 is employed for targeting the PS to EGFR expressing cells for PDT, and the non-relevant nanobody R2 is used as a negative control (Figure 1A). In addition, the internalizing biparatopic nanobody 7D129G8 is used to investigate whether more effective internalization of PS would further increase the toxicity of these nanomedicines. Similarly to the previous study[30], nanobodies were conjugated to the PS (IRdye700DX) via random NHS-mediated coupling to lysine amino acids. After purification, conjugation of the nanobodies to the PS was verified by SDS-PAGE and only traces of free PS were noticeable at the front of the gel (Figure 1B). Determination of the degree of conjugation revealed that R2, 7D12 and 7D12-9G8 were on average conjugated to 1.0, 0.5 and 1.5 molecules of PS, respectively. The production of these nanobody-PS conjugates was reproducible.

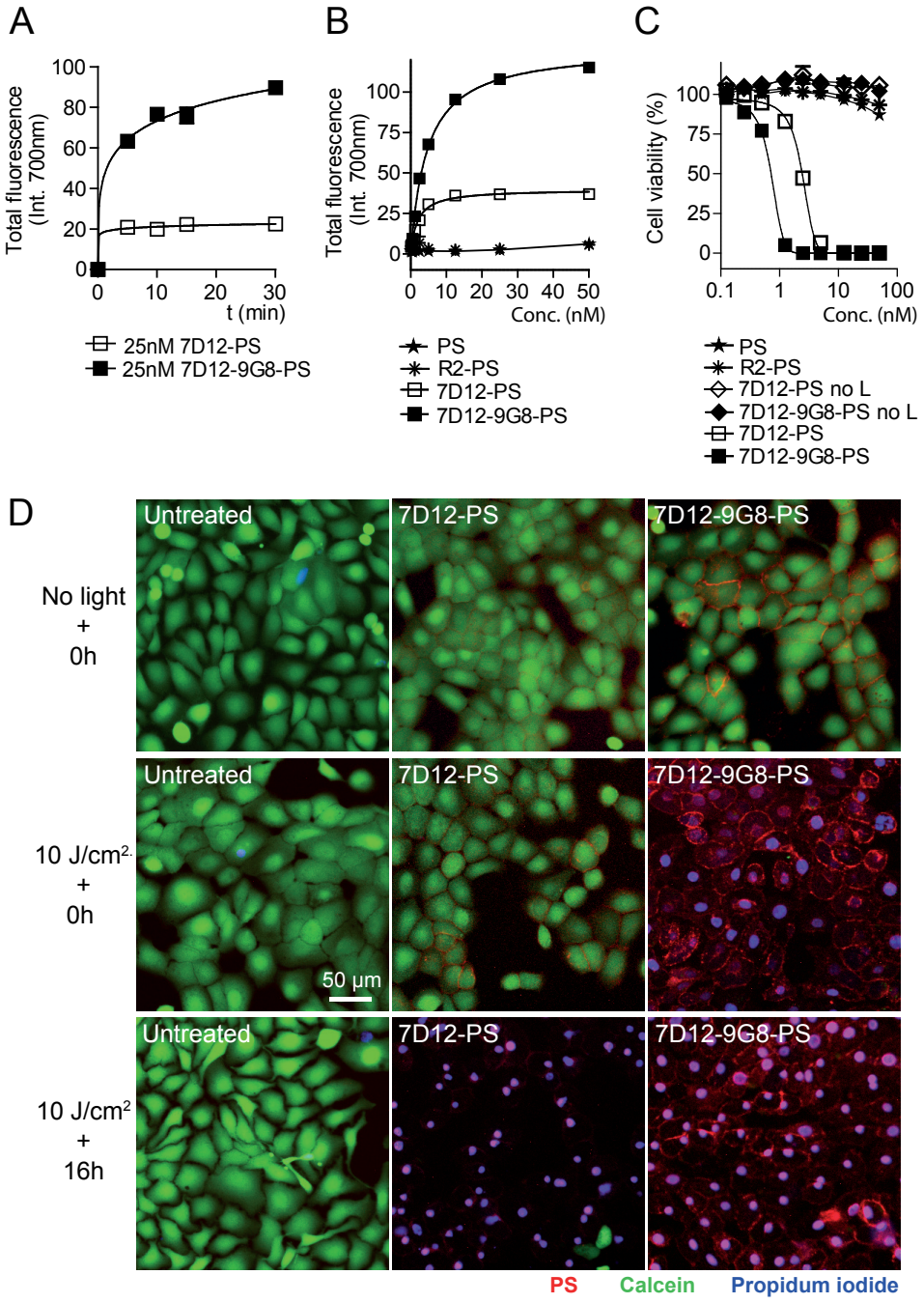
A
Total fluorescence (Int. 700nm)
100
80
60
40
20
0
0 10 20 30
t (min)
25nM 7D12-PS
25nM 7D12-9G8-PS
B
Total fluorescence (Int. 700nm)
100
75
50
25
0
0 10 20 30 40 50
Conc. (nM)
PS
R2-PS
7D12-PS
7D12-9G8-PS
C
Cell viability (%)
100
75
50
25
0
0.1 1 10 100
Conc. (nM)
PS
R2-PS
7D12-PS no L
7D12-9G8-PS no L
7D12-PS
7D12-9G8-PS
D
No light + 0h
10 J/cm2 + 0h
10 J/cm2 + 16h
Untreated
7D12-PS
7D12-9G8-PS
50 µm
PS
Calcein
Propidum iodide

Figure 2. *A. Interaction of EGFR targeted nanobody-PS conjugates with cells over time. B. Total fluorescence intensity associated with 14C cells after 30 min pulse with a concentration range of the three nanobody-PS conjugates and PS alone. C. Percentage (%) of cell viability after a 10 J/cm^2 light dose relative to untreated cells. D. Fluorescence microscopy for the detection of nanobody-PS (in red), of dead cells stained with propidium iodide (in blue) and of intact cells stained with calcein AM (in green).*

7.3.2. Nanobody-PS conjugates bind specifically to EGFR

In order to confirm that the conjugation of the PS to the nanobodies did not compromise their binding properties, binding assays were performed under non-internalizing conditions (4°C) on cell lines expressing no and different levels of EGFR. Importantly, a clear correlation was observed between the fluorescence intensity of the conjugates detected and the cellular expression level of EGFR: A431 > 14C > HeLa > 3T3 2.2, where 3T3 2.2 is negative for EGFR expression (Figure 1C). Also, the differences in B_{max} between the 7D12-PS and 7D12-9G8-PS correlated well with the difference in degree of conjugation. Binding was also assessed by fluorescence microscopy, where a similar correlation between EGFR expression level and fluorescence intensity of the nanobody-PS conjugates at the cell membrane was noticeable (Figure 1D). The apparent binding affinity of nanobodies on cells on ice were 1.4 ± 0.7 nM for 7D12-PS and 2.0 ± 0.2 nM for 7D12-9G8-PS, which is in the range of affinity values previously reported[30, 37].

7.3.3. Nanobody-PS conjugates are potent PDT agents

To explore the potential of these new conjugates for PDT, we first investigated the association kinetics of the EGFR targeted nanobody-PS conjugates to EGFR overexpressing cells. Results showed that nanobody-PS conjugates bind very rapidly to EGFR receptors (Figure 2A), early reaching approximate values of saturation, comparable to those determined by the binding assays at 4°C (Figure 1C, 14C cells). Subsequently, and in all the following experiments, cells were incubated for 30 min at 37°C (indicated as pulse), with a concentration range of the three nanobody-PS conjugates or the PS alone. Also here, the detected maximum fluorescence intensity on cells for 7D12-PS and 7D129G8-PS correlated well with the degree of conjugation (Figure 2B). No binding of free PS or R2-PS to 14C cells was detected, which indicates that there is no cell association of PS in the absence of EGFR targeted nanobodies.

After the pulse, cells were exposed to a light dose of 10 J/cm^2, to induce PDT and the cell viability was assessed the following day. Clearly, the EGFR targeted nanobody-PS conjugates are very potent PDT agents, with IC50 values of 2.3 ± 0.7 nM for 7D12-PS and of 0.6 ± 0.06 nM for 7D12-9G8-PS (Figure 2C). Furthermore, the efficacy of the PDT correlates well with the amount of PS that was present on the cells at the time of illumination. Importantly, free PS, R2-PS, and the non-illuminated EGFR targeted nanobody-PS conjugates did not affect cell viability, which highlights the specificity of this PDT approach. PDT induced toxicity was also observed

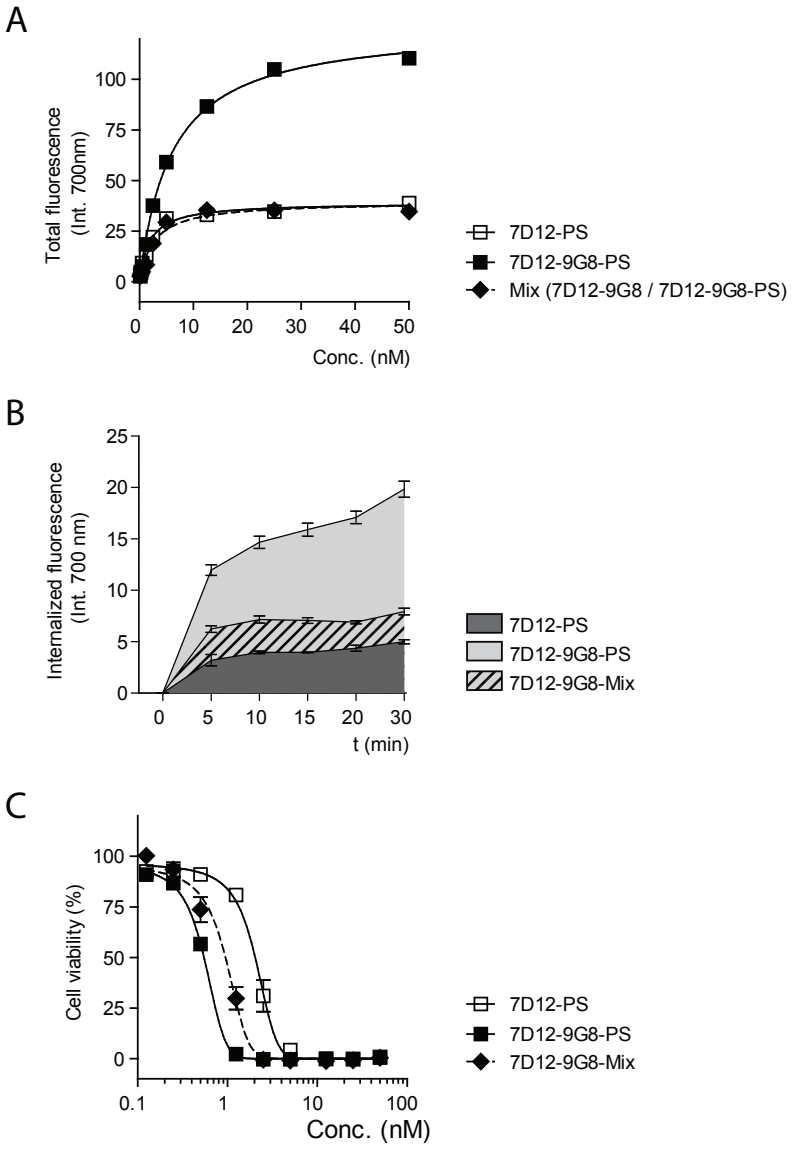

Figure 3. *A. Comparison between total nanobody-PS conjugate associated with cells with either 7D12-PS (open squares), 7D12-9G8-PS (close squares) or mixture of 7D12-9G8-PS with unconjugated 7D12-9G8 (diamonds and dashed line) containing an average degree of conjugation that is similar to that of 7D12-PS. B. Internalized nanobody-PS conjugates were determined at different time points after acid washes. C. Percentage (%) of cell viability after illumination with 10 J/cm^2, relative to untreated cells.*

by fluorescence microscopy, where dead cells, as indicated by propidium iodide staining of the nuclei, are distinguished from living cells, stained with calcein AM. Immediately after light application, all cells that were pulsed with 7D12-9G8-PS appeared dead, while in the case of 7D12-PS this was observed at a later time point. For both nanobody-PS conjugates, no cell death was observed when no light was applied after the pulse (Figure 2D).

7.3.4. The biparatopic nanobody-PS leads to more effective PDT

The nanobody 7D12-9G8 induces EGFR internalization, via receptor mediated endocytosis, and is taken up by cells more efficiently than the nanobody 7D12 (Figure S1A and S1B). This suggests that 7D12-9G8 can lead to a more effective intracellular delivery of PS, resulting in a more potent PDT (in line with studies of internalizing mAbs[31-33]). The efficacy of the PDT correlated well with the amount of PS that was present on the cells at the time of illumination (Figure 2B and 2C), resulting in the lowest IC50 (i.e. highest toxicity) for the biparatopic nanobodyPS conjugate. However, the degree of conjugation of the two nanobody-PS conjugates is different, so, to more carefully study the contribution of PS internalization via the biparatopic nanobody, we have made a mixture of 7D12-9G8 with 7D12-9G8-PS (7D12-9G8-Mix). This approach allowed comparing the two nanobody-PS formats while a similar amount of PS was associated with the cells (Figure 3A). Subsequently, acid washes were conducted to determine the fluorescence intensity of the PS located intracellularly, which showed that the 7D12-9G8-Mix accumulated in cells to a greater extent than 7D12-PS (Figure 3B). These data confirm that 7D12-9G8-PS is internalized more efficiently than 7D12-PS. More importantly, even though the total PS associated with cells is comparable, the potency of the mixture to induce PDT (IC50 1.2 ± 0.3 nM) is two times more effective than that of 7D12-PS (IC50 2.3 ± 0.7 nM). As for the 7D12-9G8-PS, which resulted in more PS associated with cells, the toxicity was evidently higher (IC50 0.6 ± 0.06 nM) (Figure 3C).

7.3.5. Illumination right after incubation leads to greater phototoxicity

The fact that nanobody-PS conjugates are internalized by cells could result in residualization of the conjugates. As this would be relevant for the subsequent illumination time point for PDT, we have investigated this aspect in more detail employing a 'pulse-chase' experimental set-up. During the chase, the amount of PS bound to the tumor cells decreased over time for both formats (41% ± 6% for 7D12-PS and 43% ± 2% for 7D12-9G8-PS), while the fraction of internalized nanobody-PS remained constant (Figure 4A). These data suggest that no recycling of the nanobodies occurs and that both formats of nanobody-PS conjugates residualize within the cells.

To gain more insight in the fate of the nanobody-PS conjugates after internalization, we studied the possibility of lysosomal degradation. After 30 min pulse and 210 min of chase, free PS was only observed in the cellular fraction and this was significantly more for the 7D12-

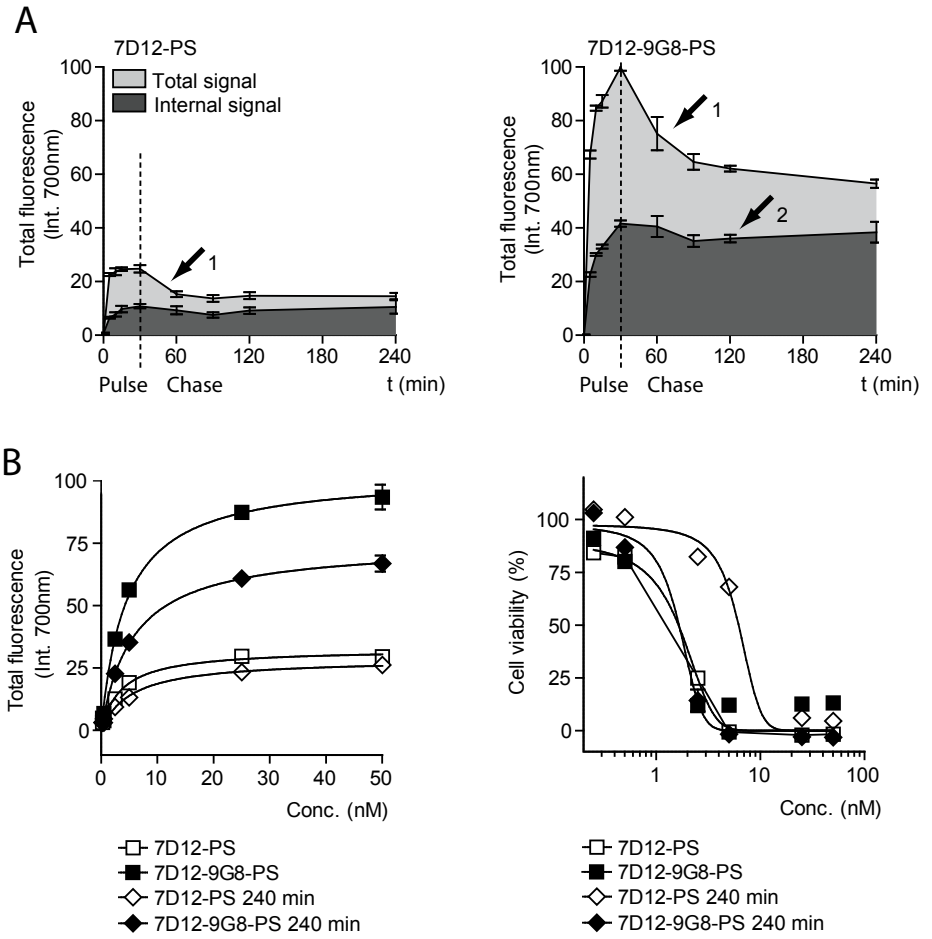

Figure 4. *A. Total (light grey) and internal (dark grey) fluorescence of nanobody-PS conjugates, during 30 min pulse and the following 210 min chase. B. Left: Total fluorescence intensity after 14C cells were pulsed with nanobody-PS conjugates or after a 210 min chase (240 min). Right: Cell viability after illumination with 10 J/cm², right after pulse or after the chase period.*

9G8-PS (20 ± 3% of the internalized fraction), as compared to 7D12-PS (6 ± 2%) (Figure S2A, $p<0.05$). The lack of free PS observed in the medium demonstrates the stability of the conjugates in culture medium. Chloroquin (CQ) prevented the degradation of 7D129G8PS, as well as the control conjugate EGF-IRDye800CW ($p<0.01$ and $p<0.001$, respectively), indicating that the conjugate is degraded in the lysosomes. Moreover, intracellular trafficking towards the lysosomes was confirmed by fluorescence microscopy (Figure S2B). Besides lysosomal degradation of the nanobody-PS conjugates, the biparatopic nanobody also induced degradation of the EGFR (Figure S2C).

To investigate how a delay in light application would affect PDT potency, 14C cells were treated as described earlier for PDT (Figure 4B, left). Cells were illuminated either right after the 30 min pulse with the nanobody-PS conjugates or after the chase period of 210 min (i.e. 240 min time point). After the chase, there was a significant decrease in potency of the 7D12PS (IC50 10.1 ± 4.4 nM), while the potency of the biparatopic nanobody-PS conjugate was less affected (IC50 1.2 ± 0.07 nM) (Figure 4B, right).

7.3.6. Nanobody-PS mediated PDT is tuneable for EGFR overexpressing tumor cells

The selectivity of the nanobody-PS induced PDT was assessed by performing the PDT on different cell lines with varying expression levels of EGFR. Similarly to the correlation observed between the level of binding of the conjugates and the expression level of these cells (Figure 1C), the potency of PDT was also correlated to the expression level of EGFR (Figure 5A). For the 7D12-PS, compared to the above mentioned IC50 on 14C cells (2.3 ± 0.7 nM), the IC50 on A431 cells was lower (1.3 ± 0.06 nM). Interestingly, no IC50 could be determined for the low EGFR expressing HeLa cells, indicating that this particular treatment is relatively ineffective towards cells with low EGFR expression. As could be expected, the 7D12-9G8-PS was more potent than the 7D12-PS, being also toxic to HeLa cells (IC50: 14C 0.59 ± 0.06 nM; A431 0.52 ± 0.10 nM; HeLa 2.29 ± 0.68 nM).

In order to reduce the potency of PDT in low EGFR expressing cells, similar PDT-assays were performed but with half the light dose (5 J/cm^2) (Figure 5B). For the 7D12-PS, this resulted in no toxicity for HeLa cells and only moderate toxicity in 14C cells (IC50 values of 39 ± 14.5 nM), but still a rather strong toxicity on A431 cells (2.3 ± 0.34 nM). In case of 7D12-9G8-PS, compared to 10 J/cm^2, the reduced light dose resulted in a higher IC50 for HeLa cells (22.8 ± 7.5 nM) and only slightly higher IC50 values for the EGFR overexpressing cell lines (1.2 ± 0.26 nM for 14C cells and 1.1 ± 0.47 nM for A431 cells).

Selectivity of the nanobody-PS conjugates was also demonstrated using co-culture experiments performed with the 14C cell line overexpressing EGFR and the HeLa cell line expressing low levels of EGFR. With 7D12-PS, immediately after the light treatment with 10 J/cm^2, no cell damage was yet observed through fluorescence microscopy. But, the next day, a clear propidium iodide staining was visible, specifically in 14C cells, while HeLa cells remained intact (Figure 5C, middle). These observations suggest that PDT mediated by 7D12-PS requires more time before the effect is detectable through fluorescence microscopy (also suggested earlier, Figure 2D). Interestingly, for 7D12-9G8-PS, immediately after the light treatment with 5 J/cm^2, cell damage was observed by the appearance of propidium iodide staining, specifically in 14C cells, while HeLa were stained with calcein AM (Figure 5C, right).

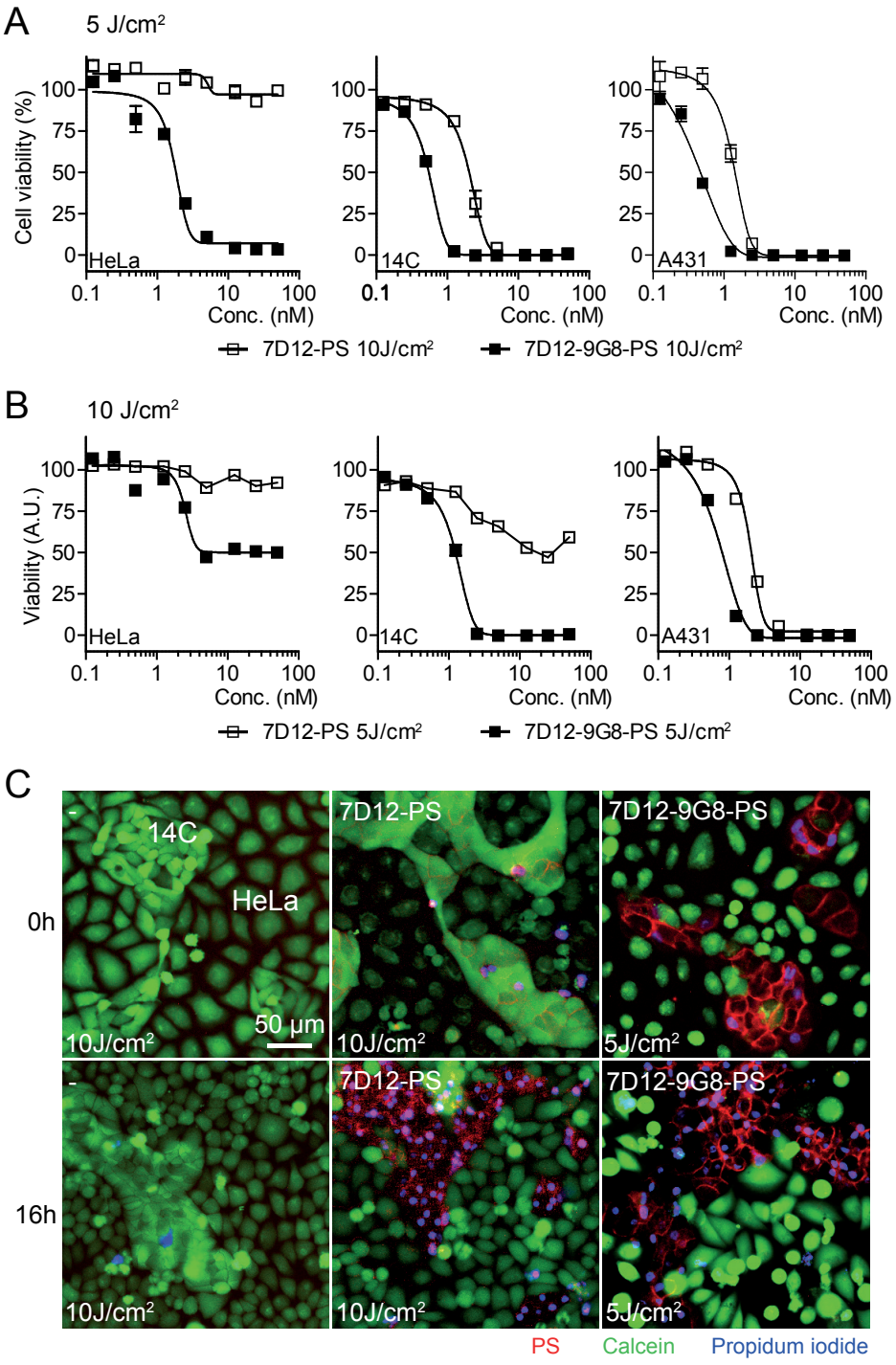
A
5 J/cm²
Cell viability (%)
HeLa
14C
A431
Conc. (nM)
7D12-PS 10J/cm²
7D12-9G8-PS 10J/cm²
B
10 J/cm²
Viability (A.U.)
HeLa
14C
A431
Conc. (nM)
7D12-PS 5J/cm²
7D12-9G8-PS 5J/cm²
C
0h
16h
14C
HeLa
50 μm
7D12-PS
7D12-9G8-PS
10J/cm²
5J/cm²
PS
Calcein
Propidum iodide

Figure 5. *A. Comparison of PDT on different cell lines pulsed with 7D12-PS (open squares) or 7D12-9G8-PS (closed squares) and illuminated with 10 J/cm^2 or B. 5 J/cm^2 light dose. C. Fluorescence microscopy of co-cultures of HeLa and 14C cells, for the detection of nanobody-PS (in red), of dead cells stained with propidium iodide (in blue) and of intact cells stained with calcein AM (in green).*

7.4. Discussion

Over the years, many efforts have been made in the field of photodynamic therapy (PDT) to target photosensitizers (PS) specifically to the site of interest (i.e. tumor)[17-20]. Monoclonal antibodies (mAbs) have been employed for this purpose (i.e. Photoimmuno-therapy) and, despite promising results reported with mAb-PS conjugates[18, 36], improvements can be made with respect of their penetration and distribution within tumor tissues, and of their clearance from blood and normal tissues. A small number of studies have reported the application of other antibody formats for targeting PS such as porphyrins and chlorins[21-23]. This small number of reports suggests that the conjugation of antibody fragments to traditional PS is not so trivial. This is partially due to the general hydrophobic character of these PS. In fact, only the newer generation of PS present better solubility in aqueous solutions[15, 16] and therefore are easier to conjugate and manipulate. In addition, the possibility of hampering binding of the antibody fragment after conjugation is also a matter of concern and, thus, alternatives have been investigated to minimize possible interferences, such as the site specific conjugation through SNAP-Tag technology[42].

In this study, we aimed to improve targeted PDT by combining the small size and high binding affinity of nanobodies with a relatively hydrophilic PS. The nanobodies here employed are robust and their binding properties are not affected by the random conjugation. Even though the conjugation reactions were performed similarly for each nanobody, different degrees of conjugation were obtained. This is an effect of the random conjugation and of the differences in the amino acid sequences of the nanobodies. This could in the future be avoided through site-directed conjugation, as recently shown with anti-HER2 nanobodies for optical imaging[48]. The PS conjugated to these nanobodies is IRDye700DX, which is relatively more hydrophilic compared to the most common PS employed and is traceable for its distribution and localization by near-infrared fluorescence imaging[36]. The first property is reflected in easiness of conjugation and purification of the nanobody-PS conjugates, while the second property facilitates *in vitro* testing by allowing its detection and the quantification of the conjugates' association level with different cell lines. This is of particular interest since, next to EGFR overexpressing cancer cells, different organs also express EGFR, albeit at a much lower level. The association of the EGFR targeted nanobody-PS conjugates and the subsequent toxicity induced on the different cell lines correlated well with their EGFR expression level.

For the EGFR targeted nanobody-PS conjugates to be cytotoxic to tumor cells *in vivo*, they have to bind specifically to tumor cells and be retained at the tumor, before they are cleared

from the bloodstream through the kidneys. From previous studies[30], it is known that the highest concentration of nanobody in the blood stream is found right after and up to 15-30 min post injection. Therefore, it was important to observe the rapid association kinetics of these conjugates (Figure 2A). In our opinion, the experimental set up employed (i.e. max 30 min pulse) is very important as it reflects the actual exposure time that could take place *in vivo*. This time period differs from what is generally used for conventional antibodies targeting PS (e.g. 6 h, 12 h, or longer[30, 33, 36]), as in that case longer serum half-lives are generally expected. Importantly, the amount of nanobody-PS associated with the cells during the 30 min pulse was sufficient to result in strong toxicity after light application, emphasizing the selectivity and potency of these conjugates for PDT (Figure 2C and 2D).

Besides different time intervals for exposure of cells to conjugates, PDT protocols may also vary in time interval between exposure and the application of light. We therefore investigated the retention of the conjugates in cells in an *in vitro* pulse-chase assay, which showed that dissociation of membrane-bound conjugates occurs over time. Consequently, somewhat less potent PDT was observed, therefore encouraging illumination as early as possible. Nevertheless, the internalization and subsequently the retention of the conjugates within cells was clearly improved by employing internalizing nanobody-PS conjugates (7D12-9G8-PS). Although the degree of conjugation was different for the monovalent and the biparatopic nanobodies, our experiment employing the mixture of 7D12-9G8 with 7D12-9G8-PS (i.e 7D12-9G8-Mix) showed that the internalization of conjugates occurred to a greater extent with the biparatopic nanobody. Subsequently, a more potent PDT was observed for the mixture compared to 7D12-PS, which is in agreement with previous studies employing internalizing mAbs for PDT[31-33]. Notably, our results are in contrast with those of Mitsunaga et al. which reported no additional effect upon internalization of a mAb-IRDye700DX conjugate[36]. However, in that study only the percentage of cell death at one concentration (67 nM) was shown, without calculating IC50 values, which could be the reason for missing the additional effect of internalization. In any case, one can also expect a different mechanism of internalization between biparatopic nanobodies and a mAb. Unlike a single mAb, biparatopic nanobodies (Chapter 3) or a combination of different mAbs[43] induce receptor clustering and consequently endocytosis. This clustering might also affect the consequent downstream trafficking. The improved efficacy and faster cell death induced by the internalizing nanobody might result from the destruction of more vital structures or organelles in the cell. Whether the mechanism through which nanobody-PS conjugates induce cell death is involving singlet oxygen only or the combination with photothermal activity proposed by Mitsunaga et al. is currently unclear. Although interesting to study the mechanism of cell death induced by PDT, for the different localizations of nanobody-PS conjugates, we consider this to be beyond the scope of this study.

The lysosomal trafficking and the lysosomal degradation of both biparatopic nanobody and EGFR correlates well with the natural negative feedback mechanism employed by EGFRs natural ligand EGF (reviewed in[44]). This is also in agreement with previous studies suggesting inhibition of endosomal recycling by antibody-induced EGFR internalization[43, 45]. Importantly, despite the lysosomal degradation, PS remains inside the cells, which in case of a necessary delay in light application, would not drastically compromise the efficacy, particularly in case of the biparatopic nanobody-PS conjugate.

So far, we have shown specific delivery of PS through nanobodies, to and into tumor cells and its efficacy in PDT has also been confirmed. However, this work needs to be translated into an *in vivo* setting in which not only the specific delivery of PS is important, but also the success of the light application. The important advantage of PDT is that light can be applied restrictedly to the sites of interest. This means that the tumor cells will receive the highest light dose, compared to the surrounding tissues. In order to gain more insights on a situation where cancer cells overexpressing EGFR are closely located to (normal) cells with low EGFR expression, co-culture experiments were performed with the 14C cell line overexpressing EGFR and the HeLa cell line expressing low levels of EGFR. These co-culture studies showed that by adjusting the light dose, the treatment could be 100% specific to the EGFR overexpressing 14C cells and safe to the low EGFR expressing HeLa cells. These data are in agreement with the concept of the threshold dose, which implies that a minimum concentration of phototoxic product (e.g. $^1O_2$) is needed to result in cellular or tissue destruction[46, 47]. The challenge *in vivo* will be to determine the appropriate settings to surpass the threshold dose, solely in targeted tissues. Penetration of light through tissues is also known to be limited due to the optical properties of tissues, which in this case also renders PDT safer for (deeper) normal tissues. In case of surgery, these traceable nanobody-PS conjugates could be employed at first for imaging and to guide the tumor resection (image-guided surgery). Thereafter, a certain light dose would be applied in the resected area for activation of the remaining conjugates for PDT of the remaining tumor cells. This approach would likely contribute to more radical tumor resections.

In conclusion, we have demonstrated that nanobodies conjugated to a PS, are suitable for specific and targeted PDT *in vitro*. Secondly, it was shown that the potency of PDT is enhanced by intracellular delivery of PS through the biparatopic nanobody. The next step is to evaluate these nanomedicines *in vivo*, in order to determine the impact and contribution of these new nanobody-PS conjugates in the field of targeted PDT, which combines tumor molecular imaging with therapy.

7.5. References

1. Raab O. Ueber die Wirkung fluorescirender Stoffe auf Infusorien. *Z Biol* 1900;**39**:524-46.
2. von-Tappeiner H, Jesionek A. Therapeutische versuche mit floureszierenden stoffen. *Muench Med Wschrf* 1903;**50**.
3. von-Tappeiner H, Jodlbauer A. Die Sensibilisierende Wirkung Fluorescierender Substanzer. Untersuchungen Uber die Photodynamische Erscheinung. *FCW Vogel Leipzig* 1907.
4. Ackroyd R, Kelty C, Brown N, Reed M. The history of photodetection and photodynamic therapy. *Photochem Photobiol* 2001;**74**:656-69.
5. Celli JP, Spring BQ, Rizvi I, Evans CL, Samkoe KS, Verma S, et al. Imaging and photodynamic therapy: mechanisms, monitoring, and optimization. *Chem Rev* 2010;**110**:2795-838.
6. Kelly JF, Snell ME. Hematoporphyrin derivative: a possible aid in the diagnosis and therapy of carcinoma of the bladder. *J Urol* 1976;**115**:150-1.
7. Dougherty TJ, Kaufman JE, Goldfarb A, Weishaupt KR, Boyle D, Mittleman A. Photoradiation therapy for the treatment of malignant tumors. *Cancer Res* 1978;**38**:2628-35.
8. Agostinis P, Berg K, Cengel KA, Foster TH, Girotti AW, Gollnick SO, et al. Photodynamic therapy of cancer: an update. *CA Cancer J Clin* 2011;**61**:250-81.
9. Allison RR, Bagnato VS, Sibata CH. Future of oncologic photodynamic therapy. *Future Oncol* 2010;**6**:929-40.
10. Moan J, Berg K. The photodegradation of porphyrins in cells can be used to estimate the lifetime of singlet oxygen. *Photochem Photobiol* 1991;**53**:549-53.
11. Hatz S, Lambert JD, Ogilby PR. Measuring the lifetime of singlet oxygen in a single cell: addressing the issue of cell viability. *Photochem Photobiol Sci* 2007;**6**:1106-16.
12. Hatz S, Poulsen L, Ogilby PR. Time-resolved singlet oxygen phosphorescence measurements from photosensitized experiments in single cells: effects of oxygen diffusion and oxygen concentration. *Photochem Photobiol* 2008;**84**:1284-90.
13. Dougherty TJ, Gomer CJ, Henderson BW, Jori G, Kessel D, Korbelik M, et al. Photodynamic therapy. *J Natl Cancer Inst* 1998;**90**:889-905.
14. Huang Z, Xu H, Meyers AD, Musani AI, Wang L, Tagg R, et al. Photodynamic therapy for treatment of solid tumors – potential and technical challenges. *Technol Cancer Res Treat* 2008;**7**:309-20.
15. O'Connor AE, Gallagher WM, Byrne AT. Porphyrin and nonporphyrin photosensitizers in oncology: preclinical and clinical advances in photodynamic therapy. *Photochem Photobiol* 2009;**85**:1053-74.
16. Gomer CJ. Preclinical examination of first and second generation photosensitizers used in photodynamic therapy. *Photochem Photobiol* 1991;**54**:1093-107.
17. Derycke AS, de-Witte PA. Liposomes for photodynamic therapy. *Adv Drug Deliv Rev* 2004;**56**:17-30.
18. van-Dongen GA, Visser GW, Vrouenraets MB. Photosensitizer-antibody conjugates for detection and therapy of cancer. *Adv Drug Deliv Rev* 2004;**56**:31-52.
19. Sibani SA, McCarron PA, Woolfson AD, Donnelly RF. Photosensitiser delivery for photodynamic therapy. Part 2: systemic carrier platforms. *Expert Opin Drug Deliv* 2008;**5**:1241-54.
20. Sharman WM, van-Lier JE, Allen CM. Targeted photodynamic therapy via receptor mediated delivery systems. *Adv Drug Deliv Rev* 2004;**56**:53-76.
21. Duska LR, Hamblin MR, Bamberg MP, Hasan T. Biodistribution of charged F(ab')2 photoimmunoconjugates in a xenograft model of ovarian cancer. *Br J Cancer* 1997;**75**:837-44.
22. Kuimova MK, Bhatti M, Deonarain M, Yahioglu G, Levitt JA, Stamati I, et al. Fluorescence characterisation of multiply-loaded anti-HER2 single chain Fv-photosensitizer conjugates suitable for photodynamic therapy. *Photochem Photobiol Sci* 2007;**6**:933-39.
23. Bhatti M, Yahioglu G, Milgrom LR, Garcia-Maya M, Chester KA, Deonarain MP. Targeted photodynamic therapy with multiply-loaded recombinant antibody fragments. *Int J Cancer* 2008;**122**:1155-63.
24. Hamers-Casterman C, Atarhouch T, Muyldermans S, Robinson G, Hamers C, Songa EB, et al. Naturally occurring antibodies devoid of light chains. *Nature* 1993;**363**:446-8.
25. Roovers RC, van-Dongen GA, en-Henegouwen PM. Nanobodies in therapeutic

applications. *Curr Opin Mol Ther* 2007;**9**:327-35.
26. Schmitz KR, Bagchi A, Roovers RC, van-Bergen-en-Henegouwen PMP, Ferguson KM. Structural evaluation of EGFR inhibition mechanisms for nanobodies/VHH domains. *Structure* 2013;*in press*.
27. Sarma VR, Silverton EW, Davies DR, Terry WD. The three-dimensional structure at 6 A resolution of a human gamma Gl immunoglobulin molecule. *J Biol Chem* 1971;**246**:3753-59.
28. Ciardiello F, Tortora G. EGFR antagonists in cancer treatment. *N Engl J Med* 2008;**358**:1160-74.
29. Vecchione L, Jacobs B, Normanno N, Ciardiello F, Tejpar S. EGFR-targeted therapy. *Exp Cell Res* 2011;**317**:2765-71.
30. Oliveira S, van-Dongen GA, Stigter-van-Walsum M, Roovers RC, Stam JC, Mali W, et al. Rapid visualization of human tumor xenografts through optical imaging with a near-infrared fluorescent anti-epidermal growth factor receptor nanobody. *Mol Imaging* 2012;**11**:33-46.
31. Mew D, Wat CK, Towers GH, Levy JG. Photoimmunotherapy: treatment of animal tumors with tumor-specific monoclonal antibody-hematoporphyrin conjugates. *J Immunol* 1983;**130**:1473-77.
32. Carcenac M, Dorvillius M, Garambois V, Glaussel F, Larroque C, Langlois R, et al. Internalisation enhances photo-induced cytotoxicity of monoclonal antibody-phthalocyanine conjugates. *Br J Cancer* 2001;**85**:1787-93.
33. Vrouenraets MB, Visser GW, Stigter M, Oppelaar H, Snow GB, van-Dongen GA. Targeting of aluminum (III) phthalocyanine tetrasulfonate by use of internalizing monoclonal antibodies: improved efficacy in photodynamic therapy. *Cancer Res* 2001;**61**:1970-75.
34. Policard A. Etudes sur les aspects offerts par des tumours experimetales examinees a la lumiere des woods. *CR Soc Biol* 1924;**91**:1423-8.
35. Rudin M, Weissleder R. Molecular imaging in drug discovery and development. *Nat Rev Drug Discov* 2003;**2**:123-31.
36. Mitsunaga M, Ogawa M, Kosaka N, Rosenblum LT, Choyke PL, Kobayashi H. Cancer cell-selective in vivo near infrared photoimmunotherapy targeting specific membrane molecules. *Nat Med* 2011;**17**:1685-91.
37. Roovers RC, Vosjan MJ, Laeremans T, el-Khoulati R, de-Bruin RC, Ferguson KM, et al. A biparatopic anti-EGFR nanobody efficiently inhibits solid tumour growth. *Int J Cancer* 2011;**129**:2013-24.
38. Roovers RC, Laeremans T, Huang L, Taeye SD, Verkleij AJ, Revets H, et al. Efficient inhibition of EGFR signalling and of tumour growth by antagonistic anti-EGFR Nanobodies. *Cancer Immunol Immunother* 2007;**56**:303–17.
39. Honegger AM, Szapary D, Schmidt A, Lyall R, Van-Obberghen E, Dull TJ, et al. A mutant epidermal growth factor receptor with defective protein tyrosine kinase is unable to stimulate proto-oncogene expression and DNA synthesis. *Mol Cell Biol* 1987;**7**:4568-71.
40. Rijcken CJ, Hofman JW, van-Zeeland F, Hennink WE, van-Nostrum CF. Photosensitiser-loaded biodegradable polymeric micelles: preparation, characterisation and in vitro PDT efficacy. *J Control Release* 2007;**124**:144-53.
41. Hofman JW, Carstens MG, van-Zeeland F, Helwig C, Flesch FM, Hennink WE, et al. Photocytotoxicity of mTHPC (temoporfin) loaded polymeric micelles mediated by lipase catalyzed degradation. *Pharm Res* 2008;**25**:2065-73.
42. Hussain AF, Kampmeier F, von-Felbert V, Merk HF, Tur MK, Barth S. SNAP-tag technology mediates site specific conjugation of antibody fragments with a photosensitizer and improves target specific phototoxicity in tumor cells. *Bioconjug Chem* 2011;**22**:2487-95.
43. Spangler JB, Neil JR, Abramovitch S, Yarden Y, White FM, Lauffenburger DA, et al. Combination antibody treatment down-regulates epidermal growth factor receptor by inhibiting endosomal recycling. *Proc Natl Acad Sci U S A* 2010;**107**:13252-57.
44. Sorkin A, Goh LK. Endocytosis and intracellular trafficking of ErbBs. *Exp Cell Res* 2008;**314**:3093-106.
45. Boersma YL, Chao G, Steiner D, Wittrup KD, Plückthun A. Bispecific designed ankyrin repeat proteins (DARPins) targeting epidermal growth factor receptor inhibit A431 cell proliferation and receptor recycling. *J Biol Chem* 2011;**286**:41273-85.
46. Patterson MS, Wilson BC, Graff R. In vivo tests of the concept of photodynamic threshold

dose in normal rat liver photosensitized by aluminum chlorosulphonated phthalocyanine. *Photochem Photobiol* 1990;**51**:343-49.
47. Farrell TJ, Wilson BC, Patterson MS, Olivo MC. Comparison of the in vivo photodynamic threshold dose for photofrin, mono- and tetrasulfonated aluminum phthalocyanine using a rat liver model. *Photochem Photobiol* 1998;**68**:394-99.
48. M.M. Kijanka, F.J. Warnders, M. El Khattabi, M. Lub-de-Hooge, G.M. van Dam, V. Ntziachristos, E.G.E. de Vries, S. Oliveira, P.M.P. van Bergen en Henegouwen, Rapid optical imaging of human breast tumor xenografts using anti-HER2 VHHs site-directly conjugated to IRDye800CW for image-guided surgery. Eur J Nucl Med Mol Imaging;*in press* (2013).

7.6. Supplementary information

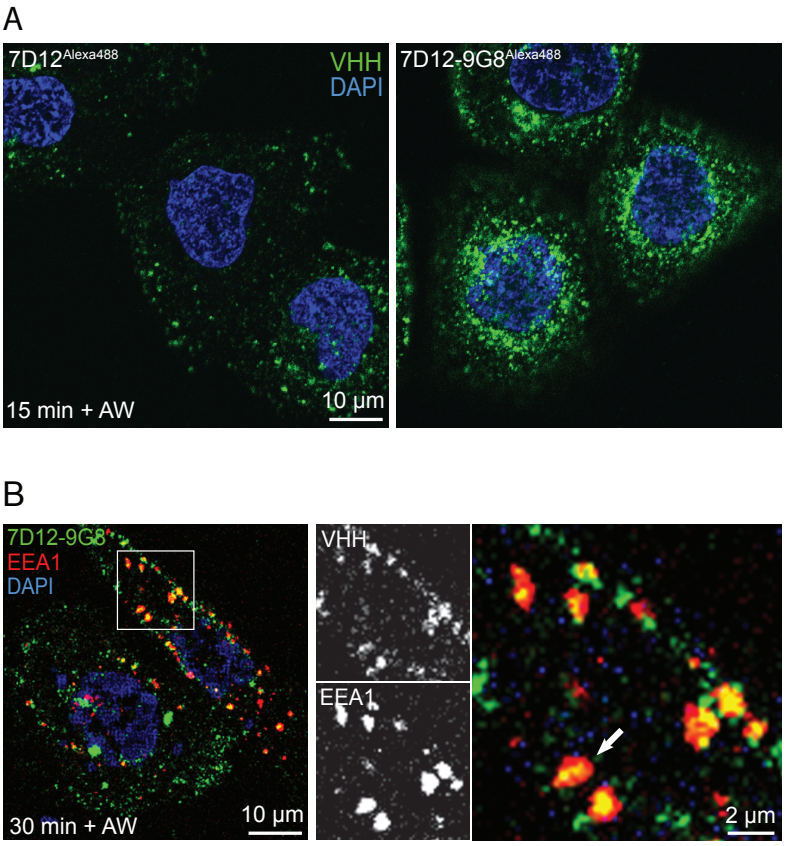

Figure S1. *Biparatopic 7D12-9G8 is internalized more efficiently than 7D12. A. Internalization of Alexa-488 conjugated nanobodies into 14C cells. 14C cells were pulsed with 7D12 or 7D12-9G8 for 15 min and membrane bound nanobody was removed by acid wash. Note the more extensive perinuclear localization and the bigger endocytotic structures of 7D12-9G8 compared to 7D12. B. 7D12-9G8 localized into early endosomes. 14C cells were pulsed with Alexa-488 conjugated 7D12-9G8 for 30 min and treated with acid wash. Early endosomes were stained with anti-EEA1 antibodies. Fluorescence microscopy imaging was performed with a confocal microscope equipped with a 63x objective.*

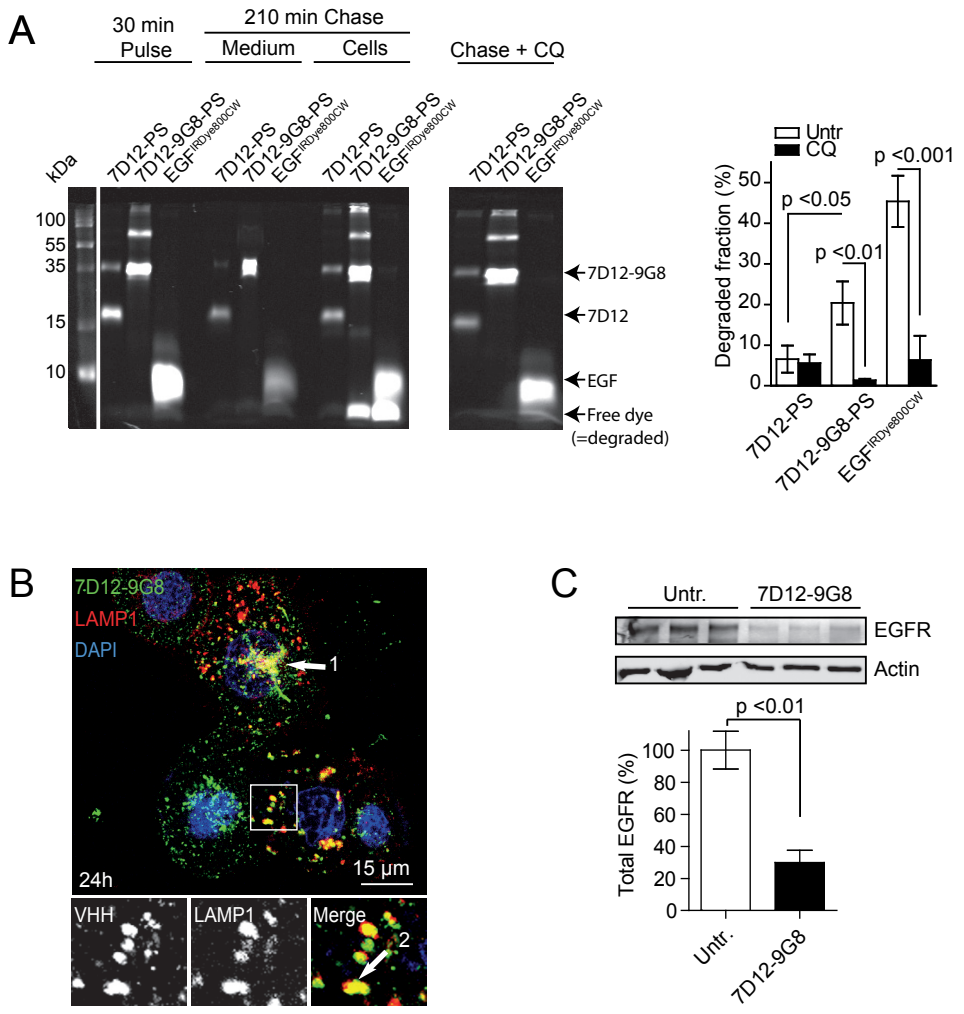

Figure S2. *Free PS is retained inside cells after lysosomal degradation of nanobody-PS. A. 14C cells were pulsed with 25 nM of either 7D12-PS, 7D12-9G8-PS or EGF-IRDye800CW for 30 min and either lysed immediately (pulse) or lysed after an additional 210 min (chase) in the absence or presence of 10 µM of Chloroquin (CQ). Degradation was visible as free dye at the front of the gel and was quantified on an Odyssey Infrared Scanner. C. Biparatopic 7D12-9G8 is trafficked to late endosomal/lysosomal compartments. 14C cells expressing LAMP1-RFP were pulsed with Alexa-488 conjugated 7D12-9G8 for 24 h after which the cells were fixed and imaged with a confocal microscope equipped with a 63x objective. D. 7D12-9G8 induces downregulation of EGFR. 14C cells were treated with 10 nM of 7D12-9G8 for 72 h after which the cells were lysed. EGFR and actin were stained by western blotting and quantified on an Odyssey Infrared scanner. P values were calculated by t-test.*

Chapter 8

Summarizing discussion

8.1. Improving the efficacy of 'naked' antibodies

In the last decades, numerous antibodies for the treatment of cancer have been developed and some have even reached the clinic [1, 2]. Nevertheless, the single target approach of these kinds of therapies (i.e. cell bound receptors or free ligands) can result in the development of resistance against those therapies, which may lead to therapeutic escape of the tumor. Therefore, more radical approaches are needed to improve the efficacy of immunotherapy. Such improvements can be found in the use of a combination of antibodies against different targets or a combination with other types of therapy [3, 4]. For example, antibody drug conjugates (ADC) combine the features of a targeting moiety with the anti-tumor activity of a cytotoxic agent [5]. Since the relatively large size of antibodies limit the distribution of such molecules through tissues and their tumor penetration, smaller antibody fragments like Fabs, Fv's, scFv's and nanobodies or VHHs have been developed [6-8]. A VHH nicely combines a small size and single domain characteristic with a high affinity binding capacity that is comparable to that of a monoclonal antibody [9]. In **Chapter 2**, several examples of the use of VHHs for anticancer therapy were described. However, both *in vitro* and *in vivo* studies show that such 'naked' antibodies primarily display cytostatic activity and lack the cytotoxic activity, which is required to eradicate the tumor. In other words, most naked antibodies do inhibit tumor growth but actually fail to remove the tumors completely [10]. Therefore, improved variations and toxic conjugates of these smaller antibody fragments are of particular interest. Examples of these modified VHHs have also been described in Chapter 2.

8.2. CIC-ME: a naturally existing uptake machinery in cells

Many cytotoxic compounds require an intracellular localization for their activity. While this is easily accomplished with small molecules that readily diffuse through cells, this is more challenging for larger molecules like proteins such as the truncated pseudomonas endotoxin a PE38 or saporin [11]. In order to successfully facilitate intracellular uptake of those therapeutic proteins, a basic understanding on the uptake machinery of tumor cells is important. For example, the internalization of EGFR is considered to be well studied and is known to involve multiple redundant and interdependent mechanisms [12, 13]. Binding of EGF induces several post-translational modifications of the intracellular EGFR domain, i.e. tyr/ser/thr phosphorylation, ubiquitination and acetylation. However, these modifications do not explain the mechanism behind ligand-induced internalization completely. Blocking all the intracellular modifications by site directed mutagenesis of the receptor does not completely inhibit the internalization [13]. Ligand binding to EGFR also results in the formation of higher order clusters on the plasma membrane [14-17]. Furthermore, clustering was believed to induce receptor-mediated internalization, as shown in multiple studies in which EGFR was clustered using antibodies or biparatopic antibody fragments [3, 18, 19]. For example, a mixture of two non-competitive anti-EGFR antibodies, Sym004, was

shown to induce EGFR internalization and degradation, which eventually resulted in enhanced anti-tumor activity [20, 21]. Nevertheless, knowledge about the mechanism behind this phenomenon is still limited. Using biparatopic VHHs, clustering-induced endocytosis and the underlying molecular determinants was studied in **Chapter 3** of this thesis. A mechanistic representation of clustering-induced internalization of EGFR by biparatopic VHHs is shown in Fig. 1A.

Receptor clustering can be studied by a variety of techniques like biochemical assays or electron microscopy [22-24]. Many of such techniques involve invasive approaches that are likely to disturb the integrity of the membrane, which might affect protein interactions. We have used a non-invasive approach to study receptor oligomerization by biparatopic VHHs. This method is based on Förster resonance energy transfer (FRET). In case FRET takes place between identical adjacent fluorescent proteins it is referred to as homo-FRET, which can be determined by fluorescence anisotropy imaging [25, 26]. Because FRET typically takes place within a distance of 10 nm, it is well suitable for studying receptor:receptor interactions in intact cells. By using biparatopic nanobodies we were able to induce EGFR clustering to a similar extend as observed with EGF but without stimulating EGFR kinase activity. This level of clustering was previously shown to correspond to higher order clustering as quantified by artificially clustered GFPs [16, 27]. Clustering of EGFR using the biparatopic nanobodies resulted in the internalization of EGFR with internalization rate constants that were four times higher than constitutive pinocytosis. As such, clustering-induced internalization with biparatopic nanobodies provides an entry mechanism for the specific delivery of therapeutic molecules into tumor cells.

As shown by dual color TIRFM, siRNA knock down and by overexpression of mutated proteins, clustering-induced internalization of EGFR was found to occur via a clathrin-, AP2 and dynamin-mediated pathway. This phenomenon is therefore referred to as clustering-induced clathrin-mediated endocytosis (CIC-ME). These findings are in line with a report showing clathrin-mediated uptake of biotinylated transferrin receptors (TfR) by extracellular clustering via multivalent streptavidin [28]. Nevertheless, not all clustering-induced internalization appears to take place via clathrin-mediated endocytosis. For example, clustering-induced internalization of EGFR via a combination of anti-EGFR (C225) and donkey-anti human IgG was clathrin-independent [29]. As this clustering was also accompanied by receptor activation, posttranslational modifications could potentially mediate additional internalization pathways. Alternatively, this way of clustering EGFR might actually generate clusters that are too large to be taken up via CME.

8.2.1. TMD dimerization motifs function in CIC-ME

The CIC-ME of EGFR, as induced by the biparatopic VHHs did not depend on the intracellular domain of EGFR, but instead revealed an important role for the transmembrane domain (TMD).

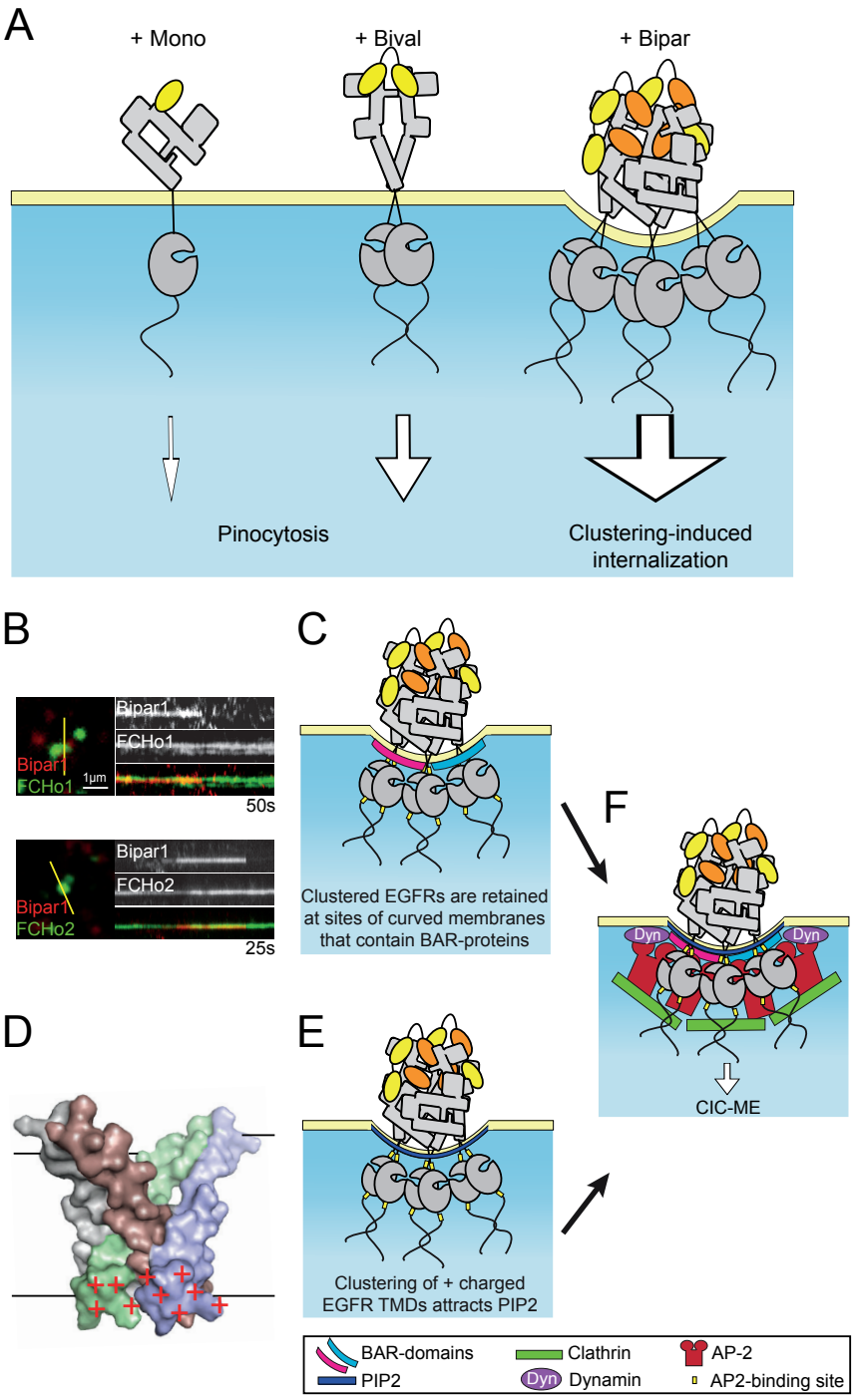
A
+ Mono
+ Bival
+ Bipar
Pinocytosis
Clustering-induced internalization
B
Bipar1
FCHo1
1µm
50s
Bipar1
FCHo2
25s
C
Clustered EGFRs are retained at sites of curved membranes that contain BAR-proteins
F
Dyn
Dyn
CIC-ME
D
E
Clustering of + charged EGFR TMDs attracts PIP2
BAR-domains
PIP2
Clathrin
Dynamin
AP-2
AP2-binding site

Figure 1. *Clustering-induced internalization of EGFR occurs via CIC-ME. (A) EGFR can be clustered on the membrane via biparatopic VHHs directed against non-overlapping epitopes on the EGFR ectodomain. Extracellular clustering of EGFR promotes its internalization, which is faster than the constitutive pinocytosis. (B) Bipar1 internalizes at pre-existing patches of FCHo1 (top) and FCHo2 (bottom). A screenshot of the live cell, dual color TIRF microscopy experiment is shown on the left. The kymograph belonging to the yellow line in the screenshot is shown on the right. (C) Clustered EGFRs with N-terminally linked TMD dimers might induce an inward membrane curvature, leading to a preferred localization in curved membrane patches that are positive for BAR-proteins like FCHo1 and FCHo2. (D) Clustering of N-terminally linked TMDs of EGFR create a positively charged patch just below the membrane. Models of two N-terminally linked TMD dimers of EGFR were docked by HADDOCK and visualized by PyMOL. The positive patch might result in local accumulation of negatively charged lipids like PIP_2 (E). Both hypothesis in C and E might lead to CIC-ME (F).*

In more detail, the GG4-like dimerization motifs in this TMD, especially the N-terminal motif, were found to be crucial for CIC-ME of EGFR. Besides functioning in CIC-ME, the TMD dimerization motifs also play a role in EGF-induced receptor internalization. TMD mutations partially inhibited the EGF-induced internalization rate. In contrast, these mutations did not affect ligand-induced receptor activation. In combination with a kinase dead mutation (K721A), even single point mutations in the TMD motifs completely blocked the uptake of EGF. Interestingly, despite all the efforts that have been put in blocking EGF internalization by mutagenesis in the last decades, this is achieved here by only two point mutations. This is actually the first report that clearly shows the relationship between TMD and endocytosis, which is in contrast with several previous reports stating their importance in receptor activation [30-32]. Nevertheless, our observations are supported by a study from Lu et al., who nicely demonstrated that EGF induces interactions between the N-terminal TMD motifs, which were not involved in receptor activation [33]. Our data indicates that EGFR endocytosis basically involves two mechanisms; the kinase-independent mechanism that depends completely on the N-terminal TMD dimerization motif and a mechanism that involves kinase activity and the consequent post-translational modifications. The kinase-independent internalization of CIC-ME is used by the biparatopic nanobodies. In ligand-induced internalization of the wild type receptor, it is reasonable to assume that these mechanisms act synergistically to facilitate the rapid uptake.

At this point, we can only speculate about the mechanism behind CIC-ME and the role of the TMD dimerization motifs in this process. A few hypotheses might be of interest for further research. One hypothesis involves the wedge shape created by EGFR TMD dimers. As observed from NMR data, N-terminally linked TMDs of EGFR cross at an angle of 46 ± 5°, creating a wedge shaped TMD dimer [34]. Similarly to the wedge-shaped protein Epsin, clustering of the wedge-shaped TMD dimers could potentially induce inwards curvature of the membrane, thereby providing the first step for receptor internalization [35, 36]. The clustering-induced remodeling of the membrane should be studied more carefully, for example by molecular dynamics simulations

or by using giant unilamellar vesicles (GUVs) [30, 37]. In case a concave membrane curvature is induced, this might form an interaction site for BAR- (Bin/Amphiphysin/Rvs) domain containing proteins which can subsequently interact with mediators of the clathrin-mediated endocytosis machinery [37, 38]. Clustering of EGFR TMDs could recruit BAR-proteins and associated CME-related proteins to the bended membrane, which could locally facilitate CME. Examples of such BAR-proteins include the F-BAR domain-containing Fer/Cip4 homology domain-only proteins 1 and 2 (FCHo1/2), which are known to be involved in clathrin-mediated endocytosis [39]. Dual color TIRF microscopy experiments already showed that biparatopic VHH-induced EGFR clusters were indeed internalized at sites where FCHo1 and FCHo2 were located (Fig. 1B). However, instead of initiating CME, these proteins appeared to be localized in pre-existing spots on the membrane. Possibly, the curved membranes of moving EGFR clusters don't initiate CME but are instead preferably retained at curved membrane patches that contain BAR-proteins and proteins of the endocytic machinery (Fig. 1C). Such pre-existing membrane sheets of clathrin were already described previously and are likely to be hot spots for endocytosis [40-42]. Another hypothesis for the role of TMDs in endocytosis involves the four positively charged amino acids just below the TMD of EGFR (arginines and histidine). Clustering of EGFR TMDs creates a dense packing of these positive charges just below the inner leaflet of the membrane (Fig. 1D). This might attract negatively charged lipids like phosphatidylinositol 4,5-bisphosphate (PIP_2), a lipid that is essential for clathrin-mediated endocytosis [43]. Different proteins involved in CME are known to bind to PIP2 including the α-subunit of adaptor protein complex 2 (AP2), dynamin and Eps15 [44-46]. Locally clustering of PIP_2 concentrates PIP_2-interacting mediators of the CME machinery (like AP2) around the EGFR clusters. The involvement of lipid domains in receptor-ligand interactions and receptor signaling were already described for several types of receptors, including EGFR [47-49]. In summary, our experiments show that intracellular uptake can be achieved by using a naturally existing uptake mechanism in tumor cells: the so-called CIC-ME. We have also demonstrated a crucial role for the TMD dimerization motifs in this process. Nevertheless, the mechanistic background behind the role of the TMD dimerization motifs in CIC-ME requires more research, but might involve membrane curvature, BAR-proteins and the formation of PIP_2 microdomains.

8.2.2. Clustering-induced internalization of the other ErbB family members

The members of the ErbB family of receptor tyrosine kinases are highly structurally related and their co-expression is common in numerous types of cancer [3, 50, 51]. Interestingly, all four members contain two GG4-like motifs involved in TMD dimerization [52-54]. In contrast to EGFR and ErbB4, ErbB2 doesn't have a known ligand and ErbB3 lacks a functional kinase. Therefore, these receptors require trans-activation by other members of the ErbB family for kinase-activation or C-terminal tyrosine-phosphorylation [51, 55]. Their relatively high molecular similarity does provide

an opportunity to speculate about the internalization mechanisms of these other EGFR family members. In general, the internalization rates of both ErbB2 and ErbB3 are slower than that of EGFR [56]. In the absence of the trans-activation via the fully functional EGFR or ErbB4, both ErbB2 and ErbB3 are in their inactive state and their internalization is per definition kinase-independent. Most likely, inactive ErbB2 receptors reside on the membrane as monomers or perhaps predimers, similar to EGFR. This means that ErbB2 alone has no natural signal for internalization and will therefore not be internalized efficiently. Internalization studies using ErbB2/EGFR chimeric proteins and truncated ErbB2 receptors showed that removing the C-terminus of ErbB2 enhances its internalization, suggesting a potential role for the TMD in its endocytosis [57, 58, 59]. Therefore, it is reasonable to believe that internalization of inactive ErbB2 can be induced only via artificial clustering of the receptor. This hypothesis is supported by the numerous observations of clustering-induced internalization/downregulation of ErB2 [18, 60].

Internalization of ErbB3 is less well studied but was also shown to be independent of its C-terminal part [61]. Inactive ErbB3 might still be clustered upon ligand-induced conformational changes and this might drive its internalization [62]. Furthermore, antibody-induced internalization was also observed for ErbB3 [63]. Taken together, TMD-mediated clustering-induced internalization might be part of the conventional internalization mechanism of all four ErbB family members. In fact, clustering-induced internalization might even be more essential for the uptake of ErbB2 and ErbB3, as compared to EGFR, due to their lack of a natural ligand or kinase activity. In any case, this entry route of ErbB2 and ErbB3 has great potential for therapeutic nanobullets.

Clustering-induced internalization could also be used for EGFR mutants, which are often observed in tumors and relate to tumor progression [64, 65, 66]. Interestingly, the TMD and in particular the TMD dimerization motifs in many of these EGFR mutants are not mutated. One of the most common EGFR mutants is EGFR-vIII, which lacks 267 amino acids from its extracellular domain (amino acid 6-273) and is expressed in various types of glioblastoma [67-69]. Despite its constitutively active kinase, this mutant displays an impaired internalization, compared to the full length EGFR [70]. Since the TMD dimerization motifs of EGFR-vIII are intact, CIC-ME might provide a good entry mechanism for therapeutic drug delivery into EGFR-vIII expressing tumor cells.

8.2.3. The fate of EGFR upon CIC-ME

Upon internalization, EGFR is known to either recycle back to the membrane or traffic further downstream towards lysosomal degradation [71, 72]. In **Chapter 4** of this thesis, the fate of EGFR upon CIC-ME was studied in more detail by using the previously published triepitopic anti-EGFR constructs that were known to very efficiently induce sequestering of EGFR from the plasma membrane without activating the receptors kinase [73]. Similarly to the biparatopic VHHs

or its natural ligand EGF, fluorescence anisotropy imaging showed that the triepitopic constructs induced higher-order clustering of EGFR without kinase activation. The triepitopic constructs induced CIC-ME and sub-cellular trafficking towards late endosomes/lysosomes, resulting in a comparable level of degradation of EGFR as observed with EGF. This is in sharp contrast with the model proposed by Sigismund et al., stating that EGF-induced clathrin-mediated uptake of EGFR sustains signaling by mediating recycling from the early endosomes to the plasma membrane [74]. Furthermore, the authors also suggest that the non-clathrin mediated endocytosis of EGFR via the 'raft' route results in the observed ubiquitin-dependent lysosomal sorting [74, 75]. It must be noted that these hypotheses involve an activated EGFR, while in our experiments involved clustered but non-activated receptors.

In an attempt to find out which mechanism is responsible for this lysosomal sorting of EGFR upon CIC-ME, we studied the level of ubiquitination of the receptor. While ubiquitination is considered to be the main determinant for ligand-induced lysosomal trafficking of EGFR, no triepitopic-induced phosphorylation or ubiquitination of the receptor was detected. It is therefore currently unclear what actually mediates the lysosomal trafficking of EGFR upon CIC-ME. The lack of ubiquitination implies a non-essential role for ubiquitin-binding proteins like Hrs, STAM or proteins of the ESCRT complex in this process [12]. Other mediators for the formation of multiple vesicular bodies (MVB) and lysosomal sorting might be involved, such as sorting nexin family members [76, 77]. This should be determined experimentally.

Possibly, receptor clustering is by itself a signal for lysosomal targeting. Clustering-mediated trafficking is not completely uncommon in biology as some GPCRs and complexes of polymeric IgA receptor (pIgA-R) and transferrin (TfR) are known to translocate through polarized cells via oligomerization [78, 79]. The hypothesis of clustering-induced trafficking of EGFR is supported by the observation that internalized EGFR remains clustered inside endosomes after 20 min (Chapter 4, Fig. S1). Like with endocytosis, clustering of TMDs might create protein and lipid domains that drive trafficking as a result of avidity interactions between multiple low affinity interacting proteins. For example, such interactions may involve the two dileucine motifs in EGFR (LL-679/680 and LL-1010/1011), which are known to be involved in EGFR degradation [80, 81]. Similarly to the model in which concave, inward membrane curvature N-terminally linked TMDs initiate endocytosis, clustering of C-terminally linked TMDs could potentially induce convex, outward curvature that would allow the formation of intralumenal vesicles (ILVs) in MVBs. The possible existence of C-terminally linked TMD dimers was supported by a high probability in a docking experiment with EGFR TMD models (Fig. 1D) and by recently published simulation data [30]. However, so far, this hypothesis is opposed by our observation that mutation of the C-terminal TMD dimerization motif did not significantly affect antibody-induced degradation of EGFR (Chapter 4). The role of clustering in MVB formation should be studied in more detail.

In addition, it would be of general interest to determine a biological function for the C-terminal TMD dimerization motif. In particular, the role of this motif in the formation of MVBs and the related exosomes might be interesting for future research.

8.3. Employing CIC-ME for cancer therapy

Our observation that CIC-ME results in lysosomal degradation of EGFR has clear therapeutic potential. CIC-ME could reduce the overexpression of all members of the ErbB family of receptors in different types of tumors. Moreover, this approach has the potential to downregulate the expression of EGFR mutants like the EGFR-vIII. This constitutively active mutant is internalized slower than EGFR and is subsequently recycled back to the plasma membrane, rather than being sorted for lysosomal degradation [70]. In that respect, CIC-ME might actually be employed to selectively downregulate the surface expression of EGFR mutants like EGFR-vIII. Moreover, if clustering-induced downregulation is a more general phenomenon for membrane proteins, it could potentially be used to downregulate all receptors with comparable TMD-GG4 motifs. Besides stimulating receptor degradation of different types of receptors, CIC-ME can facilitate the targeted intracellular delivery and lysosomal release of anti-cancer drugs. This approach increases the therapeutic efficacy and reduces off-target cytotoxicity in healthy tissues. Well known examples of such carriers include targeted liposomes, polymeric nanoparticles and micelles and albumin-based nanoparticles, but also monoclonal antibodies or antibody-related fragments (see also Chapter 2) [82, 83].

8.3.1. Intracellular delivery via tumor targeted nanobody-decorated nanoparticles

In **Chapter 5** and **6**, receptor-mediated internalization was employed by glutaraldehyde crosslinked albumin nanoparticles to facilitate the intracellular delivery and release of therapeutic molecules. Similar albumin nanoparticles have previously been functionalized by decorating them with monoclonal antibodies or other targeting ligands [84-88]. In Chapter 5, the nanoparticles were surface-coated with polyethylene glycol 3500 (PEG) and an anti-EGFR nanobody (EGa1), creating the so-called nanobody-albumin nanoparticles (NANAPs). The targeted nanoparticles showed a 40-fold higher binding to EGFR-positive 14C cells compared to PEGylated nanoparticles and were internalized by clathrin-mediated endocytosis and ultimately digested in lysosomes. This clathrin-mediated uptake and lysosomal sorting of the NANAPs is comparable to the CIC-ME and subsequent lysosomal sorting of EGFR induced by biparatopic VHHs and the triepitopic antibody constructs. This might suggest that the multivalency of the anti-EGFR NANAPs induce similar internalization and subcellular sorting via clustering of EGFR.

As a therapeutic molecule, the multikinase inhibitor 17864 was chosen. This is structurally closely related to sunitinib and targets several growth-factor signaling pathways like

PDGFR and c-Kit by inhibiting ATP binding [89]. In order to achieve specific release of the cargo inside those EGFR-expressing cells, 17864 was conjugated to the albumin particles via an L_x-linker (also known as the universal linker system (ULS)) [90, 91]. This platinum-based linker forms an interaction between pyridyl moieties of 17864 and methionine or cysteine residues of the albumin particles. This interaction dissociates in low pH and thiol environments like endosomal compartments including lysosomes. Our data showed that the intracellular routing of the targeted nanoparticles indeed facilitated the release of 17864-L_x, which consequently resulted in a more pronounced inhibition of proliferation.

In **Chapter 6**, a similar approach was used with nanoparticles directed against Met-expressing tumor cells. Met overexpression is correlated with aggressive cancers, such as brain, liver, pancreatic cancers and gastric carcinoma [92-94]. Originally, anti-Met immunotherapy focused on blocking Met activation by sequestering HGF or by competitive binding to the ligand-binding spots on Met ectodomain [95, 96]. However, since highly Met-overexpressing tumors display constitutive activation of the receptor, ligand blocking is often ineffictive [94, 97]. In that case, prevention of dimerization or complete removal of Met from the plasma membrane is more effective [98-101]. By using anti-Met NANAPs, we aimed to internalize, sequester and downregulate Met in tumor cells. Furthermore, the anti-Met NANAPs would provide a good biomaterial for the intracellular delivery of therapeutic compounds.

Recently, Lu *et al*. reported the use of anti-Met single chain antibodies for targeting of quantum dots or doxorubicin loaded liposomes [88]. Nanobodies have several advantages with respect to single chain antibodies, which include high binding affinity, stability and relatively easy production [9]. In our study, anti-Met VHHs were selected by phage display and these were SATA modified like previously done with the EGFR VHH [102, 103]. The binding affinity of the selected VHHs was 10 fold higher than the reported scFv's and this was unaffected by SATA modification. The constructed NANAPs bound and internalized specifically in Met-expressing cells. The nanoparticles also activated Met, but whether this contributed to Met receptor internalization is currently unknown. Possibly, internalization is also induced by clustering and a similar mechanism as CIC-ME is involved. Subsequently, the G2-PEG-NPs were targeted to the lysosomes where they were degraded. This internalization and subcellular routing provides a good basis for intracellular drug release via reversible linkers like the platinum-based L_x-linker that was described above. The lysosomal trafficking and degradation of the nanoparticles was also accompanied by downregulation of total Met protein, which could potentially contribute to the inhibition of tumor growth as previously demonstrated with EGFR [102]. Similarly, Met downregulation via antibody-induced shedding followed by proteasomal degradation was already shown to reduce tumor size [99]. An indication for such an intrinsic anti-tumor activity of the G2-PEG-NPs was observed in the *in vitro* scratch wound assay, where they partially inhibit wound

healing in A549 cells. However, the therapeutic efficacy of the anti-Met NANAPs should be improved, for example by reversibly conjugating them to inhibitors or toxic molecules.

8.3.2. Photodynamic therapy is improved by intracellular delivery of photosensitizer

The relatively large size of albumin particles provides an enormous loading capacity for therapeutic molecules, but it also seriously hampers their tumor penetration and thereby their efficacy [104, 105]. As observed with similar nanoparticles, there is a high chance that *in vivo*, the large particles are cleared from the blood very rapidly and accumulate in the lungs and the liver [106, 107]. In contrast, VHHs like the biparatopic ones that induce CIC-ME offer less conjugation sites, but do display a rapid tumor accumulation and distribution ([108] and Oliveria et al., manuscript in preparation).

Since a VHH only has on average only a few sites for conjugation of a therapeutic molecule, this molecule needs to be very potent. In order to facilitate a tumor-specific cytotoxic effect instead of a cytostatic one, a toxic compound should be used instead of a specific kinase inhibitor. A good example of such an approach is found in photodynamic therapy (PDT). Depending on the type of photosensitizers (PS), excitation of a PS either results in a local raise in temperature (photothermal) or in the generation of the very toxic singlet oxygen ($^1O_2$) (photodynamic), which lethally damages cells [109]. Site-specific cytotoxicity is generally induced by local illumination of the PS. Although PDT a considered to be a very potent anti-tumor strategy, it is traditionally accompanied by many side effects like off-target cytotoxicity due to high hydrophobicity of the photosensitizer and a lack of tumor targeting [110]. Recently, more hydrophilic types of PS have been developed and were conjugated to targeting ligands like antibodies or antibody fragments [111, 112, 113]. More importantly, intracellular delivery of PS was shown to improve the efficacy of PDT even further. In **Chapter 7**, nanobodies and in particular internalizing biparatopic VHHs were used to target photosensitizers to and into EGFR-positive tumor cells.

The PS used in this study, the previously published IRDye700DX, is considered to be relatively hydrophilic compared to the parental phthalocyanines [114]. When excited with low light intensity, this PS emits near infra-red fluorescent light, which enables the visualization of the tumor localization *in vivo*. Labeling of the nanobodies with 1 to 1.5 molecules of IRDye700DX per nanobody did not affect their binding affinities. Also, cellular association and toxicity correlated well with the EGFR expression levels in different cell lines. In general, PDT-induced cytotoxicity can be improved by conjugating more PS to a nanobody. However, one should be careful with this, since this also harms the binding capacity of the nanobody, increases the hydrophobicity of the conjugate and might even result in quenching of the PS-fluorophores as a result of FRET [115].

In correlation to the study described in Chapter 3, the biparatopic VHH-PS conjugates mediated intracellular delivery of the PS and this enhanced the potency of the PDT. The mechanism behind this enhanced cytotoxicity upon internalization is currently unclear, but

this might involve the destruction of more vital structures or organelles in the cell via either a photodynamic or photothermal mode of action. The internalizing biparatopic VHH-PS conjugate eventually trafficked to the lysosomes, in which both VHH and receptor were degraded. This process is comparable to the natural negative feedback mechanism of activated EGFR and is in agreement with the results obtained with the triepitopic antibody constructs in Chapter 4 and the anti-EGFR NANAPs in Chapter 5 [71]. This subcellular trafficking of biparatopic VHHs upon CIC-ME is likely to ensure longer *in vivo* tumor retention. However, it might also result in leakage and clearance of free therapeutic compounds. Nevertheless, since IRDye700DX residualizes inside cells, it is expected to be retained in the tumor upon degradation of the targeting ligand, where it could function for PDT. This tumor retention and the effect of the endosomal environment, like low pH, on the quantum yield of the PS are currently being investigated in an *in vivo* study.

8.4. Summarizing conclusions

Taken together, the work in this thesis has lead to the following conclusions:

- Higher order clustering of EGFR results in kinase-independent, clustering-induced clathrin-mediated endocytosis, which is abbreviated as CIC-ME.
- CIC-ME of EGFR requires the N-terminal TMD dimerization motif and leads to ubiquitin-independent lysosomal degradation of both receptor and cargo.
- Receptor-mediated endocytosis and subsequent lysosomal degradation by nanobody-albumin nanoparticles (NANAPS) facilitate intracellular delivery and release of therapeutic molecules in tumor cells.
- Nanobodies are suitable and promising targeting ligands for photosensitizers in photodynamic therapy of cancer.
- The efficacy of photodynamic therapy is improved by intracellular delivery of the photosensitizer via CIC-ME.

8.5. References

1. Scott, A. M., Wolchok, J. D. & Old, L. J. Antibody therapy of cancer *Nat. Rev. Cancer.* **12**, 278-287 (2012).
2. Elbakri, A., Nelson, P. N. & Abu Odeh, R. O. The state of antibody therapy *Hum. Immunol.* **71**, 1243-1250 (2010).
3. Ferraro, D. A. *et al*. Inhibition of triple-negative breast cancer models by combinations of antibodies to EGFR *Proc. Natl. Acad. Sci. U. S. A.* **110**, 1815-1820 (2013).
4. Nieder, C., Pawinski, A., Dalhaug, A. & Andratschke, N. A review of clinical trials of cetuximab combined with radiotherapy for non-small cell lung cancer *Radiat. Oncol.* **7**, 3-717X-7-3 (2012).
5. Iyer, U. & Kadambi, V. J. Antibody drug conjugates - Trojan horses in the war on cancer *J. Pharmacol. Toxicol. Methods* **64**, 207-212 (2011).
6. Altintas, I., Kok, R. J. & Schiffelers, R. M. Targeting epidermal growth factor receptor in tumors: from conventional monoclonal antibodies via heavy chain-only antibodies to nanobodies *Eur. J. Pharm. Sci.* **45**, 399-407 (2012).
7. Roovers, R. C., van Dongen, G. A. & van Bergen en Henegouwen, P. M. Nanobodies in therapeutic applications. *Curr. Opin. Mol. Ther.* **9**, 327-335 (2007).
8. Revets, H., De Baetselier, P. & Muyldermans, S. Nanobodies as novel agents for cancer therapy. *Expert Opin. Biol. Ther.* **5**, 111-124 (2005).
9. Harmsen, M. M. & De Haard, H. J. Properties, production, and applications of camelid single-domain antibody fragments. *Appl. Microbiol. Biotechnol.* **77**, 13-22 (2007).
10. Roovers, R. C. *et al*. A bi-paratopic anti-EGFR nanobody efficiently inhibits solid tumour growth. *Int. J. Cancer* (2011).
11. Kawakami, K., Nakajima, O., Morishita, R. & Nagai, R. Targeted anticancer immunotoxins and cytotoxic agents with direct killing moieties *ScientificWorldJournal* **6**, 781-790 (2006).
12. Sorkin, A. & Goh, L. K. Endocytosis and intracellular trafficking of ErbBs. *Exp. Cell Res.* **314**, 3093-3106 (2008).
13. Goh, L. K., Huang, F., Kim, W., Gygi, S. & Sorkin, A. Multiple mechanisms collectively regulate clathrin-mediated endocytosis of the epidermal growth factor receptor. *J. Cell Biol.* **189**, 871-883 (2010).
14. Saffarian, S., Li, Y., Elson, E. L. & Pike, L. J. Oligomerization of the EGF receptor investigated by live cell fluorescence intensity distribution analysis *Biophys. J.* **93**, 1021-1031 (2007).
15. Clayton, A. H., Tavarnesi, M. L. & Johns, T. G. Unligated epidermal growth factor receptor forms higher order oligomers within microclusters on A431 cells that are sensitive to tyrosine kinase inhibitor binding *Biochemistry* **46**, 4589-4597 (2007).
16. Hofman, E. G. *et al*. Ligand-induced EGF receptor oligomerization is kinase-dependent and enhances internalization. *J. Biol. Chem.* **285**, 39481-39489 (2010).
17. Clayton, A. H., Orchard, S. G., Nice, E. C., Posner, R. G. & Burgess, A. W. Predominance of activated EGFR higher-order oligomers on the cell surface *Growth Factors* **26**, 316-324 (2008).
18. Friedman, L. M. *et al*. Synergistic down-regulation of receptor tyrosine kinases by combinations of mAbs: implications for cancer immunotherapy. *Proc. Natl. Acad. Sci. U. S. A.* **102**, 1915-1920 (2005).
19. Spangler, J. B. *et al*. Combination antibody treatment down-regulates epidermal growth factor receptor by inhibiting endosomal recycling. *Proc. Natl. Acad. Sci. U. S. A.* **107**, 13252-13257 (2010).
20. Pedersen, M. W. *et al*. Sym004: a novel synergistic anti-epidermal growth factor receptor antibody mixture with superior anticancer efficacy. *Cancer Res.* **70**, 588-597 (2010).
21. Koefoed, K. *et al*. Rational identification of an optimal antibody mixture for targeting the epidermal growth factor receptor *MAbs* **3**, 584-595 (2011).
22. van Belzen, N. *et al*. Direct visualization and quantitative analysis of epidermal growth factor-induced receptor clustering *J. Cell. Physiol.* **134**, 413-420 (1988).
23. Moriki, T., Maruyama, H. & Maruyama, I. N. Activation of preformed EGF receptor dimers by ligand-induced rotation of the transmembrane domain *J. Mol. Biol.* **311**, 1011-1026 (2001).
24. Yu, X., Sharma, K. D., Takahashi, T., Iwamoto, R. & Mekada, E. Ligand-independent dimer formation of epidermal growth factor receptor (EGFR) is a step separable from ligand-induced EGFR signaling *Mol. Biol. Cell* **13**, 2547-2557 (2002).

25. Bader, A. N., Hofman, E. G., van Bergen En Henegouwen, P. M. & Gerritsen, H. C. Imaging of protein cluster sizes by means of confocal time-gated fluorescence anisotropy microscopy. *Opt. Express* **15**, 6934-6945 (2007).
26. Ghosh, S., Saha, S., Goswami, D., Bilgrami, S. & Mayor, S. Dynamic imaging of homo-FRET in live cells by fluorescence anisotropy microscopy *Methods Enzymol.* **505**, 291-327 (2012).
27. Bader, A. N., Hofman, E. G., Voortman, J., en Henegouwen, P. M. & Gerritsen, H. C. Homo-FRET imaging enables quantification of protein cluster sizes with subcellular resolution *Biophys. J.* **97**, 2613-2622 (2009).
28. Liu, A. P., Aguet, F., Danuser, G. & Schmid, S. L. Local clustering of transferrin receptors promotes clathrin-coated pit initiation *J. Cell Biol.* **191**, 1381-1393 (2010).
29. Berger, C., Madshus, I. H. & Stang, E. Cetuximab in combination with anti-human IgG antibodies efficiently down-regulates the EGF receptor by macropinocytosis *Exp. Cell Res.* **318**, 2578-2591 (2012).
30. Arkhipov, A. *et al*. Architecture and membrane interactions of the EGF receptor *Cell* **152**, 557-569 (2013).
31. Cymer, F. & Schneider, D. Transmembrane helix-helix interactions involved in ErbB receptor signaling *Cell. Adh Migr.* **4**, 299-312 (2010).
32. Burke, C. L., Lemmon, M. A., Coren, B. A., Engelman, D. M. & Stern, D. F. Dimerization of the p185neu transmembrane domain is necessary but not sufficient for transformation *Oncogene* **14**, 687-696 (1997).
33. Lu, C. *et al*. Structural evidence for loose linkage between ligand binding and kinase activation in the epidermal growth factor receptor *Mol. Cell. Biol.* **30**, 5432-5443 (2010).
34. Mineev, K. S. *et al*. Spatial structure of the transmembrane domain heterodimer of ErbB1 and ErbB2 receptor tyrosine kinases *J. Mol. Biol.* **400**, 231-243 (2010).
35. Horvath, C. A., Vanden Broeck, D., Boulet, G. A., Bogers, J. & De Wolf, M. J. Epsin: inducing membrane curvature *Int. J. Biochem. Cell Biol.* **39**, 1765-1770 (2007).
36. Ford, M. G. *et al*. Curvature of clathrin-coated pits driven by epsin *Nature* **419**, 361-366 (2002).
37. Itoh, T. & De Camilli, P. BAR, F-BAR (EFC) and ENTH/ANTH domains in the regulation of membrane-cytosol interfaces and membrane curvature *Biochim. Biophys. Acta* **1761**, 897-912 (2006).
38. Gallop, J. L. & McMahon, H. T. BAR domains and membrane curvature: bringing your curves to the BAR *Biochem. Soc. Symp.* **(72)**, 223-231 (2005).
39. Henne, W. M. *et al*. FCHo proteins are nucleators of clathrin-mediated endocytosis. *Science* **328**, 1281-1284 (2010).
40. Scott, M. G., Benmerah, A., Muntaner, O. & Marullo, S. Recruitment of activated G protein-coupled receptors to pre-existing clathrin-coated pits in living cells *J. Biol. Chem.* **277**, 3552-3559 (2002).
41. Heuser, J. E., Keen, J. H., Amende, L. M., Lippoldt, R. E. & Prasad, K. Deep-etch visualization of 27S clathrin: a tetrahedral tetramer *J. Cell Biol.* **105**, 1999-2009 (1987).
42. den Otter, W. K. & Briels, W. J. The generation of curved clathrin coats from flat plaques *Traffic* **12**, 1407-1416 (2011).
43. Martin, T. F. PI(4,5)P(2) regulation of surface membrane traffic *Curr. Opin. Cell Biol.* **13**, 493-499 (2001).
44. Gaidarov, I., Chen, Q., Falck, J. R., Reddy, K. K. & Keen, J. H. A functional phosphatidylinositol 3,4,5-trisphosphate/phosphoinositide binding domain in the clathrin adaptor AP-2 alpha subunit. Implications for the endocytic pathway. *J. Biol. Chem.* **271**, 20922-20929 (1996).
45. Salim, K. *et al*. Distinct specificity in the recognition of phosphoinositides by the pleckstrin homology domains of dynamin and Bruton's tyrosine kinase. *EMBO J.* **15**, 6241-6250 (1996).
46. Naslavsky, N., Rahajeng, J., Chenavas, S., Sorgen, P. L. & Caplan, S. EHD1 and Eps15 interact with phosphatidylinositols via their Eps15 homology domains. *J. Biol. Chem.* **282**, 16612-16622 (2007).
47. Hofman, E. G. *et al*. EGF induces coalescence of different lipid rafts. *J. Cell. Sci.* **121**, 2519-2528 (2008).
48. Hofman, E. G., Bader, A. N., Gerritsen, H. C. & van Bergen En Henegouwen, P. M. EGF induces rapid reorganization of plasma membrane microdomains. *Commun. Integr. Biol.* **2**, 213-214 (2009).
49. Pike, L. J. Growth factor receptors, lipid rafts and caveolae: an evolving story *Biochim. Biophys. Acta* **1746**, 260-273 (2005).
50. Hsieh, A. C. & Moasser, M. M. Targeting

HER proteins in cancer therapy and the role of the non-target HER3 *Br. J. Cancer* **97**, 453-457 (2007).
51. Yarden, Y. & Pines, G. The ERBB network: at last, cancer therapy meets systems biology *Nat. Rev. Cancer.* **12**, 553-563 (2012).
52. Sternberg, M. J. & Gullick, W. J. A sequence motif in the transmembrane region of growth factor receptors with tyrosine kinase activity mediates dimerization *Protein Eng.* **3**, 245-248 (1990).
53. Mendrola, J. M., Berger, M. B., King, M. C. & Lemmon, M. A. The single transmembrane domains of ErbB receptors self-associate in cell membranes *J. Biol. Chem.* **277**, 4704-4712 (2002).
54. Russ, W. P. & Engelman, D. M. The GxxxG motif: a framework for transmembrane helix-helix association *J. Mol. Biol.* **296**, 911-919 (2000).
55. Earp, H. S., Dawson, T. L., Li, X. & Yu, H. Heterodimerization and functional interaction between EGF receptor family members: a new signaling paradigm with implications for breast cancer research *Breast Cancer Res. Treat.* **35**, 115-132 (1995).
56. Baulida, J., Kraus, M. H., Alimandi, M., Di Fiore, P. P. & Carpenter, G. All ErbB receptors other than the epidermal growth factor receptor are endocytosis impaired *J. Biol. Chem.* **271**, 5251-5257 (1996).
57. Sorkin, A., Di Fiore, P. P. & Carpenter, G. The carboxyl terminus of epidermal growth factor receptor/erbB-2 chimerae is internalization impaired *Oncogene* **8**, 3021-3028 (1993).
58. Tikhomirov, O. & Carpenter, G. Geldanamycin induces ErbB-2 degradation by proteolytic fragmentation *J. Biol. Chem.* **275**, 26625-26631 (2000).
59. Lerdrup, M. *et al*. Endocytic down-regulation of ErbB2 is stimulated by cleavage of its C-terminus *Mol. Biol. Cell* **18**, 3656-3666 (2007).
60. Wartlick, H. *et al*. Highly specific HER2-mediated cellular uptake of antibody-modified nanoparticles in tumour cells *J. Drug Target.* **12**, 461-471 (2004).
61. Waterman, H., Sabanai, I., Geiger, B. & Yarden, Y. Alternative intracellular routing of ErbB receptors may determine signaling potency *J. Biol. Chem.* **273**, 13819-13827 (1998).
62. Cho, H. S. & Leahy, D. J. Structure of the extracellular region of HER3 reveals an interdomain tether *Science* **297**, 1330-1333 (2002).
63. Belleudi, F. *et al*. Monoclonal antibody-induced ErbB3 receptor internalization and degradation inhibits growth and migration of human melanoma cells *Cell. Cycle* **11**, 1455-1467 (2012).
64. Voldborg, B. R., Damstrup, L., Spang-Thomsen, M. & Poulsen, H. S. Epidermal growth factor receptor (EGFR) and EGFR mutations, function and possible role in clinical trials *Ann. Oncol.* **8**, 1197-1206 (1997).
65. Yeang, C. H., McCormick, F. & Levine, A. Combinatorial patterns of somatic gene mutations in cancer *FASEB J.* **22**, 2605-2622 (2008).
66. Cancer Genome Atlas Network. Comprehensive molecular portraits of human breast tumours *Nature* **490**, 61-70 (2012).
67. Pedersen, M. W., Meltorn, M., Damstrup, L. & Poulsen, H. S. The type III epidermal growth factor receptor mutation. Biological significance and potential target for anti-cancer therapy *Ann. Oncol.* **12**, 745-760 (2001).
68. Gan, H. K., Burgess, A. W., Clayton, A. H. & Scott, A. M. Targeting of a conformationally exposed, tumor-specific epitope of EGFR as a strategy for cancer therapy *Cancer Res.* **72**, 2924-2930 (2012).
69. Kuan, C. T., Wikstrand, C. J. & Bigner, D. D. EGF mutant receptor vIII as a molecular target in cancer therapy *Endocr. Relat. Cancer* **8**, 83-96 (2001).
70. Grandal, M. V. *et al*. EGFRvIII escapes down-regulation due to impaired internalization and sorting to lysosomes *Carcinogenesis* **28**, 1408-1417 (2007).
71. Sorkin, A. & Goh, L. K. Endocytosis and intracellular trafficking of ErbBs. *Exp. Cell Res.* **315**, 683-696 (2009).
72. Wiley, H. S. Trafficking of the ErbB receptors and its influence on signaling. *Exp. Cell Res.* **284**, 78-88 (2003).
73. Spangler, J. B., Manzari, M. T., Rosalia, E. K., Chen, T. F. & Wittrup, K. D. Triepitopic antibody fusions inhibit cetuximab-resistant BRAF and KRAS mutant tumors via EGFR signal repression *J. Mol. Biol.* **422**, 532-544 (2012).
74. Sigismund, S. *et al*. Clathrin-mediated internalization is essential for sustained EGFR signaling but dispensable for degradation. *Dev. Cell.* **15**, 209-219 (2008).

75. Sigismund, S. *et al*. Threshold-controlled ubiquitination of the EGFR directs receptor fate *EMBO J.* **32**, 2140-2157 (2013).
76. Kurten, R. C., Cadena, D. L. & Gill, G. N. Enhanced degradation of EGF receptors by a sorting nexin, SNX1 *Science* **272**, 1008-1010 (1996).
77. Gullapalli, A. *et al*. A role for sorting nexin 2 in epidermal growth factor receptor down-regulation: evidence for distinct functions of sorting nexin 1 and 2 in protein trafficking *Mol. Biol. Cell* **15**, 2143-2155 (2004).
78. Wallrabe, H., Bonamy, G., Periasamy, A. & Barroso, M. Receptor complexes cotransported via polarized endocytic pathways form clusters with distinct organizations *Mol. Biol. Cell* **18**, 2226-2243 (2007).
79. Canals, M., Lopez-Gimenez, J. F. & Milligan, G. Cell surface delivery and structural re-organization by pharmacological chaperones of an oligomerization-defective alpha(1b)-adrenoceptor mutant demonstrates membrane targeting of GPCR oligomers *Biochem. J.* **417**, 161-172 (2009).
80. Huang, F., Jiang, X. & Sorkin, A. Tyrosine phosphorylation of the beta2 subunit of clathrin adaptor complex AP-2 reveals the role of a di-leucine motif in the epidermal growth factor receptor trafficking. *J. Biol. Chem.* **278**, 43411-43417 (2003).
81. Tsacoumangos, A., Kil, S. J., Ma, L., Sonnichsen, F. D. & Carlin, C. A novel dileucine lysosomal-sorting-signal mediates intracellular EGF-receptor retention independently of protein ubiquitylation *J. Cell. Sci.* **118**, 3959-3971 (2005).
82. Duncan, R. & Gaspar, R. Nanomedicine(s) under the microscope *Mol. Pharm.* **8**, 2101-2141 (2011).
83. Zamboni, W. C. *et al*. Best practices in cancer nanotechnology: perspective from NCI nanotechnology alliance *Clin. Cancer Res.* **18**, 3229-3241 (2012).
84. Bae, S. *et al*. Doxorubicin-loaded human serum albumin nanoparticles surface-modified with TNF-related apoptosis-inducing ligand and transferrin for targeting multiple tumor types *Biomaterials* **33**, 1536-1546 (2012).
85. Bunschoten, A. *et al*. Targeted non-covalent self-assembled nanoparticles based on human serum albumin *Biomaterials* **33**, 867-875 (2012).
86. Kratz, F. Albumin as a drug carrier: design of prodrugs, drug conjugates and nanoparticles *J. Control. Release* **132**, 171-183 (2008).
87. Low, K., Wacker, M., Wagner, S., Langer, K. & von Briesen, H. Targeted human serum albumin nanoparticles for specific uptake in EGFR-Expressing colon carcinoma cells *Nanomedicine* **7**, 454-463 (2011).
88. Lu, R. M., Chang, Y. L., Chen, M. S. & Wu, H. C. Single chain anti-c-Met antibody conjugated nanoparticles for in vivo tumor-targeted imaging and drug delivery *Biomaterials* **32**, 3265-3274 (2011).
89. Harmsen, S. *et al*. Development of a cell-selective and intrinsically active multikinase inhibitor bioconjugate *Bioconjug. Chem.* **22**, 540-545 (2011).
90. Temming, K., Fretz, M. M. & Kok, R. J. Organ- and cell-type specific delivery of kinase inhibitors: a novel approach in the development of targeted drugs *Curr. Mol. Pharmacol.* **1**, 1-12 (2008).
91. Dolman, M. E. *et al*. Targeting of a platinum-bound sunitinib analog to renal proximal tubular cells *Int. J. Nanomedicine* **7**, 417-433 (2012).
92. Corso, S., Comoglio, P. M. & Giordano, S. Cancer therapy: can the challenge be MET? *Trends Mol. Med.* **11**, 284-292 (2005).
93. Knudsen, B. S. & Vande Woude, G. Showering c-MET-dependent cancers with drugs *Curr. Opin. Genet. Dev.* **18**, 87-96 (2008).
94. Mitra, A. K. *et al*. Ligand-independent activation of c-Met by fibronectin and alpha(5) beta(1)-integrin regulates ovarian cancer invasion and metastasis *Oncogene* **30**, 1566-1576 (2011).
95. Toschi, L. & Janne, P. A. Single-agent and combination therapeutic strategies to inhibit hepatocyte growth factor/MET signaling in cancer *Clin. Cancer Res.* **14**, 5941-5946 (2008).
96. Martens, T. *et al*. A novel one-armed anti-c-Met antibody inhibits glioblastoma growth in vivo *Clin. Cancer Res.* **12**, 6144-6152 (2006).
97. Nakamura, Y. *et al*. Constitutive activation of c-Met is correlated with c-Met overexpression and dependent on cell-matrix adhesion in lung adenocarcinoma cell lines *Cancer. Sci.* **99**, 14-22 (2008).
98. Hammond, D. E., Urbe, S., Vande Woude, G. F. & Clague, M. J. Down-regulation of MET, the receptor for hepatocyte growth factor *Oncogene* **20**, 2761-2770 (2001).
99. Petrelli, A. *et al*. Ab-induced ectodomain shedding mediates hepatocyte growth factor

receptor down-regulation and hampers biological activity *Proc. Natl. Acad. Sci. U. S. A.* **103**, 5090-5095 (2006).
100. Lefebvre, J. *et al*. Met degradation: more than one stone to shoot a receptor down *FASEB J.* **26**, 1387-1399 (2012).
101. Greenall, S. A. *et al*. Non-agonistic bivalent antibodies that promote c-MET degradation and inhibit tumor growth and others specific for tumor related c-MET *PLoS One* **7**, e34658 (2012).
102. Oliveira, S. *et al*. Downregulation of EGFR by a novel multivalent nanobody-liposome platform. *J. Control. Release* **145**, 165-175 (2010).
103. van der Meel, R. *et al*. Tumor-targeted Nanobullets: Anti-EGFR nanobody-liposomes loaded with anti-IGF-1R kinase inhibitor for cancer treatment *J. Control. Release* **159**, 281-289 (2012).
104. Wittrup, K. D., Thurber, G. M., Schmidt, M. M. & Rhoden, J. J. Practical theoretic guidance for the design of tumor-targeting agents *Methods Enzymol.* **503**, 255-268 (2012).
105. Schmidt, M. M. & Wittrup, K. D. A modeling analysis of the effects of molecular size and binding affinity on tumor targeting *Mol. Cancer. Ther.* **8**, 2861-2871 (2009).
106. Polyak, A. *et al*. In vitro and biodistribution examinations of Tc-99m-labelled doxorubicin-loaded nanoparticles *Nucl. Med. Rev. Cent. East. Eur.* **14**, 55-62 (2011).
107. Ilium, L. *et al*. Blood clearance and organ deposition of intravenously administered colloidal particles. The effects of particle size, nature and shape *Int. J. Pharm.* **12**, 135-146 (1982).
108. Oliveira, S. *et al*. Rapid visualization of human tumor xenografts through optical imaging with a near-infrared fluorescent anti-epidermal growth factor receptor nanobody *Mol. Imaging* **11**, 33-46 (2012).
109. Celli, J. P. *et al*. Imaging and photodynamic therapy: mechanisms, monitoring, and optimization *Chem. Rev.* **110**, 2795-2838 (2010).
110. Ackroyd, R., Kelty, C., Brown, N. & Reed, M. The history of photodetection and photodynamic therapy *Photochem. Photobiol.* **74**, 656-669 (2001).
111. van Dongen, G. A., Visser, G. W. & Vrouenraets, M. B. Photosensitizer-antibody conjugates for detection and therapy of cancer *Adv. Drug Deliv. Rev.* **56**, 31-52 (2004).
112. Sharman, W. M., van Lier, J. E. & Allen, C. M. Targeted photodynamic therapy via receptor mediated delivery systems *Adv. Drug Deliv. Rev.* **56**, 53-76 (2004).
113. Vrouenraets, M. B. *et al*. Targeting of aluminum (III) phthalocyanine tetrasulfonate by use of internalizing monoclonal antibodies: improved efficacy in photodynamic therapy *Cancer Res.* **61**, 1970-1975 (2001).
114. Mitsunaga, M. *et al*. Cancer cell-selective in vivo near infrared photoimmunotherapy targeting specific membrane molecules *Nat. Med.* **17**, 1685-1691 (2011).
115. Petrasek, Z. & Phillips, D. A time-resolved study of concentration quenching of disulfonated aluminium phthalocyanine fluorescence *Photochem. Photobiol. Sci.* **2**, 236-244 (2003).

List of abbreviations

List of abbreviations

ADC	Antibody drug conjugates
ADCC	Antibody-dependent cellular cytotoxicity
ADCP	Antibody-dependent cellular phagocytosis
AP2	Adaptor protein complex 2
BAR	Bin Amphiphysin Rvs
Bipar	Biparatopic VHH
CDC	Complement-dependent cytotoxicity
CDR	Complementarity-determining region
CEA	Carcinoembriogenic antigen
CH	Constant domain of the heavy chain
CHC	Clathrin heavy chain
CIC-ME	Clustering-induced, clathrin-mediated endocytosis
CIE	Clathrin-independent endocytosis
CME	Clathrin-mediated endocytosis
CTB	Cholera toxin B
DARPin	Designed ankyrin repeat protein
DLS	Dynamic light scattering
DMEM	Dulbecco's modified eagle's medium
EGF	Epidermal growth factor
EGFR	Epidermal growth factor receptor
ELISA	Enzyme-linked immunosorbent assay
Eps15	Epidermal growth factor receptor pathway substrate 15
ErbB	Erythroblastosis oncogene B
ERK	Extracellular signal-regulated kinase
ESCRT	Endosomal sorting complexes required for transport
Fab	Antigen-binding fragment
FACS	Fluorescence activated cell sorter
Fc	Fragment crystallizable region
FCHo	Fer/Cip4 homology domain-only
FCS	Fetal calf serum
FDA	Food and drug administration
FGFR	Fibroblast growth factor receptor
FKBP	FK506-binding protein
FLIM	Fluorescence lifetime imaging microscopy

FRET	Fluorescence resonance energy transfer
Fv	Variable fragment
GFP	Green fluorescent protein
GPCR	G-protein coupled receptor
GUV	Giant unilamellar vesicle
HcAb	Heavy chain antibody
HGF	Hepatocyte growth factor
HGFR	Hepatocyte growth factor receptor (Met)
HSA	Human serum albumin
ILV	Intralumenal vesicles
IRDye	Infrared dye
mAb	Monoclonal antibody
MAPK	Mitogen-activated protein kinase
mGFP	Monomeric green fluorescent protein
MVB	Multiple vesicular body
NANAP	Nanobody-albumin nanoparticle
NFκB	Nuclear factor kappa-light-chain-enhance of activated B-cells
NP	Nanoparticle
NR	Non-relevant
PB	Phosphate buffer
PDT	Photodynamic therapy
PE38	Pseudomonas exotoxin A, truncated, 38 kDa
PEG	Polyethylene glycol
PET	Positron emission tomography
PFA	Paraformaldehyde
PI3K	Phosphoinositide 3 kinase
PIP2	Phosphatidylinositol 4,5-biphosphate
PKB	Protein kinase B
PLC	Phospholipase C
PS	Photosensitizer
RTK	Receptor tyrosine kinase
scFv	Single chain variable fragment
sdAb	Single domain antibody
SEM	Standard error of the mean
siRNA	Small interfering RNA
SPECT	Single-photon emission computed tomography

STAT	Signal transducer and activator of transcription
TEM	Transmission electron microscopy
TfR	Transferrin receptor
TIRF-M	Total internal reflection fluorescence microscopy
TK	Tyrosine kinase
TMD	Transmembrane domain
Trf	Transferrin
VEGF	Vascular endothelial growth factor
VEGFR	Vascular endothelial growth factor receptor
VH	Variable domain of the heavy-chain
VHH	Variable domain of the heavy-chain from a heavy chain-only antibody

English summary

English summary

Cancer is characterized by uncontrolled growth or proliferation of cells. Cancer cells have acquired self-sufficiency in growth signalling and/or unlimited replication. Besides surgery or chemo- or radiation therapy, cancer therapies can focus on targeting specific tumor-related molecules. Examples of targeted therapies include small molecule inhibitors, small interfering RNAs (siRNA) and immunotherapy, the latter of which involves the use of antibodies that either activate the immune system or block tumor-related signalling cascades. Unfortunately, antibody treatments are often not sufficient to remove a tumor completely and more aggressive measures are welcome. A way to improve the specific anti-tumor activity is using so-called antibody-drug conjugates (ADC). Combining the tumor-specificity of an antibody with the cytotoxicity of a therapeutic agent enhances the potency of the antibody and reduces the off-target toxicity of chemotherapy.

For optimal tumor targeting and penetration, specificity, binding affinity and size of the targeting ligand matter. In that respect, conventional antibodies are relatively large and therefore display poor tumor penetration/distribution. This is why several types of smaller antibody fragments or scaffold proteins have been developed in the last decades. An example of such a small antibody fragment is the variable domain of the heavy chain of heavy chain only antibodies (VHH or nanobody). An overview of the use of nanobodies for cancer-therapy is given in **Chapter 2**. Nanobodies that are being used for the delivery of therapeutic molecules can be referred to as so-called "Nanobullets". Because many therapeutic, and in this case cytotoxic compounds require an intracellular localization for their activity, ideal Nanobullets should not only target to tumor cells but should also facilitate intracellular delivery. In order to achieve an efficient intracellular delivery of Nanobullets, a basic understanding of the biology behind cellular uptake is essential.

The epidermal growth factor receptor (EGFR) and the hepatocyte growth factor (HGF) receptor (Met) are receptor tyrosine kinases that are overexpressed in many cancers, making them attractive targets for cancer therapy. EGFR serves as a model receptor and its activation and internalization are well studied. Ligand-induced signalling of both receptors is silenced by a negative-feedback mechanism consisting of rapid internalization and subsequent degradation of the receptor-ligand complex. Internalization of EGFR is regulated by many ligand-induced post-translational modifications like phosphorylation, ubiquitination and acetylation. However, these modifications do not explain the observed internalization completely. Because ligand-binding also results in the formation of higher order clusters of EGFR on the plasma membrane, clustering was recently suggested to be involved in receptor internalization also. However, the mechanism behind clustering-induced internalization is still unclear.

In this thesis, the mechanism behind clustering-induced endocytosis was studied using multi-epitopic antibody constructs directed against the extracellular part of EGFR (**Chapter 3**). EGFR clustering via biparatopic (binding two non-overlapping epitopes) VHH constructs results in the clustering-induced, clathrin mediated endocytosis (CIC-ME) of the receptor-antibody complex. CIC-ME is kinase-independent and therefore does not activate signalling cascades towards growth and proliferation. CIC-ME also revealed a previously unrecognized role for the transmembrane dimerization motifs of EGFR in internalization. Subsequently, EGFR clustering via tri-epitopic antibody-fibronectin constructs induces unconventional, ubiquitin-independent trafficking of EGFR towards lysosomal degradation (**Chapter 4**). The knowledge of achieving kinase-independent internalization into tumor cells was put to practice by developing different internalizing Nanobullets for intracellular drug delivery. Nanobody-decorated, albumin-based nanoparticles (NANAPs) were generated for the intracellular release of the platinum-linked multikinase inhibitor 17864-Lx in lysosomes of EGFR-expressing tumor cells (**Chapter 5**). Anti-Met NANAPs displayed similar internalization, lysosomal trafficking and degradation and could therefore serve as a novel biomaterial for drug delivery into Met-expressing cells (**Chapter 6**). Finally, nanobodies were turned into Nanobullets for photodynamic therapy (PDT) by conjugating them to the relatively hydrophilic photosensitizer IRDye700DX (**Chapter 7**). Illumination of such photosensitizers (PS) with near-infra red light locally generates the very toxic $^1O_2$. The nanobody-PS conjugates display a specific and strong anti-tumor activity, which can be improved even further by employing internalizing, biparatopic Nanobullets (100% specific cell death, IC50 of ~1nM).

Taken together, this thesis (I) describes the use of nanobodies for cancer therapy, (II) provides a fundamental background behind clustering-mediated uptake and trafficking in tumor cells and (III) gives three examples of nanobullets for cancer therapy. Because of their small size, high specificity and high potency, internalizing nanobody-PS conjugates are considered to be the most promising examples of Nanobullets, which clearly deserve further *in vivo* testing.

Addendum

Nederlandse samenvatting

Nederlandse samenvatting

Kanker wordt gekenmerkt door ongecontroleerde groei en deling van cellen. Kankercellen zijn in staat zichzelf te voorzien van groeisignalen en/of kunnen zich onbeperkt repliceren. Naast chirurgie, bestraling en chemotherapie kan een anti-kanker behandeling ook bestaan uit therapieën die zich richten tegen specifieke tumor-gerelateerde moleculen. Voorbeelden hiervan zijn small molecule inhibitors, siRNAs en immunotherapie. De laatstgenoemde aanpak maakt gebruik van antilichamen die het immuunsysteem activeren of specifieke tumor-gerelateerde signaleringspaden blokkeren. Helaas wordt de tumorgroei vaak alleen geremd door de antilichamen en wordt de tumor niet volledig verwijderd. De specifieke anti-kanker activiteit kan verbeterd worden door de tumor-specificiteit van antilichamen te combineren met de toxiciteit van een therapeutisch middel. Deze antilichaam-geneesmiddel conjugaties (antibody-drug conjugates, ADC) verhogen de effectiviteit van antilichamen waardoor de kans op bijwerkingen van de chemotherapie wordt verminderd.

Voor een optimale ophoping en verdeling van zulke ADCs in de tumor zijn de specificiteit, bindingsaffiniteit, en de grootte van het antilichaam belangrijk. Conventionele antilichamen zijn relatief groot, wat leidt tot een relatief slechte tumorpenetratie en distributie. Daarom zijn er in de laatste decennia verschillende soorten kleinere antilichaamfragmenten ontwikkeld. Een voorbeeld hiervan is het variabele domein van de zware-keten-antilichamen van lama's (VHH of nanobody). Een overzicht van het gebruik van nanobodies bij anti-kanker therapie wordt gegeven in Hoofdstuk 2. Nanobodies die gebruikt worden voor het bezorgen van therapeutische moleculen worden 'Nanobullets' genoemd. Omdat vele therapeutische, en in dit geval toxische moleculen intracellulair functioneren, binden ideale Nanobullets niet alleen aan tumorcellen, maar regelen ze ook de intracellulaire afgifte van het therapeutisch molecuul. Voor het ontwikkelen van een Nanobullet met een efficiënte intracellulaire afgifte, is een gedegen kennis van de biologie van cellulaire opname essentieel.

De epidermale groei factor receptor (EGFR) en de hepatocyte groei factor (HGF) receptor (Met) zijn tumor-gerelateerde, celmembraan gebonden receptor tyrosine kinases en daarom aantrekkelijke doelwitten voor therapie. EGFR dient al jaren als model receptor en de activatie en internalisatie van EGFR zijn goed bestudeerd. Ligand-geïnduceerde signalering van beide receptoren wordt geneutraliseerd door een negatieve-feedback mechanisme dat bestaat uit een snelle internalisatie en afbraak van het receptor-ligand complex. De internalisatie wordt gereguleerd door meerdere ligand-geïnduceerde post-translationele modificaties zoals fosforylering, ubiquitinering en acetylering. Deze modificaties verklaren de ligand-geïnduceerde internalisatie echter niet volledig. Sinds kort wordt er gesuggereerd dat de activatie-geïnduceerde clustering van EGFR op het plasmamembraan ook betrokken zou zijn bij internalisatie. Echter, het mechanisme van deze clustering-geïnduceerde internalisatie is nog onduidelijk.

In dit proefschrift wordt clustering-geïnduceerde internalisatie van EGFR en het mechanisme hierachter onderzocht met behulp van multi-epitoop-bindende antilichaam constructen gericht tegen het extracellulaire deel van EGFR (Hoofdstuk 3). EGFR clustering via biparatope VHHs (die twee niet-overlappende epitopen binden) resulteert in de internalisatie van het receptor-antilichaam complex via zogenaamde clustering-geïnduceerde, clathrine-gemedieerde endocytose (CIC-ME). CIC-ME is kinase-onafhankelijk en activeert de groei en proliferatieve signalering van tumor cellen niet. CIC-ME onthulde een voorheen onbekende rol van de transmembraan dimerisatie motieven van EGFR in internalisatie. EGFR clustering via tri-epitopische antilichaam-fibronectine constructen leidt vervolgens tot een onconventioneel, ubiquitine-onafhankelijk transport van EGFR richting lysosomale afbraak (Hoofdstuk 4).

De opgedane kennis omtrent kinase-onafhankelijke internalisatie en lysosomale transport in tumorcellen werd vervolgens toegepast bij de ontwikkeling van verschillende soorten internaliserende Nanobullets. Albumine nanodeeltjes werden gedecoreerd met nanobodies (NANAPs) voor de specifieke intracellulaire afgifte van de multi-kinase remmer 17864 in EGFR-positieve tumor cellen (Hoofdstuk 5). Lysosomale afgifte van 17864, door middel van een reversibele platinum-verbinding (Lx) tussen het albumine en 17864, zorgde voor remming van celdeling. Anti-Met NANAPs laten een soortgelijke internalisatie, lysosomaal transport en afbraak zien en kunnen beschouwd worden als een nieuw biomateriaal voor de intracelulaire afgifte van therapeutische moleculen in Met-positieve tumor cellen (Hoofdstuk 6). Ten slotte werden de nanobodies van de eerste internalisatie studies omgezet in Nanobullets voor fotodynamische therapie (PDT) door ze te koppelen aan de relatief hydrofiele photosensitizer (PS) IRDye700DX (Hoofdstuk 7). Na bestraling van deze PS met bijna infra-rood licht, vormt zich het zeer toxische $^1O_2$. Nanobody-PS-conjugaten laten een erg specifieke en hoge anti-tumor activiteit zien, die nog verder verbeterd wordt door internaliserende biparatope Nanobullets (100 % specifieke celdood met een IC50 van ~1 nM).

Samengevat, dit proefschrift (I) beschrijft het gebruik van nanobodies voor de behandeling van kanker tot dusver, (II) geeft inzicht in de fundamentele biologie achter clustering-geïnduceerde opname en transport in tumor cellen en (III) geeft drie voorbeelden van potentiele Nanobullets voor de behandeling van kanker. Door hun kleine formaat, de hoge specificiteit en hoge anti-tumor activiteit, zijn internaliserende nanobody-PS conjugaten de meest veelbelovende voorbeelden van Nanobullets die daardoor erg interessant voor verdere in vivo testen.

Addendum

Curriculum Vitae

Curriculum Vitae

Raimond Heukers was born on the 11th of July in 1983 in Emmen, The Netherlands. He attended secondary school at the Esdal College in Klazienaveen at which he obtained his MAVO degree. He respectively obtained his technician degrees from the Drenthe College in Emmen and Saxion Hogeschool in Enschede and his MSc degree in biomedical sciences at the University of Utrecht. Subsequently, he started his PhD project under the supervision of dr. Paul van Bergen en Henegouwen at the Cell Biology department at Utrecht University.

Education

2009 - Recent	PhD in Cell Biology/Molecular Oncology. Utrecht University, Utrecht, the Netherlands. Research school: Institute of Biomembranes Promotor: Prof. dr. Casper C. Hoogenraad Copromotor: Dr. Paul M.P. van Bergen en Henegouwen
2006 - 2008	Master of Science (MSc) Biology of Disease, Graduate School of Life Sciences, Utrecht University, Utrecht, The Netherlands
2003 - 2006	Bachelor of Applied Science (BAS) Biology and Medical Laboratory Research, Saxion Hogeschool, Enschede, The Netherlands
1999 - 2003	Upper Secondary Vocational Education (MBO) Analytical Chemistry, with a bio-analytical differentiation, Drenthe College, Emmen, The Netherlands
1995 - 1999	MAVO secondary school, Esdal College, Klazienaveen, The Netherlands

Internships

- Cellular Architecture and Dynamics, Utrecht University
  (6 months, supervisor: dr. Paul M.P. van Bergen en Henegouwen)
- Department of Medical Physiology, University Medical Centre Utrecht
  (9 months, supervisor: dr. Marcel A.G. van der Heyden).
- Cancer Biomarkers and Prevention Group, Department of Biochemistry, University of Leicester, Leicester, United Kingdom
  (6 months, supervisors: dr. Elena P. Moiseeva and prof. dr. Margaret M. Manson)
- Department of Pathology and lab. medicine, University of Groningen
  (6 months, supervisor dr. Barry van der Strate).
- Department of Molecular Biology of Plants, University of Groningen
  (6 months, supervisor dr. Onno M.H. de Vries).

Work experience

2009 - Recent	PhD candidate Cell Biology/Molecular Oncology, Utrecht University
2009 - 2011	Collaboration with arGEN-X BV, Zwijnaarde, Belgium Project: Selection and characterization of antagonistic anti-Met antibodies from *Llama* using the SIMPLE platform.
2009	Research Assistant. Ablynx NV, Zwijnaarde, Belgium Project description: Characterizing selected Nanobodies against new targets in the second 'Landgrab' project.
2008	Junior Consultant Taxations at Capgemini, Utrecht
2006	Junior Consultant Diagnosis Treatment Combinations (DBC), financial department, Leveste Scheper Ziekenhuis, Emmen

Certificates

Health Physics level 4B Radiation course, Technical University Delft. 2009
Course on Modern Laser Microscopy, University of Groningen. 2008
Course on Laboratory animal science (Art. 9). Utrecht University. 2007
IELTS Academic Language Test. Overall Score: 7.5. Amsterdam. 2006
Nomination for 'Saxion scriptieprijs' for bachelor thesis. Enschede. 2006

Further activities

Committee member of the Intercity Young Scientist Meeting (IYSM). 2012-Recent
PhD committee of the Institute of Biomembranes, Utrecht. 2011-2013
MSc Representative. Grad. School of Life Sciences, Utrecht University. 2008-2009
Active member of several student associations. 2004-2010

Poster presentations

- IIAS-ISF Conference on "Epidermal growth Factor Receptor - Future Directions", Jerusalem, Israel, 17-20 Nov 2013
- EMBO meeting, Amsterdam, September 2013
- ICREA symposium, "Visualizing signalling nanoplatforms at *higher* spatiotemporal *resolution*", Barcelona, Spain, 29-31 May 2013
- Scientific Meeting NWO- study groups Protein Research, Nucleic acids and Lipids & Biomembranes, Veldhoven, The Netherlands. 10-11 December 2012
- Beatson International Cancer Conference, Glasgow, Scotland. 1-4 July 2012
- Scientific Meeting NWO- study groups Protein Research, Nucleic acids and Lipids & Biomembranes, Veldhoven, The Netherlands. 6-7 December 2010

Invited talks

- Institute of Biomembranes AIO day, Utrecht, 31th of October 2013. Title: CIC-ME for cancer therapy
- Molecular and Cell Biology Meeting. Biopharmacy, Utrecht University. 12th of October 2012. Title: Cell Biology tools for Biopharmacy purposes
- Scientific Meeting NWO- study groups Protein Research, Lipids & Biomembranes,
- NCMLS, Nijmegen, The Netherlands. 8th of June 2012. Title: EGFR endocytosis requires both its kinase activity and the transmembrane GG4 motif
- MPEP meeting. Bijvoet Institute, Utrecht. 6th of June 2012. Title: EGFR endocytosis requires both its kinase activity and the transmembrane GG4 motif
- Virology division. Department of Infectious Disease and Immunology. Veterinary medicine. Utrecht University. 1st of June 2012. Title: EGFR endocytosis is regulated by its N-terminal transmembrane GG4 dimerization motif
- CHAINS2011 Chemistry As INnovating Science Conference. NWO/KNCV, Maarssen, the Netherlands, 28-30 November 2011. Title: Clathrin-dependent endocytosis and degradation of EGFR by VHH-induced receptor clustering
- Met-project meeting at arGEN-X. Ghent, Belgium.13th of July 2011. Title: Extracellular clustering of transmembrane receptors induces clathrin-dependent endocytosis
- Guest lecture. Saxion Hogeschool, Enschede, The Netherlands. 17th of May 2010. Title: Improved anti-tumor strategies: From idea, via research, to therapy

Patents:

Method for intracellular delivery of bioactive agents into mammalian cells by homobody transporters. **Raimond Heukers,** Sabrina Oliveira, Rob C. Roovers, Paul M. P. van Bergen en Henegouwen. Utrecht University, Provisional Application number 61732953. 04/12/2012.

List of publications:

Heukers R., van Bergen en Henegouwen P.M.P., Oliveira S., Novel nanobody-photosensitizer conjugates for targeted photodynamic therapy. Nanomedicine, *under revision*

de Heus C., Kagie N.J.A., **Heukers R**., van Bergen en Henegouwen P.M.P., Gerritsen H.C., Analysis of EGF receptor oligomerization by homo-FRET, Methods Cell Biol. 2013;117:305-21.

Heukers R., Altintas I., Raghoenath S., de Zan E., Pepermans R., Roovers R.C., Haselberg R., Henning W.E., Schiffelers R.M. Kok R.J., van Bergen en Henegouwen P.M.P., Targeting hepatocyte growth factor receptor (Met) positive tumor cells using internalizing nanobody-decorated albumin nanoparticles. Biomaterials. 2014 Jan;35(1):601-10.

Oliviera S., **Heukers R**., Somkom J., Kok R.J., van Bergen en Henegouwen P.M.P., Targeting tumors with nanobodies for cancer therapy. J Control Release. 2013 Sep 11;172(3):607-617.

Heukers R., Vermeulen J.F., Fereidouni F., Bader A.N., Voortman J., Roovers R.C., Gerritsen H.C., van Bergen en Henegouwen P.M.P., EGFR endocytosis requires its kinase activity and N-terminal transmembrane dimerization motif. J Cell Sci. 2013 Nov 1;126(Pt 21):4900-12.

van der Meel R., Oliveira S., Altintas I., **Heukers R.**, Pieters E.H., van Bergen en Henegouwen P.M.P., Storm G., Hennink W.E., Kok R.J., Schiffelers R.M., Inhibition of tumor growth by targeted anti-EGFR/IGF-1R Nanobullets depends on efficient blocking of cell survival pathways., Mol Pharm. 2013 Oct 7;10(10):3717-27.

Varkevisser R., Houtman M.J., Waasdorp M., Man J.C., **Heukers R.**, Takanari H., Tieland R.G., van Bergen en Henegouwen P.M.P., Vos M.A., van der Heyden M.A., Inhibiting the clathrin-mediated endocytosis pathway rescues K(IR)2.1 downregulation by pentamidine., Pflugers Arch. 2013 Feb;465(2):247-59.

Altintas I., **Heukers R.**, van der Meel R., Lacombe M., Amidi M., van Bergen En Henegouwen P.M.P., Hennink WE, Schiffelers R.M., Kok R.J., Nanobody-albumin nanoparticles (NANAPs) for the delivery of a multikinase inhibitor 17864 to EGFR overexpressing tumor cells., J Control Release. 2013 Jan 28;165(2):110-8.

Moiseeva, E.P. and **Heukers, R**., Indole-3-carbinol-induced modulation of NF-kappaB signalling is breast cancer cell-specific and does not correlate with cell death. Breast Cancer Res Treat. 2008 Jun;109(3):451-62.

Moiseeva, E.P., **Heukers, R**. and Manson, M.M., EGFR and Src are involved in indole-3-carbinol-induced death and cell cycle arrest of human breast cancer cells. Carcinogenesis. 2007 Feb;28(2):435-45.

Moiseeva, E., **Heukers, R**., Manson, M., Complexity of constitutive NF-kappaB activity as a therapeutic target in breast cancer cells. Abstract in European journal of cancer. 2006 Nov; 12(4);180.

Dankwoord

Dankwoord

Nu is dan eindelijk het moment aangebroken om de mensen te bedanken zonder wie dit 'prachtige' boekje nooit gemaakt had kunnen worden. Na regen komt zonneschijn en na wetenschap komt het dankwoord. In kan het natuurlijk kort houden om drukkosten te besparen, maar omdat ik niet van plan ben nog een proefschrift te schrijven, neem ik lekker de ruimte.

Zoals bij veel aio's is de inhoud van het dankwoord grotendeels al jaren voor de promotie bedacht. Helaas, zoals ook bij vele aio's, zijn de meeste prachtzinnen al verdampt ten tijde van het schrijven en kom je vervolgens op de proppen met totaal iets anders. Dit betekent, hoewel het natuurlijk met alle liefde en de beste bedoelingen geschreven is, dat onderstaande tekst niet te letterlijk genomen dient te worden. Ik heb iedereen namelijk in gedachten ook al in heel veel andere/betere bewoordingen bedankt. Nu ik mij alvast voor de hier op volgende woordkeuzes heb ingedekt, zou ik me ook alvast even willen verontschuldigen voor de personen die ik straks ga vergeten te bedanken. Dus, voor iedereen die ook maar in de verste verte iets met dit proefschrift te maken heeft gehad of zelfs denkt dat hij of zij heeft bijgedragen en hieronder niet genoemd staat: Bedankt! Daarnaast is de volgorde van de namen volstrekt willekeurig en bestaat er dus geen 'directe correlatie' tussen de positie en waardering.

Welnu, de persoon die aanzienlijk heeft bijgedragen aan mijn opleiding, onderzoek en werk, en die ik dus als eerste wil bedanken, is mijn copromotor Paul van Bergen en Henegouwen. Paul, je zegt altijd dat de mensen om je heen niet gek genoeg kunnen zijn. Hoe gekker, hoe beter. Ik heb de afgelopen jaren dan ook van alles meegemaakt. Maar naast jouw onconventionele ziens- en werkwijzen ben je ook erg enthousiast en kritisch en dat heeft mijn tijd in jou groep en het onderzoek zeker goed gedaan. Heel fijn om met iemand te werken voor wie alle hypotheses bespreekbaar zijn. Er zijn minder betrokken begeleiders. Over het 'buiten de box denken', soms kreeg ik de indruk dat je niet eens wist dat er überhaupt een box is. Ik denk dat 5 jaar werken met jou mijn manier van denken voorgoed heeft veranderd. Bedankt voor deze leerzame periode en leuke tijd.

Daarnaast wil ik graag mijn promotor Casper Hoogenraad bedanken voor zijn heldere blik op zaken en het uitstekend uitvoeren van de bij de professor titel behorende bevoegdheden. Schijnbaar probleemloos werd de ene na de andere bureaucratische hobbel genomen. Ik kan nog veel van je leren. Naast de serieuze zaken hebben we ook erg gelachen en als leerling van Paul weet ik dat dat ook belangrijk is. Anna, ik wil jou ook graag bedanken voor alle input, goede gesprekken en de kritische noot. Ik ben er scherper door geworden. Ik ben jullie ook erg dankbaar voor de manier

waarop wij een paar jaar geleden zijn opgenomen in de nieuwe celbiologie groep. Ik denk dat we inmiddels aardig goed gemengd zijn en ik heb gemerkt dat de goede samenwerkingen nu al zijn meerwaarde heeft bewezen en dat we nog elke dag van elkaar leren. Ik hoop dan ook dat jullie deze symbiose nog een tijdje volhouden.

Na het afronden van het proefschrift is deze beoordeeld door een, wat mij betreft, zeer kundige leescommissie bestaande uit Anna Akhmanova, Hans de Haard en Wim Hennink van de Universiteit Utrecht, Peter van der Sluijs van het Universitair Medisch Centrum Utrecht en Wouter Moolenaar van het Nederlands Kanker Instituut in Amsterdam. Bedankt voor jullie tips, trucs en carrière advies. Hans en Anna extra bedankt voor het attenderen op de spelfouten en inconsistenties.

Jarno Voortman wil ik graag bedanken voor ALLES! Vanaf de eerste dag dat ik het lab binnen kwam als Heukie Beukie wisten we al dat dit een goede samenwerking zou worden. ‘Werken met dat kadaver!’ We hebben dan ook veel voor elkaar gekregen en ik zal de vele radioactieve experimenten op de 3^{e} nooit meer vergeten. Mijn duim ook niet. Ik heb met betrekking tot het begeleiden van studenten ook aardig wat van je geleerd. Met onze positieve insteek hebben we samen heel wat studenten enthousiast gemaakt. Oh ja, en ook nog bedankt dat het hele lab even draaiende hebt gehouden voor, tijdens en na de vehuizingen. Ik hoop dat je je vermaakt als lenzenslijper en dat we nog een keer een pilsje gaan pakken. Het zou leuk zijn als moeder de vrouw dan ook mee komt.

En dan hebben we natuurlijk onze Erik Hofman a.k.a. der Hofmeister. Ik wil je graag heeeeeeel erg bedanken voor al het voorwerk dat je zo mooi hebt opgeschreven in jouw proefschrift en voor alle hulp bij het opstarten van mijn project. Dat was echt geweldig met de neus in de boter vallen in de eerste jaren. Jij wist immers precies waar alles lag en hoe het allemaal het beste werkte. En vooral ook wat niet werkte. Daarnaast ben ik ook de andere postdocs bij Paul in de groep erg dankbaar voor leuke, leerzame en vooral productieve samenwerkingen. Rob Roovers voor de goede verhalen/kennis en dat we altijd gebruik konden maken van jouw praktische probleem-oplossend vermogen (cloneren). Oh ja, en voor de hulp bij bijna al het nanobody werk natuurlijk. Mijn buurvrouw (zowel op het werk als thuis) Sabrina Oliveira voor het eeuwige optimisme (op het lab zelfs nog na 19:00 uur) en voor de farmaceutische insteek in onze groep. Dat inzicht vond ik erg waardevol en het heeft mij regelmatig aan het denken gezet over onze celbiologische onderzoekjes. Ik denk dat we samen een geweldig mooi werk hebben afgeleverd en ik denk ook dat er een mooie toekomst voor jou in de wetenschap ligt. Maar vergeet alsjeblieft niet dat interessante ontdekkingen soms uit onverwachte hoeken komen. Ga dus gerust eens van de paden

af en houdt de ogen goed open. Feel free to drop by for an English translation.

Alles goed en wel, maar dit boekje was er natuurlijk nooit gekomen als ik niet zelf ook nog even met dat pipetje in mijn handen in de krochten van het Kruytgebouw aan een labtafeltje had gezeten. Ik wil dus graag mijn stagebegeleiders: Jarno Voortman (UU), Marcel van der Heyden (UMC), Toon van Veen (UMC), Marien Houtman (UMC), Bart Kok (UMC), Maggie Manson (Leicester University), Elena Moiseeva (Leicester University), Barry van der Strate (UMCG), Marie Geerlings (UMCG) en Onno de Vries (RUG) graag bedanken voor alle energie die ze in mij gestopt hebben. Tjonge, wat heb ik veel moeten leren zeg. Ik denk dat goede coaches en mentoren net zo belangrijk, zo niet belangrijker zijn, als/dan theorie colleges. Het uitdunnen van onderwijspersoneel en het verhogen van de publicatiedruk op de onderwijzende onderzoekers lijkt mij op de lange termijn dan ook vooral kapitaalvernietiging.

Zonder de speciale en ongeëvenaarde sfeer op ons lab had ik het pipetteren waarschijnlijk niet volgehouden. Van Bingo FM tot de WC experience. Van muziekale diepgang tot optimale werksfeer. Vandaar dat ik naast Jarno, Rob, Erik ook de andere grondleggers van deze unieke werksfeer graag wil bedanken: Edward Dolk, Renée de Bruin, Jord Stam, Rachid El Khoulati en Smiriti Raghoenath. Wat een beestenboel. Daarnaast zijn er natuurlijk ook nog de andere labgenootjes die de tijd op de 5e verdieping zeker ook onvergetelijk hebben gemaakt: Mohammed El Khattabi, Theo Verrips, Bart de Haan, Elsa Regan, Lucy Rutten, Mireille Koenders, Ava Sadi, Jan Andries Post, Chris Schneijdenberg, Hans Meeldijk, Willie Geerts, Wally Müller, Karin Vocking, Jose Bijvelt, Frits Kindt en Ronald Leito. De aio's worden hieronder even apart genomen. Ik wil in het bijzonder Fons Cremers bedanken voor het enthousiasme en interesse in mijn project en in de algemene stand van zaken. Het is al vaker gezegd, maar je bent een bijzondere vent. Bij jou op de afdeling zitten was heel goed voor mijn extracurriculaire activiteiten en het ontplooien van mijn begeleidingscompetenties. Ik heb veel van je geleerd. Ik hoop dat je je nog lang kan inzetten voor het algemeen belang en dat je daarna mag genieten van een welverdiend pensioen. En dat Cremers-standbeeld komt er nog wel.

Naast de lijn11- en lijn12-busladingen Bachelor studenten die we begeleid hebben tijdens hun cursussen, heb ik ook nog de hulp gehad van Master stagiairs/stagiaires. Mohamed Kaplan, bedankt voor je hulp tijdens je stage en voor het op de proef stellen van mijn wetenschappelijk en literaire kennis, mijn filosofisch inzicht en mijn geduld. De resultaten van jouw stage waren steevast contra-intuïtief en druisten altijd tegen onze hypotheses in. Maar ik ben blij dat ze uiteindelijk allemaal bleken te kloppen en dat we ze in een mooi artikel hebben kunnen verwerken. Veel succes met het afronden van jouw promotie. Ik ben er van overtuigd dat met jouw intellect,

eigenwijsheid en doorzettingsvermogen, een mooi academische carrière in het verschiet ligt. Cilia de Heus, heel erg bedankt voor het uitvoeren en eenvoudig lijken van experiment die voor anderen onmogelijke lijken. Jouw werk-mentaliteit was erg goed voor de data-acquisitie en ik hoop dat dat harde werken uiteindelijk beloond wordt met veel publicaties tijdens jouw promotie-traject. Ook bedankt dat ik, als volwaardig begeleider, de laudatio mocht uitspreken tijdens je diploma-uitreiking en leuk dat je in onze groep bent blijven hangen. Kim Bouwman, bedankt voor je onuitputtelijke doorzettingsvermogen tijdens je schijnbaar onmogelijke stageproject. Ook al leek er steeds niets uit te komen, jouw werk heeft het project wel aan de praat gehouden. Momenteel lijkt het erop dat het toch nog een redelijk succesvol staartje gaat krijgen. Naast deze MSc-studenten heb ik het laatste jaar ook mogen genieten van de blot-productie-machine Ian Kercher. Ian, zoals het zich een waar analist betaamd heb jij binnen no-time een compleet artikel bij elkaar geblot. Geen gelul, gewoon pipetteren. Heel erg bedankt hiervoor, want dat heeft toch een mooi hoofdstuk opgeleverd met data dat sowieso nog een keer ergens gepubliceerd gaat worden. Dat beloof ik. En ik ga ook echt nog whisky kopen bij pa Kercher. Ook heb ik twee scriptie-studenten mogen begeleiden, Marjolein Haagsman en Thijs Gruntjes. Hoewel dit voor mij ook een leerzame ervaring was, hoop ik dat jullie er (behalve jullie cijfer) ook nog iets aan hebben gehad. Bedankt voor de research en voor de prettige samenwerking in elk geval.

Heel veel donkere uurtjes (zelfs op de prachtige zomerse dagen met blauwe lucht) heb ik doorgebracht in de kelder van Moleculaire Biofysica. Hans Gerritsen, bedankt dat ik de experiment bij jullie mocht uitvoeren en bedankt voor de input in de soms ogenschijnlijk ondoenbare experimenten. Arjen Bader en Farzad Fereidouni uiteraard bedankt voor de goede en prettige samenwerking. Zonder jullie was het allemaal niet gelukt. Jullie expertise was onmisbaar en ik heb ontzettend veel van jullie geleerd. Dat laatste geldt overigens ook voor Dave van den Heuvel, Gerhard Blab, Hoa Truong en de aio's Johan van Voskuilen, Helene Knaus en Tim van Werkhoven. Nivard Kagie, bedankt voor het harde werken, doorzetten en uiteindelijk redden van onze publicatie.

Lichtere tijden heb ik meegemaakt bij Biofarmacie. Wat een leuke samenwerkingen heb ik gehad met mensen uit dat schitterende en lichte gebouw aan de overkant van de straat. Markus de Raadt, Afrouz Yousefi, Erik Teunissen, Maryam Amidi, Enrico Mastrobatista en de Nanobullet mensen Robbert Jan Kok, Raymond Schiffelers, Wim Hennink, Isil Altinas en Roy van der Meel, bedankt. Ik voelde me altijd erg welkom bij jullie. Dit geldt overigen ook voor Remko van Vught en Eefjan Breukink van Membraan Biochemie en Biofysica.

The Nanobulleteers in particular, deserve a little more attention. This was a very good collaboration between Chemistery, Pharmacy and Cell biology. I'm very happy that I could be part of such a nice team of people. It was not only a good team for science, but I also enjoyed our Nanodiners and Nanobeers very much. Priceless!
Isil, I'm especially very happy with our collaboration. Gladly, despite our different backgrounds, we were both always open for each other suggestions and arguments. This lead to two very nice Nanobullet papers, which would have been impossible to make individually. One third of my experimental chapters were made with you! We've also had a lot of fun and coffee and I hope we will work together more often in the future.
Roy, wij hadden ook wel drie van zulke papers kunnen maken als het lot ons iets beter gezind was. De particles van Isil waren nu eenmaal makkelijker onder de microscoop. Ben wel blij dat het nog wel tot een paper heeft geleidt en dat ik dus heb mogen meedoen aan het liposomen werk. Terwijl ik dit schrijf heb jij net je promotie gehad, dus je hebt al genoeg veren in je rectum, maar je bent een topkerel om mee te werken. Ik hoop ook dat we nog even collega's worden in het UMC en dat we anders sowieso enorm gaan samenwerken.
Remko, bedankt voor alle hulp bij kloneringen of producties en voor jouw unieke zienswijzes op proeven doen. Die bak kennis van jou kwam bij mij ook regelmatig van pas. Dus ook hier was het Nanobullet-project goed voor. Ik weet niet of wij zo veel hadden overlegd als we niet in het zelfde team zouden zitten. Jouw papers komen er ook aan en dan ben ik erg benieuwd wat je allemaal daarna nog gaat uitvinden. Wie weet hebben ook wij elkaar nog een keertje nodig in de toekomst en dan mag je bij mij in elk geval altijd aankloppen.
Zoals blijkt uit de vele publicaties die deze Focus&Massa project Nanobullets heeft opgeleverd, is dit een enorm succesvolle actie geweest. Ik tel zo een stuk of 11 hoofstukken uit onze proefschriften die in goede tijdschriften zijn gepubliceerd. Wat mij betreft gaan we nog een paar jaar door als Nanobullet team. Of er moet een nieuw Nanobullet team komen, want er zit volgens mij nog veel meer in het vat.

Een paar jaar geleden werd ons lab geannexeerd door een legio Rotterdammers. Echter, dit heeft heel goed uitgepakt en ik ben blij dat ik in zo'n goede groep heb mogen werken. Daarom wil ik sowieso Phebe Wulf bedanken voor het pico bello regelen van het één, dan wel het ander en de rest. En daarnaast natuurlijk de rest van de groep: Esther de Graaff, Lucas Kapitein, Phillip Schatzle, Inez Ferreira, Corette Wierenga, Martin Hartemink, Marina Mikhaylova, Kai Jiang, Ilya Grigoriev, Benjamin Bouchet, Eugene Katrukha, Elena Tortosa, Lauri Gumi, Karin Boekhoorn. Sinds de komst van Anna en Casper zijn de banden met ontwikkelingsbiologie ook verder ontwikkeld en zou ik dus Sander van den Heuvel, Mike Boxem, Inge The ook graag willen bedanken voor het meedenken tijdens de werkbesprekingen en Adrie Thomas (alsmede Toon de

Kroon) voor de hulp bij de bureaucratische rompslomp rond het radioactiviteitslab.

Ger Arkesteijn bedankt voor het sorteren van die vreselijk slecht expresserende cellen van me. Ze waren eigenlijk een vernedering voor dat prachtige apparaat. Ik had nog graag dat projectje van ons verder uit willen werken, maar je kan nou eenmaal niet alles tegelijk. Als het even meezit, gaan wij elkaar in de nabije toekomst nog vaak bij de Influx treffen.

Een deel van mijn aio-schap bestond uit een samenwerking met arGENx. Dit heeft niet alleen een groot deel van mijn aio-tijd betaald, maar het heeft mij ook erg veel geleerd en een kijkje in de keuken van een farmaceutisch bedrijf geboden. Hiervoor wil ik graag Hans de Haard, Tim van Hauwermeiren en Michael Saunders bedanken. Laten we hopen dat onze lead spoedig de wereld zal veroveren. In het bijzonder wil ik Anna Hultberg, Natalie de Jonge en Els Vestjens bedanken voor de fijne samenwerking. Anna, heel veel succes. Geniet van het leven en ik hoop dat we ooit nog eens zo kunnen samenwerken.

Over het algemeen betekend het gezamenlijk volgen van een opleiding ook het delen van de daarbij behorende pieken en dalen. Dit maakt tegenslagen bespreekbaar en zorgt ervoor dat je elkaar op de juiste momenten net even dat steuntje in de rug kan geven. Of, je kan elkaar soms ook genadeloos weer met de benen op de grond zetten. Al met al heeft dit tot mooie vriendschappen geleid. Onvergetelijke dingen hebben we meegemaakt met de aio's en dat had ik voor geen goud willen missen. Promoveren heeft het voor mij ook mogelijk gemaakt om vriendschappen op te bouwen met onvoorstelbaar intelligente, maar toch lieve mensen. Ik vind het een eer om me met de volgende mensen te mogen vergezellen: Chris Emmerson, Bram Dorresteijn, Vincent Krouwer, Andrea Gorlani, Milla Summanen-Paalanen en Matthia Winter-Karreman. Maar ook jullie aanhang natuurlijk: Dorien, Maaike, Laura, Antti en Victor. Ik heb veel van jullie geleerd en ik heb via jullie ook veel van mezelf geleerd. Kumma kana is in Finland inmiddels een begrip op het Himmos festival. Mos Kiitos for all those trips Milla, Antti and the rest the Paalanen family. Het Tvtas weekend is een succes gebleken en ik hoop dat we dat nog jaren volhouden. Dat ene weekend in het jaar, in de winter notabene, alle stress opzij zetten door lekker te sleeën, zwemmen, vliegeren of in de sauna, is goed voor lijf en leden. Lijkt mij. En dit jaar gaat versie 5 alweer van start. Naar DEUTSCHLAND!!!! Bedankt voor de leuke tijd en laten we vooral contact houden.

Eigenlijk wil ik alle aio's bedanken en succes wensen met het afronden van hun boekje. Ten eerste Alex Klarenbeek. Zet hem op he, en laat je niet gek maken. Wat wordt dat straks een feest, niet normaal. Zal ik de Pathe bioscoop al reserveren voor de film 'What happened to Alex in Gent'?

En natuurlijk de andere aio's (al dan niet al klaar): Nika Strokappe, Emine Korkmaz, Matthijs de Winter, Els van der Vlist, Oliver Wicht, Susanna Abrue, Kay Wai Man, Mariella Franker, Joanna lipka, Marijn Kuipers, Josta Kevenaar, Robert van den Berg, Petra van Bergeijk, Max Adrian, Amol Aher, Sam van Beuningen, Bas Cloin, Marleen van Coevorden, Catia Frias, Hai Yin Hu, Ivar Noordstra, Marta Silva, Jingchao Wu, Carol Yu, Vincent Portegijs, Tim van Mourik, Christiaan Berends, Thijs Koorman, Suzanne Ruijtenberg, Selma Waaijers, Sander Kooijman, Susan van Dommelen en natuurlijk de vele PhD studenten van het Institute of Biomembranes.

Samen met Caspar Jonker, Michiel van Veen en Dorothee van Breevoort heb ik een kleine bijeenkomst voor jonge onderzoekers in de cell biologie georganiseerd, genaamd de Intercity Young Scientist Meeting (IYSM). Dat was erg leerzaam, nuttig en gezellig met z'n vieren en ik wens jullie heel veel succes met het afronden van jullie boekjes.

Vrienden die me al een paar jaar vergezellen en gerust stellen in tijden van klaagzang zijn de twee blonde dames van de drie musketeers: Malin Boezelman-Jonsson en Eva Herold. Dat wij nog steeds actief vrienden zijn vind ik echt super en waar we ook ooit terecht komen, ik hoop dat we elkaar in de gaten blijven houden. Sinds Jan Willem en Jan er de laatste jaren bij gekomen zijn, is het alleen maar gezelliger geworden. Eigenlijk horen Michiel Boekhout en Evelien Berends hier ook een beetje bij. Boekie, om jou nog maar eens even apart te nemen, we hebben het er al vaker over gehad en ik weet niet hoe, maar jij gaat ooit een boel voor elkaar krijgen. Ik heb het gevoel dat ik jou ooit ga bellen of je niet alsjeblieft een baan voor me hebt. Het is trouwens bij jullie allemaal bewonderingswaardig hoe jullie die hoge intelligentie combineren met een goed EQ. Zo zijn jullie toch een beetje mijn voorbeelden.

Goed, genoeg over bèta-wetenschappers. Ik heb een uitstekend studentenleven gehad met hele bijzondere huisgenootjes als Ruben Zoethout in Groningen, Marijn Bosch, Peter Mueller, Maarten Pieterson en Nicky Haitel in Utrecht, Rutger Kortman, Jan Willem Meppelink, Casper Meppelink (soort van huisgenoot), Hylke de Vriend, Martin Krikke en Jeroen Raven in Enschede en Froukje Brands en Els Buist in Groningen. Een gemêleerd gezelschap die jarenlang als thuis, spreekbuis en feestmaatjes functioneerden. Liters jonge…. Liters…. Eigenlijk spreek ik jullie allemaal nog regelmatig en dat doet me goed. Juist die uiteenlopende achtergronden en interesses zorgt ervoor dat we elkaar altijd iets te vertellen hebben en dat we van elkaar blijft leren. Leuk, voor erbij dan hé.

Tijdens mijn studententijd in Utrecht heb ik ook Ben Govers ontmoet bij de studentenvereniging voor internationale betrekkingen (SIB). Ben, bedankt voor die onvergetelijke ervaringen in

Midden-Amerika en voor de vele filosofie-uurtjes. En voor de muzieklessen. Ook bedankt voor alle interesse in een voor jouw zo onbegrijpelijke materie als cel biologie. De andere import Utrechters, Willem Bartelink (in het bijzonder, we go way back namelijk) en Carina Clemens, Martijn Langereis en Shofie Langereis-Jacobs, Pepijn Schellen en Willeke Versteeg, Ronald Jacobi en Mijke Jacobi-Vogels wil ik ook graag bedanken voor de mentale ondersteuning en versnaperingen. Gezellig buurtje zo hè. Toch moeten we vaker mountainbiken.

Gert Vos, sinds de eerste week op het MBO zijn we al vrienden en jarenlang hebben we gefilosofeerd over diploma's, wetenschap, ambities en onzin. En hoewel we aanvankelijk voornamelijk verantwoordelijk waren voor de economische bloei van de horeca in het centrum van Emmen, denk ik dat we ons aardig aan elkaar hebben opgetrokken en ik ben dan ook enorm dankbaar voor de vele discussies en de leuke tijd tijdens onze studies. Ik hoop dat je met Natalie een gelukkig gezinnetje wordt en dat je mij ook de komende jaren een beetje scherp blijft houden. Keertje poolen?

Over sport gesproken, de afgelopen jaren heb ik proberen te badmintonnen. En mijn team bestaande uit Ernst de Boer en Manon van Gestel, Els Brakkee, Marcel Heijnen, Lotte Rijpstra en Michiel de Graaff moesten altijd aanhoren hoe druk ik wel niet was. Sorry nog daarvoor en bedankt voor de gezellige en sportieve afwisseling met het onderzoek.

Aan één club nogal uiteenlopende mensen heb ik extra veel te danken: de jongens uit Drenthe: Raimon Wegkamp, Ronald Alberts en Rianne Wiers, Dennis Huizing en Rosemarijn Huizing-Boelema, Alex Bos en Loesje Heijmans, Raymon Luchjenbroers en Anita de Haan, Reinier Wiering en Isabelle Diependaal, Klaus Harm en Petra Timmerman. Nou ja, Drenthe, inmiddels wonen en werken jullie ook overal. Ik ben jullie heel erg dankbaar voor het feit dat jullie er altijd waren als ik aan kwam waaien. Wij kennen elkaar natuurlijk al eeuwen, maar met jullie in de Boogie Bar, de Brasserie, de Corner, tuin, op de bank of op vakantie was en is nog altijd super gezellig. Bij jullie vond ik vaak respectvolle sociale controle. Altijd kritsch, maar ook altijd vol respect en bewondering voor elkaar. Ik hoop dat jullie door dit boekje een beetje een beter beeld krijgen van wat ik de afgelopen jaren heb gedaan. En anders leg ik het wel een keer uit met een pilsje. Eéntje dan he, Dennis.

Ik ben blij dat ik straks twee sterke kerels naast mij heb staan om me te verdediging tegen de aantijgingen van het oppositiecommissie. Mocht het uit de hand lopen dat weet ik zeker dat ik op mijn blot-brother Rachid en mijn big-brother Harald kan rekenen. Rachid, het was heel fijn om je op het lab te hebben de afgelopen jaren en ik ben blij dat je het er zo naar je zin hebt. We gaan nog

samen pipetteren, dat voel ik gewoon. Het is die Rachid op die mike. Altijd hitten, altijd hype....

En Harald, ik kan je niet genoeg bedanken voor het zijn van mijn grote broer. Ja, jij kan daar ook niks aan doen, dat weet ik. Maar het is voor een jongere broertje heel fijn om alles bij een grote broer af te kunnen kijken. Zo werden jaren geleden de grote stappen als verhuizen naar de grote stad en studeren een stuk minder groot en kon ik leren van jouw ervaringen. Wij delen de drive om iets neer te zetten, ongeacht wat. Volgens jouw redenering is namelijk alles mogelijk. Die levenshouding werkt heel inspirerend. En hoewel jij in een totaal andere branche werkt, ben je altijd geinteresseerd in mijn vakgebied. Het is dan ook altijd leuk om samen met jou successen te vieren, ideeen en plannen te bespreken en te filosoferen over het nut van alledag en hoe het beste hiervan te genieten. Ik ben blij dat we weer wat dichter bij elkaar wonen en dat we elkaar regelmatig zien. Je bent goed bezig!

Nu we bij familie zijn aangekomen, wil ik de familie Hiddink en Eskes graag bedanken voor de warme woorden, aandacht, interesse en sociale controle. Ab, Ria, Sieneke, Ivo, Rienk, Nadia, Oma Eskes en de vele ooms en tantes en neefjes en nichtjes, jullie maakten van de verjaardagen, familiedagen, gewone bezoekjes, maar ook de tentfeesten altijd een welkome onderbrekingen van al dat gedoe in Utrecht. Zeker in tijden dat alles op het lab mislukt is het fijn om opgevangen te worden door een club nuchtere achterhoekers. Datzelfde geldt ook voor Wietske Wolters en Wilmen Hoekstra, Rianne Memelink en Sake Boere en Ingrid van den Nieuwenhuizen. Prachtig mooi daar trouwens, de Achterhoek.

Maar er gaat natuurlijk niks boven echt thuis. Ook thuis in Klazienaveen vond ik altijd een luisterend oor. Ik wil graag mijn oma bedanken voor de boerenwijsheid: "*Leer joe de kop nie gek, want je kun'n 't nie metneemn*". Ik heb daar de afgelopen 10 jaar wel eens aan gedacht en het vervolgens als argument gebruikt voor een weekendje niets doen. Het moet wel leuk blijven natuurlijk.

Pa, Ma en Joury, ontzettend bedankt voor alles. Voor de enorme stimulerende omgeving thuis en voor het mogelijk maken dat Harald en ik zo lang mochten studeren als dat we wilden. Het is eigenlijk ook best fijn dat jullie al 20 jaar in hetzelfde huis wonen. Dan voelt het voor ons ook echt als thuis als we langs komen. Onder het motto 'zolang je maar weet wat je doet en je je best doet' hebben jullie ons al vroeg geleerd dat we zelf onze verantwoordelijkheid moesten dragen voor onze keuzes. Toch fijn dat jullie, als goede ouders, ons toch altijd in de gaten houden en het aangeven wanneer we stom bezig zijn. Pa, ik ben de opmerking die je maakte na mijn eerste stage in Groningen nooit vergeten: "*Het was misschien wel lastig, maar als je deze stap vooruit zo mooi*

vond, dan moet je dat volhouden en hierna geen stap meer terug doen". Uit de toegewijde manier waarop je Harald en mij altijd dingen probeert te leren blijkt dat je een goede leraar had kunnen worden. Nou ja, dat ben je dus eigenlijk al. De wandelingen met Joury langs het kanaal zijn goede rust- en uitwaaimomentjes en bovendien onbetaalbaar. Bedankt voor je nuchtere probleemoplossend vermogen en je calvinistische arbeidsethos (zoek maar op). En ma, jouw ernorme verwondering voor de natuur is erg aanstekelijk gebleken. Omdat we vroeger thuis eigenlijk geen van allen veel biologische kennis, deelden we het enthousiasme over al die rare planten en beestjes rondom het huis. Erg leuk en interessant om dat samen allemaal te ontdekken en uit te zoeken. En de creativiteit die ik van jou heb georven is de afgelopen jaren ook erg vaak van pas gekomen tijdens het bedenken van experimenten en het maken van een biologische modellen. PA en ma, bedankt voor deze onbedoelde thuisopleidingen en Boxumse creativiteit en ik hoop dat we nog jaren samen die rare wereld om ons heen mogen bewonderen.

Het mooist heb ik natuurlijk voor het laatst bewaard. Lieve Wietske, wat ben ik blij dat ik mijn aio-schap met jou heb mogen doorbrengen. Sterker nog, wat ben ik blij dat ik de afgelopen 10 jaar met je heb mogen doorbrengen. En hopelijk nog veel langer. Hoewel ik het je al doezend keer heb gezegd, ik kan me geen betere partner wensen. Wat zijn wij een team. Ik ben blij dat je me de afgelopen jaren zo hebt geholpen met mijn aio-dipjes, aio-topjes, tijdsplanningen, vrije tijd, filosofische vraagstukken, lekker avondeten, rehydratie en nog veel meer. Heel fijn om zo veel liefde, nuchterheid, stabiliteit en intellect in mijn buurt te hebben. Stimulerend gezelschap. Ik ben enorm trots op wat jij de afgelopen jaren hebt gepresteerd. Dat jij, naast een promoverend vriendje (met zijn geneuzel), een goede baan en een actief sociaal leven, gewoon nog even je MSc diploma gehaald hebt, is fantastisch! Woehoe! We hebben ons de afgelopen jaren aardig uit de naad gewerkt. Vanaf nu gaan we ook avonden en weekenden vrij nemen en gaan we elk jaar op vakantie. Net als normale mensen. Beloofd.

Ik zou mijn dankwoord graag willen samenvatten en afsluiten met een passend citaat van zeker niet één van mijn meest favoriete schrijvers:

' "Het is gezien," mompelde hij, "het is niet onopgemerkt gebleven." Hij strekte zich uit en viel in een diepe slaap.'

Gerard Kornelis van het Reve (De Avonden, 1947)

Bedankt.
Raimond

p.s. deze pagina is om op te tekenen